

**CARBOXAMIDE RUTHENIUM(II) AND MANGANESE(II) COMPLEXES:  
STRUCTURAL, KINETIC AND MECHANISTIC STUDIES IN TRANSFER  
HYDROGENATION OF KETONES**

**BY**

**ROBERT TETTEY KUMAH (216076619)**

**A THESIS SUBMITTED IN PARTIAL FULFILMENT OF THE ACADEMIC  
REQUIREMENTS FOR THE DEGREE OF DOCTOR OF PHILOSOPHY IN  
CHEMISTRY**

**SCHOOL OF CHEMISTRY AND PHYSICS**

**COLLEGE OF AGRICULTURE, ENGINEERING AND SCIENCE,**

**UNIVERSITY OF KWAZULU-NATAL, SOUTH AFRICA**

**SUPERVISOR: PROF. STEPHEN OJWACH**

**MAY 2022**

## DECLARATION

I, Robert Tetey Kumah, declare that;

The research reported in this thesis, “*Carboxamide ruthenium(II) and manganese(II) complexes: structural, kinetic, and mechanistic studies in the transfer hydrogenation of ketones*”, except where otherwise indicated, is my original research.

1. This thesis has not been submitted for any degree or examination at any other university.
2. This thesis does not contain other persons’ data, pictures, graphs, or other information unless specifically acknowledged as being sourced from other persons.
3. This thesis does not contain other persons' writing, unless specifically acknowledged as being sourced from other researchers. Where other written sources have been quoted, then:
  - i. Their words have been re-written, but the general information attributed to them has been referenced.
  - ii. Where their exact words have been used, then their writing has been placed in italics and inside quotation marks and referenced.
4. This thesis does not contain text, or tables copied and pasted from the internet, unless specifically acknowledged, and the source being detailed in the thesis and in the References sections.

Signed:



Date: 20-05-2022

As the candidate’s supervisor, I have approved this thesis for submission.

Name: Prof. Stephen Ojwach

Signed: —



Date: 20-05-2022

## **DEDICATION**

*This thesis is dedicated to*

*My mother, Ms Florence Yawa Tsorhey*

## **ACKNOWLEDGEMENTS**

Professor Stephen Ojwach, my supervisor, deserves special thanks for his patience, guidance, and support during this study. Your ideas and outstanding supervisory role, profound knowledge in chemistry, insightful and instructive comments on this study offered me a lot of optimism in my research. I extend a debt of gratitude to the University of KwaZulu-Natal for providing the necessary facilities, without which none of this would have been possible.

I am grateful to the academic, technical, and administrative staff of the School of Chemistry and Physics, University of KwaZulu-School Natal, for their assistance in completing this study. Thank you for resolving the X-ray crystallographic structures, Mr Sizwe Zamisa. To my colleagues in the Catalysis Research Group, thank you for your friendship, support, and the wonderful times we had together. The Pietermaritzburg Chemistry Postgraduate community is also recognized for their support while conducting this research.

A special thanks to my mother and siblings for their unwavering support and encouragement. Thank you, my lovely son, Robertson Elikem Kumah, for your enduring and steadfast love.



## PREFACE

The development of new catalysts with improved catalytic efficiency for specific organic transformations has attracted the interest of researchers in the field of catalysis and organic synthesis in recent years. The first and second-row transition metals, in particular, have been widely employed in academia and industry to transform substrates such as ketones and aldehydes into valuable agrochemical, pharmaceutical and fine chemical products. The main focus areas of this thesis are catalyst activity and stability in transfer hydrogenation reactions. The architecture of the ligands is fundamental in balancing the electronic and steric properties of the catalyst. The main focus is catalytic activity and stability of the metal complexes in the transfer hydrogenation reactions of ketones. In this thesis, we aimed to achieve the balance between catalyst activity and the cost of catalyst establishment by using ruthenium(II) and manganese(II) complexes supported on multifunctional carboxamide ligands in catalytic transfer hydrogenation of ketones. This thesis is presented in seven chapters.

**Chapter 1** gives a general introduction to catalytic reduction reactions. The Chapter also discusses the role of metal catalysts in the transfer hydrogenation reactions and highlights some of the industrial applications of the transfer hydrogenation reactions. In addition, the relevant literature on transfer hydrogenation of ketones catalysed by ruthenium(II) and manganese(II) based catalysts is captured.

**Chapter 2** presents the general materials, instrumentation, detailed experimental procedures, methods and spectroscopic data analyses. It includes the general experimental design, syntheses and characterisation of the carboxamide ligands and their corresponding ruthenium(II) and manganese(II) complexes. The general methods of the transfer hydrogenation of ketones, kinetics and mechanism are also presented here.

**Chapter 3** describes the synthesis and characterisation of carboxamide ligands and their corresponding carbonyl-ruthenium(II) complexes and detailed structural studies of the complexes. The catalytic applications of the ruthenium complexes as catalysts in the transfer hydrogenation of ketones, the role of the catalyst structures and the mechanism of transfer hydrogenation of ketones are discussed. The findings of this chapter have been published in *New Journal of Chemistry*, 2022, **46**, 3146-3155.

**Chapter 4** focuses on improving the catalytic activities of the complexes described in Chapter 3 by developing new mono- and dinuclear organo-ruthenium(II) complexes supported on dipicolinamide ligands. It presents the detailed synthesis and coordination chemistry of the organo-ruthenium(II) complexes and gives a detailed study of the complexes as catalysts in transfer hydrogenation. The mechanism of transfer hydrogenation of ketones catalysed by the ruthenium complexes has been presented in this chapter.

In **Chapter 5**, the preparation, structural studies and catalytic application of dinuclear half-sandwich ruthenium(II) complexes of pyridine/pyrazine quinoline-carboxamides are discussed. The Chapter presents the role of catalyst structures in the transfer hydrogenation of ketones and aldehydes. The study further compared the impact of the pyridine *versus* pyrazine motifs on the kinetics of transfer hydrogenation of ketones. The Chapter also applies low-resolution ESI- mass spectrometry techniques to elucidate reactive intermediates in the transfer hydrogenation of ketones.

**Chapter 6** reports the synthesis of low-cost earth abundance, dinuclear manganese(II) complexes supported on dipicolinamide and its application as potential catalysts in the transfer hydrogenation of ketones. It highlights the effects of reactions of the catalytic activities of the

manganese(II) in the transfer hydrogenation of ketones. Finally, the overall conclusions on the key findings of this study and future prospects are presented in **Chapter 7**.

## RESEARCH OUTPUTS AND MANUSCRIPTS UNDER REVIEW

### Publications:

- I. Robert T. Kumah, Paranthaman Vijayan and Stephen O. Ojwach, Carboxamide carbonyl-ruthenium(II) complexes: detailed structural and mechanistic studies in the transfer hydrogenation of ketones. *New Journal of Chemistry*, **2022**,46, 3146-3155.
- II. Robert T. Kumah, and Stephen O. Ojwach, Mononuclear and dinuclear (pyridyl)carboxamide Ru(II) complexes: Ligand controlled coordination diversity and catalytic transfer hydrogenation of ketones, (Manuscript submitted to *Organometallics: om-2022-00231s*).
- III. Robert T. Kumah, and Stephen O. Ojwach, Diruthenium(II) half-sandwich complexes of dipicolinamide complexes: synthesis, structure studies and applications as catalysts for transfer hydrogenation of ketones, (Manuscript under review, *Inorganics* journal).
- IV. Robert T. Kumah, and Stephen O. Ojwach, Piano-stool diruthenium(II) complexes of quinoline-carboxamide: structure, mechanistic studies, and transfer hydrogenation of ketones, (Manuscript under preparation to be submitted to *European Journal of Inorganic Chemistry*).

- V. Robert T. Kumah, and Stephen O. Ojwach, Dinuclear manganese(II) complexes of dipyridyl-carboxamides, structural studies and transfer hydrogenation of ketones, (Manuscript under preparation to be submitted to *ChemSusChem*).

**Conference presentations:**

- I. Robert T. Kumah and Stephen O. Ojwach. *Dinuclear manganese(II) complexes of multidentate (phenylene)dipicolinamide: synthesis, structural elucidation, and application as catalysts for transfer hydrogenation of ketones*. CATSA 2021 Conference- Virtual and hosted by the University of KwaZulu-Natal, South Africa, **7<sup>th</sup> -10<sup>th</sup> November 2021**.

## ABSTRACT

The carboxamide ligands *N*-(benzo[d]thiazol-2-yl)pyrazine-2-carboxamide (**HL1**), *N*-(1H-benzo[d]imidazol-2-yl)pyrazine-2-carboxamide (**HL2**), were prepared by condensation of pyrazine-carboxylic acid and appropriate heteroaromatic amines. Reactions of **HL1** and **HL2** with ruthenium(II) precursors,  $[\text{RuH}(\text{CO})\text{Cl}(\text{PPh}_3)_3]$  and  $[\text{RuH}_2(\text{CO})(\text{PPh}_3)_3]$  afforded the mononuclear complexes  $[\text{RuL1}(\text{PPh}_3)_2(\text{CO})\text{Cl}]$  (**Ru1**),  $[\text{RuL1}(\text{PPh}_3)_2(\text{CO})\text{H}]$  (**Ru2**),  $[\text{RuL2}(\text{PPh}_3)_2(\text{CO})\text{Cl}]$  (**Ru3**),  $[\text{RuL2}(\text{PPh}_3)_2(\text{CO})\text{H}]$  (**Ru4**). The solid-state structures of complexes **Ru1**, **Ru2**, and **Ru4** reveal bidentate modes of coordination of the ligands and distorted octahedral geometries around the Ru(II) centre. The complexes formed active catalysts in the transfer hydrogenation of ketones and achieved turnover number (TON) up to 530 in 6 h. The ruthenium(II)–hydride complexes, **Ru2** and **Ru4**, were capable of catalysing transfer hydrogenation of ketones reactions under base free reaction conditions and demonstrated higher catalytic activities compared to the corresponding non-hydride analogues (**Ru1** and **Ru3**). An inner sphere monohydride mechanism involving dissociation of one  $\text{PPh}_3$  group was proposed from *in situ*  $^{31}\text{P}\{^1\text{H}\}$  NMR spectroscopy studies.

Dipicolinamide ligand system, *N,N'*-(1,4 phenylene)dipicolinamide (**H2L3**), *N,N'*-(1,2-phenylene)dipicolinamide (**H2L4**), *N,N'*-(4,5-dimethyl-1,2-phenylene)dipicolinamide (**H2L5**), *N,N'*-(4-methoxy-1,2-phenylene)dipicolinamide (**H2L6**) were synthesised following a similar protocol described for **HL1** and **HL2**. Treatment of the ligands **H2L3** and **H2L4** with  $\text{RuH}(\text{CO})\text{Cl}(\text{PPh}_3)_3$  afforded bimetallic complexes  $[\text{Ru}_2(\text{H2L3})(\text{PPh}_3)_4(\text{CO})_2][2\text{Cl}]$  (**Ru5**),  $[\text{Ru}_2(\text{H2L3})(\text{H})_2(\text{PPh}_3)_4(\text{CO})_2]$  (**Ru5b**),  $[\text{Ru}_2(\text{H2L4})(\text{PPh}_3)_3(\text{CO})_2\text{Cl}_3]$  (**Ru6**) and a mononuclear complex  $[\text{RuCl}_2\text{L4}(\text{PPh}_3)_2(\text{CO})]$  (**Ru7**). The solid-state structure of the dinuclear ruthenium(II) complexes confirmed a bidentate coordinate mode, with  $\text{PPh}_3$ , CO, and chlorido auxiliary ligands occupying the remaining coordinating sites to afford distorted trigonal bipyramidal

geometries (**Ru5** and **Ru6**) while the mononuclear complex **Ru7** adopted a distorted octahedral geometry around its ruthenium(II) atom. The reaction of the ligands **H2L4-H2L6** with the  $[\text{RuCl}_2(\eta^6\text{-}p\text{-cymene})]_2$  precursor produces half-sandwich diruthenium complexes  $[\{\text{Ru}(\eta^6\text{-}p\text{-cymene})\}_2\text{-}\mu\text{-Cl}(\text{L4})][\text{Ru}(\eta^6\text{-}p\text{-cymene})\text{Cl}_3]$  (**Ru8**),  $[\{\text{Ru}(\eta^6\text{-}p\text{-cymene})\}_2\text{-}\mu\text{-Cl}(\text{L4})][\text{PF}_6]$  (**Ru9**),  $[\{\text{Ru}(\eta^6\text{-}p\text{-cymene})\}_2\text{-}\mu\text{-Cl}(\text{L5})][\text{PF}_6]$  (**Ru10**), and  $[\{\text{Ru}(\eta^6\text{-}p\text{-cymene})\}_2\text{-}\mu\text{-Cl}(\text{L6})][\text{PF}_6]$  (**Ru11**). The molecular structure of cationic complexes, **Ru8-Ru11**, was confirmed by single-crystal X-ray crystallography analysis. The complexes **Ru8-Ru11** display a bidentate  $\text{N}_{\text{pyridine}} \wedge \text{N}_{\text{amidate}}$  mode of coordination to give *pseudo*-octahedral geometry (piano-stool-like geometry). The ruthenium(II) complexes demonstrated remarkable enhanced catalytic activity (TON values up to  $1.71 \times 10^4$ ) in the transfer hydrogenation of ketones at a very low catalyst loading of  $2.75 \times 10^{-2}$  mol% (275 ppm). The dinuclear ruthenium(II) complexes showed higher catalytic activity compared to the corresponding mononuclear complex **Ru5**. The half-sandwich diruthenium complexes **Ru8-Ru11** displayed relatively higher catalytic activity than the ruthenium complexes **Ru5** and **Ru6** bearing the  $\text{PPh}_3$  co-ligands. Monohydride inner-sphere catalytic cycle was proposed for the transfer hydrogenation of ketones catalysed by both **Ru1** and **Ru9**, and the formation of the reactive intermediates was supported with low-resolution mass spectrometry data.

The dinuclear ruthenium complexes of pyridine and pyrazine-carboxamide bearing quinolinyl motif were synthesised by reacting, *N*-(quinolin-8-yl)pyrazine-2-carboxamide, (**HL7**), 5-methyl-*N*-(quinolin-8-yl)pyridine-2-carboxamide, (**HL8**), 5-chloro-*N*-(quinolin-8-yl)pyridine-2-carboxamide, (**HL9**), and 2-pyrazine-carboxylic acid (**HL10**) with equimolar  $[\text{RuCl}_2(\eta^6\text{-}p\text{-cymene})]_2$  to afford the dinuclear complexes  $[\{\text{Ru}(\eta^6\text{-}p\text{-cymene})\}_2\text{Cl}_3(\text{L10})]$  (**Ru12**),  $[\{\text{Ru}(\eta^6\text{-}p\text{-cymene})\text{Cl}\}_2(\text{L7})][\text{PF}_6]$  (**Ru13**),  $[\{\text{Ru}(\eta^6\text{-}p\text{-cymene})\text{Cl}\}_2(\text{L8})][\text{Ru}(\text{L8})\text{Cl}_3]$  (**Ru14**), and  $[\{\text{Ru}(\eta^6\text{-}p\text{-cymene})\text{Cl}\}_2(\text{L9})][\text{PF}_6]$  (**Ru15**), respectively. The solid-state

structures of the dinuclear complexes **Ru12** and **Ru13** reveal a typical piano-stool geometry around the Ru(II) ions. The dinuclear ruthenium complexes **Ru12-Ru15** were used as catalysts in the transfer hydrogenation of a broad spectrum of aldehydes and ketones and demonstrated excellent catalytic activity, TON values up to  $4.8 \times 10^4$ , using catalyst loading of  $2.0 \times 10^{-3}$  mol% (20 ppm). The catalytic performance of the complexes was affected by the ligand architecture and the substituents on the pyridyl ring. Complexes **Ru13-15** exhibited higher catalytic activities compared to the complex **Ru12** which could be ascribed to the role of quinoline in stabilising the complexes. The pyridine and pyrazine motifs have a significant impact on the reactivity and the catalytic activity of the complexes. *In-situ* low-resolution ESI-MS analyses of the reactive intermediates aided in proposing a monohydride inner-sphere mechanism for the transfer hydrogenation of ketones catalysed by **Ru15**.

To develop a more sustainable, environmentally compatible and cost-efficient protocol for transfer hydrogenation of ketones, a new catalytic system based on manganese(II) metal was synthesised. New manganese(II) complexes **Mn1-Mn4**, ligated on dipicolinamide ligands were synthesized by treating the *N,N'*-(1,4-phenylene)dipicolinamide (**H<sub>2</sub>L3**), *N,N'*-(1,2-phenylene)dipicolinamide (**H<sub>2</sub>L4**), *N,N'*-(4-methoxy-1,2-phenylene)dipicolinamide (**H<sub>2</sub>L5**) and *N,N'*-(4,5-dimethyl-1,2-phenylene)dipicolinamide (**H<sub>2</sub>L6**) with MnCl<sub>2</sub>·4H<sub>2</sub>O salt to afford dinuclear manganese(II) complexes [Mn<sub>2</sub>(**H<sub>2</sub>L3**)<sub>2</sub>Cl<sub>4</sub>] (**Mn1**), [Mn<sub>2</sub>(**H<sub>2</sub>L4**)<sub>2</sub>Cl<sub>4</sub>] (**Mn2**), [Mn<sub>2</sub>(**H<sub>2</sub>L5**)<sub>2</sub>(Cl)<sub>4</sub>] (**Mn3**) and [Mn<sub>2</sub>(**H<sub>2</sub>L6**)<sub>2</sub>Cl<sub>4</sub>] (**Mn4**). The solid-state structure of complex **Mn2** showed a six-coordinate dinuclear complex with the two Mn(II) ions adopting a distorted octahedral environment surrounded by two tetradentate ligands and chlorido co-ligands, respectively. The Mn(II) complexes formed active catalysts in transfer hydrogenation of ketones to achieve TON values up to  $5.12 \times 10^4$ . The presence of electron-donating substituents -OCH<sub>3</sub> and -CH<sub>3</sub> in complexes **Mn3** and **Mn4** displayed minor effects in the transfer



hydrogenation of ketones. The new carboxamide-manganese(II) complexes are among the most active manganese-based catalysts capable of hydrogenating a large scope of ketones ranging from aliphatic to aromatic ketones. A dihydride catalytic cycle has been proposed and supported with *in-situ* low-resolution mass spectrometry data.

## TABLE OF CONTENTS

DECLARATION .....	i
DEDICATION .....	ii
ACKNOWLEDGEMENTS .....	iii
PREFACE .....	iv
RESEARCH OUTPUTS AND MANUSCRIPTS UNDER REVIEW .....	vii
ABSTRACT.....	ix
TABLE OF CONTENTS.....	xiii
LIST OF FIGURES .....	xviii
LIST OF SCHEMES.....	xxvii
LIST OF TABLES.....	xxix
ABBREVIATIONS .....	xxxi
CHAPTER 1 .....	1
1. INTRODUCTION AND LITERATURE REVIEW .....	1
1.1 Introduction to transition metal catalysis .....	1
1.1.1 Background information.....	1
1.1.2. Reduction of ketones .....	2
1.1.3. High-pressure hydrogenation of ketones .....	3
1.1.4. Hydroboration (HB) of ketones .....	4
1.1.5. Hydrosilylation (HS) of ketones .....	5
1.1.6. Biocatalytic reduction (BCR) of ketones.....	5
1.1.7. Transfer hydrogenation of ketones .....	6
1.2. Literature review of transfer hydrogenation of ketones catalysed by ruthenium(II) and manganese(I/II) complexes .....	15
1.2.1. General background on transition metal catalysts in transfer hydrogenation of ketones .....	15
1.2.2. Manganese(I)-based catalysts for transfer hydrogenation of ketones .....	35
1.3. Statement of the problem .....	37
1.4. The rationale of the study.....	38

1.5. General Aim and objectives .....	39
1.5.1. General aim.....	39
1.6. References .....	40
CHAPTER 2 .....	48
2.0 EXPERIMENTAL, INSTRUMENTATION AND METHODS.....	48
2.1. General information .....	48
2.2. General Materials .....	48
2.3. General Instrumentation.....	49
2.3.1. X-ray crystallography .....	49
2.4. Synthesis and characterisation of pyrazine-carboxamide ligands ( <b>HL1</b> and <b>HL2</b> ).....	50
2.4.1. <i>N</i> -(benzo[d]thiazol-2-yl) pyrazine-2-carboxamide ( <b>HL1</b> ) .....	50
2.4.2. <i>N</i> -(1H-benzo[d]imidazol-2-yl)pyrazine-2-carboxamide ( <b>HL2</b> ).....	51
2.5. Synthesis and characterisation of phenyl-dipicolinamide ligands ( <b>H2L3</b> – <b>H2L6</b> ) .....	51
2.5.1. <i>N,N'</i> -(1,4-phenylene)dipicolinamide ( <b>H2L3</b> ) .....	51
2.5.2. <i>N,N'</i> -(1,2-phenylene)dipicolinamide ( <b>H2L4</b> ) .....	52
2.5.3. <i>N,N'</i> -(4,5-dimethyl-1,2-phenylene)dipicolinamide ( <b>H2L5</b> ).....	53
2.5.4. <i>N,N'</i> -(4-methoxy-1,2-phenylene)dipicolinamide ( <b>H2L6</b> ).....	53
2.6. Synthesis and characterisation of <i>N</i> -pyrazyl/Pyridyl(quinolin-8-yl)pyrazine-2-carboxamide ligands ( <b>HL7-HL9</b> ) .....	54
2.6.1. <i>N</i> -(quinolin-8-yl)pyrazine-2-carboxamide ( <b>HL7</b> ).....	54
2.6.2. 5-methyl- <i>N</i> -(quinolin-8-yl)pyrazine-2-carboxamide ( <b>HL8</b> ) .....	54
2.6.3. 5-Chloro- <i>N</i> -(quinolin-8-yl)pyridine-2-carboxamide ( <b>HL9</b> ).....	55
2.7. Synthesis and characterisation of carbonyl-ruthenium(II) complexes of pyrazine-carboxamide ligands (Ru1-Ru4) .....	56
2.7.1. [Ru( <b>L1</b> )(CO)Cl(PPh <sub>3</sub> ) <sub>2</sub> ] ( <b>Ru1</b> ) .....	56
2.7.2. [Ru( <b>L1</b> )(CO)H(PPh <sub>3</sub> ) <sub>2</sub> ] ( <b>Ru2</b> ) .....	57
2.7.3. [Ru( <b>L2</b> )(CO)Cl(PPh <sub>3</sub> ) <sub>2</sub> ] ( <b>Ru3</b> ) .....	57
2.7.4. [Ru( <b>L2</b> )(CO)H(PPh <sub>3</sub> ) <sub>2</sub> ] ( <b>Ru4</b> ) .....	58
2.8. Synthesis and characterisation of carbonyl-ruthenium(II) complexes of phenyl-dipicolinamide ligands, (Ru5-Ru7) .....	58
2.8.1. [Ru <sub>2</sub> ( <b>H2L3</b> )(PPh <sub>3</sub> ) <sub>4</sub> (CO) <sub>2</sub> ][4Cl] ( <b>Ru5</b> ).....	58
2.8.2. [Ru <sub>2</sub> ( <b>H2L4</b> )(CO) <sub>2</sub> Cl <sub>2</sub> (PPh <sub>3</sub> ) <sub>3</sub> ] ( <b>Ru6</b> ).....	59
2.8.3. [Ru( <b>H2L4</b> )Cl{(CO)(PPh <sub>3</sub> ) <sub>2</sub> } <sub>2</sub> ] ( <b>Ru7</b> ) .....	60
2.8.4. [(RuHCO{PPh <sub>3</sub> } <sub>2</sub> ) <sub>2</sub> ( <b>H2L5</b> )] [2Cl] ( <b>Ru5b</b> ) .....	61
2.8.5. [{Ru(η <sup>6</sup> - <i>p</i> -cymene) <sub>2</sub> -μ-Cl] <sub>2</sub> <b>L4</b> ] [RuCl <sub>3</sub> (η <sup>6</sup> <i>p</i> -cymene)] ( <b>Ru8</b> ).....	61

2.8.6. [ $\{\text{Ru}(\eta^6\text{-}p\text{-cymene})_2\text{-}\mu\text{-Cl}\}_2\text{L4}\}$ ][PF <sub>6</sub> ] ( <b>Ru9</b> ).....	62
2.8.7. [ $\{\text{Ru}(\eta^6\text{-}p\text{-cymene})_2\text{-}\mu\text{-Cl}\}_2\text{L5}\}$ ][PF <sub>6</sub> ] ( <b>Ru10</b> ).....	63
2.8.8. [ $\{\text{Ru}(\eta^6\text{-}p\text{-cymene})_2\text{-}\mu\text{-Cl}\}_2\text{L6}\}$ ][PF <sub>6</sub> ] ( <b>Ru11</b> ).....	64
2.9. Synthesis and characterisation of dinuclear Ru(II) complexes of <i>N</i> -pyrazyl/Pyridyl(quinolin-8-yl)pyrazine-2-carboxamide ligands ( <b>Ru12-Ru15</b> ) .....	64
2.9.1. [ $\{\text{Ru}(\eta^6\text{-}p\text{-cymene})\text{Cl}\}_2(\text{L10})$ ] ( <b>Ru12</b> ).....	64
2.9.2. [ $\{\text{Ru}(\eta^6\text{-}p\text{-cymene})\text{Cl}\}_2(\text{L7})$ ][PF <sub>6</sub> ] ( <b>Ru13</b> ) .....	65
2.9.3. [ $\{\text{RuCl}(\eta^6\text{-}p\text{-cymene})\text{Cl}\}_2(\text{L8})$ ][Ru(L8)Cl <sub>3</sub> ] ( <b>Ru14</b> ) .....	66
2.9.4. [ $\{\text{RuCl}(\eta^6\text{-}p\text{-cymene})\}_2(\text{L9})$ ][PF <sub>6</sub> ] ( <b>Ru15</b> ).....	66
2.10. Synthesis and characterisation of dinuclear manganese(II) complexes of dipyridyl(phenylene)-dicarboxamides (Mn1-Mn4) .....	67
2.10.1. [Mn <sub>2</sub> (H <sub>2</sub> L3) <sub>2</sub> Cl <sub>4</sub> ] ( <b>Mn1</b> ).....	67
2.10.2. [Mn <sub>2</sub> (H <sub>2</sub> L4) <sub>2</sub> Cl <sub>4</sub> ] ( <b>Mn2</b> ).....	67
2.10.3. [Mn <sub>2</sub> (H <sub>2</sub> L5) <sub>2</sub> Cl <sub>4</sub> ] ( <b>Mn3</b> ).....	68
2.10.4. [Mn <sub>2</sub> (H <sub>2</sub> L6) <sub>2</sub> Cl <sub>4</sub> ] ( <b>Mn4</b> ).....	68
2.11. Typical procedure of the transfer hydrogenation of ketones.....	68
2.11.1. Isolation and characterisation of the TH products.....	69
2.11.2. Mercury poisoning test .....	70
2.11.3. Mechanistic studies of transfer hydrogenation.....	70
2.12. References .....	70
CHAPTER 3 .....	72
3. CARBOXAMIDE CARBONYL-RUTHENIUM(II) COMPLEXES: DETAILED STRUCTURAL AND MECHANISTIC STUDIES IN THE TRANSFER HYDROGENATION OF KETONES .....	72
3.1. Introduction.....	72
3.2. Results and discussion.....	74
3.2.1. Synthesis and characterisation of compounds .....	74
3.2.2. Solid-state structure of complexes <b>Ru1</b> , <b>Ru2</b> , and <b>Ru4</b> .....	81
3.2.3. Application of complexes Ru1-Ru4 in the transfer hydrogenation of ketones .....	87
3.2.3.1. Optimisation of catalyst loading using complex <b>Ru3</b> .....	87
3.3. Conclusions .....	99
3.4. References .....	100
CHAPTER 4 .....	105

4. MONONUCLEAR AND DINUCLEAR (BIPYRIDYL)-CARBOXAMIDE RUTHENIUM(II) COMPLEXES: LIGAND CONTROLLED COORDINATION DIVERSITY AND CATALYTIC TRANSFER HYDROGENATION OF KETONES .....	105
4.1. Introduction .....	105
4.2. Results and discussion.....	106
4.2.1. Synthesis and characterisation of ligands and complexes .....	106
4.2.2. Molecular structure of the complexes <b>Ru5-Ru8</b> and <b>Ru11</b> .....	121
4.2.3. Transfer hydrogenation of ketones .....	131
4.3. Conclusions .....	146
4.4 References .....	147
CHAPTER 5 .....	151
5. PIANO-STOOL DIRUTHENIUM(II) COMPLEXES OF QUINOLINYL-CARBOXAMIDE: STRUCTURAL, MECHANISTIC STUDIES AND TRANSFER HYDROGENATION OF KETONES .....	151
5.1. Introduction .....	151
5.2. Results and discussion.....	152
5.2.1 Synthesis and characterisation of complexes <b>Ru12-Ru15</b> .....	152
5.2.2. Solid-state structures of the dinuclear half-sandwich complexes <b>Ru12</b> and <b>Ru14</b> .....	163
5.2.3. Transfer hydrogenation of ketones and aldehydes .....	168
5.3. Conclusions .....	181
5.4. References .....	182
CHAPTER 6 .....	186
DINUCLEAR MANGANESE(II) COMPLEXES OF DIPYRIDYL-CARBOXAMIDES: STRUCTURAL STUDIES AND TRANSFER HYDROGENATION OF KETONES .....	186
6.1. Introduction .....	186
6.2. Results and discussion.....	188
6.2.1. Synthesis and characterisation of carboxamide Mn(II) complexes.....	188
6.2.2. Molecular structure of the dinuclear <b>Mn2</b> complex .....	192
6.2.3. Transfer hydrogenation of ketones .....	195
6.2.4. Effect of catalyst structure on the transfer hydrogenation of acetophenone .....	197
6.2.5. Substrate scope studies using complex <b>Mn4</b> .....	200
6.2.6. Plausible catalytic cycle for transfer of ketones using <b>Mn2</b> as catalysts .....	203

6.3. Conclusions .....	205
6.4. References .....	205
CHAPTER 7 .....	209
7.GENERAL CONCLUSION AND FUTURE PROSPECTS .....	209
7.1. Overall concluding remarks .....	209
7.2. General summary .....	212
7.3. Future prospects .....	213

## LIST OF FIGURES

<b>Figure 1.1.</b> NHC-Ru-arene complexes ( <b>1a-d</b> ) for transfer hydrogenation of ketones. <sup>101</sup>	18
<b>Figure 1.2.</b> Half-sandwich Ru-NHC complexes ( <b>2a-2e</b> ) reported by Ozdemir and co-workers. <sup>102</sup>	19
<b>Figure 1.3.</b> Structure of Ru(II) complexes bearing hemilabile NHC-pyrazole (NCN) pincer ligands reported by Messerle. <sup>103</sup>	20
<b>Figure 1.4.</b> Structure of pyridyl carboximine Ru(II) half-sandwich complexes used in TH of ketones reported by Omondi and co-workers. <sup>105</sup>	21
<b>Figure 1.5.</b> Half sandwich Ru(II) bearing Schiff-base backbones used in TH of ketones. <sup>108</sup>	21
<b>Figure 1.6.</b> Structure of ferrocenyl-imino-thiazolidine Ru(II) complexes reported by Gomez and co-workers. <sup>110</sup>	22
<b>Figure 1.7.</b> Ru(II) acetate complexes ( <b>7a-7j</b> ) anchored on bulky diphosphine and ferrocenyl-pyridyl amine ligands. <sup>110</sup>	23
<b>Figure 1.8.</b> Ru(II) complexes bearing <i>N</i> -tridentate pincer-type pyridyl-bis(pyridylidene) carboxamide ligands reported by Albrecht and co-workers. <sup>112</sup>	25
<b>Figure 1.9.</b> Modified Ru(II) complexes bearing <i>N,N,N</i> -tridentate pincer-type pyridyl-bis(pyridylidene) carboxamide ligands used for TH of ketones. <sup>113</sup>	26
<b>Figure 1.10.</b> Ru(II) phosphine-carboxamide complexes ( <b>11a -11e</b> ) reported by Gupta and co-workers. <sup>114</sup>	27
<b>Figure 1.11.</b> Dinuclear Ru(II)- arene complexes derived from monodentate organophosphine complexes used TH of ketones. <sup>115</sup>	28
<b>Figure 1.12.</b> Structural representation of Ru(II)-NNN pincer complexes derived from fused bis(pyrazolyl)-imidazolyl ligands. <sup>116</sup>	29

<b>Figure 1.13.</b> Diruthenium(II)-NNN complexes derived from unsaturated 16-electron mononuclear ruthenium(II)-pyrazolyl-imidazolyl-pyridine complex and 4,4'-linked bipyridine ligands. <sup>117</sup>	30
<b>Figure 1.14.</b> Trinuclear Ru(II) complexes anchored on amino-phosphine and phosphinite ligands used as catalysts for TH of ketones by Aydemir and co-workers. <sup>118</sup>	31
<b>Figure 1.15.</b> Bimetallic Ru(II)-NNN cationic complexes assembled by C-C rotated methylene linker reported by Yu and co-workers. <sup>120</sup>	32
<b>Figure 1.16.</b> Structure of polynuclear Ru(II) complexes ( <b>16a-16d</b> ) supported on central substituted pyridyl benzene backbone. <sup>119</sup>	33
<b>Figure 1.17.</b> Structure of neutral and cationic Ru(II)-NHC complexes <b>17a-17d</b> reported by Danaboyina and co-workers. <sup>121</sup>	34
<b>Figure 1.18.</b> Mn(I) catalysts ( <b>18a-18d</b> ) based on a nitrogen-donor system developed from amino methyl-pyridine reported by Sortais <i>et al.</i> <sup>124</sup>	35
<b>Figure 1.19.</b> Structure of Mn(I) complexes <b>19a-19f</b> supported on benzimidazole-amine ligands and catalytic activities under similar reaction conditions. <sup>125</sup>	36
<b>Figure 1.20.</b> Chiral Mn(I) complexes supported on P-N donor ligands bearing chiral ferrocene group reported for ATH of ketones by Kirchner <i>et al.</i> <sup>126</sup>	37
<b>Figure 1.21.</b> Chiral Mn(I) complexes ( <b>21a-21c</b> ) supported on mixed P-N donor ligands system reported by Morris and co-workers. <sup>127</sup>	37
 <b>Figure 2.1.</b> <sup>1</sup> H NMR spectrum of the crude product of TH of acetophenone using complex <b>Ru8</b> , 0.0015 mol% (15ppm) as a catalyst. An aliquot was taken and analysed after 4 h of reaction. The integral values of methyl protons of acetophenone and 1-phenylethanol corresponding to percentage conversion and yield = 42%. .....	69



<b>Figure 3.1.</b> A comparison in the shift between the $^1\text{H}$ NMR spectra of (a) <b>HL1</b> (N-H <sub>amide</sub> at 12.68 ppm) and (b) <b>Ru2</b> (N-H <sub>amide</sub> : absent, Ru-H signal at $\delta_{\text{H}}$ : -13.08 ppm).....	76
<b>Figure 3.2.</b> A comparison in shift between the $^{13}\text{C}\{^1\text{H}\}$ NMR spectra of (a) <b>HL1</b> (-C=O at $\delta$ : 161.3) and (b) complex <b>Ru1</b> (C=O signal at $\delta$ : 166.9 ppm).....	78
<b>Figure 3.3.</b> $^{31}\text{P}\{^1\text{H}\}$ NMR spectrum of complex <b>Ru4</b> showing a signal at $\delta$ : 23.2 ppm implicating the presence of two equivalent $\text{PPh}_3$ <i>trans</i> to each other. ....	79
<b>Figure 3.4.</b> LC-MS spectrum of <b>Ru2</b> showing the $m/z$ at 911, $[\text{M}^+ + 100\%]$ . The simulated theoretical mass distribution plot (inset).....	81
<b>Figure 3.5.</b> The ORTEP view of complex <b>Ru1</b> with thermal ellipsoids at a 50% probability level. All hydrogen atoms and $\text{CH}_2\text{Cl}_2$ are omitted for clarity. Selected bond length ( $\text{\AA}$ ): Ru(1)-C(13), 1.984(7) Ru(1)-N(1), 2.113(3), Ru(1)-N(2), 2.115(3), Ru(1)-P(1), 2.400(11), Ru(1)-Cl(1), 2.426(10). Bond angle( $^\circ$ ): C(13)-Ru(1)-N(1), 176.32(16), N(1)-Ru(1)-N(2), 77.84(13), C(13)-Ru(1)-P(2), 89.04(13), N(1)-Ru(1)-P(2), 91.12(9), and P(2)-Ru(1)-P(1), 176.88(4). ...	83
<b>Figure 3.6.</b> The ORTEP view of complex <b>Ru2</b> with thermal ellipsoids at a 50% probability level. All aromatic hydrogen atoms and $\text{CH}_2\text{Cl}_2$ are omitted for clarity. Selected bond length ( $\text{\AA}$ ): Ru(1)-C(13), 1.984(7), Ru(1)-N(1), 2.118(14), Ru(1)-N(2), 2.116(15), Ru(1)-P(1), 2.364(4), Ru(1)-H(1A), 1.550(10). Bond angle( $^\circ$ ): C(13)-Ru(1)-N(1), 177.73(7), N(1)-Ru(1)-N(2), 76.13(5), C(13)-Ru(1)-P(2), 90.76(5), N(1)-Ru(1)-P(2), 88.31(4), and P(2)-Ru(1)-P(1), 165.302(16).....	84
<b>Figure 3.7.</b> The ORTEP view of complex <b>Ru4</b> with thermal ellipsoids at a 50% probability level. All aromatic atoms and $\text{CH}_2\text{Cl}_2$ are omitted for clarity. Selected bond length ( $\text{\AA}$ ): Ru(1)-C(13), 1.984(7), Ru(1)-N(1), 2.115(6), Ru(1)-N(2), 2.118(5), Ru(1)-P(1), 2.410(11), Ru(1)-H(1A), 1.967(10). Bond angle( $^\circ$ ): C(13)-Ru(1)-N(1), 100.81(10), N(1)-Ru(1)-N(2), 76.24(8), C(13)-Ru(1)-P(2), 89.05(8), N(1)-Ru(1)-P(2), 95.06(6), and P(2)-Ru(1)-P(1), 168.60(2). ....	85

<b>Figure 3.8.</b> Plots of percentage conversion, turnover number (TON) vs time showing the effects of catalyst loading on the catalytic activity in the TH of acetophenone using complex <b>Ru3</b> .	88
<b>Figure 3.9. (a)</b> A plot of percentage conversion vs time showing the effects of catalyst structure on the catalytic activity of TH of acetophenone reaction using complexes <b>Ru1-Ru4</b> . <b>(b)</b> a plot of $\ln[\text{acetophenone}]_t/[\text{acetophenone}]_0$ vs $\ln[t]$ for determination of the rate constants of each catalyst in TH of acetophenone reaction.	92
<b>Figure 3.10.</b> $^{31}\text{P}\{^1\text{H}\}$ NMR spectral of complex $[\text{RuHCO}(\text{L4})(\text{PPh}_3)_2]$ , <b>Ru4</b> in the presence of acetophenone, $i\text{PrOH}$ and $\text{K}^t\text{BuO}$ for 6 h. Spectrum, <b>(i)</b> shows a signal at $\delta$ 23.2 ppm corresponding to two equivalent $\text{PPh}_3$ groups in the complex at $t = 0$ . Spectra <b>(ii)</b> and <b>(iii)</b> show signals for the free $\text{PPh}_3$ at $\delta$ -4.7 and 5.28 ppm after 4 h and 6 h, respectively.	97
<b>Figure 4.1.</b> A comparison in shift between the $^1\text{H}$ NMR spectra of <b>(a) H<sub>2</sub>L3</b> ( $\text{N-H}_{\text{amide}}$ at $\delta$ : 10.07 ppm) and <b>(b) Ru5</b> ( $\text{N-H}_{\text{amide}}$ at $\delta$ : 11.07 ppm).	111
<b>Figure 4.2.</b> $^1\text{H}$ NMR spectrum of complex <b>Ru5b</b> obtained from <b>Ru5</b> showing two signals for $\text{N-H}_{\text{iminolate}}$ protons at 13.48ppm and 13.68 ppm and $\text{Ru-H}$ at -10.21 ppm and -1603 ppm.	112
<b>Figure 4.3.</b> A comparison in shift between the $^1\text{H}$ NMR spectra of <b>(a) H<sub>2</sub>L4</b> ( $\text{N-H}_{\text{amide}}$ at $\delta$ : 10.07 ppm) and <b>(b) Ru9</b> ( $\text{N-H}_{\text{amide}}$ : absent).	114
<b>Figure 4.4.</b> A comparison in shift between the $^{13}\text{C}\{^1\text{H}\}$ NMR spectra of <b>(a) H<sub>2</sub>L4</b> ( $\text{C}_{\text{amide}}$ at $\delta$ : 162.9 ppm) and <b>(b) Ru9</b> ( $\text{C}_{\text{amide}}$ at $\delta$ : 169.6 ppm).	115
<b>Figure 4.5.</b> $^{31}\text{P}\{^1\text{H}\}$ NMR spectrum of complex <b>Ru5</b> showing a typical septet signal at $\delta$ : 44.6 ppm indicating the presence of two equivalent $\text{PPh}_3$ trans to each other.	116
<b>Figure 4.6.</b> $^{31}\text{P}\{^1\text{H}\}$ NMR of complex <b>Ru11</b> showing signal between 131 and 157 ppm confirming the presence of $[\text{PF}_6]^-$ counterion.	117

- Figure 4.7.**  $^{19}\text{F}$  NMR of complex **Ru11** showing a doublet signal between ~69 and ~79 ppm confirming the presence of  $[\text{PF}_6]^-$  counterion. .... 117
- Figure 4.8.** ESI -MS (positive mode) of complex **Ru5** showing the molecular ion peak at  $m/z = 1626$   $[\text{M}^{2+}, 100]$ . Simulated isotopic mass distribution of the cationic species, **Ru5** (Inset). .... 120
- Figure 4.9.** ESI -MS (positive mode) of complex **Ru9** showing the molecular ion peak at  $m/z = 825$   $[\text{M}^+, 100]$  corresponding to the cationic species with formula,  $\text{C}_{92}\text{H}_{74}\text{N}_4\text{O}_4\text{P}_4\text{Ru}_2$ . Theoretical isotopic mass distribution of the cationic species of the complex, **Ru9** (inset). 121
- Figure 4.10.** An ORTEP view of **Ru5** showing displacement ellipsoids represented at 50% and atom labelling. All hydrogen atoms, chloride ions and solvents are omitted for the purpose of clarity. Selected bond distances ( $\text{\AA}$ ): Ru(1)-N(1), 2.153(2); Ru(1)-O(1), 2.1530(18); Ru(1)-P(1), 2.3443(7); Ru(1)-P(2), 2.3728(7); Ru(1)-C(1), 1.833(8). Selected bond angles ( $^\circ$ ): N(1)-Ru(1)-O(1), 74.10(5); N(1)-Ru(1)-P(1), 93.12; N(1)-Ru(1)-P(2), 95.78(6); N(1)-Ru(1)-C(1), 101.84(13); C(1)-Ru(1)-O(1), 175.80(13); C(1)-Ru(1)-P(1), 93.12(2); C(1)-Ru(1)-P(2), 96.14(8), P(1)-Ru(1)-O(1), 85.68(5); P(1)-Ru(1)-P(2), 165.68(5). .... 123
- Figure 4.11.** An ORTEP view of **Ru6** showing displacement ellipsoids represented at 50% and atom labelling. All hydrogen atoms and diethyl ether are omitted for clarity. Selected bond distances ( $\text{\AA}$ ): Ru(1)-N(1), 2.153(2); Ru(1)-O(1), 2.1530(18); Ru(1)-P(1), 2.3443(7); Ru(1)-P(2), 2.3728(7); Ru(1)-C(1), 1.833(8). Selected bond angles ( $^\circ$ ): N(1)-Ru(1)-O(1), 67.64(5); N(1)-Ru(1)-P(1), 93.12; N(1)-Ru(1)-P(2), 95.78(6); N(1)-Ru(1)-C(1), 101.84(13); C(1)-Ru(1)-O(1), 175.80(13); C(1)-Ru(1)-P(1), 93.12(2); C(1)-Ru(1)-P(2), 96.14(8), P(1)-Ru(1)-O(1), 85.68(5); P(1)-Ru(1)-P(2), 165.68(5). .... 124
- Figure 4.12.** An ORTEP view of **Ru7** showing displacement ellipsoids represented at 50% and atom labelling. All hydrogen atoms and chloroform are omitted for clarity. Bond length ( $\text{\AA}$ ): N(1)-Ru(1), 2.151(7); O(1)-Ru(1), 2.094(5); Ru(1)-P(1), 2.3735(18); Ru(1)-C(55), 2.094(5);

Ru-Cl(1), 2.367(6). Bond angle (°): N(1)-Ru(1)-P(1), 91.40(17); N(1)-Ru(1)-C(55), 168.3(7); N(1)-Ru(1)-Cl(1), 95.42(19); O(1)-Ru(1)-P(1), 91.03(15); O(1)-Ru(1)-N(1), 75.8(2), O(1)-Ru(1)-C(55), 92.5(6) and O(1)-Ru-Cl(1), 171.20(17); P(1)-Ru(1)-P(2), 175.07(6) and P(1)-Ru(1)-Cl(1), 88.72(9)..... 125

**Figure 4.13.** Solid state structure of complex **Ru5b** drawn at displacement 50% thermal ellipsoids. All aromatic and amide hydrogen atoms are omitted for clarity. Selected bond distances (Å): Ru(1)-N(1), 2.188(4); Ru(1)-O(1), 2.1510(3); Ru(1)-P(1), 2.3703(11); Ru(1)-P(2), 2.3421(10); Ru(1)-C(1)O, 1.833(5), O(1)-C(7), 1.840(4). Ru(1)-H, 1.54(3). Selected bond angles (°): N(1)-Ru(1)-O(1), 74.10(5); N(1)-Ru(1)-P(1), 95.85(9); N(1)-Ru(1)-P(2), 95.88(7); N(1)-Ru(1)-C(1)O, 101.46(19); OC(1)-Ru(1)-O(1), 175.55(19); OC(1)-Ru(1)-P(1), 95.80(15); P(1)-Ru(1)-O(1), 85.68(5); P(1)-Ru(1)-P(2), 164.79(4), N(1)-Ru(1)-H, 92.75(4). ..... 126

**Figure 4.14.** An ORTEP view of **Ru8** showing displacement ellipsoids represented at 50% and atom labelling. All hydrogen atoms are omitted for clarify. Bond length (Å): N(1)-Ru(1), 2.093(2); N(2)-Ru(1), 2.1090(2); Ru(1)-Cl(1), 2.460(6); Ru(3)-Cl(2), 2.392(3). Bond angle(°): N(1)-Ru(1)-N(2), 77.55(18); N(1)-Ru(1)-Cl(1), 85.39(14); N(2)-Ru-Cl(1), 86.95(13); Cl(2)-Ru(3)-Cl(3), 87.65(5)..... 127

**Figure 4.15.** An ORTEP view of **Ru11** showing displacement ellipsoids represented at 50% and atom labelling. All hydrogen atoms are omitted for clarify. Bond length(Å): N(1)-Ru(1), 2.093(2); N(2)-Ru(1), 2.1090(2); Ru(1)-Cl(1), 2.460(6); Ru(3)-Cl(2), 2.392(3). Bond angle(°): N(1)-Ru(1)-N(2), 77.55(18); N(1)-Ru(1)-Cl(1), 85.39(14); N(2)-Ru-Cl(1), 86.95(13); Cl(2)-Ru(3)-Cl(3), 87.65(5)..... 128

**Figure 4. 16.** Time-dependent transfer hydrogenation reaction of acetophenone catalysed by **Ru5-Ru11**:  $5.00 \times 10^{-3}$  mol% (50 ppm);  $K^t$ BuO: 4.0 mol%; temperature 82 °C. (a) and (c)

Conversion[%] vs time plots, (b) and (d)  $-\ln[\text{Ac.}]_t/[\text{Ac.}]_0$  vs time plot of the **Ru9-Ru11** catalysts in the TH of acetophenone. .... 137

**Figure 4.17.** Hydride region of  $^1\text{H}$  NMR spectra of the Ru-H species (**Ru1b**), obtained from the reactions of **Ru5** with [iPrOH/ $^t\text{BuOK}$ ] at 80 °C in (a) 30 min, (b) 1 h, (c) 1: 30 min and (d) 2 h..... 142

**Figure 4.18.**  $^{31}\text{P}$  NMR spectra of original complex **Ru5** (a) showing the signal at 23.2 ppm corresponding to the two  $\text{PPh}_3$  groups in **Ru5** and (b) showing the signals at 29.2 ppm corresponding two  $\text{PPh}_3$  of group in **Ru5b**, (c) intermediates showing the signals at ~4.7 ppm and 28.5 ppm corresponding dissociated  $\text{PPh}_3$  and coordinated  $\text{PPh}_3$  of intermediate **Ru5c** respectively at 80 °C after 6 h. .... 143

**Figure 5.1.** A comparison in chemical shifts in the  $^1\text{H}$  NMR spectra of (a) **HL10** ( $\text{H}_{\text{pyrazine}}$ : 9.18-8.79 ppm) and (b) **Ru12** ( $\text{H}_{\text{pyrazine}}$ : 9.40-8.92 ppm)..... 156

**Figure 5.2.** A comparison in the chemical shifts in the  $^{13}\text{C}\{^1\text{H}\}$  NMR spectra of (a) **HL10** ( $\text{C}=\text{O}_{\text{amide}}$  at  $\delta$ : 166.5 ppm) and (b) **Ru12** ( $-\text{C}-\text{O}_{\text{hemi-amide}}$  at  $\delta$ : 169.7 ppm). .... 157

**Figure 5.3.** A comparison in the chemical shifts in the  $^1\text{H}$  NMR spectra of (a) **HL9** ( $\text{N}-\text{H}_{\text{amide}}$  at  $\delta$ : 11.65 ppm) and (b) **Ru15** ( $\text{N}-\text{H}_{\text{amide}}$  absent)..... 158

**Figure 5.4.** A comparison in the chemical shifts in the  $^{13}\text{C}\{^1\text{H}\}$  NMR spectra of (a) **HL9** ( $-\text{C}=\text{O}_{\text{amide}}$  at  $\delta$ : 162.8 ppm) and (b) **Ru15** ( $-\text{C}=\text{O}_{\text{amide}}$  at  $\delta$ : 167.9 ppm). .... 159

**Figure 5.5.**  $^{31}\text{P}\{^1\text{H}\}$  NMR of complex **Ru14** showing signal between ~131 and ~157 ppm confirming the presence of  $[\text{PF}_6]^-$  counterion. .... 160

**Figure 5. 6.**  $^{19}\text{F}$  NMR of complex **Ru11** showing a doublet signal between ~69 and ~79 ppm confirming the presence of  $[\text{PF}_6]^-$  counterion. .... 161

**Figure 5.7.** ESI-MS spectrum of **Ru14**, showing  $m/z = 804.95$  [ $\text{M}^+$ , 100%] and consistent with theoretical isotopic mass distribution (inset). .... 162

**Figure 5.8.** ORTEP representation of **Ru12** at 50% probability thermal ellipsoids level. Hydrogen atoms and solvent, CHCl<sub>3</sub> have been removed for clarity. Bond length(Å): Ru(1)-N(1), 2.117(3) Ru(2)-N(2), 2.097(3), Ru(1)-Cl(1), 2.173(4), Ru(1)-O(2), 2.091(2). Bond angle(°): N(1)-Ru(1)-Cl(1), 86.95(8), O(2)-Ru(1)-N(1), 77.83(10), N(2)- Ru(1)-Cl(3), 81.24(8), and O(1)- Ru(1)-Cl(3), 84.76(7). ..... 165

**Figure 5.9.** ORTEP representation of **Ru14** at 50% probability thermal ellipsoids level. Hydrogen atoms and counterion of **Ru3**, RuCl<sub>3</sub>(L<sup>3</sup>) have been removed for clarity. Bond length (Å): Ru(1)-N(1), 2.089(4), Ru(2)-N(2), 2.173(4), Ru(1)-Cl(1), 2.391(14), Ru(2)-N(3), 2.173(4), Ru(1)-O(2), 2.120(3). Bond angle (°): N(1)-Ru(1)-Cl(1), 93.83(13), O(2)-Ru(1)-N(1), 84.03(12), N(2)- Ru(1)-Cl(3), 77.75(16), and O(1)- Ru(1)-Cl(3), 86.04(10). ..... 166

**Figure 5.10.** A plot of catalysts loading (mol%) vs conversion [%] and TON was used to determine optimised catalyst loading..... 170

**Figure 5.11.** Time-dependence plots of the TH of acetophenone reactions catalysed by **Ru12**-**Ru15**. (a) Percentage conversion vs time/h, (b) ln[Ac.]/[Ac.]<sub>o</sub> vs time/h. .... 173

**Figure 6.1.** ESI-MS spectrum of complex **Mn1** showing the m/z = 852 [M<sup>+</sup>- Cl, 100] and 885 [M<sup>+</sup>, 40%]. The simulated theoretical isotopic mass distribution pattern (inset). ..... 191

**Figure 6.2.** ORTEP plot of symmetric unit of complex **Mn2** (atomic displacement ellipsoid at 50% probability). All hydrogen atoms are omitted for clarity. Bond lengths (Å): Mn(1)-N(2), 2.266(4), Mn(2)-Cl(2), 2.4023(11), Mn(2)-O(10), 2.262(4). Bond angles (°): O(10)-Mn(2)-N(3), 73.04(12), O(10)-Mn(2)-O(20), 81.56(10), N(3)-Mn(2)-N(4), 143.92(13), N(4)-Mn(2)-Cl(2), 98.10(10). ..... 195

**Figure 7.1.** Selected Ru (II) and Mn(II) complexes displaying the highest and lowest catalytic activities in TH of ketones. .... 211

**Figure 7.2.** The general structure of the proposed diruthenium(II) complexes for TH of quinoline and quinoline.....214

**Figure 7.3.** General structure of Mn(I) carbonyl complexes supported on mesoporous material, MCM-41. ....215

## LIST OF SCHEMES

<b>Scheme 1.1.</b> A representative reaction scheme for HPH of ketone catalysed by transition metal catalyst. ....	3
<b>Scheme 1.2.</b> Hydroboration of ketone catalysed by transition metal catalyst.....	4
<b>Scheme 1.3.</b> Catalytic hydrosilylation of ketones using PhSiH <sub>3</sub> as a source of hydrogen. ....	5
<b>Scheme 1.4.</b> Bio-catalytic reduction of ketone to optically active alcohol. ....	6
<b>Scheme 1.5.</b> A representative reaction scheme for transfer hydrogenation of unsaturated substrates catalysed by a TMC. ....	7
<b>Scheme 1.6.</b> Typical reaction pathway for direct hydride transfer hydrogenation of ketones (Meerwein–Ponndorf–Verley). <sup>54</sup> .....	9
<b>Scheme 1.7.</b> A typical monohydride inner-sphere mechanism for transfer hydrogenation of ketones. ....	10
<b>Scheme 1.8.</b> A typical outer-sphere mechanism for transfer hydrogenation of ketones.....	11
<b>Scheme 1.9.</b> Dihydride mechanism (inner-sphere) as proposed by Henbest et al. using Ru(PPh <sub>3</sub> ) <sub>3</sub> Cl <sub>2</sub> as catalyst. <sup>60</sup> .....	12
<b>Scheme 1.10.</b> Transfer deuteration of alkynes and alkene using deuterated dioxane-d <sub>8</sub> as a source of deuterium and solvent. ....	13
<b>Scheme 1.11.</b> Synthesis of propargylic alcohol and biaryl alcohol via <b>(a)</b> tandem Sonogashira C-C coupling-transfer hydrogenation and <b>(b)</b> Suzuki-Miyaura C-C coupling-transfer hydrogenation methods, respectively.....	15
 <b>Scheme 3.1.</b> Synthesis of carboxamide Ru(II) complexes <b>Ru1-Ru4</b> . ....	75
<b>Scheme 3.2.</b> A proposed monohydride reaction pathway for transfer hydrogenation of ketone catalysed by <b>Ru4</b> .....	98



<b>Scheme 4.1.</b> Rearrangement reactions within the ligand prior to the formation of dinuclear Ru(II) complexes <b>Ru5-Ru7</b> .....	107
<b>Scheme 4.2.</b> Synthesis of carbonyl ruthenium(II) complexes, <b>Ru5 - Ru7</b> . ....	108
<b>Scheme 4.3.</b> Synthesis of half-sandwich ruthenium(II) complexes <b>Ru8-Ru11</b> .....	109
<b>Scheme 4.4.</b> Proposed monohydride mechanism for the transfer hydrogenation of acetophenone catalysed by <b>Ru5</b> as deduced from NMR spectroscopy and structural characterisation of the Ru-H intermediate. ....	144
<b>Scheme 4.5.</b> A plausible mechanism for transfer hydrogenation of acetophenone catalysed by <b>Ru9</b> . The reactive intermediates were identified by low-resolution ES-MS analysis.....	146
 <b>Scheme 5.1.</b> Synthesis of half-sandwich dinuclear Ru(II) complexes <b>Ru12-Ru15</b> .....	154
<b>Scheme 5.2.</b> Monohydride mechanism proposed for TH of acetophenone catalysed by <b>Ru15</b> . ....	181
 <b>Scheme 6.1.</b> Synthesis of bimetallic manganese(II) carboxamide complexes <b>Mn1-Mn4</b> ....	189
<b>Scheme 6.2.</b> The proposed outer-sphere dihydride mechanism of TH of acetophenone using complex <b>Mn2</b> .....	204

## LIST OF TABLES

<b>Table 3.1.</b> Selected FT-IR spectroscopic data of the complexes <b>Ru1-Ru4</b> and corresponding ligands <b>HL1-HL2</b> .	80
<b>Table 3.2.</b> Crystal data and structure refinement for complexes <b>Ru1, Ru2</b> and <b>Ru4</b>	86
<b>Table 3.3.</b> Optimisation of catalyst loading for effective TH of acetophenone using complex <b>Ru3<sup>a</sup></b>	88
<b>Table 3.4.</b> Optimisation of base loading for effective TH of acetophenone using complexes <b>Ru3</b> and <b>Ru4<sup>a</sup></b>	90
<b>Table 3.5.</b> Transfer hydrogenation of acetophenone data of complexes <b>Ru1-Ru4<sup>a</sup></b>	92
<b>Table 3.6.</b> Result of substrate scope studies using complex <b>Ru4<sup>a</sup></b>	95
<b>Table 4.1.</b> Selected FT-IR spectroscopic data of the complexes <b>Ru5-Ru11</b> and corresponding ligands <b>H<sub>2</sub>L3-H<sub>2</sub>L6</b> .	119
<b>Table 4.2.</b> A summary of crystallographic parameters and refinement data for complexes <b>Ru5-Ru7</b> .	129
<b>Table 4.3.</b> Summary of crystallographic parameters and refinement data of <b>Ru8</b> and <b>Ru11</b> .	130
<b>Table 4.4.</b> Effects of catalyst concentration and base on TH of acetophenone using complexes <b>Ru5</b> and <b>Ru9</b> as a catalysts. <sup>a</sup>	133
<b>Table 4.5.</b> Effects of catalyst structure on the transfer hydrogenation of acetophenone catalysed by complexes <b>Ru5 – Ru11</b> . <sup>a</sup>	135
<b>Table 4.6.</b> Result of substrate scope studies using complexes <b>Ru5</b> and <b>Ru9</b> as catalysts. <sup>a</sup>	140

<b>Table 5.1.</b> Selected FT-IR spectroscopic data of the complexes <b>Ru12-Ru15</b> and corresponding ligands <b>HL7-HL10</b> .	161
<b>Table 5.2.</b> Summary of crystallographic data and structural refinement data for complexes <b>Ru12</b> and <b>Ru14</b> .	167
<b>Table 5.3.</b> Optimisation of reaction conditions for transfer hydrogenation of acetophenone using <b>Ru13<sup>a</sup></b> .	169
<b>Table 5.4.</b> Effects of catalyst structure on transfer hydrogenation of acetophenone <sup>a</sup> .	172
<b>Table 5.5.</b> Substrate scope investigation using the dinuclear complex <b>Ru15</b> . <sup>a</sup>	176
<b>Table 5.6.</b> Result of transfer hydrogenation of aldehydes catalysed by complex <b>Ru15</b> . <sup>a</sup>	179
 <b>Table 6.1.</b> Selected FT-IR spectroscopic data of the complexes <b>Mn1-Mn4</b> and corresponding ligands <b>H2L3-H2L6</b> .	 190
<b>Table 6.2.</b> Crystal and structural refinement data for complex <b>Mn2</b> .	194
<b>Table 6.3.</b> The results of reaction conditions optimisation for TH of ketones using <b>Mn2<sup>a</sup></b> .	197
<b>Table 6.4.</b> Investigation of effects of catalyst structure in the transfer hydrogenation of acetophenone. <sup>a</sup>	199
<b>Table 6.5.</b> Results of substrate scope studies using complex <b>Mn4<sup>a</sup></b>	202
 <b>Table 7.1.</b> Catalytic activity (TON and $k_{\text{ob}}/\text{h}^{-1}$ ) of selected Ru(II) and Mn(II) complexes...	 212

## ABBREVIATIONS

NMR	Nuclear Magnetic Resonance
FT-IR	Fourier transform infrared
ESI-MS	Electron spray ionisation mass spectrometry
LC-MS	Liquid chromatography mass spectrometry
s	singlet
d	doublet
m	multiplet
ppm	Part per million
TMC	Transition metal complex
TON	Turn over number
TOF	Turn over frequency
<i>J</i>	Coupling constant
DCM	Dichloromethane
TH	Transfer hydrogenation
HS	hydrosilylation
BCR	Biocatalytic reduction
L	Ligands
HB	Hydroboration
M	Metal
<i>ee</i>	Enantiomeric excess
$\delta$	Chemical shift
PPh <sub>3</sub>	Triphenylphosphine
HPH	High Pressure Hydrogenation

DMSO- <i>d</i> <sub>6</sub>	Deuterated Dimethyl sulfoxide
CDCl <sub>3</sub> - <i>d</i>	Deuterated chloroform
TOF <sub>50</sub>	Turnover frequency at 50% conversion

## CHAPTER 1

### 1. INTRODUCTION AND LITERATURE REVIEW

This chapter deals with the fundamental concepts, mechanism, and industrial applications of transfer hydrogenation catalysis. It also covers literature review on transfer hydrogenation of ketones catalysed by ruthenium(II) and manganese(I/II) based complexes.

#### 1.1 Introduction to transition metal catalysis

##### 1.1.1 Background information

The primary objective of a catalyst in any chemical reaction is to accelerate the kinetics of the reaction toward the formation of a thermodynamically stable product by following different reaction pathways with lower activation energy.<sup>1-2</sup> Catalysis is a subject with the highest impact on the chemical industries.<sup>3-4</sup> It is one of the most attractive and promising techniques in various fields of academic and industrial processes that involve chemical syntheses.<sup>3, 5</sup> In the last two decades, it was estimated that about 85% of all the existing industrial chemical processes and almost all newly developed transformations involved the application of catalysts.<sup>6-7</sup> Presently, catalysts made from transition metals are extensively used in the manufacturing of agrochemicals, pharmaceuticals, polymers, flavours, fuels, among others chemical products.<sup>6, 8</sup> From the perspective of chemical scientists, catalysis can be subcategorised into: heterogeneous and homogeneous catalysis. The catalyst involved in the heterogeneous reaction is usually solid, whilst the co-catalyst, substrate, solvent, and products exist in the fluid/gaseous phase.<sup>9</sup> Refinery processes such as cracking or catalytic reforming of petroleum crude products and manufacturing of ammonia, sulfuric, and nitric acid are among the few that make use of heterogeneous catalysis.<sup>9-10</sup> In contrast, homogeneous catalysis involves the reactants, products, and the catalytic active species all in a single phase, typically

the fluidic phase.<sup>9-10</sup> Catalysts developed from transition metal complexes are often used in homogeneous catalysis.<sup>11-12</sup>

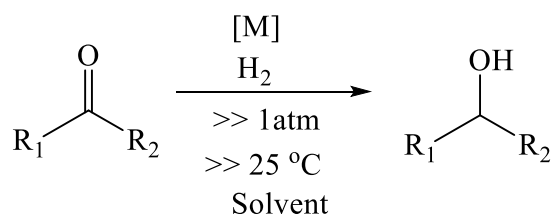
Transition metal catalysts (TMCs) are versatile and widely used in the synthetic community. TMCs are commonly applied in a number of industrial transformations, including hydrogenation, polymerisation, Fisher Tropsch processes, hydroformylation of alkenes, olefin oligomerization, carbonylation of methanol, oxidation, cross-coupling reactions, and in the synthesis of various target molecules.<sup>13-14</sup> TMCs are unavoidable in most industrial transformations due to their high selectivity, stability and activity.<sup>15-16</sup> TMCs help minimise the formation of by-products and improve the overall efficiencies with which desired transformation is achieved.<sup>15</sup> TMCs play vital roles in organic transformations, including the manufacturing of petrochemicals, inorganic chemicals, fuel cells, pollution abatements, and bio-based compounds.<sup>17-18</sup> The following sections capture brief discussions of various methods of hydrogenation reactions.

### **1.1.2. Reduction of ketones**

Reduction transformation is an essential synthetic protocol used to synthesise several chemical products. There are five main known strategies for carrying out reduction reactions, *viz*: high-pressure hydrogenation (HPH), hydroboration (HB), hydrosilylation (HS), enzymatic (biocatalytic) reduction (ER) and transfer hydrogenation (TH). These methods are briefly discussed in the following sub-sections.

### 1.1.3. High-pressure hydrogenation of ketones

High-pressure hydrogenation (HPH) of a ketone is the addition of molecular hydrogen ( $\text{H}_2$ ) across the polar pi bond ( $-\text{C}=\text{O}$ ) to produce the corresponding alcohol. This reaction is carried out in the presence of a TMC at high pressure (**Scheme 1.1**).<sup>19</sup> HPH is not only limited to ketones, but has been extended to other unsaturated organic compounds such as alkenes, imines, and enamines, heteroaromatics (quinoline, pyridine, pyrazine). The use of BINAP-Ru(II) catalysts [BINAP = 2,2'-bis(diphenylphosphino)-1, 1'-binaphthyl]<sup>20</sup>, for instance, has been proven to be exceptionally efficient for the stereoselective hydrogenation of functionalised ketones, and has been advanced for the industrial synthesis of antibiotic carbapenems and antibacterial Levofloxacin.<sup>21-22</sup> However, HPH has a number of challenges that limits its applications in a number of industrial processes. HPH is expensive and requires sophisticated apparatus in its operations, and reaction conditions also pose safety challenges since high pressure and temperature conditions are often employed.<sup>18, 23</sup>



[M] = metal-based catalysts

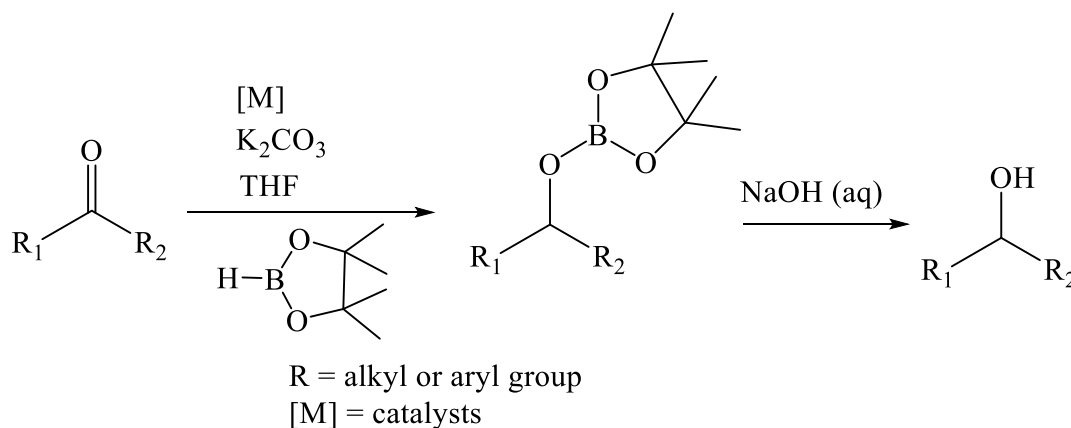
R = hydrogen, alkyl or aryl group

**Scheme 1.1.** A representative reaction scheme for HPH of ketone catalysed by transition metal catalyst.



#### 1.1.4. Hydroboration (HB) of ketones

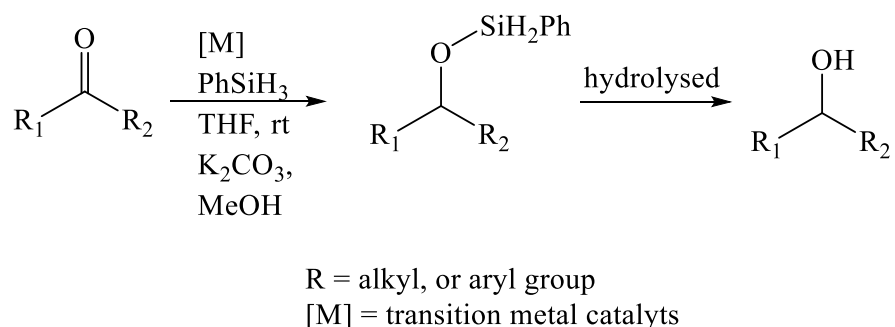
Hydroboration (HB) of a ketone is an efficient way of accessing secondary alcohols. HB involves the formation of an organoborate intermediate, which hydrolyses to form the desired alcohol (**Scheme 1.2**). Catalytic hydroboration of a ketone is an atom-economical, selective and highly cost-effective synthetic approach for accessing functionalised alcohols under mild reaction conditions.<sup>24-25</sup> HB provides a substantial safety advantage compared to HPH that uses hazardous metal-hydride and harsh reaction conditions. Hydroboranes are stable, easy to handle, and compatible with other functional groups in developing new synthetic strategies for transition-metal-catalysed reactions.<sup>25</sup> TMCs, including main group and lanthanide metal complexes, have been employed in the hydroboration of ketones.<sup>26-27</sup> A number of hydroboration agents, such as Corey's CBC reagent,  $\text{BH}_3\cdot\text{THF}$ ,  $\text{B}_2\text{H}_6$ , theoxylborane, catecholborane, dioxaborolane, and pinacolborane (Bpin) have been developed to effectively reduce ketones at relatively mild temperatures.<sup>28-29</sup> HB has been extended to the reduction of other unsaturated substrates such as olefins, alkynes, nitriles, imine, among others. The use of complex borane ligands, which must be synthesised *via* tedious processes, is a drawback of the hydroboration reaction.<sup>26</sup> In addition, the use of hydroboration method of reducing ketones generate borates side products which does not comply with the principles of green chemistry (atom economy).<sup>26</sup>



**Scheme 1.2.** Hydroboration of ketone catalysed by transition metal catalyst.

### 1.1.5. Hydrosilylation (HS) of ketones

The addition of Si-H (silanes or siloxanes) to the polar pi ( $\pi$ ) bonds ( $\text{-C=O}$ ) of ketones to form the corresponding silyl ether intermediates is known as hydrosilylation of ketone. Hydrosilylation (HS) of ketone yields silyl-ether intermediates, which eventually undergo hydrolysis to form the respective secondary alcohols under acidic or basic conditions (**Scheme 1.3**).<sup>30-31</sup> HS is also applicable to the reduction of multiple bonds in carbon-carbon, carbon-heteroatom, and, in rare situations, heteroatomic bonds.<sup>32</sup> HS provides an alternative method of accessing various organosilicon compounds for hydrogenation.<sup>33-34</sup> Silanes such as  $\text{PhSiH}_3$ ,  $\text{Ph}_2\text{SiH}_2$ ,  $\text{Et}_2\text{SiH}_2$ ,  $(\text{EtO})_2\text{MeSiH}$  are usually the primary source of hydrogen.<sup>35</sup> Hydrosilylation has a number of advantages over molecular hydrogenation, for example, takes place under mild reaction conditions. Relatively safe reagents without the need for additional precautions are used. Hydrosilylation is a direct synthetic protocol, and is applicable in the synthesis of silylated (protected) alcohols, which is particularly important in multistep synthesis.<sup>33</sup>



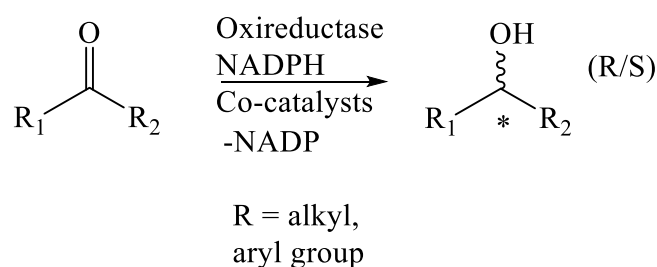
**Scheme 1.3.** Catalytic hydrosilylation of ketones using  $\text{PhSiH}_3$  as a source of hydrogen.

### 1.1.6. Biocatalytic reduction (BCR) of ketones

Biocatalysts are capable of catalysing reduction reactions with excellent stereo-, regio- and chemoselectivity. Biocatalysis provides a good alternative and a classical synthetic route for accessing highly functionalised alcohol products.<sup>36</sup> BCR is an efficient method of installing

stereogenic centres in organic compounds while introducing new functionality (**Scheme 1.4**).<sup>37-</sup>

<sup>38</sup> Oxidoreductases are structurally well-defined enzymes that place reducing agents at stereocenters of prochiral ketones to give enantiopure alcohols. Biocatalytic reductions, like any other non-enzymatic reduction reaction, require reducing agents. The nicotinamide adenine dinucleotide cofactors NADH NADPH are among the few reducing agents used in the biocatalytic reduction of ketones. The application of biocatalysts in the reduction of ketones faces a number of challenges.<sup>36, 39</sup> Biocatalysts are sensitive to temperature and pH changes. Furthermore, biochemical pathway development and modification for the effective reduction of ketones are difficult tasks, and only a few biocatalysts are commercially available in tiny quantities.<sup>39</sup> Biocatalysts are often specific and prefer a single type of substrate.<sup>38</sup> These reduction agents are expensive to regenerate and used in stoichiometric amounts.

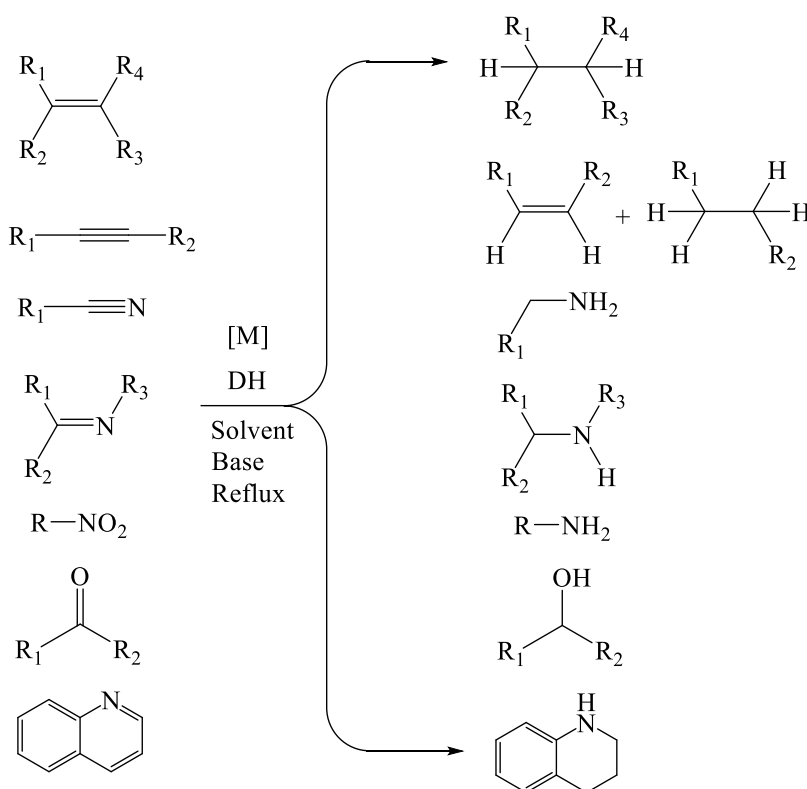


**Scheme 1.4.** Bio-catalytic reduction of ketone to optically active alcohol.

### 1.1.7. Transfer hydrogenation of ketones

The transformation reaction that involves the addition of hydrogen atoms across unsaturated pi bonds in a molecule from sources other than molecular hydrogen is known as a transfer hydrogenation reaction.<sup>40</sup> This protocol is often used to transform ketones, nitrile, imines, alkene, and alkynes, and *N*-heterocyclic substrates such as quinoline,<sup>41-42</sup> indole,<sup>42</sup> pyridine,<sup>41</sup> fluorobenzenes,<sup>43</sup> among others (**Scheme 1.5**). Hydrogen donors such as isopropyl alcohol, water/silane, HCOOH/Et<sub>3</sub>N, HCOOH/HCOONa azeotropic mixtures and Hantzsch ester<sup>44</sup> have been used as the alternative source of hydrogen atoms. Recently, ammonia borane

( $\text{BH}_3\cdot\text{NH}_3$ ) has attracted considerable attention as a hydrogen donor molecule owing to its stability and high hydrogen storage density (19.6 wt%).<sup>41</sup> TMCs are usually employed for efficient hydride transfer from the donor molecules to the substrates. Ruthenium(II), rhodium(II/III), osmium(II), and iridium(I/III) complexes have been extensively used in this reaction since the first report by Noyori and his group.<sup>40, 45</sup> In recent years, the focus has been on developing homogeneous catalysts for TH based on earth-abundant transition metals such as Fe, Co, and Mn as a sustainable alternative to noble metal catalysts.<sup>45-46</sup> TH presents a number of advantages. For example, high pressurised, flammable gas and a sophisticated setup are not required in its operation. TH is greener and operates under milder reaction conditions compared to molecular hydrogenation reaction.<sup>47-48</sup>



[M] = metal-based catalysts

R = hydrogen, alkyl or aryl group

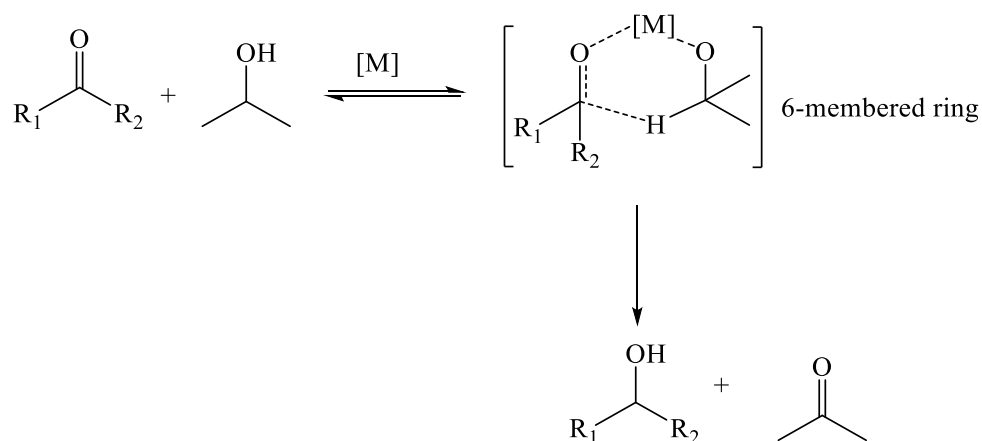
DH = hydrogen donor

**Scheme 1.5.** A representative reaction scheme for transfer hydrogenation of unsaturated substrates catalysed by a TMC.

#### 1.1.7.1. Mechanism of transfer hydrogenation reactions of ketones

Transfer hydrogenation reactions occur through two fundamental catalytic cycles: a direct H-transfer (metal-templated concerted process) and a hydridic route (metal-hydride mediated multi-step process).<sup>48-49</sup> TH of unsaturated molecules involves the application of transition metal catalysts. Hydrogen-donor molecules are generally required to generate the metal-hydride species. The hydride is usually transferred from the metal-hydride intermediate to the substrate to form the desired products.<sup>48, 50</sup> The hydridic route (metal-hydride mediated multi-step process) of TH involves the dissolution of labile co-ligand(s) to create vacant orbitals, binding of the donor molecule with pre-catalyst,  $\beta$ -hydride elimination, metal-hydride formation (active species), insertion of a substrate, migration of hydride and elimination of the product and regeneration of the catalytically active species.<sup>50</sup>

The direct hydride transfer mechanism (**Scheme 1.6**) proceeds *via* the formation of a complex intermediate in which the donor and acceptor are bound to the metal and kept in close proximity.<sup>51</sup> In this reaction, the catalyst usually functions as a template to facilitate the proper orientation for concerted hydride transfer.<sup>52-53</sup> The transition state of direct hydride transfer is purported to take place through the Meerwein–Ponndorf–Verley pathway.<sup>54</sup>

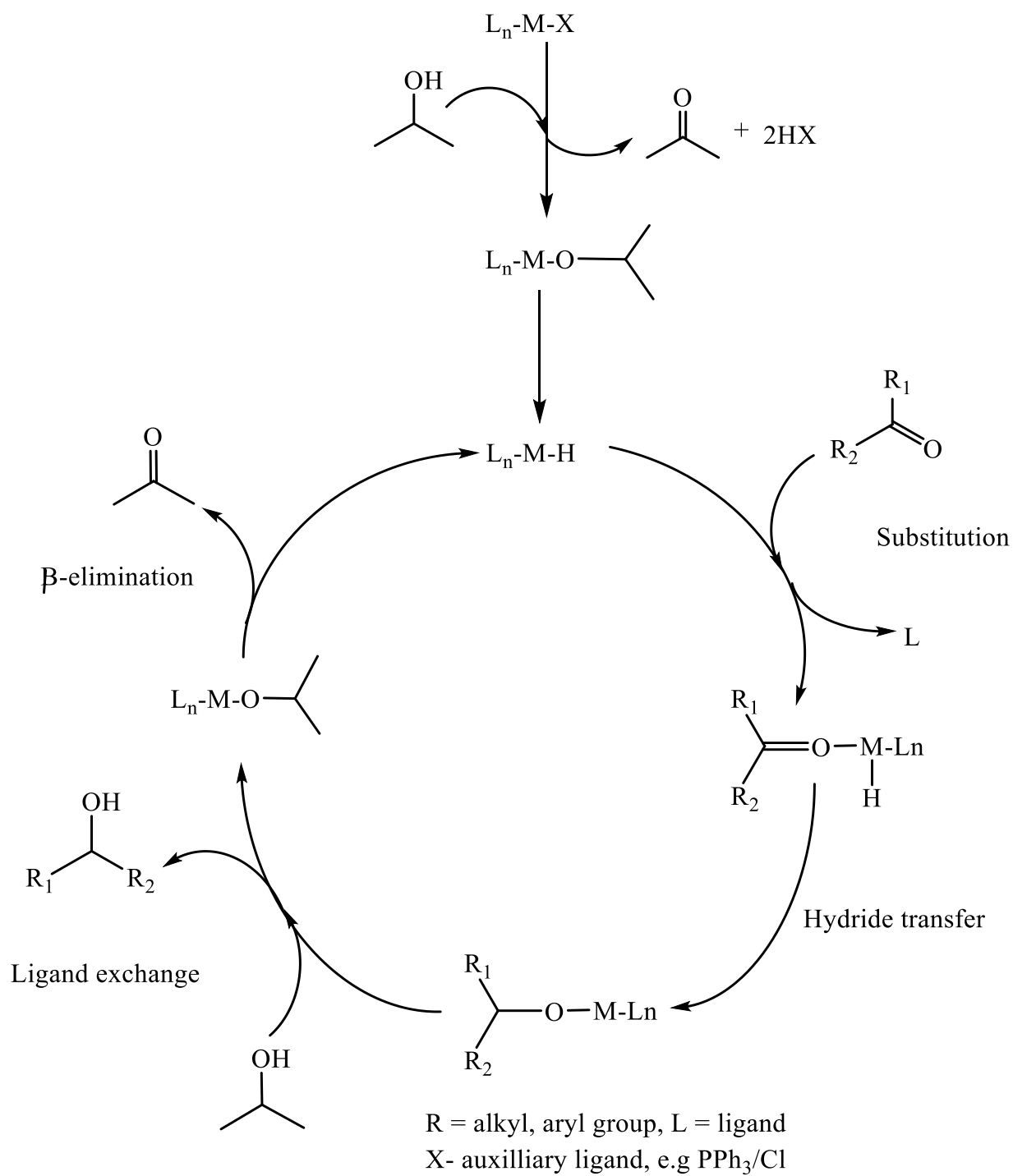


R = alkyl or aryl group; [M] = catalyst

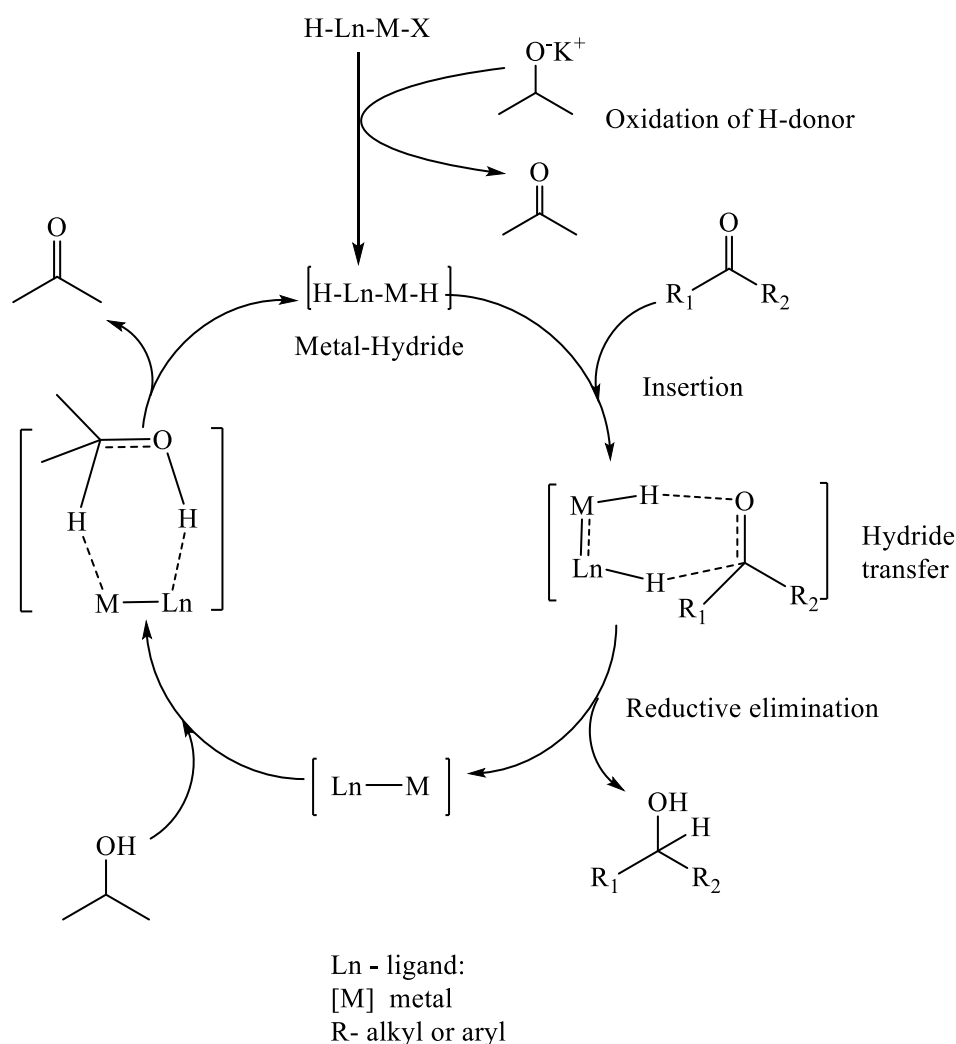
**Scheme 1.6.** Typical reaction pathway for direct hydride transfer hydrogenation of ketones (Meerwein-Ponndorf-Verley).<sup>54</sup>

The hydridic route involves the formation of metal hydride as the active intermediate from the interaction of the catalyst with the hydrogen donor and transfer of hydride from the metal centre to the substrate.<sup>48</sup> In this pathway, the hydrogen donor and acceptor molecules interact sequentially with the TMC. The metal hydride mechanism occurs *via* either the monohydride or dihydride pathways.<sup>48, 55</sup>

A monohydride mechanism takes place through either an inner- or outer-sphere pathway. In the former, the substrate interacts directly with the metal centre (**Scheme 1.7**). In contrast, the outer-sphere pathway involves the reactant slipping into a 'pocket' of the active site of the catalyst and interacts through hydrogen bonding (**Scheme 1.8**).<sup>55-56</sup> The hydride migrates through the formation of a four/six-membered cyclic ring which eventually disintegrates to give the desired product.<sup>57-58</sup>



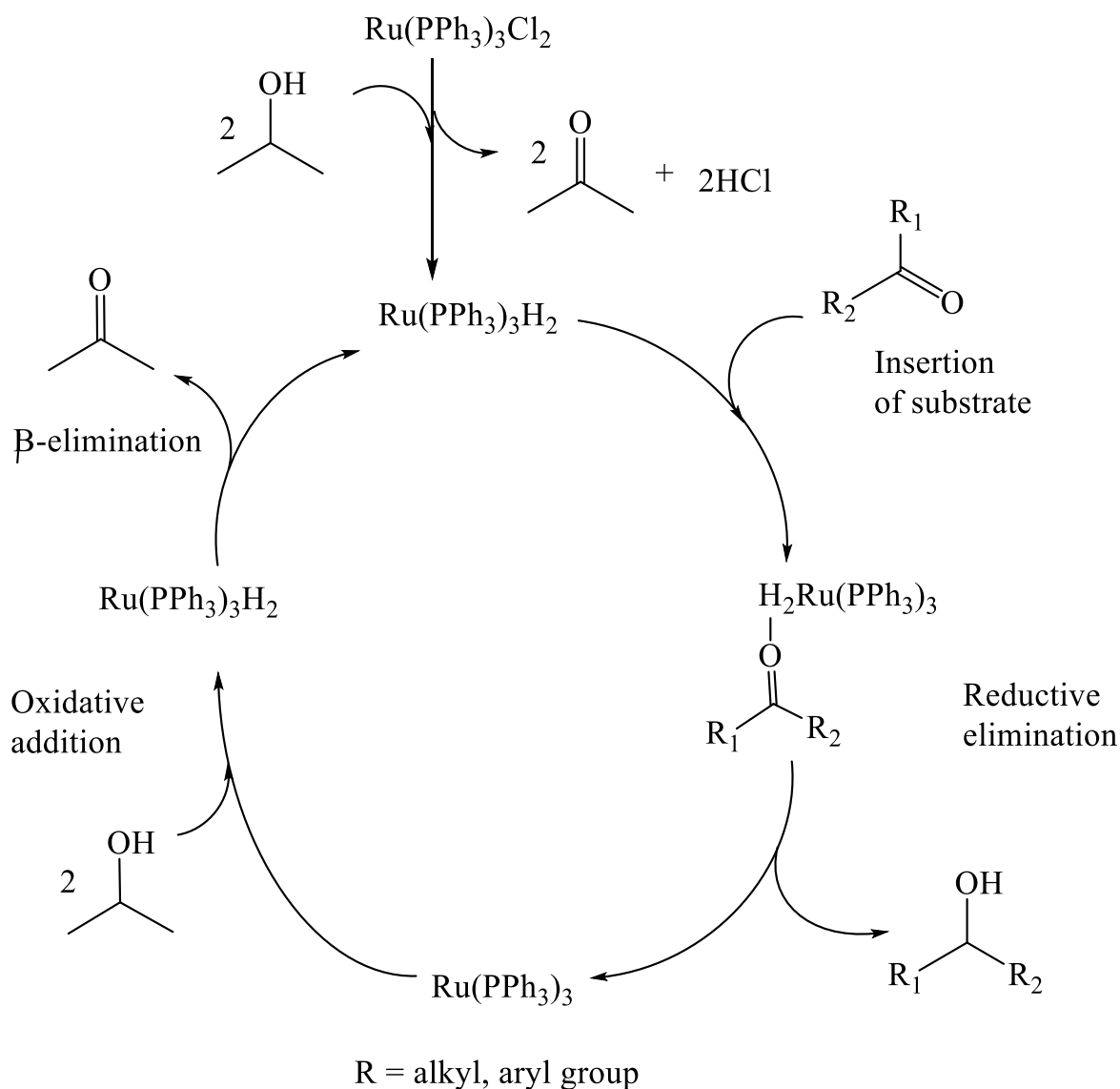
**Scheme 1.7.** A typical monohydride inner-sphere mechanism for transfer hydrogenation of ketones.



**Scheme 1.8.** A typical outer-sphere mechanism for transfer hydrogenation of ketones.

The dihydride mechanism involves the formation of a metal-dihydride intermediate (**M-H<sub>2</sub>**) as the active species.<sup>59</sup> In the dihydride mechanism, the active species (**M-H<sub>2</sub>**) are formed and transferred to the substrates *via* either an outer- or inter-sphere pathway.<sup>58</sup> A typical illustration is the mechanism proposed by Henbest using **Ru(PPh<sub>3</sub>)<sub>3</sub>Cl<sub>2</sub>** as a catalyst in transfer hydrogenation of ketones (**Scheme 1.9**), where the catalyst reacts with the isopropyl alcohol to form the ruthenium-dihydride species in the presence of a base.<sup>59</sup> The next step involves hydride transfer to the substrate followed by reductive elimination to give the desired product, and formation of Ru(0) species which, by oxidative addition of the hydrogen-donor molecule, leads to regeneration of the dihydride active species.<sup>58-59</sup>





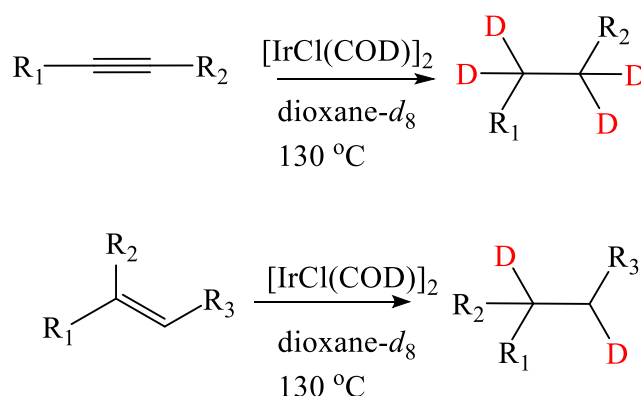
**Scheme 1.9.** Dihydride mechanism (inner-sphere) as proposed by Henbest *et al.* using  $\text{Ru(PPh}_3)_3\text{Cl}_2$  as catalyst.<sup>60</sup>

### 1.1.7.2. Applications of transfer hydrogenation

Transfer hydrogenation has proven to be an excellent synthetic approach for introducing new functionalities into many complex compounds. TH reactions have become well established synthetic protocol for installing stereogenic centres into many biologically relevant molecules.<sup>40, 46</sup> TH has provided an excellent synthetic protocol for the effective reduction of

carbonyl compounds to their corresponding products. For example, ketone substrates ranging from aromatic to alkyl ketones bearing various substituents are reduced to their corresponding alcohols under mild reaction conditions (**Scheme 1.5**).<sup>40</sup> TH of  $\alpha$ - $\beta$ -unsaturated carbonyl substrates, where the carbonyl functional group, C=O, are preferentially reduced to give the corresponding carbinol has been considered an important tool in the multistep synthesis of natural products. For example, with  $\text{RuCl}_2(\eta^6\text{-}p\text{-cymene})$  supported on chiral ephedrine ligand,  $\beta$ -ketoesters could be transformed into enantiopure  $\beta$ -hydroxy esters.<sup>61</sup> Also, regioselective reduction of the ketoisophorone proceeds with excellent chemoselectivity in the presence of Ru-catalyst supported on chiral amino alcohol ligands.<sup>56, 62</sup>

TH of olefins and alkynes also occur using isopropyl alcohols as the source of hydrogen atoms.<sup>63</sup> Conjugated C=C pi bonds could be chemoselectively hydrogenated to their corresponding aliphatic products under mild reaction conditions.<sup>62</sup> TH has become a powerful technique for incorporating deuterium atoms into small molecules such as alkenes and alkynes *via* transfer deuteration using deuterium formic acids (DCOOD), dioxane- $d_8$ , and tetrahydrofuran- $d_8$ , among others (**Scheme 1.10**).<sup>64-65</sup>

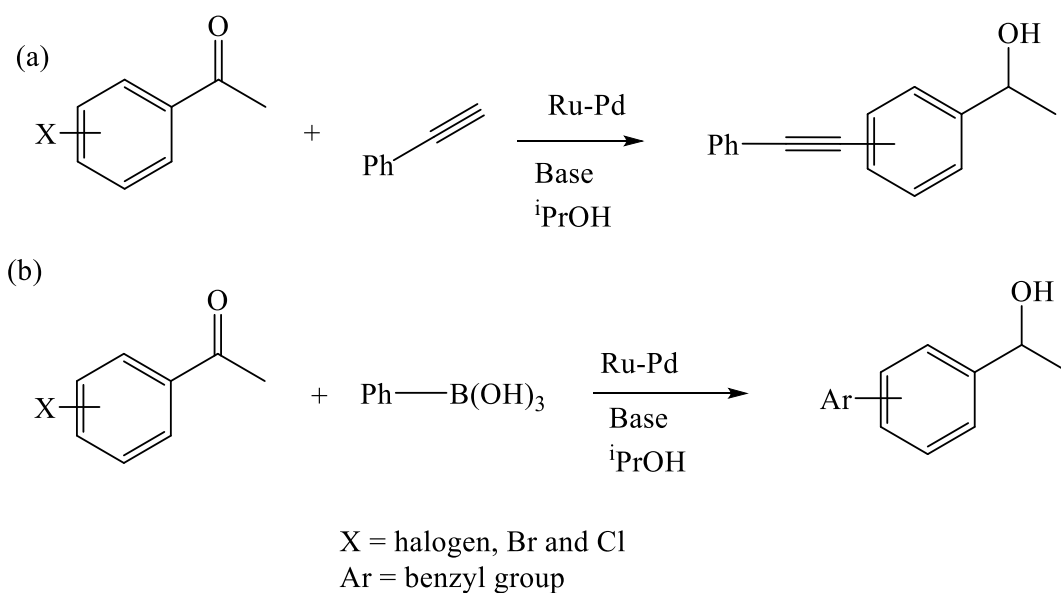


**Scheme 1.10.** Transfer deuteration of alkynes and alkene using deuterated dioxane- $d_8$  as a source of deuterium and solvent.

Asymmetric transfer hydrogenation of imines has become a prominent protocol for accessing enantiopure amines (**Scheme 1.5**) using chiral catalysts.<sup>66-67</sup> The asymmetric transfer hydrogenation (ATH) has been effectively used in total synthesis of *N*-heterocyclics such as morphine, dihydroquinoline which are key intermediates in the syntheses of pharmaceuticals, agrochemicals, dyes, and alkaloids, among other fine chemical products.<sup>68-69</sup>

Carbon-carbon coupling reactions in tandem with TH of ketones are efficiently used in the preparation of various functionalised alcohols, which are essential syphons in the synthesis of natural products.<sup>70-71</sup> For example, propargylic alcohols are obtained *via* tandem Sonogashira-coupling-transfer hydrogenation protocol.<sup>72</sup> Miyuara-Suzuki C-C coupling in tandem with transfer hydrogenation is also well-known for synthesising chiral biaryl alcohols (**Scheme 1.11**).<sup>70-71</sup>

TH catalysts have been found suitable for promoting kinetic resolution of racemic alcohols. For example, a number of Ru(II) catalysts have been reported to have high efficiency in the resolution of racemic secondary alcohols, such as 3-hydroxymethyl-1-tetralols and 3-hydroxymethyl-1-indanols.<sup>73-74</sup>



**Scheme 1.11.** Synthesis of propargylic alcohol and biaryl alcohol *via* (a) tandem Sonogashira C-C coupling-transfer hydrogenation and (b) Suzuki-Miyaura C-C coupling-transfer hydrogenation methods, respectively.

## 1.2. Literature review of transfer hydrogenation of ketones catalysed by ruthenium(II) and manganese(I/II) complexes

### 1.2.1. General background on transition metal catalysts in transfer hydrogenation of ketones

The impact of homogeneous catalysis on industrial processes has expanded over the years. Increasing catalytic processes in industry have been devised due to new knowledge about the structure and reactivity of organometallic compounds.<sup>75</sup> A considerable number of novel compounds have been made in the last two decades to catalyse TH of ketone reactions effectively.<sup>76-78</sup>

In developing homogeneous catalysts, an increasing impetus has been placed on designing organic ligands to regulate the electronic and steric parameters and enhance the stability,

catalytic activity, and chemo-selectivity.<sup>79</sup> A number of organic-based ligands with various donor atoms and functionalities have been developed to achieve appreciable catalytic properties. Relevant examples of these ligand systems include *N*-heterocyclic carbene (NHC),<sup>80-81</sup> amino-phosphine,<sup>81-82</sup> imino-phosphine,<sup>83</sup> carboxamides,<sup>84</sup> sulphur-nitrogen, thiocarbamate and semi-thiocarbamate,<sup>85</sup> amino-alcohols,<sup>86-87</sup> phosphoramidite,<sup>88</sup> and selenium-based ligands.<sup>89</sup> Each has unique electronic and steric properties that regulate the catalyst's overall reactivity, stability, and catalytic activity. Through the specific coordination chemistry of these ligand systems, the oxidation states of the metal centres are varied with concerted activation of the catalyst in fundamental catalytic steps of organic transformation.<sup>90-</sup>

91

In the last two decades, a considerable number of transition metals, including lanthanides and actinides, have been exploited for their potential catalytic properties in the transfer hydrogenation of ketones, and diverse catalytic activities have been reported.<sup>3, 40</sup> Ru(II), Ir(II/III), Os(II), Rh(II/III), Fe(II), Ni(II), Co(II), and Mn(I) are examples of transition metals that have been investigated for their prospective catalytic properties in transfer hydrogenation of ketones.<sup>40, 47</sup> Through several structural modifications to the functionalities within ligands, a number of novel complexes endowed with a wide range of potential catalytic properties have been developed.<sup>3, 92</sup> Recently, a number of mononuclear and polynuclear transition metal-based complexes with their respective catalytic activities have been reported as a new class of catalysts.<sup>93</sup> In this review, a selected number of Ru(II) and Mn(I) complexes will be discussed with respect to their catalytic properties in the transfer hydrogenation of ketones.

### 1.2.2. Ruthenium(II) complexes as catalysts in transfer hydrogenation of ketones

Several ruthenium-based complexes for TH of ketones have been reported with remarkable catalytic activities over the years. The choice of the ligand is a key issue of consideration toward the development of catalysts for practical TH of ketones.<sup>40</sup> For clarity, the Ru(II) -based complexes will be categorized and discussed based on their ligand structures.

#### 1.2.2.1. *N*-heterocyclic carbene (NHC)-ruthenium(II) complexes as catalysts in the transfer hydrogenation of ketones

A series of *N*-heterocyclic carbene (NHC) ligands has been at the frontline of organometallic chemistry and catalysis since its first isolation as a free ligand by Arduengo *et al.* in 1991.<sup>94</sup> NHC ligands are versatile and widely encountered in the design of organometallic compounds, more significantly, toward catalysis.<sup>95-96</sup> NHC exhibited a wide range of electronic properties and formed stable complexes with a wide range of transition metals.<sup>97-98</sup> These ligands act in many cases as sigma ( $\sigma$ )-donor ligands while keeping their fair pi ( $\pi$ )-back-donating tendency.<sup>95</sup> NHC ligands demonstrate similar properties as phosphines in terms of stability, electronic and steric effects and reactivity.<sup>99-100</sup> Relating the structure and catalytic efficiency of Ru(II)-NHC complexes is complicated in TH; hence, only a few examples relevant for TH of ketones have been highlighted. For example, well-defined half-sandwich NHC-Ru(II) complexes **1a** and **1b**<sup>101</sup> (**Figure 1.1**) have been developed and evaluated as catalysts for TH of ketones by Ozdemir and co-workers. Remarkably, a 1/400 ratio of the catalysts to KOH could reduce acetophenone and its derivatives up to 90% within 30 minutes. The catalytic activities of these complexes were not significantly affected by the substituents on the imidazolyl ring of the organic moieties.

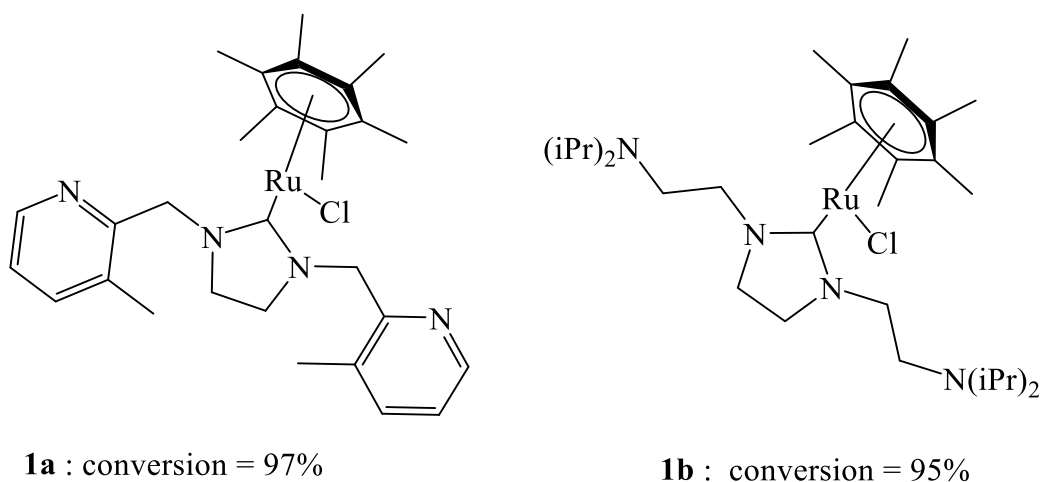


**Figure 1.1.** NHC-Ru-arene complexes (**1a-d**) for transfer hydrogenation of ketones.<sup>101</sup>

Ozdemir and co-workers have also reported a similar NHC-Ru(II) system, **2a-2e** (**Figure. 1.2**), with catalytic activity between 88-95% after 12 h of TH of ketones reaction using 2-propyl alcohol and KOH.<sup>102</sup> The influence of the catalyst structure on the catalytic activity remains unclear, although **2a** and **2c** bearing *N,N'* dimesitylmethylperhydrobenzimidazolyliidene moiety showed slightly higher yields compared to **2b** and **2d**.

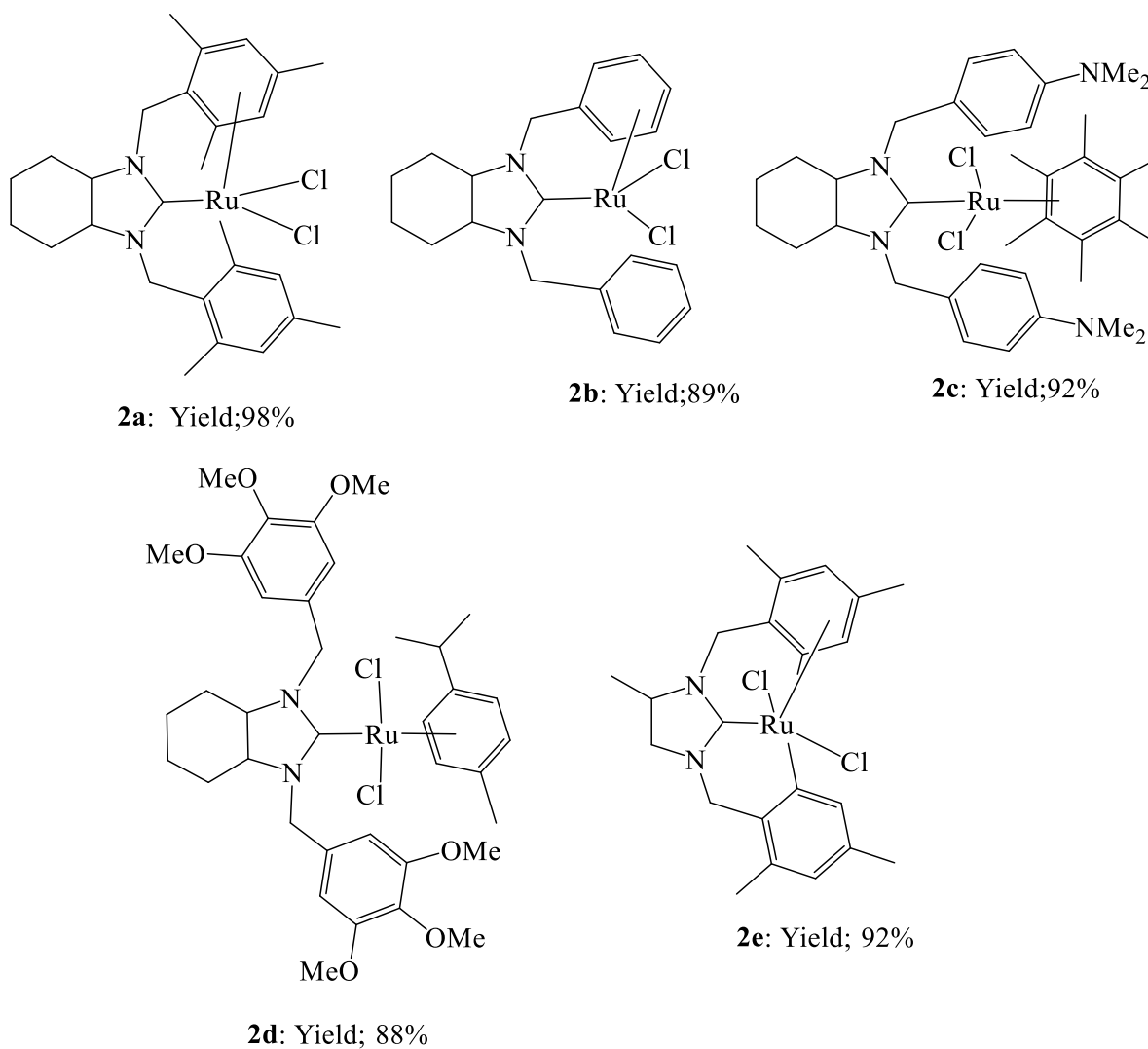


**Figure 1.2.** Half-sandwich Ru-NHC complexes (**2a-2e**) reported by Ozdemir and co-workers.<sup>102</sup>

Recently, NHC Ru(II) complexes (**Figure 1.3, 3a-3f**) bearing a hemilabile *N*-heterocycle carbene (NHC)-pyrazole pincer moiety were also developed and studied for their catalytic efficiency in TH of ketones.<sup>103</sup> The impact of the counterions on the catalytic activities were also investigated, where  $[\text{B}_5\text{O}_6(\text{OH})_4]^-$  appeared to have shown higher activity compared to those bearing the counterion  $[\text{BPh}_4]^-$ . Significant differences in catalytic activities were



observed for **3c** and analogues **3d-3f**, which was attributed to the *hapto*-bonding effect and relative stability of Ru- *p*-cymene moiety in prolonging the lifetime of complexes **3d-3f**.<sup>103</sup>

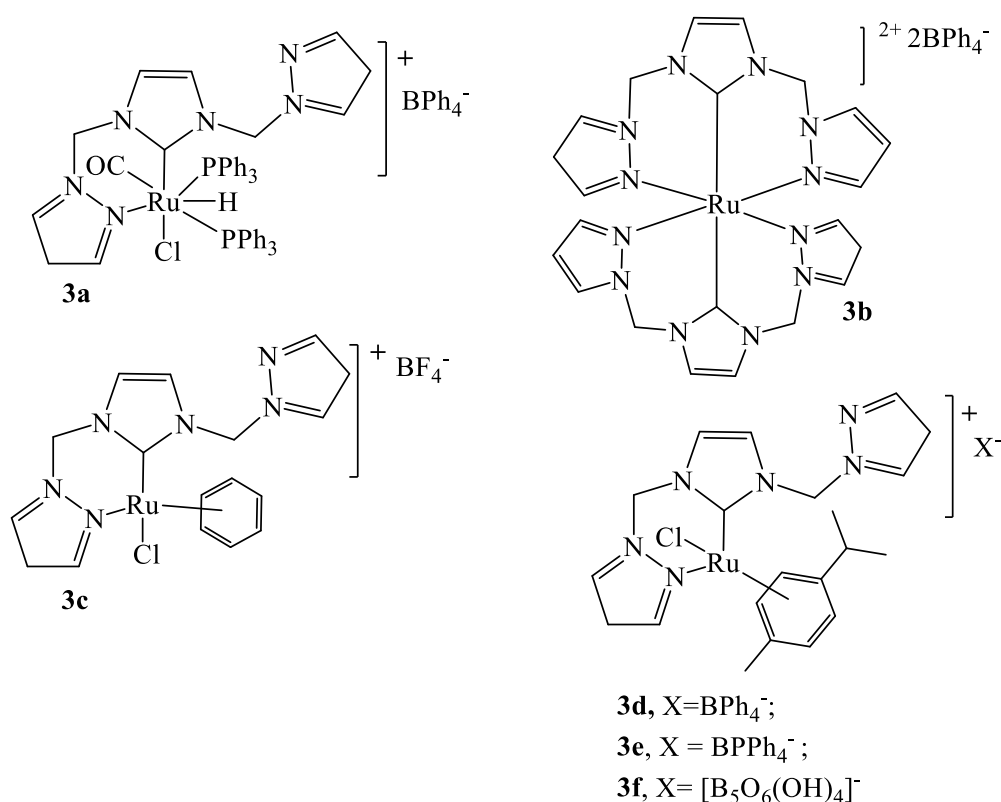


**Figure 1.3.** Structure of Ru(II) complexes bearing hemilabile NHC-pyrazole (NCN) pincer ligands reported by Messerle.<sup>103</sup>

### 1.2.1.3. Ru(II) complexes supported on carboximine ligands

Carboximine or Schiff base ligands have been considered useful and extensively employed in synthesising transition metal complexes, including Ru(II) compounds.<sup>104</sup> Pyridyl-carboximine ligands are a class of *N*, *N*-donor ligands with good pi (π)-electron donor ability suitable for binding ruthenium(II) precursors.<sup>105-106</sup> A number of half-sandwich Ru(II) complexes coordinated to pyridyl-carboximine ligands with functionalised substituents have been applied as catalysts in TH of ketones in the last two decades, and are still receiving significant attention due to their promising catalytic activities.<sup>105, 107</sup> For example, pyridine-carboximine complexes (**Figure 1.4**) have been reported with TOF up to 920 h<sup>-1</sup> by Omondi and workers.<sup>105</sup>

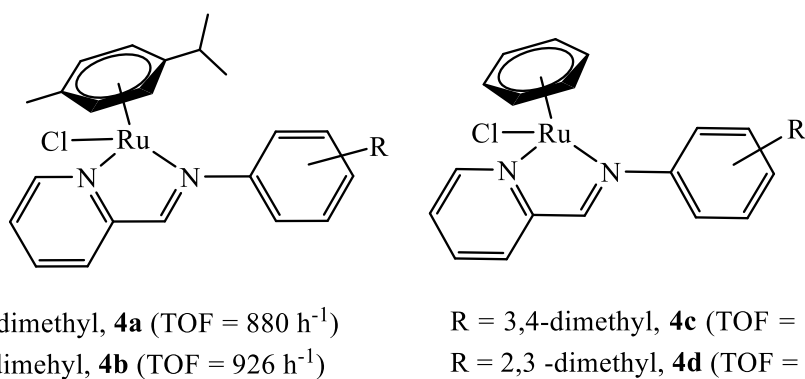


**Figure 1.4.** Structure of pyridyl carboximine Ru(II) half-sandwich complexes used in TH of ketones reported by Omondi and co-workers.<sup>105</sup>

Venkatachalam *et al.* have also reported Ru(II) complexes (**5a-5c**) of pyridyl-imine ligands (**Figure 1.5**), and evaluated their catalytic efficiency in transfer hydrogenation of ketones. The Ru(II) complexes exhibited catalytic activity up to 95 % with catalyst loading of 0.100 mol% in 12 h.<sup>108</sup>

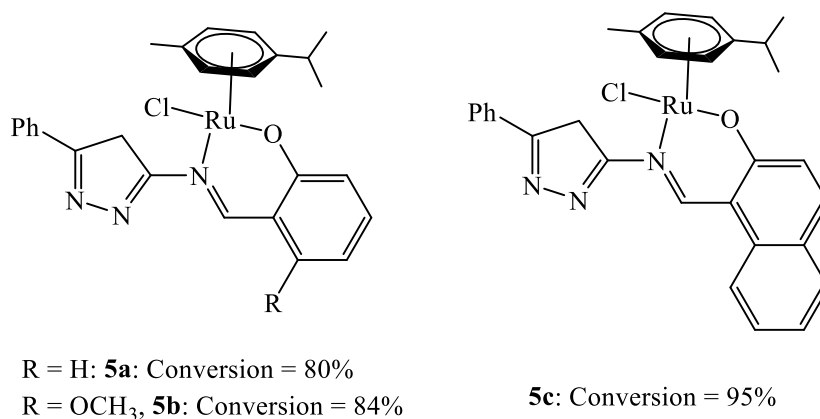
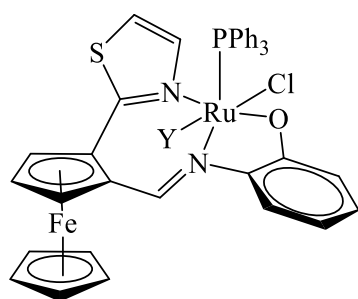


**Figure 1.5.** Half sandwich Ru(II) bearing Schiff-base backbones used in TH of ketones.<sup>108</sup>

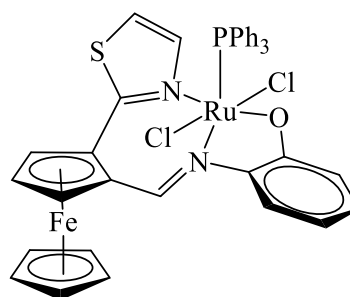
#### 1.2.1.4. Ruthenium(II) complexes anchored on ferrocene base ligands

Ferrocene has a unique sandwich structure that piqued the interest of organometallic chemists, and it is one of the most important structural motifs.<sup>109</sup> Ferrocene has numerous desirable characteristics, including thermal stability and good tolerance to moisture and oxygen.<sup>110-111</sup> In

the last two decades, a number of Ru(II) complexes have been made from ferrocene based ligands and which have been evaluated for their catalytic potentials in TH of ketones (**Figure 1.6**). For instance, Gomez and co-workers have reported Ru(II) complexes (**6a-6b**) supported on 2-ferrocenyl-2-thiazoline Schiff base ligands for TH of ketones.<sup>110</sup> These complexes gave up to 99% conversion in 6 h with catalyst loading of 0.75 mol%. Recently, Baratta and co-workers have reported a series of Ru(II) complexes supported on ferrocene moiety for efficient TH of ketones (**Figure 1.7**). These catalysts were found to be catalytically active and achieved TOF up to  $81.0 \times 10^3 \text{ h}^{-1}$ .<sup>106</sup>



**6a**: Conversion = 98%,  
Y = CH<sub>3</sub>CN



**6b**: Conversion = 87%

**Figure 1.6.** Structure of ferrocenyl-imino-thiazolidine Ru(II) complexes reported by Gomez and co-workers.<sup>110</sup>

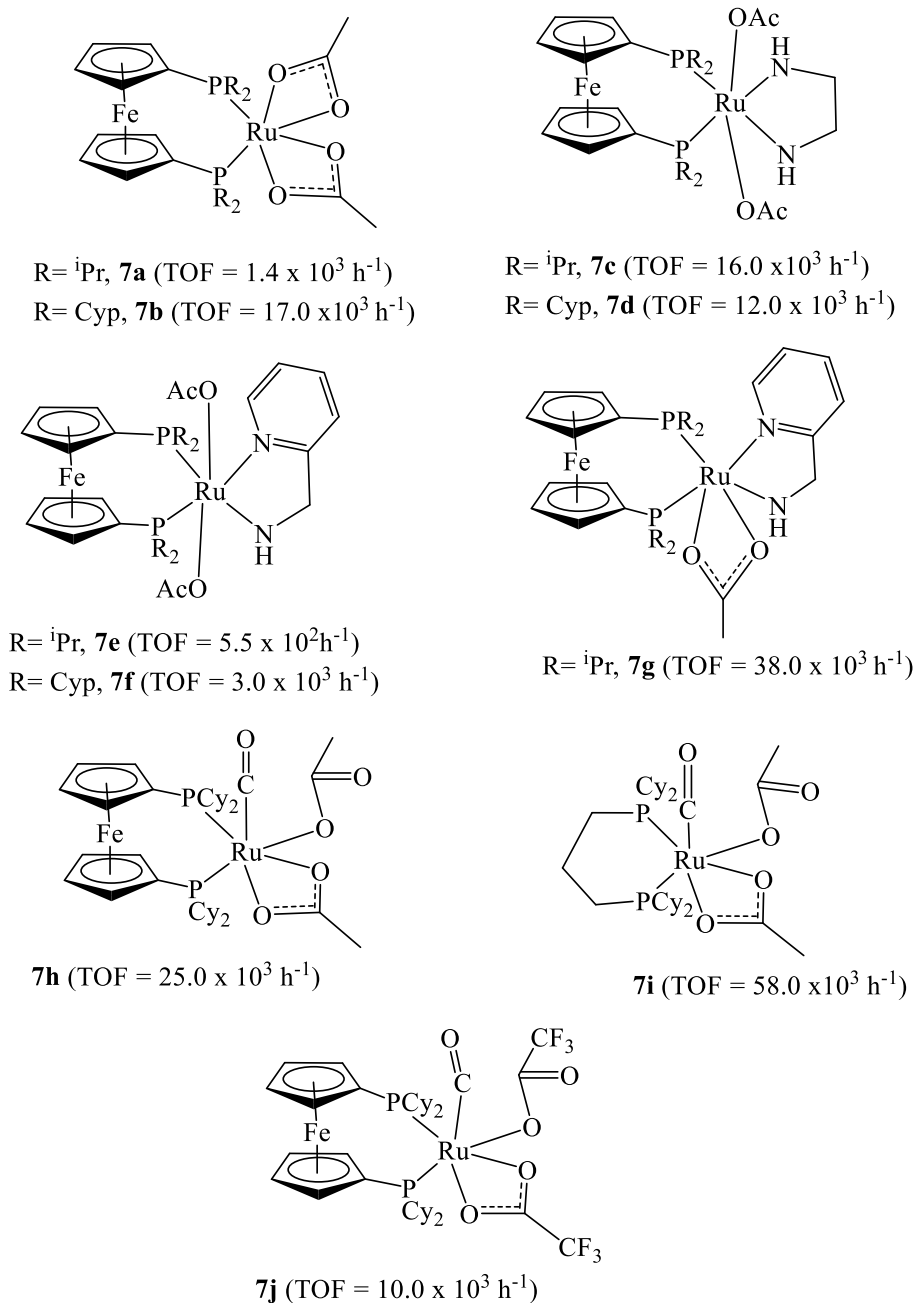
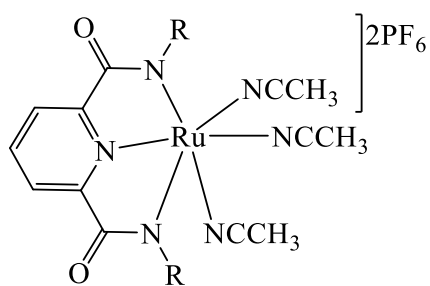


**Figure 1.7.** Ru(II) acetate complexes (**7a-7j**) anchored on bulky diposphine and ferrocenyl-pyridyl amine ligands.<sup>110</sup>

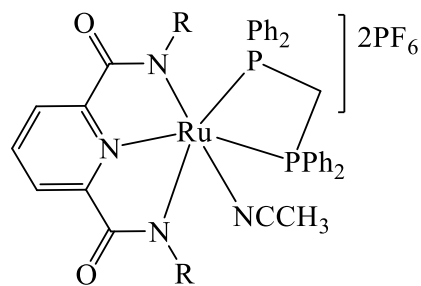
#### 1.2.1.5. Ru(II) complexes supported on carboxamide ligands

Ruthenium(II)-carboxamide catalysts for transfer hydrogenation of ketones have attracted significant attention in recent years.<sup>84</sup> Carboxamide ligands containing PNP and PNN donors are exceptionally versatile and catalytically active in TH of ketones. For example, Ru(II)

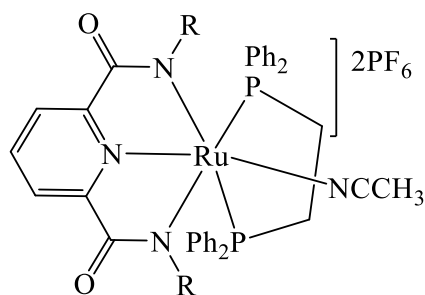
complexes (**8a-8f**) bearing *N,N,N*-tridentate pyridyl-bis(pyridylidene) carboxamide ligands (**Figure 1.8**) were developed by Albrecht and co-workers.<sup>112</sup> These complexes have proven to be catalytically active in TH of ketones and showed turnover frequency at 50% conversion (TOF<sub>50</sub>) between  $1.00 \times 10^2 \text{ h}^{-1}$  and  $4.0 \times 10^3 \text{ h}^{-1}$  in TH of ketones.<sup>112</sup> In an attempt to enhance the catalytic activity of the Ru(II)- pyridyl-bis(pyridylidene) carboxamide complexes, Albrecht and co-workers modified the parent structure of **9a-9e** by placing the various substituents on the pyridyl arms (**Figure 1.9**). TOF up to  $210\,000 \text{ h}^{-1}$  using catalyst loading of 25 ppm was achieved in the TH of benzophenone derivatives.<sup>112</sup>



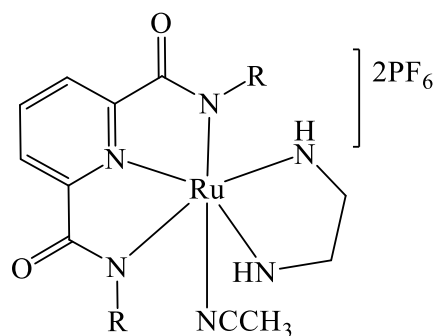
**8a:** TOF = 100 h<sup>-1</sup>



**8b:** TOF = 300 h<sup>-1</sup>

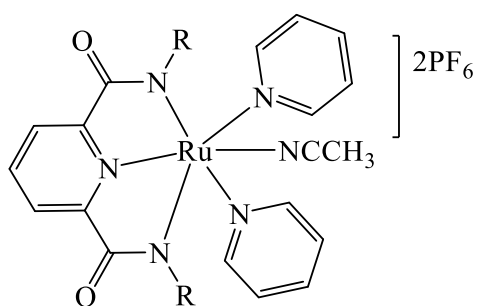


**8c:** TOF = 300 h<sup>-1</sup>

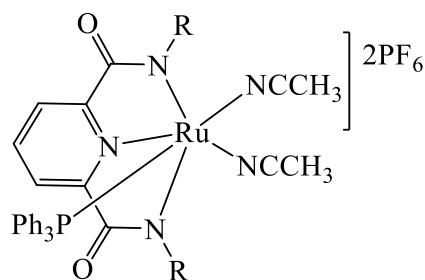


**8d:** TOF = 150 h<sup>-1</sup>

R = 1-methyl-2-pyridine



**8e:** TOF = 40 h<sup>-1</sup>



**8f:** TOF = 450 h<sup>-1</sup>

**Figure 1.8.** Ru(II) complexes bearing *N*-tridentate pincer-type pyridyl-bis(pyridylidene) carboxamide ligands reported by Albrecht and co-workers.<sup>112</sup>

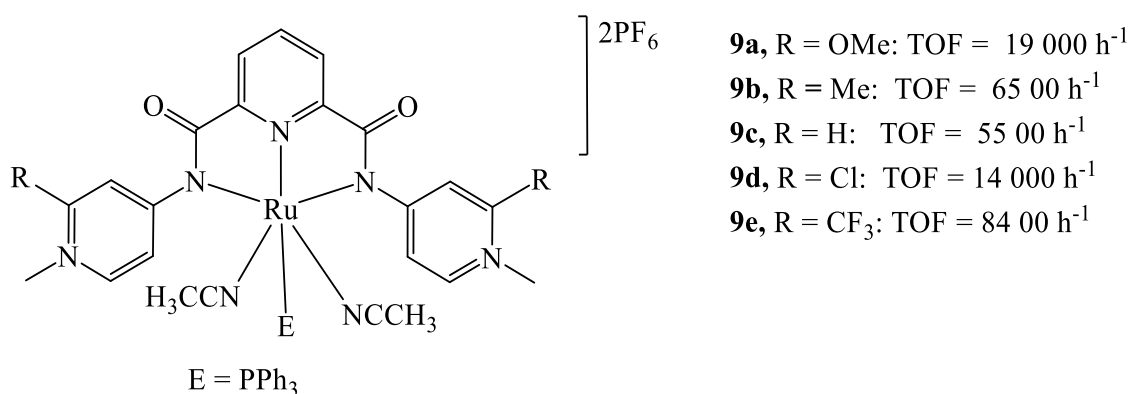


**Figure 1.9.** Modified Ru(II) complexes bearing *N,N,N*-tridentate pincer-type pyridyl-bis(pyridylidene) carboxamide ligands used for TH of ketones.<sup>113</sup>

Recently, Gupta and co-workers have also reported PNN-Ru(II) complexes (**10a-10f**) supported on phosphine-carboxamide ligands (**Figure 1.10**) for TH of ketones.<sup>114</sup> The Ru(II) complexes demonstrated good catalytic activity with a percentage yield up to 99 % in the presence of a stoichiometric amount of KOH. A number of biologically active ketones were also transformed into corresponding alcohols using these Ru(II) catalysts.<sup>114</sup>

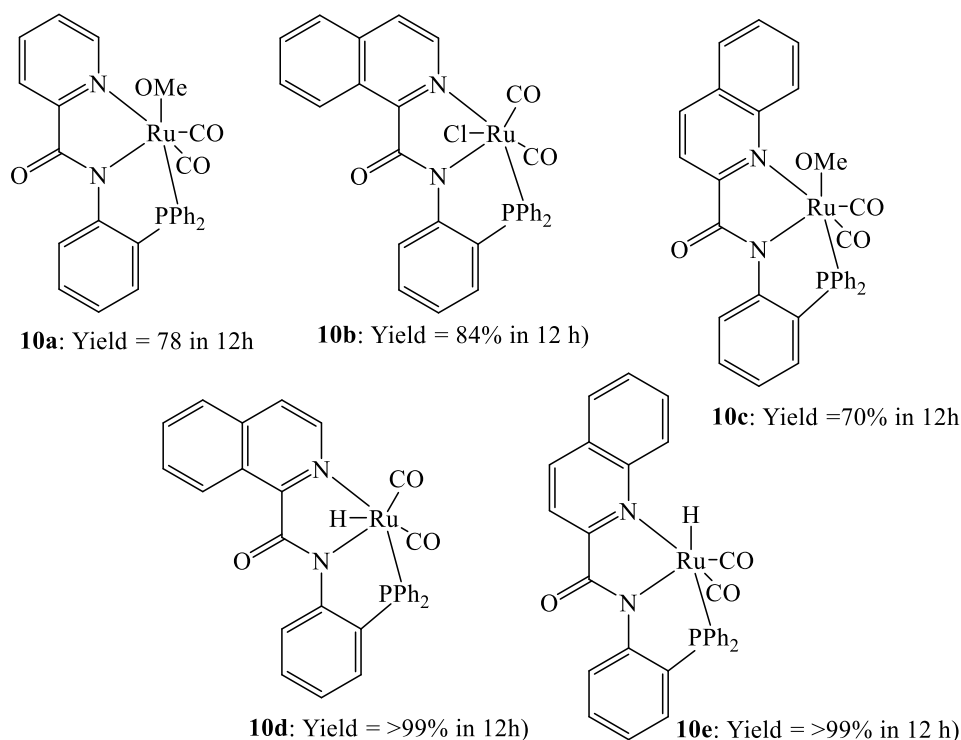


**Figure 1.10.** Ru(II) phosphine-carboxamide complexes (**11a-11e**) reported by Gupta and co-workers.<sup>114</sup>

#### 1.2.1.6. Multinuclear Ru(II) complexes in transfer hydrogenation of ketones

Multinuclear complex catalysts have recently received much attention primarily due to probable electronic interactions between metal centres and cooperative activation of the substrates, leading to higher reactivity than mononuclear complexes.<sup>40</sup> Multinuclear complexes of Ru(II) with remarkable catalytic efficiency in TH of ketones have been reported. Ayedmir *et al.* reported structurally defined bimetallic Ru(II) complexes (**11a-11b**) (**Figure 1.11**) derived from organo-phosphinite-imino ligands. The complexes showed an excellent catalytic activity up to 530 h<sup>-1</sup> using a substrate/base/catalyst ratio of 100:5:1.<sup>115</sup>



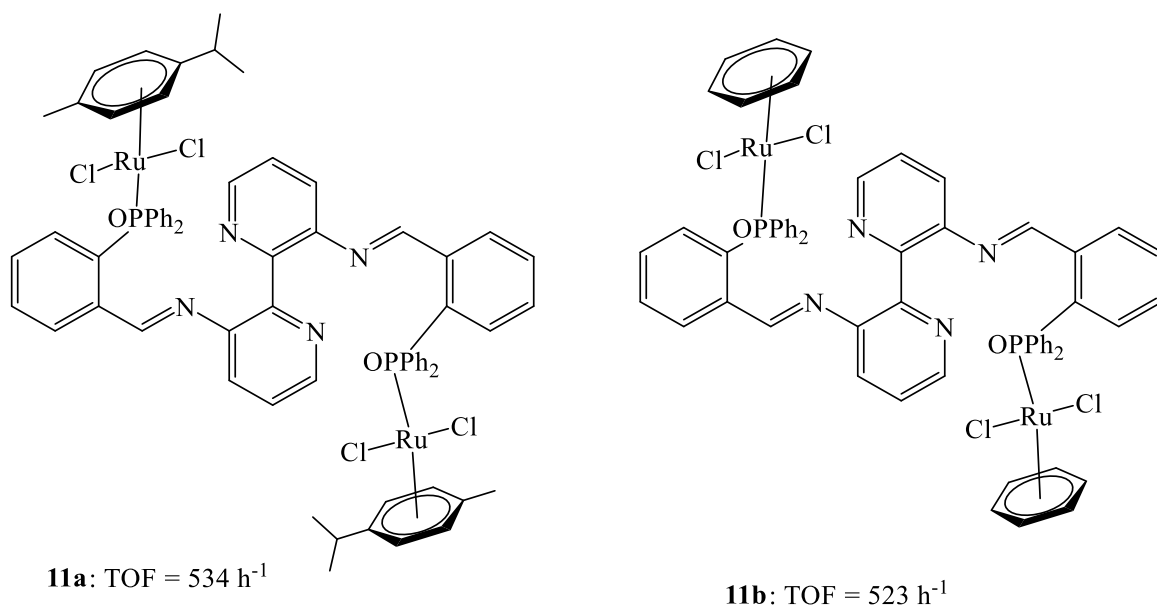


**Figure 1.11.** Dinuclear Ru(II)- arene complexes derived from monodentate organophosphine complexes used TH of ketones.<sup>115</sup>

Recently, Yu and co-workers have reported catalytically active dinuclear Ru(II)-NNN pincer complexes anchored on bis(pyrazolyl)-imidazolyl moiety fused with  $\pi$ -ring (**Figure 1.12**) for TH of ketones.<sup>116</sup> A high catalytic activity with TOF up to  $1.3 \times 10^7 \text{ h}^{-1}$  was attained with catalyst loading of 0.03 mol% in the presence of 1.00 mol% KOH.<sup>116</sup> The remarkable catalytic activity of the dinuclear complexes was attributed to stability and cooperativity between two coordinated Ru(II) metal centres.

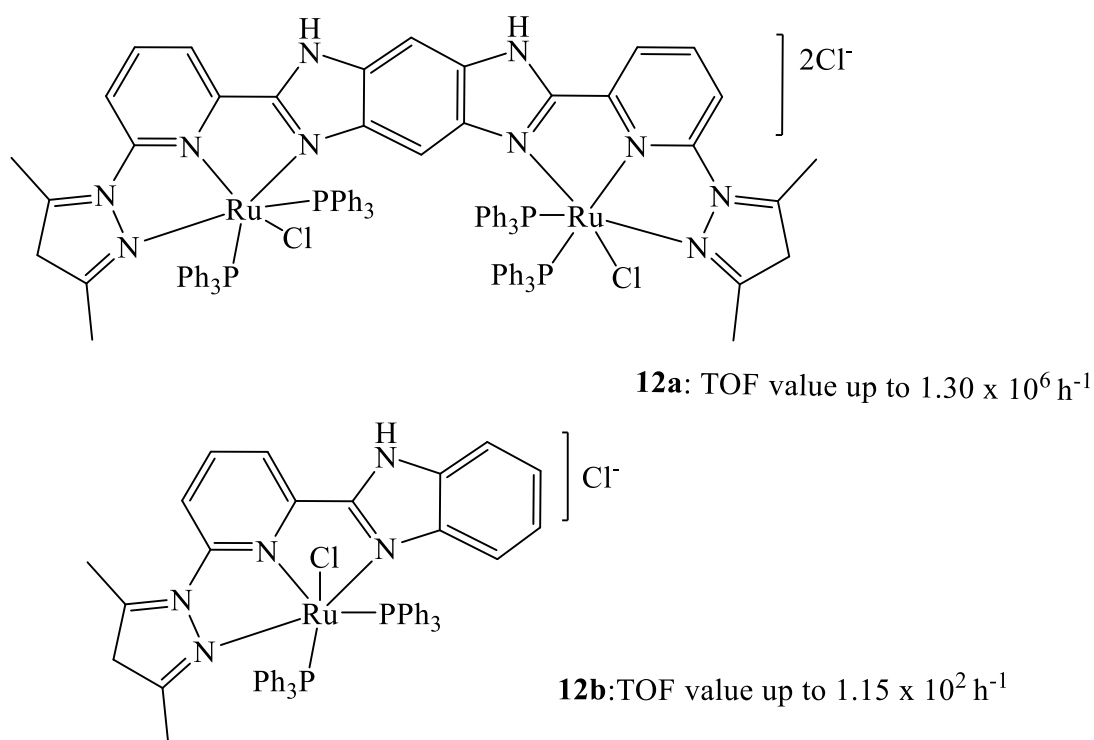
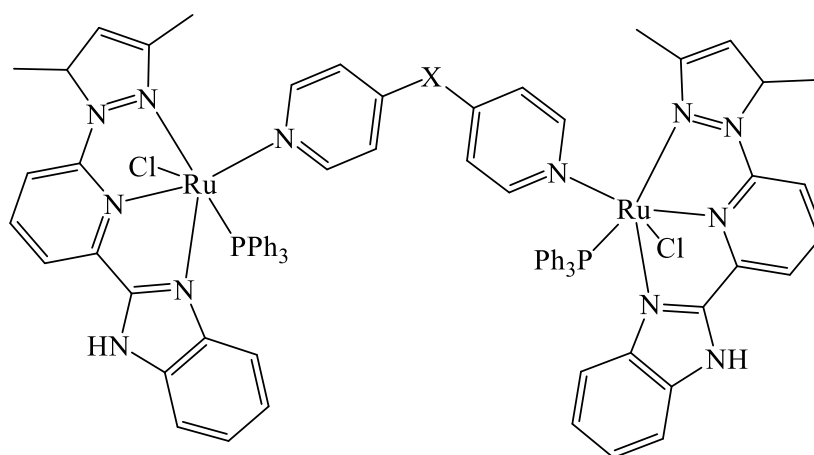


**Figure 1.12.** Structural representation of Ru(II)-NNN pincer complexes derived from fused bis(pyrazolyl)-imidazolyl ligands.<sup>116</sup>

The application of aromatic linkers such as 4,4'-bipyridine has provided a facile synthetic route for assembling 16e<sup>-</sup> mononuclear Ru(II) units (**13a -13d**). The multinuclear Ru(II) N<sup>^</sup>N<sup>^</sup>N<sup>^</sup> complexes (**13a -13d**) demonstrated exceptionally higher catalytic activity (TOF up to  $1.4 \times 10^7 \text{ h}^{-1}$ ) as well as excellent cooperative effects in the transformation of ketones into their respective products (**Figure 1.13**).<sup>117</sup>



X = (CH<sub>2</sub>)<sub>1</sub>, **13a**; TOF up to 8.45 x 10<sup>6</sup> h<sup>-1</sup>

X = (CH<sub>2</sub>)<sub>2</sub>, **13b**; TOF up to 1.25 x 10<sup>7</sup> h<sup>-1</sup>

X = (CH<sub>2</sub>)<sub>3</sub>, **13c**; TOF up to 1.37 x 10<sup>7</sup> h<sup>-1</sup>

X = (CH<sub>2</sub>)<sub>4</sub>, **13d**; TOF up to 1.43 x 10<sup>7</sup> h<sup>-1</sup>

**Figure 1.13.** Diruthenium(II)-NNN complexes derived from unsaturated 16-electron mononuclear ruthenium(II)-pyrazolyl-imidazolyl-pyridine complex and 4,4'-linked bipyridine ligands.<sup>117</sup>

The trinuclear ruthenium(II) complexes (**14a** and **14b**) supported on tridentate amino-phosphine–phosphinite and phosphinite ligands were found to be effective catalysts for the transfer hydrogenation of ketones by Aydemir and co-workers (**Figure 1.14**).<sup>118</sup> The trinuclear complexes attained turnover frequency up to 1.12 x 10<sup>3</sup> h<sup>-1</sup> in the presence of NaOH.

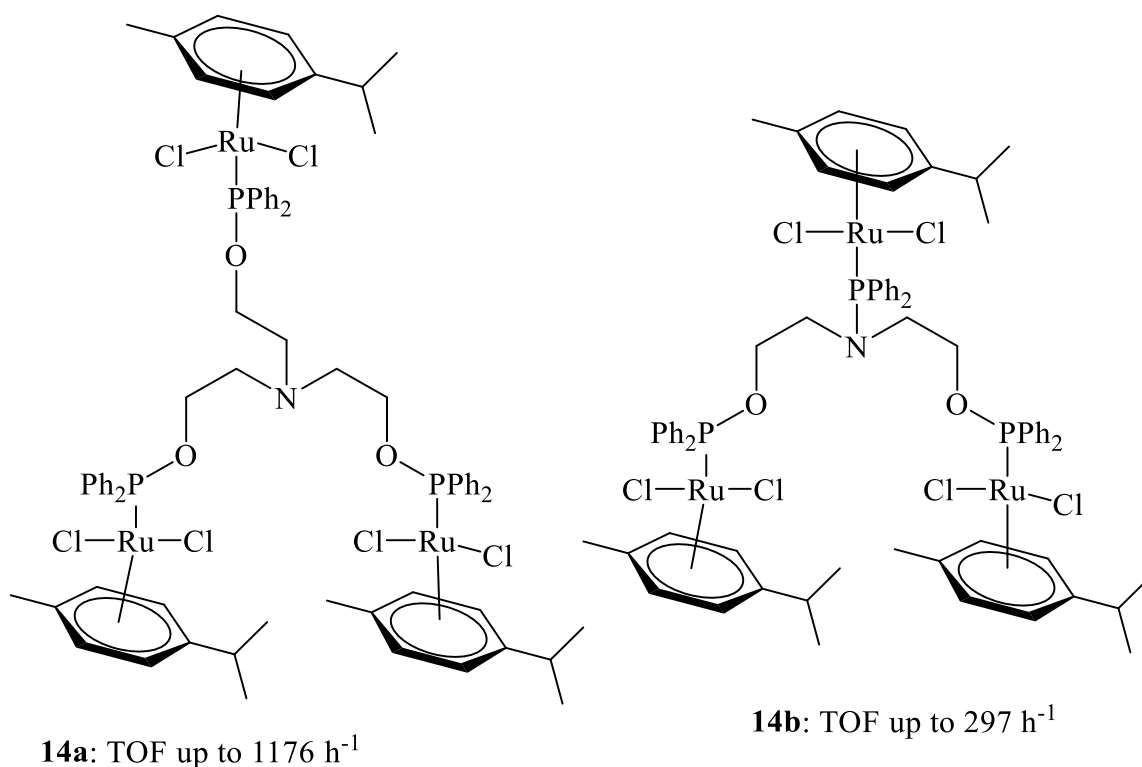


**Figure 1.14.** Trinuclear Ru(II) complexes anchored on amino-phosphine and phosphinite ligands used as catalysts for TH of ketones by Aydemir and co-workers.<sup>118</sup>

Recently Yu and co-workers have been developing a number of dinuclear Ru(II) complexes which showed remarkable catalytic activities in the TH of ketones.<sup>116-117, 119-120</sup> For example, dinuclear Ru(II) complexes (**15a and 15b**) derived from bis(pyrazolyl-imidazolyl pyridine) (**Figure 1.15**) have been reported with high catalytic activity (TOF up to  $4.3 \times 10^6 \text{ h}^{-1}$ ) in transfer hydrogenation of ketones.<sup>120</sup> The catalytic properties of these Ru(II)-NNN complexes were primarily influenced by the chelating effect of pyrazolyl and pyridyl moieties within the ligand architecture and the degree of metal-metal interaction.<sup>120</sup> Similarly, tri- and hexanuclear Ru(II) complexes  $[\text{Ru(II)-NNN}]_n$  (**16a and 16d**) which were assembled from 16e- mononuclear Ru(II)-pyrazolyl-imidazolyl pyridine units and oligo-pyridine linker (**Figure 1.15**) have also been reported with excellent catalytic activity.<sup>119</sup> The multinuclear Ru(II)-NNN complexes exhibited higher TOF value up to  $7.10 \times 10^7 \text{ h}^{-1}$  using catalyst loading of 0.0125 mol%. The

excellent catalytic activities exhibited by the multinuclear complexes were attributed to the excellent cooperativity and stability of the complexes in TH of ketones.<sup>119</sup>

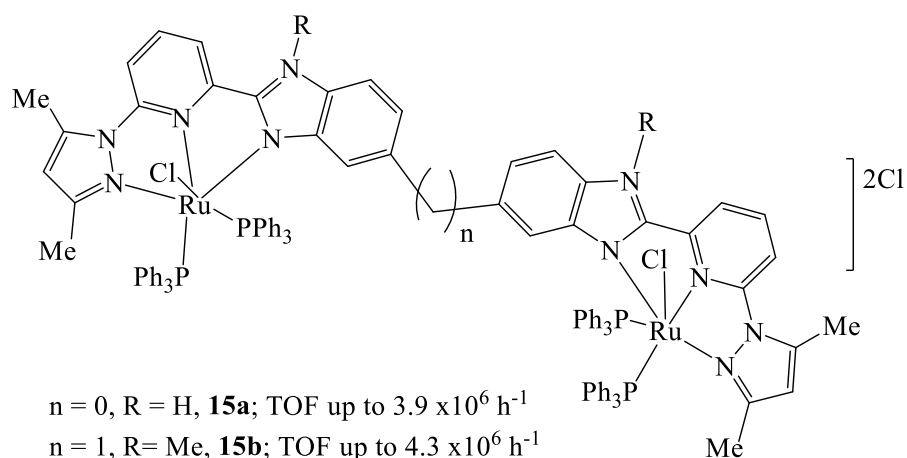


**Figure 1.15.** Bimetallic Ru(II)-NNN cationic complexes assembled by C-C rotated methylene linker reported by Yu and co-workers.<sup>120</sup>

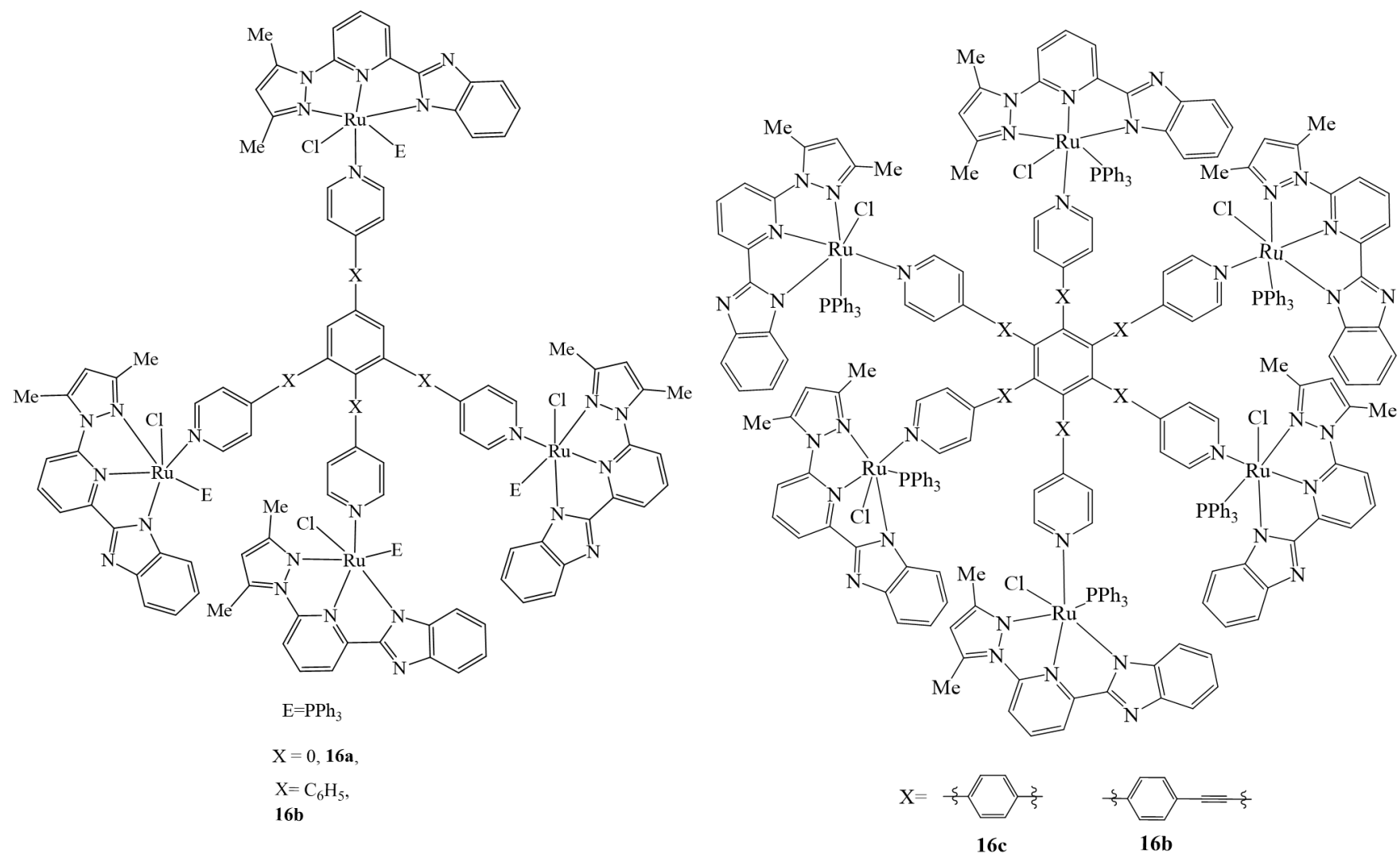


**Figure 1.16.** Structure of polynuclear Ru(II) complexes (**16a-16d**) supported on central substituted pyridyl benzene backbone.<sup>119</sup>

Half-sandwich Ru(II)-NHC complexes, **17a-17d** (**Figure 1.17**), have been synthesised and evaluated for their catalytic efficiency in TH of ketones. With catalyst loading of 0.25 -2.00 mol%, the catalysts **17a-17b** demonstrated TOF up to 200 h<sup>-1</sup> within 2 h of reaction.<sup>121</sup>

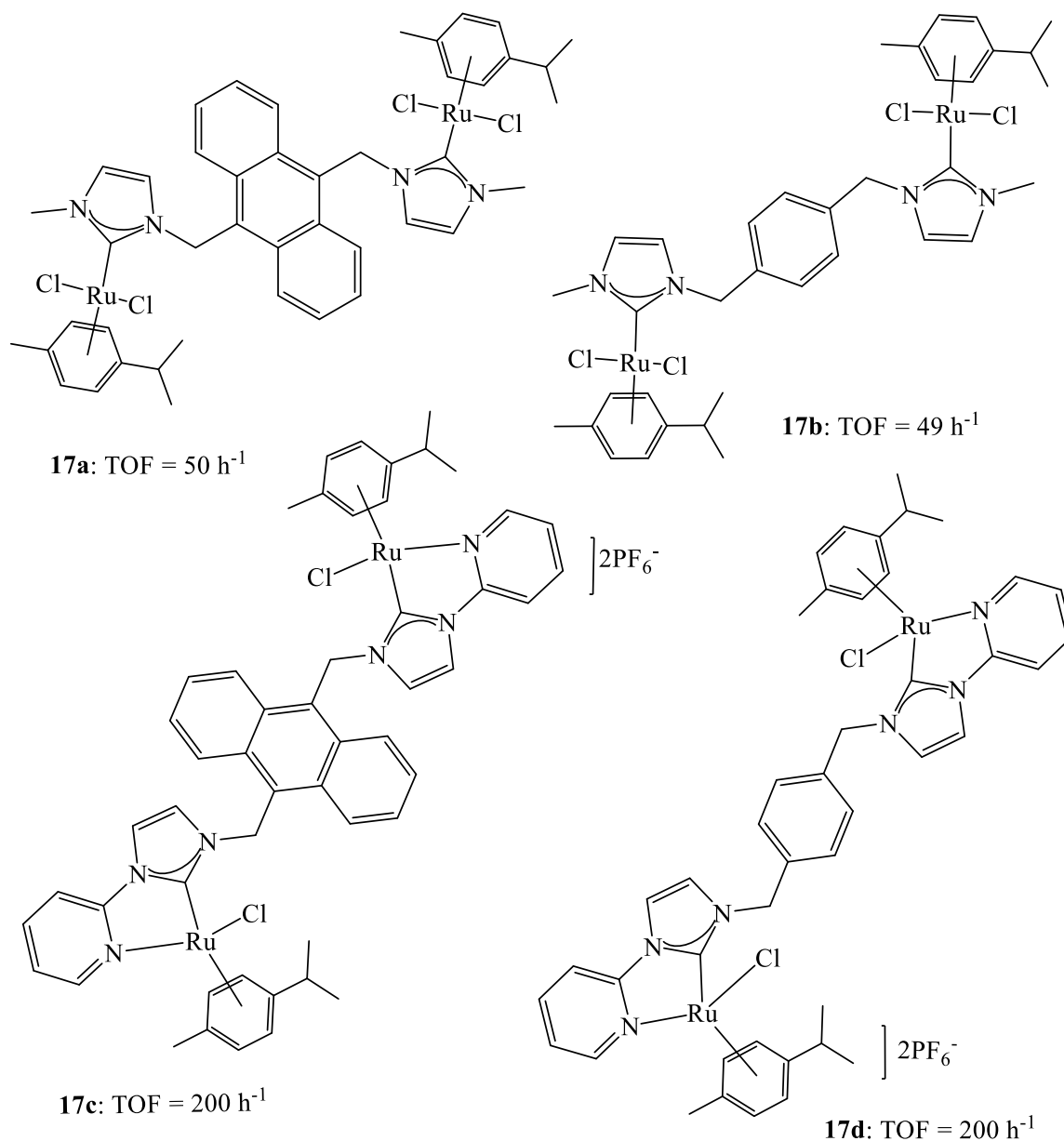


**Figure 1.17.** Structure of neutral and cationic Ru(II)-NHC complexes **17a-17d** reported by Danaboyina and co-workers.<sup>121</sup>

### 1.2.2. Manganese(I)-based catalysts for transfer hydrogenation of ketones

The application of manganese-based catalysts has emerged as a more reliable alternative for noble metal-base catalysts and has attracted considerable attention.<sup>122-123</sup> Manganese(I)-based complexes for transfer hydrogenation of ketones have emerged with promising catalytic activities.

#### 1.2.2.1. Manganese complexes supported on nitrogen-donor ligands

Nitrogen donor ligands are generally used to enhance stability, regulate the steric and electronic parameters and improve the reactivity of a metal centre. Recently, a number of Mn(I) complexes supported on nitrogen donor ligands have been evaluated as catalysts for TH of ketones. For instance, the Mn(I) complexes, **18a-18d** (**Figure 1.18**) anchored on amino-pyridine ligands, have been studied by Sortais *et al.* for TH of ketones. These complexes (**18a-18d**) were found to be catalytically active and showed high TOF up to 3600 h<sup>-1</sup> at room temperature with a very low catalyst concentration of 0.1 mol %.<sup>124</sup>

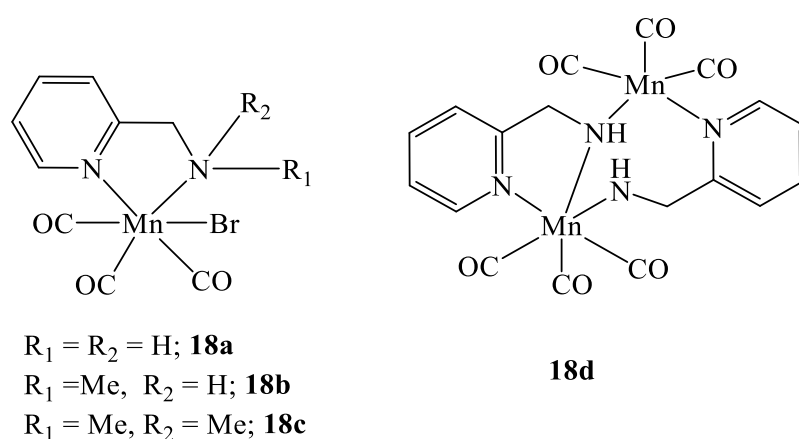
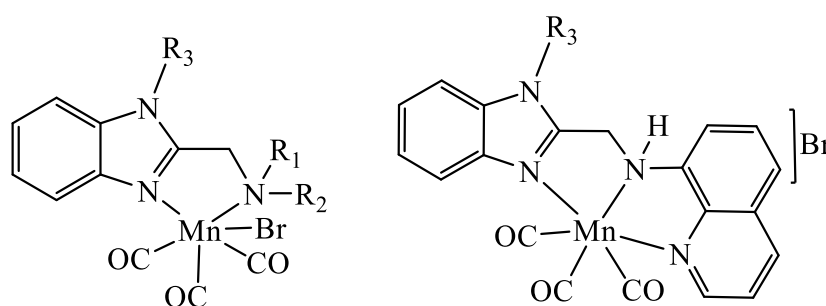


**Figure 1.18.** Mn(I) catalysts (**18a-18d**) based on a nitrogen-donor system developed from amino methyl-pyridine reported by Sortais *et al.*<sup>124</sup>



Recently, Kundu and co-workers also reported Mn(I) carbonyl complexes, **19a-19e** bearing N-H heterocyclic (benzimidazole) amines (**Figure 1.19**).<sup>125</sup> The Mn(I) complex made up of *N*-(1H-benzimidazol-2-yl)methyl aniline fragment **19a** showed higher catalytic activity compared to **19d** and **19e**. Both the benzimidazole and amine fragments were noted to enhance the catalytic activity in TH of ketones under similar reaction conditions.<sup>125</sup>



$R_1 = \text{Ph}, R_2 = R_3 = \text{H}$ , **19a**: Conversion = 96%

$R_1 = \text{Me}, R_2 = \text{H}, R_3 = \text{Me}$ , **19b**: Conversion = 35%

$R_1 = R_2 = \text{Me}, R_3 = \text{H}$ , **19c**: Conversion = 52%

$R_1 = \text{Me}, R_2 = R_3 = \text{H}$ , **19d**: Conversion = 68%

$R_1 = R_2 = \text{Ph}, R_3 = \text{H}$ , **19e**: Conversion = 28%

**19f**: Conversion = 62% in 2h

**Figure 1.19.** Structure of Mn(I) complexes **19a-19f** supported on benzimidazole-amine ligands and catalytic activities under similar reaction conditions.<sup>125</sup>

#### 1.2.2.2. Mixed phosphine and nitrogen donor Mn(I) complexes

Mixed phosphine-nitrogen-donor Mn(I) complexes have been fairly studied in the transfer hydrogenation of ketones. The application of Mn(I) complexes anchored on mixed phosphine and nitrogen donor ligands has been motivated by the demand for environmentally compatible catalysts for the fine chemical and pharmaceutical industries. The mixed P-N donor systems are Mn(I) complexes **20a-20c** (**Figure 1.20**), developed by Kirchner and co-workers.<sup>126</sup> The Mn(I) complexes **20a-20c** showed catalytic activity up to 96%, with *ee* up to 86% in TH of acetophenone derivatives.

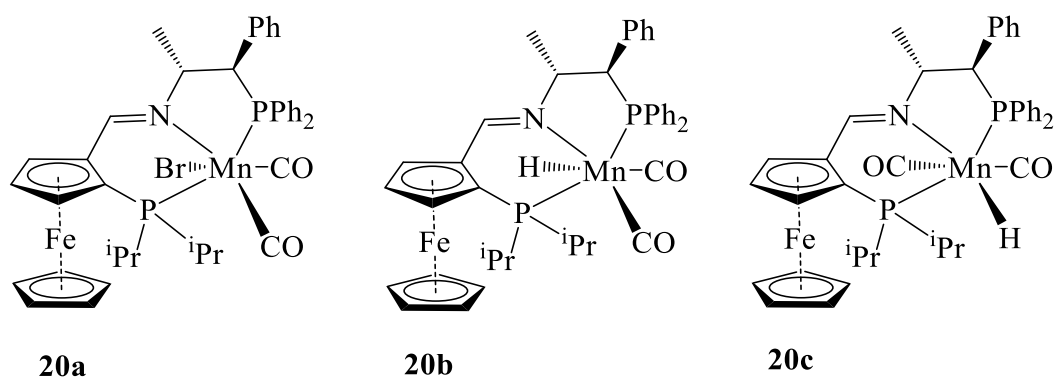


**Figure 1.20.** Chiral Mn(I) complexes supported on P-N donor ligands bearing chiral ferrocene group reported for ATH of ketones by Kirchner *et al.*<sup>126</sup>

Morris and co-workers also contributed to the TH of ketones by using Mn(I) complexes, **21a-21c** supported on P-N donor ligands (**Figure 1.21**). The pre-catalysts **21a-21c** demonstrated catalytic activity up to 98 % in 1 h with *ee* up to 42% in TH of acetophenone.<sup>127</sup>

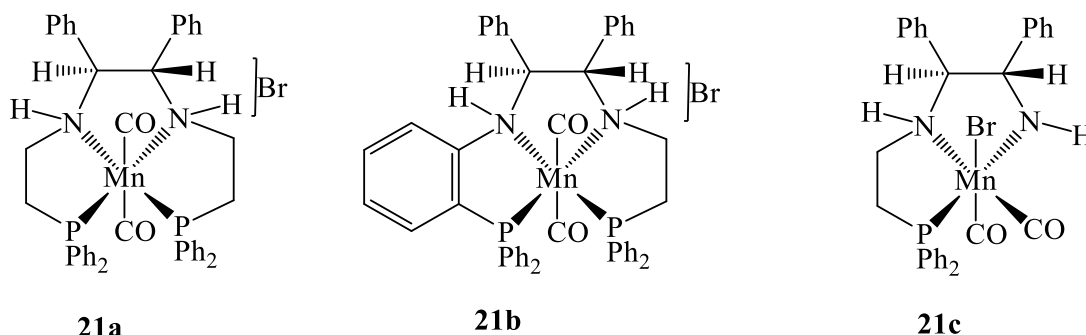


**Figure 1.21.** Chiral Mn(I) complexes (**21a-21c**) supported on mixed P-N donor ligands system reported by Morris and co-workers.<sup>127</sup>

### 1.3. Statement of the problem

Catalysis is one of the most impactful and transformative research fields in academia and the synthetic industry.<sup>128</sup> Drug discovery, alternative energy, and materials synthesis are the few subjects enabled by this field of study.<sup>129-130</sup> Transition metal complexes are the most

successful and well-known catalysts for practical TH of ketones due to their high catalytic activity, selectivity and stability. TMCs have predominated the field of TH of ketones for decades.<sup>78, 128</sup> The search for efficient, more stable, and economical catalysts for effective industrial TH reactions remains a continuous process. However, most existing catalytic systems for transfer hydrogenation reactions often face challenges such as high cost of establishment, instability, lack of selectivity, and toxicity. Therefore, new catalytic systems for effective transfer hydrogenation reactions to circumvent these challenges are worthy of endeavour.

#### **1.4. The rationale of the study**

Transition metal catalysts (TMCs) supported on nitrogen and phosphorus-donor ligands are known to display high reactivity, stability and are easily synthesised under relatively mild reaction conditions.<sup>131</sup> The nitrogen and phosphorus donor ligands also aid in modulating steric and electronic properties, thus enhancing catalytic activity, selectivity, stability and solubility.<sup>132</sup> While manganese(I/II) complexes have been less studied in TH of ketones,<sup>133</sup> the ruthenium(II) complexes predominated the interest of many researchers for decades due to their favourable catalytic properties.<sup>134-135</sup> In addition, ruthenium half-sandwich, carbonyl and phosphine-based complexes have been extensively studied as catalysts in TH of ketones in the last two decades. This is primarily due to their improved reactivity, stability, and ability to crystallize readily, which are beneficial for catalyst usage and purification.<sup>109, 135</sup> For these reasons, we aim to design efficient ruthenium and manganese-based catalysts for transfer hydrogenation of ketones with a good understanding of their performance at the molecular level in terms of kinetics.

## **1.5. General Aim and objectives**

### **1.5.1. General aim**

These projects aimed to design mono- and dinuclear carboxamide ruthenium(II) and manganese(II) complexes for the effective transfer hydrogenation of ketones.

### **1.5.2. Specific objectives**

From the general aim, the following specific objectives can be formulated:

1. To synthesise and characterise novel carboxamide ruthenium(II) and manganese(II) complexes.
2. To study new carboxamide ruthenium(II) and manganese(II) complexes as catalysts in transfer hydrogenation of ketones.
3. To investigate the impact of carboxamide and ancillary ligands such as triphenylphosphine, carbonyl, and para--cymene group on the performance of the catalysts.
4. To carry out mechanistic studies of the transfer hydrogenation reactions using *in situ* mass spectrometry,  $^1\text{H}$  and  $^{31}\text{P}\{^1\text{H}\}$  NMR spectroscopy experiments.

The outcomes of these studies are described in detail in the subsequent Chapters 2-6, and the key findings are summarised in Chapter 7.

## 1.6. References

1. Leitner, W., *Acc. Chemical Res.* **2002**, *35*, 746-756.
2. Hagen, J., *Industrial catalysis: a practical approach*. John Wiley & Sons: 2015.
3. Van Leeuwen, P. W., *Homogeneous catalysis: understanding the art*. Springer Science & Business Media: 2006.
4. Ding, S.; Hülsey, M. J.; Pérez-Ramírez, J.; Yan, N, *Joule* **2019**, *3*, 2897-2929.
5. Prima, D. O.; Kulikovskaya, N. S.; Galushko, A. S.; Mironenko, R. M.; Ananikov, V. P., *Curr. Opin. Green Sustain. Chem.* **2021**, *31*, 100502.
6. Hayler, J. D.; Leahy, D. K.; Simmons, E. M., *Organometallics* **2018**, *38*, 36-46.
7. Singh, B.; Sharma, V.; Gaikwad, R. P.; Fornasiero, P.; Zboril, R.; Gawande, M. B., *Small* **2021**, *17*, 2006473.
8. Chen, F.; Jiang, X.; Zhang, L.; Lang, R.; Qiao, B., *Chin. J. Catal.* **2018**, *39*, 893-898.
9. Cui, X.; Li, W.; Ryabchuk, P.; Junge, K.; Beller, M., *Nat. Catal.* **2018**, *1*, 385-397.
10. Kakaei, K.; Esrafil, M. D.; Ehsani, A., *Interface Sci. Technol.* **2019**, *27*, 1-21.
11. Gebbink, R. J. K.; Moret, M.-E., *Non-Noble Metal Catalysis: Molecular Approaches and Reactions*. John Wiley & Sons: 2019.
12. Drake, T.; Ji, P.; Lin, W., *Acc. Chem. Res.* **2018**, *51*, 2129-2138.
13. Behr, A.; Vorholt, A. J.; Seidensticker, T., *ChemBioEng Reviews* **2015**, *2*, 6-21.
14. Bhaduri, S.; Mukesh, D., *Homogeneous catalysis: mechanisms and industrial applications*. John Wiley & Sons: 2014.
15. Shende, V. S.; Saptal, V. B.; Bhanage, B. M., *Chem. Rec.* **2019**, *19*, 2022-2043.
16. Kumar, S.; Mohan, B.; Tao, Z.; You, H.; Ren, P., *Catal. Sci. Technol.* **2021**, *11*, 5734-5771.
17. Masters, C., *Homogeneous transition-metal catalysis: a gentle art*. Springer Science & Business Media: 2012.

18. Cokoja, M.; Bruckmeier, C.; Rieger, B.; Herrmann, W. A.; Kuehn, F. E., *Angew. Chem. Int. Ed.* **2011**, *50*, 8510-8537.
19. Gray, J.; Russell, L., *J. Am. Oil Chem. Soc.* **1979**, *56*, 36-44.
20. Noyori, R., *Acta Chem. Scand.* **1996**, *50*, 380-390.
21. Palmer, A. M.; Zanotti-Gerosa, A., *Curr. Opin. Drug Discov. Devel.* **2010**, *13*, 698-716.
22. Genet, J.-P., *Acc. Chem. Res.* **2003**, *36*, 908-918.
23. Gandolfi, C.; Heckenroth, M.; Neels, A.; Laurenczy, G.; Albrecht, M., *Organometallics* **2009**, *28*, 5112-5121.
24. Zhang, G.; Cheng, J.; Davis, K.; Bonifacio, M. G.; Zajackowski, C., *Green Chem.* **2019**, *21*, 1114-1121.
25. Shegavi, M. L.; Bose, S. K., *Catal. Sci. Technol.* **2019**, *9*, 3307-3336.
26. Lau, S.; Provis-Evans, C. B.; James, A. P.; Webster, R. L., *Dalton Trans.* **2021**, *50*, 10696-10700.
27. Klein, J.; Dunkelblum, E., *Tetrahedron* **1968**, *24*, 5701-5710.
28. Brown, H. C.; Ramachandran, P. V., *Pure Appl. Chem.* **1991**, *63*, 307-316.
29. Burkhardt, E. R.; Matos, K., *Chem. Rev.* **2006**, *106*, 2617-2650.
30. Raya-Baron, A.; Ona-Burgos, P.; Fernandez, I., *ACS Catal.* **2019**, *9*, 5400-5417.
31. Riant, O.; Mostefai, N.; Courmarcel, J., *Synthesis* **2004**, *2004*, 2943-2958.
32. Royo, B., *Adv. Organomet. Chem.* **2019**, *72*, 59-102.
33. Uvarov, V. M.; de Vekki, D. A., *J. Organomet. Chem.* **2020**, *923*, 121415.
34. Diez-Gonzalez, S.; Nolan, S. P., *Org. Prep. Proced. Int.* **2007**, *39*, 523-559.
35. Marciniak, B.; Guliński, J., *J. Organomet. Chem.* **1993**, *446*, 15-23.
36. Hollmann, F.; Opperman, D. J.; Paul, C. E., *Angew. Chem. Int. Ed.* **2021**, *60*, 5644-5665.

37. Wohlgemuth, R., *Development of Sustainable Biocatalytic Reduction Processes for Organic Chemists*. Brenna, E **2014**, 1-25.
38. Kar, S.; Sanderson, H.; Roy, K.; Benfenati, E.; Leszczynski, J., *Chem. Rev.* **2022**, 122, 3, 3637–3710.
39. Sheldon, R. A.; Woodley, J. M., *Chem. Rev.* **2018**, 118, 801-838.
40. Wang, D.; Astruc, D., *Chem. Rev.* **2015**, 115, 6621-6686.
41. Cui, X.; Huang, W.; Wu, L., *Org. Chem. Front.* **2021**, 8, 5002-5007.
42. Pang, M.; Chen, J.-Y.; Zhang, S.; Liao, R.-Z.; Tung, C.-H.; Wang, W., *Nat. Commun.* **2020**, 11, 1-9.
43. Gelis, C.; Heusler, A.; Nairoukh, Z.; Glorius, F., *Chem. Eur. J.* **2020**, 26, 14090.
44. Guo, Q. S.; Du, D. M.; Xu, J., *Angew. Chem.* **2008**, 120, 771-774.
45. Noyori, R.; Hashiguchi, S., *Acc. Chem. Res.* **1997**, 30, 97-102.
46. Foubelo, F.; Najera, C.; Yus, M., *Tetrahedron: Asymmetry* **2015**, 26, 769-790.
47. Wang, C.; Wu, X.; Xiao, J., *Chem. Asian J.* **2008**, 3, 1750-1770.
48. Štefane, B.; Požgan, F., *Top. Curr. Chem.* **2016**, 374, 18.
49. Wu, X.; Liu, J.; Di Tommaso, D.; Iggo, J. A.; Catlow, C. R. A.; Bacsá, J.; Xiao, J., *Chem. Eur. J.* **2008**, 14, 7699-7715.
50. Demianets, I.; Cherepakhin, V.; Maertens, A.; Lauridsen, P. J.; Sharada, S. M.; Williams, T. J., *Polyhedron* **2020**, 182, 114508.
51. Shiner, V.; Whittaker, D., *J. Am. Chem. Soc.* **1963**, 85, 2337-2338.
52. Klomp, D.; Maschmeyer, T.; Hanefeld, U.; Peters, J. A., *Chem. Eur. J.* **2004**, 10, 2088-2093.
53. Zhang, M.; Li, R.; Wu, Y.; Yu, Y., *Ind. Eng. Chem. Res.* **2021**, 60, 2871-2880.
54. Kumbhar, P. S.; Sanchez-Valente, J.; Lopez, J.; Figueras, F., *Chem. Commun.* **1998**, 535-536.

55. Rautenstrauch, V.; Hoang-Cong, X.; Churlaud, R.; Abdur-Rashid, K.; Morris, R. H., *Chem. Eur. J.* **2003**, *9*, 4954-4967.
56. Gladiali, S.; Alberico, E., *Chem. Soc. Rev.* **2006**, *35*, 226-236.
57. Echeverria, P.-G.; Ayad, T.; Phansavath, P.; Ratovelomanana-Vidal, V., *Synthesis* **2016**, *48*, 2523-2539.
58. Prokopchuk, D. E.; Morris, R. H., *Organometallics* **2012**, *31*, 7375-7385.
59. Clapham, S. E.; Hadzovic, A.; Morris, R. H., *Coord. Chem. Rev.* **2004**, *248*, 2201-2237.
60. Trocha-Grimshaw, J.; Henbest, H., *Chem. Commun.* **1967**, 544-544.
61. Deshpande, S. H., Synthesis of chiral ligands and their applications to asymmetric hydrogenation using transition metal complexes. PhD Thesis **2013**. Savitribai Phule Pune University, <http://hdl.handle.net/10603/192681>.
62. Alshakova, I. D.; Gabidullin, B.; Nikonov, G. I., *ChemCatChem* **2018**, *10*, 4860-4869.
63. Zhang, G.; Yin, Z.; Tan, J., *RSC Adv.* **2016**, *6*, 22419-22423.
64. Li, L.; Hilt, G., *Org. Lett.* **2020**, *22*, 1628-1632.
65. Vang, Z. P.; Hintzsche, S. J.; Clark, J. R., *Chem. Eur. J.* **2021**, *27*, 9988-10000.
66. Peñafiel, I.; Mangas-Sánchez, J.; Claver, C., Asymmetric (Transfer) Hydrogenation of Imines. *Asymmetric Hydrogenation and Transfer Hydrogenation* **2021**, 281-305.
67. Deng, L.; Liu, X.; Song, S., *Org. Chem. Front.* **2022**, *9*, 874-889
68. Barrios-Rivera, J.; Xu, Y.; Clarkson, G. J.; Wills, M., *Tetrahedron* **2022**, *103*, 132562.
69. Kehner, R. A.; Hewitt, M. C.; Bayeh-Romero, L., *ACS Catal.* **2022**, *12*, 1758-1763.
70. Dehury, N.; Maity, N.; Tripathy, S. K.; Basset, J.-M.; Patra, S., *ACS Catal.* **2016**, *6*, 5535-5540.
71. Dehury, N.; Tripathy, S. K.; Sahoo, A.; Maity, N.; Patra, S., *Dalton Trans.* **2014**, *43*, 16597-16600.
72. Xu, J.; Cheng, T.; Zhang, K.; Wang, Z.; Liu, G., *Chem. Commun.* **2016**, *52*, 6005-6008.



73. Hashiguchi, S.; Fujii, A.; Haack, K. J.; Matsumura, K.; Ikariya, T.; Noyori, R., *Angew. Chem. Int. Ed.* **1997**, *36*, 288-290.
74. Kitamura, M.; Kasahara, I.; Manabe, K.; Noyori, R.; Takaya, H., *J. Org. Chem.* **1988**, *53*, 708-710.
75. Herrmann, W. A.; Cornils, B., *Angew. Chem. Int. Ed.* **1997**, *36*, 1048-1067.
76. Copéret, C.; Chabanas, M.; Petroff Saint-Arroman, R.; Basset, J. M., *Angew. Chem. Int. Ed.* **2003**, *42*, 156-181.
77. Cornils, B.; Herrmann, W. A., *J. Catal.* **2003**, *216*, 23-31.
78. Cornils, B.; Herrmann, W. A.; Beller, M.; Paciello, R., *Applied homogeneous catalysis with organometallic compounds: a comprehensive handbook in four volumes*. John Wiley & Sons: 2017; Vol. 4.
79. Crabtree, R. H., *The organometallic chemistry of the transition metals*. John Wiley & Sons: 2009.
80. Piyasaengthong, A.; Williams, L. J.; Yufit, D. S.; Walton, J. W., *Dalton Trans.* **2022**, *51*, 340-351.
81. Neshat, A.; Mastroilli, P.; Mousavizadeh Mobarakeh, A., *Molecules* **2022**, *27*, 95.
82. Vue, B., PhD. Thesis. *Ruthenium (II)-catalyzed asymmetric transfer hydrogenation of aromatic ketones using new ferrocene-based amino-phosphine ligands featuring planar chirality*. California State University, Fresno: 2008.
83. Del Zotto, A.; Baratta, W.; Ballico, M.; Herdtweck, E.; Rigo, P., *Organometallics* **2007**, *26*, 5636-5642.
84. Yadav, S.; Vijayan, P.; Gupta, R., *J. Organomet. Chem.* **2021**, *954*, 122081.
85. Lorraine, S. C.; Lawrence, M. A.; Celestine, M.; Holder, A. A., *J. Mol. Struct.* **2020**, *1222*, 128829.
86. Guijarro, D.; Pablo, Ó.; Yus, M., *Tetrahedron Lett.* **2011**, *52*, 789-791.

87. Takehara, J.; Hashiguchi, S.; Fujii, A.; Inoue, S.-i.; Ikariya, T.; Noyori, R., *Chem. Commun.* **1996**, 233-234.
88. Minnaard, A. J.; Feringa, B. L.; Lefort, L.; De Vries, J. G., *Acc. Chem. Res.* **2007**, *40*, 1267-1277.
89. Dresch, L. C.; de Araújo, B. B.; Casagrande, O. d. L.; Stieler, R., *RSC Adv.* **2016**, *6*, 104338-104344.
90. Gessner, V. H., *Modern Ylide Chemistry: Applications in Ligand Design, Organic and Catalytic Transformations*. Springer: 2018; Vol. 177.
91. Bongers, N.; Krause, N., *Angew. Chem. Int. Ed.* **2008**, *47*, 2178-2181.
92. Suss-Fink, G.; Meister, G., *Adv. Organomet. Chem.* **1993**, *35*, 41-134.
93. Matsuzawa, A.; Harvey, J. N.; Himo, F., *Top. Catal.* **2021**, 1-9.
94. Arduengo III, A. J.; Harlow, R. L.; Kline, M., *J. Am. Chem. Soc.* **1991**, *113*, 361-363.
95. Koy, M.; Bellotti, P.; Das, M.; Glorius, F., *Nat. Catal.* **2021**, *4*, 352-363.
96. Bellotti, P.; Koy, M.; Hopkinson, M. N.; Glorius, F., *Nat. Rev. Chem.* **2021**, *5*, 711-725.
97. Kumar, A.; Kisan, H. K.; Huynh, H. V., *Organometallics* **2021**, *40*, 1699-1705.
98. Arduengo III, A. J.; Dias, H. R.; Harlow, R. L.; Kline, M., *J. Am. Chem. Soc.* **1992**, *114*, 5530-5534.
99. Zhao, Q.; Meng, G.; Nolan, S. P.; Szostak, M., *Chem. Rev.* **2020**, *120*, 1981-2048.
100. Dragutan, V.; Dragutan, I.; Delaude, L.; Demonceau, A., *Coord. Chem. Rev.* **2007**, *251*, 765-794.
101. Gürbüz, N.; Özcan, E. Ö.; Özdemir, İ.; Cetinkaya, B.; Şahin, O.; Büyükgüngör, O., *Dalton Trans.* **2012**, *41*, 2330-2339.
102. Yiğit, B.; Yiğit, M.; Özdemir, İ.; Çetinkaya, E., *Trans. Met. Chem.* **2012**, *37*, 297-302.
103. Nair, A. G.; McBurney, R. T.; Walker, D. B.; Page, M. J.; Gatus, M. R.; Bhadbhade, M.; Messerle, B. A., *Organometallics* **2016**, *45*, 14335-14342.

104. Uematsu, N.; Fujii, A.; Hashiguchi, S.; Ikariya, T.; Noyori, R., *J. Am. Chem. Soc.* **1996**, *118*, 4916-4917.
105. Gichumbi, J. M.; Friedrich, H. B.; Omondi, B., *J. Mol. Catal.* **2016**, *416*, 29-38.
106. Gichumbi, J. M.; Friedrich, H. B.; Omondi, B., *Trans. Met. Chem.* **2016**, *41*, 867-877.
107. Gichumbi, J. M.; Friedrich, H. B., *J. Organomet. Chem.* **2018**, *866*, 123-143.
108. Ramesh, M.; Venkatachalam, G., *J. Organomet. Chem.* **2019**, *880*, 47-55.
109. Liu, D.; Li, W.; Zhang, X., *Org. Lett.* **2002**, *4*, 4471-4474.
110. Badillo-Gómez, J.; Sánchez-Rodríguez, E.; Toscano, R.; Gouygou, M.; Ortega-Alfaro, M.; López-Cortés, J., *J. Organomet. Chem.* **2021**, *932*, 121630.
111. Gómez Arrayás, R.; Adrio, J.; Carretero, J. C., *Angew. Chem. Int. Ed.* **2006**, *45*, 7674-7715.
112. Melle, P.; Manoharan, Y.; Albrecht, M., *Inorg. Chem.* **2018**, *57*, 11761-11774.
113. Melle, P.; Thiede, J.; Hey, D. A.; Albrecht, M., *Chem. Eur. J.* **2020**, *26*, 13226-13234.
114. Yadav, S.; Vijayan, P.; Yadav, S.; Gupta, R., *Dalton Trans.* **2021**, *50*, 3269-3279.
115. Liu, T.; Chai, H.; Wang, L.; Yu, Z., *Organometallics* **2017**, *36*, 2914-2921.
116. Liu, T.; Wu, K.; Wang, L.; Fan, H.; Zhou, Y.-G.; Yu, Z., *Organometallics* **2019**, *39*, 93-104.
117. Aydemir, M.; Durap, F.; Baysal, A.; Meric, N.; Buldağ, A.; Gümgüm, B.; Özkar, S.; Yıldırım, L. T., *J. Mol. Catal. Chem.* **2010**, *326*, 75-81.
118. Chai, H.; Wang, Q.; Liu, T.; Yu, Z., *Dalton Trans.* **2016**, *45*, 17843-17849.
119. Meriç, N.; Durap, F.; Aydemir, M.; Baysal, A., *Appl. Organomet. Chem.* **2014**, *28*, 803-808.
120. Chai, H.; Liu, T.; Zheng, D.; Yu, Z., *Organometallics* **2017**, *36*, 4268-4277.
121. Viji, M.; Tyagi, N.; Naithani, N.; Ramaiah, D., *New J. Chem.* **2017**, *41*, 12736-12745.
122. Wen, J.; Wang, F.; Zhang, X., *Chem. Soc. Rev.* **2021**, *50*, 3211-3237.

123. Yang, W.; Chernyshov, I. Y.; van Schendel, R. K.; Weber, M.; Müller, C.; Filonenko, G. A.; Pidko, E. A., *Nat. Commun.* **2021**, *12*, 1-8.
124. Bruneau-Voisine, A.; Wang, D.; Dorcet, V.; Roisnel, T.; Darcel, C.; Sortais, J.-B., *Org. Lett.* **2017**, *19*, 3656-3659.
125. Ganguli, K.; Shee, S.; Panja, D.; Kundu, S., *Dalton Trans.* **2019**, *48*, 7358-7366.
126. Zirakzadeh, A.; de Aguiar, S. R.; Stöger, B.; Widhalm, M.; Kirchner, K., *ChemCatChem* **2017**, *9*, 1744-1748.
127. Demmans, K. Z.; Olson, M. E.; Morris, R. H., *Organometallics* **2018**, *37*, 4608-4618.
128. Chirik, A *ACS Catal.* **2015**, *5*, 5584-5585.
129. Olivier-Bourbigou, H.; Chizallet, C.; Dumeignil, F.; Fongarland, P.; Geantet, C.; Granger, P.; Launay, F.; Löfberg, A.; Massiani, P.; Mauge, F., *ChemCatChem* **2017**, *9*, 2029-2064.
130. Wang, X.; Chen, W.; Zhang, L.; Yao, T.; Liu, W.; Lin, Y.; Ju, H.; Dong, J.; Zheng, L.; Yan, W., *J. Am. Chem. Soc.* **2017**, *139*, 9419-9422.
131. Deb, B.; Dutta, D. K., *J. Coord. Chem.* **2018**, *71*, 1205-1213.
132. Peacock, D. M.; Jiang, Q.; Hanley, P. S.; Cundari, T. R.; Hartwig, J. F., *J. Am. Chem. Soc.* **2018**, *140*, 4893-4904.
133. Azouzi, K.; Valyaev, D. A.; Bastin, S.; Sortais, J.-B., *Curr. Opin. Green Sustain. Chem.* **2021**, *31*, 100511.
134. Garg, N.; Sarkar, A.; Sundararaju, B., *Coord. Chem. Rev.* **2021**, *433*, 213728.
135. Baidilov, D.; Hayrapetyan, D.; Khalimon, A. Y., *Tetrahedron* **2021**, *98*, 132435.

## CHAPTER 2

### EXPERIMENTAL, INSTRUMENTATION AND METHODS

#### 2.1. General information

This Chapter presents the materials, instrumentation, detailed experimental procedures, and characterisation methods used in this thesis. The Chapter covers the experimental design, synthesis and characterisation of the carboxamide ligands and their corresponding mononuclear and dinuclear ruthenium(II) and manganese(II) complexes. The  $^1\text{H}$ ,  $^{13}\text{C}$ ,  $^{19}\text{F}$ ,  $^{31}\text{P}$ , NMR spectroscopic, FT-IR spectroscopic, mass spectrometry, elemental analysis, and magnetic moment measurement data obtained from the characterisation of the compounds are presented in this Chapter.

#### 2.2. General Materials

All the reagents were purchased from Sigma-Aldrich and used without further purification. Standard procedures were followed in the purification and drying of solvents.<sup>1</sup> All solvents were of analytical grade. Diethyl ether was dried over sodium and molecular sieves while, dichloromethane, isopropyl alcohol (*i*PrOH), and ethanol were purified by distillation and dried over benzophenone,  $\text{CaCl}_2$ , and molecular sieves before use. All reactions were performed under an oxygen-free environment unless stated otherwise. The prefabricated ruthenium precursors  $[\text{RuH}(\text{CO})(\text{PPh}_3)_3\text{Cl}]$  and  $[\text{RuH}_2(\text{PPh}_3)_3(\text{CO})]$  were synthesised by adopting a modified procedure.<sup>2-4</sup> Chemical reagents such as pyridine-2-carboxylic acid, 8-aminoquinoline, 4-methyl-2-picolinic acid (> 99%), 4-chloro-2-picolinic acid (> 99%), pyrazine-2-carboxylic acid (> 99%), triphenylphosphate (> 99%), sodium methoxide (> 99%), pyridine-2-carboxylic acid (> 99%), *p*-phenylenediamine, *o*-phenylenediamine (> 97%), 4-methoxy

benzene-1,2-diamine (> 99%), 5-methyl-pyrazine-2-carboxylic acid (> 99%), 4,5-dimethylbenzene-1,2-diamine (> 99%), acetophenone (> 99%), 4-amino acetophenone (> 99%), 4-methyl acetophenone (> 99%), 2-methyl acetophenone (> 99%), 2-nitroacetophenone (> 99%), 1-acetylimidazole, 2-acetylpyridine (> 99%), 1-acetylnaphthalene (> 99%), 2-acetylnaphthalene (> 99%), 2-chloroacetophenone (> 99%), 4-chloroacetophenone (> 99%), 4-hydroxyacetophenone (> 99%), 2-pentanone (> 97%), 2-methylcyclohexanone (> 99%), manganese(II) chloride tetrahydrate salt (> 99%) and  $[\text{RuCl}_2(p\text{-cymene})]_2$  (> 99%) dimer were used without further purifications.

### 2.3. General Instrumentation

$^1\text{H}$  and  $^{13}\text{C}$  NMR spectra were recorded on a Bruker Ultrashield 400 ( $^1\text{H}$  NMR 400 MHz,  $^{13}\text{C}\{^1\text{H}\}$  NMR 100 MHz) spectrometer in  $\text{CDCl}_3$  solution at room temperature, and chemical shifts ( $\delta$ ) were determined relative to internal TMS and recorded in ppm relative to  $\text{CHCl}_3$   $\delta_{\text{H}}$ : 7.26 ppm and  $\delta_{\text{C}}$ : 77.6 ppm and  $\text{DMSO-d}_6$   $\delta_{\text{H}}$ : 2.50 ppm. Coupling constants ( $J$ ) were reported in Hertz (Hz), and splitting patterns were indicated as s (singlet), d (doublet), dd (doublet of doublet), t (triplet), and m (multiplet).  $^{31}\text{P}\{^1\text{H}\}$  NMR spectra were obtained from 400 MHz in  $\text{CDCl}_3$  at room temperature and referenced to the external standard  $\text{H}_3\text{PO}_4$  ( $\delta_{\text{P}}$  0.00 ppm). Elemental analyses were performed on Thermal Scientific Flash 2000, and ESI mass spectra were recorded on an LC premier micro-mass spectrometer. The FT-IR spectra were recorded on a PerkinElmer spectrum 100 in the 4000–650  $\text{cm}^{-1}$  range.

#### 2.3.1. X-ray crystallography

X-ray data were recorded on the Bruker Apex Duo equipped with the Oxford Instruments Cryojet operating at 100(2) K and the Incoatec micro source operating at 30 W X-ray power.

The data were collected with Mo K $\alpha$  ( $\lambda = 0.71073$  Å) and Cu K $\alpha$  ( $\lambda = 1.54184$  Å) radiations at a crystal-detector distance of 50 mm. The following conditions were used for data collection: omega and *phi* scan with exposures at 30 W X-ray power and 0.50° frame widths using APEX2.<sup>5</sup> Data were reduced using outlier rejection, scanning speed scaling, and standard Lorentz and polarisation correction factors with the SAINT41 program.<sup>6</sup> A correction of the SADABS semi-empirical multi-scan absorption was applied to the data. Direct methods, SHELXS-2014 and WinGX,<sup>7</sup> have been used to solve all three structures. All non-hydrogen atoms were located on the difference Fourier map and anisotropically refined with SHELXL-97.<sup>8</sup> All hydrogen atoms were fixed by HFIX at ideal positions and were included in the refinement process using riding model with isotropic thermal parameters. All hydrogen atoms were included as idealized contributors in the least squares process. Their positions were calculated using a standard riding model with C–H<sub>aromatic</sub> distances of 0.93 Å and Uiso = 1.2Ueq and C–H<sub>methylene</sub> distances of 0.99 Å and Uiso = 1.2Ueq and C–H<sub>methyl</sub> distances of 0.98 Å and Uiso = 1.5Ueq.

## 2.4. Synthesis and characterisation of pyrazine-carboxamide ligands (HL1 and HL2)

### 2.4.1. *N*-(benzo[d]thiazol-2-yl) pyrazine-2-carboxamide (HL1)

The ligand *N*-(benzo[d]thiazol-2-yl)pyrazine-2-carboxamide (**HL1**) was synthesised according to literature procedures.<sup>9-11</sup> Pyrazine-2-dicarboxylic acid (1.00 g, 5.02 mmol) and 2-aminobenzothiazole (0.75 g, 5.02 mmol) were dissolved in 20 mL pyridine and then heated with stirring for 15 minutes at 110 °C. Triphenylphosphite P(OPh)<sub>3</sub> (1.55 g, 5.00 mmol) was introduced drop-wise to the resulting solution and then allowed to stir at 90 °C for 12 h. The crude product was poured into ice-cold water, filtered, and washed with cold water and cold methanol. The yellow crude powder was recrystallised from methanol and toluene. Yield: 1.54 g (74%). <sup>1</sup>H NMR (400 MHz, *d*<sub>6</sub>-DMSO): 9.37 (s, 1H<sub>amidate</sub>), 8.98 (d, <sup>3</sup>J<sub>HH</sub> = 2.4 Hz, 1H<sub>pyrazine</sub>),

8.90 – 8.85 (m, 1H<sub>pyrazine</sub>), 8.07 (d,  $^3J_{\text{HH}} = 7.8$  Hz, 1H<sub>pyrazine</sub>), 7.84 (d,  $^3J_{\text{HH}} = 8.0$  Hz, 1H<sub>benzene</sub>), 7.50 (t,  $^3J_{\text{HH}} = 7.6$  Hz, 1H<sub>benzene</sub>), 7.38 (t,  $^3J_{\text{HH}} = 7.6$  Hz, 1H<sub>benzene</sub>).  $^{13}\text{C}\{^1\text{H}\}$  NMR (101 MHz, CDCl<sub>3</sub>)  $\delta$ : 161.3(C<sub>carbonyl</sub>), 156.8(C<sub>pyrazine</sub>), 148.6(C<sub>pyrazine</sub>), 145.0(C<sub>pyrazine</sub>), 143.1(C<sub>pyrazine</sub>), 142.5(C<sub>benzothiole</sub>), 132.5(C<sub>benzothiole</sub>), 126.5(C<sub>benzothiole</sub>), 124.4(C<sub>benzothiole</sub>), 121.5(C<sub>benzothiole</sub>), 121.4(C<sub>benzothiole</sub>). FT-IR spectrum (Zn-Se ATR, cm<sup>-1</sup>): 3324 (N–H), 1691 (C=O), 1533 (C=N). HR ESI-MS spectrum, m/z: Calcd. for C<sub>12</sub>H<sub>8</sub>N<sub>4</sub>SO; 256.0419; Found 257.0497 [M + H]<sup>+</sup>.

#### 2.4.2. *N*-(1H-benzo[d]imidazol-2-yl)pyrazine-2-carboxamide (HL2)

Pyrazine-2-dicarboxylic acid (1.00 g, 5.00 mmol), 2-aminobenzothiazole (0.75 g, 5.00 mmol), and P(OPh)<sub>3</sub> (1.55 g, 5.00 mmol). Recrystallization was achieved from methanol to obtain a pale-yellow solid. Yield: 1.04 g (72%).  $^1\text{H}$  NMR (400 MHz, DMSO)  $\delta$ : 12.20 (s, 1H<sub>amidate</sub>), 9.37 (d,  $^3J_{\text{HH}} = 1.2$  Hz, 1H<sub>pyrazine</sub>), 8.86 (d,  $^3J_{\text{HH}} = 35.5, 1.9$  Hz, 2H<sub>pyrazine</sub>), 7.51 (d,  $^3J_{\text{HH}} = 5.9, 3.2$  Hz, 2H<sub>benzene</sub>), 7.18 (dd,  $^3J_{\text{HH}} = 5.9, 3.2$  Hz, 2H<sub>benzene</sub>).  $^{13}\text{C}\{^1\text{H}\}$  NMR (101 MHz, CDCl<sub>3</sub>)  $\delta$ : 163.2(C<sub>carbonyl</sub>), 149.9(C<sub>pyrazine</sub>), 149.0(C<sub>pyrazine</sub>), 138.6(C<sub>pyrazine</sub>), 131.5(C<sub>pyrazine</sub>), 127.6(C<sub>benzoimidazole</sub>), 126.1(C<sub>benzoimidazole</sub>), 126.5(C<sub>benzoimidazole</sub>), 127.6(C<sub>benzoimidazole</sub>), 126.1(C<sub>benzoimidazole</sub>), 122.9(C<sub>benzoimidazole</sub>). FT-IR spectrum ((Zn-Se ATR, cm<sup>-1</sup>): 3251 (N–H) amidate, 1684 (C=O)<sub>amidate</sub>, 1546 (C=N)<sub>pyrazine</sub>. HR ESI-MS spectrum, m/z: Calcd. for C<sub>12</sub>H<sub>9</sub>N<sub>5</sub>O; 239.0807; Found 240.0885 [M + H]<sup>+</sup>.

### 2.5. Synthesis and characterisation of phenyl-dipicolinamide ligands (H<sub>2</sub>L3 – H<sub>2</sub>L6)

#### 2.5.1. *N,N'*-(1,4-phenylene)dipicolinamide (H<sub>2</sub>L3)

The ligand, **H<sub>2</sub>L3** and **H<sub>2</sub>L4** were synthesised by a simple condensation reaction between appropriate amines and dicarboxylic acid using a modified literature procedure.<sup>12-14</sup> To a solution of a picolinic acid (0.50 g, 4.061 mmol) in pyridine (10 mL) was added *ap*-phenylenediamine (0.26 g, 2.413 mmol) and triphenylphosphate (1.00 mL) and refluxed at 110



°C for 6h to form a suspension. The reaction mixture was cooled to room temperature, 20 ml of distilled water was added and filter under vacuum to obtained white crude product. The crude was then washed with dry ethanol (30 mL) and dried in vacuum to obtain white crystalline solid. Yield = 0.660 g (86%). <sup>1</sup>H NMR (400 MHz, CDCl<sub>3</sub>) δ<sub>H</sub>: 10.07 (s, 2H<sub>amide</sub>), 8.65 (m, <sup>3</sup>J<sub>HH</sub> = 5.6 Hz, 2H<sub>pyridine</sub>), 8.34 (d, <sup>3</sup>J<sub>HH</sub> = 6.4Hz, 2H<sub>pyridine</sub>), 7.94(t, <sup>3</sup>J<sub>HH</sub> = 6.4H, 2H<sub>pyridine</sub>) 7.85(s, 2H<sub>pyridine</sub>), 7.52(d, <sup>3</sup>J<sub>HH</sub> = 10 Hz, 4H<sub>benzene</sub>). <sup>13</sup>C{<sup>1</sup>H}NMR (101 MHz, CDCl<sub>3</sub>) δ: 162.9, 149.7, 148.2, 137.5, 130.2, 126.5, 124.7, 122.6. FT-IR (cm<sup>-1</sup>): (νC=O)<sub>amide</sub> = 3331; (νN-H)<sub>amide</sub> = 1660. HR ESI-MS, m/z(%): HR ESI-MS, m/z(%): Calcd for C<sub>18</sub>H<sub>15</sub>N<sub>4</sub>O<sub>2</sub>; 318.1117, Found: 319.1195 [M + H]<sup>+</sup>.

The carboxamide ligands **HL4-HL6** were synthesised by following the same procedure as described for **HL3**.

### 2.5.2. *N,N'*-(1,2-phenylene)dipicolinamide (**H<sub>2</sub>L4**)

A picolinic acid (0.50 g, 4.061 mmol), *o*-phenylenediamine (0.261 g, 2.413 mmol) and triphenylphosphate (1.00 mL), and refluxed at 110 °C for 6h. The crude product was washed with ethanol(30 mL) to obtain a pale-yellow solid. A white crystalline solid was obtained. Yield = 0.660 g (86%). <sup>1</sup>H NMR (400 MHz, CDCl<sub>3</sub>) δ<sub>H</sub>: 10.71 (s, 2H<sub>amide</sub>), 8.65(t, <sup>3</sup>J<sub>HH</sub> = 5.6 Hz, 2H<sub>pyridine</sub>), 8.19 (d, <sup>3</sup>J<sub>HH</sub> = 6.4Hz, 2H<sub>pyridine</sub>), 8.06 (d, <sup>3</sup>J<sub>HH</sub> = 6.4Hz, 2H<sub>pyridine</sub>), 7.79(t, <sup>3</sup>J<sub>HH</sub> = 6.4Hz, 2H<sub>pyridine</sub>) 7.67(m, <sup>3</sup>J<sub>HH</sub> = 6.4Hz 2H<sub>benzene</sub>), 7.32(d, <sup>3</sup>J<sub>HH</sub> = 10 Hz, 2H<sub>benzene</sub>). <sup>13</sup>C{<sup>1</sup>H} NMR (101 MHz, CDCl<sub>3</sub>) δ: 163.3, 149.9, 149.0, 138.6, 131.4, 127.5, 126.2, 125.7, 122.9. FT-IR (cm<sup>-1</sup>): (νC=O)<sub>amide</sub> = 1664; (νN-H)<sub>amide</sub> = 3312. HR ESI-MS, m/z(%): Calcd. C<sub>18</sub>H<sub>15</sub>N<sub>4</sub>O<sub>2</sub>; 318.1117, Found: 319.1195 [M + H]<sup>+</sup>.

### 2.5.3. *N,N'*-(4,5-dimethyl-1,2-phenylene)dipicolinamide (H<sub>2</sub>L5)

A picolinic acid (0.50 g, 3.62 mmol), 4,5-dimethylbenzene-1,2-diamine (0.26 g, 2.41 mmol), triphenylphosphate (1.10 mL, 3.62 mmol), and refluxed at 110 °C for 6h. White compound was obtained. Yield = 0.637 g (86%). <sup>1</sup>H NMR (400 MHz, CDCl<sub>3</sub>) δ: 10.17 (s, 2H<sub>amide</sub>), 8.57 (m, <sup>3</sup>J<sub>HH</sub> = 5.6 Hz, 2H<sub>pyridine</sub>), 8.31 (m, <sup>3</sup>J<sub>HH</sub> = 4.8 Hz, 2H<sub>pyridine</sub>), 7.91 (m, <sup>3</sup>J<sub>HH</sub> = 4.8 Hz, 2H<sub>pyridine</sub>), 7.64 (s, 2H<sub>benzene</sub>), 7.45 (m, <sup>3</sup>J<sub>HH</sub> = 6.2 Hz, 2H<sub>pyridine</sub>), 3.71 (s, 3H), 2.34 (s, 6H, CH<sub>3</sub>). <sup>13</sup>C{<sup>1</sup>H} NMR (101 MHz, CDCl<sub>3</sub>) δ: 162.8, 149.9, 148.2, 137.4, 134.8, 127.8, 126.3, 125.7, 122.5, 19.8. FT-IR (cm<sup>-1</sup>): (νN-H)<sub>amide</sub> = 3325; (νC=O)<sub>amide</sub> = 1663. HR-ESI-MS: m/z(%); Calcd for C<sub>20</sub>H<sub>18</sub>N<sub>4</sub>O<sub>2</sub>; 346.1430, Found: 347.1508 [M + H]<sup>+</sup>.

### 2.5.4. *N,N'*-(4-methoxy-1,2-phenylene)dipicolinamide (H<sub>2</sub>L6)

A picolinic acid (0.50 g, 3.62 mmol), 4-methoxybenzene-1,2-diamine (0.26 g, 2.41 mmol), triphenylphosphate (1.10 mL, 3.62), and refluxed at 110 °C for 6h. Off-white solid compound was obtained. Yield = 0.74 g (91%). <sup>1</sup>H NMR (400 MHz, CDCl<sub>3</sub>) δ: 10.63 (s, 1-H<sub>amide</sub>), 10.58 (s, H<sub>amide</sub>), 8.69 (d, <sup>3</sup>J<sub>HH</sub> = 5.6 Hz, 2H<sub>pyridine</sub>), 8.58 (d, <sup>3</sup>J<sub>HH</sub> = 5.6 Hz, 2H<sub>pyridine</sub>), 8.18 (m, <sup>3</sup>J<sub>HH</sub> = 6.4 Hz, 1H<sub>pyridine</sub>), 8.08 (m, <sup>3</sup>J<sub>HH</sub> = 6.4 Hz, 2H<sub>pyridine</sub>), 7.68 (m, <sup>3</sup>J<sub>HH</sub> = 6.4 Hz, 2H<sub>pyridine</sub>), 7.64 (m, <sup>3</sup>J<sub>HH</sub> = 6.4 Hz, 2H<sub>pyridine</sub>), 6.89 (d, <sup>3</sup>J<sub>HH</sub> = 7.2 Hz, H<sub>benzene</sub>), 6.83 (d, <sup>3</sup>J<sub>HH</sub> = 7.2 Hz, H<sub>benzene</sub>), 7.36 (s, H<sub>benzene</sub>), 3.71 (s, 3H, -OCH<sub>3</sub>). <sup>13</sup>C{<sup>1</sup>H} NMR (101 MHz, CDCl<sub>3</sub>) δ: 163.6, 162.8, 157.7, 150.1, 149.7, 149.6, 148.0, 148.6, 138.7, 138.5, 133.2, 127.6, 127.4, 123.4, 122.8, 111.2, 109.8, 55.8. FT-IR (cm<sup>-1</sup>): (νN-H)<sub>amide</sub> = 3323; (νC=O)<sub>amide</sub> = 1663. HR-ESI-MS: m/z(%); Calcd. for C<sub>19</sub>H<sub>16</sub>N<sub>4</sub>O<sub>3</sub>; 348.1222 Found: 349.1301 [M + H]<sup>+</sup>.

## 2.6. Synthesis and characterisation of *N*-pyrazyl/Pyridyl(quinolin-8-yl)pyrazine-2-carboxamide ligands (HL7-HL9)

### 2.6.1. *N*-(quinolin-8-yl)pyrazine-2-carboxamide (HL7)

To a suspension of 8-amino-quinoline (1.08 g, 10.0 mmol), pyrazine-2-carboxylic acid (1.24 g, 10.0 mmol), and tetrabutylammonium tetrafluoroborate (3.22 g, 10.0 mmol) in pyridine (20.0 mL) was added triphenyl phosphite (TPPO) (2.80 mL, 10.00 mmol). The reaction mixture was refluxed at 100 °C for 12 h. The mixture was cooled to room temperature and poured into ice-cold water (40 mL). The resulting dark brown precipitate was collected by suction filtration, washed with copious amount of cold methanol and dried. Yield: 1.88 g (76%). <sup>1</sup>H NMR (400 MHz, DMSO-d<sub>6</sub>): δH (ppm): 11.91 (s, H<sub>amide</sub>), 9.39 (d, <sup>3</sup>J<sub>HH</sub> = 12, H<sub>pyrazine</sub>); 8.99 (d, <sup>3</sup>J<sub>HH</sub> = 12, H<sub>pyrazine</sub>); 8.97 (s, H<sub>pyrazine</sub>); 8.91 (d, <sup>3</sup>J<sub>HH</sub> = 4, H<sub>quinoline</sub>); 8.87 (d, <sup>3</sup>J<sub>HH</sub> = 4, H<sub>quinoline</sub>); 8.85 (dd, <sup>3</sup>J<sub>HH</sub> = 4, H<sub>quinoline</sub>); 8.46 (dd, <sup>3</sup>J<sub>HH</sub> = 12, 1H<sub>quinoline</sub>); 7.77 (dd, <sup>3</sup>J<sub>HH</sub> = 12, H<sub>quinoline</sub>); 7.66 (m, <sup>3</sup>J<sub>HH</sub> = 12, H<sub>quinoline</sub>); <sup>13</sup>C{<sup>1</sup>H} NMR (DMSO-d<sub>6</sub>): δ<sub>C</sub> (ppm): 143.52 (CH<sub>pyrazine</sub>); 144.61 (CH<sub>pyrazine</sub>); 147.64 (CH<sub>pyrazine</sub>); 148.81 (C<sub>pyrazine</sub>); 157.65 (C<sub>pyridine</sub>); 163.06 (C=O). FT-IR (cm<sup>-1</sup>): ν(N-H) = 3313; ν(C=O) = 1660<sub>amide</sub> and ν(C-N)<sub>amide</sub> = 1469. HR-MS (ESI): m/z Calcd for C<sub>14</sub>H<sub>10</sub>N<sub>4</sub>O; 250.0855, Found: 251.0933 [M + H]<sup>+</sup>

The carboxamide ligands **HL8-HL9** were synthesised by following the same procedure as described for **HL2** using the appropriate carboxylic acids and 8-aminoquinoline.

### 2.6.2. 5-methyl-*N*-(quinolin-8-yl)pyrazine-2-carboxamide (HL8)

8-aminoquinoline (1.44 g, 10.00 mmol), 5-methyl-pyrazine-2-carboxylic acid (1.24 g, 10.00 mmol), triphenyl phosphite (TPPO) (2.80 mL, 10.00 mmol). and tetrabutylammonium tetrafluoroborate (3.22 g, 10.0 mmol). Light brown solid: Yield: 0.92 g (94%). Slow diffusion

of diethyl ether into a solution of the compound in ethanol afforded a single crystal suitable for X-ray crystallography analysis.  $^1\text{H}$  NMR (400 MHz, DMSO- $d_6$ ):  $\delta_{\text{H}}$  (ppm): 12.02(s,  $\text{H}_{\text{amide}}$ ), 9.45 (d,  $^3J_{\text{HH}} = 12$ ,  $\text{H}_{\text{pyridine}}$ ); 9.02 (d,  $^3J_{\text{HH}} = 12$ ,  $\text{H}_{\text{pyridine}}$ ); 8.98 (s,  $\text{H}_{\text{pyridine}}$ ); 8.62 (d,  $^3J_{\text{HH}} = 4$ ,  $\text{H}_{\text{quinoline}}$ ) 8.23 (d,  $^3J_{\text{HH}} = 4$ ,  $\text{H}_{\text{quinoline}}$ ); 7.62 (dd,  $^3J_{\text{HH}} = 4$ ,  $\text{H}_{\text{quinoline}}$ ); 7.52 (dd,  $^3J_{\text{HH}} = 12$ ,  $\text{H}_{\text{quinoline}}$ ); 7.51 (m,  $^3J_{\text{HH}} = 12$ ,  $1\text{H}_{\text{quinoline}}$ ); 2.37(s,  $3\text{H}_{\text{methyl}}$ ).  $^{13}\text{C}$  NMR ( $d_6$ -DMSO):  $\delta_{\text{C}}$  (ppm): 116.06 ( $\text{C}_{\text{quinoline}}$ ); 122.42 ( $\text{C}_{\text{quinoline}}$ ); 122.73 ( $\text{C}_{\text{quinoline}}$ ); 127.02 ( $\text{C}_{\text{quinoline}}$ ); 127.85 ( $\text{C}_{\text{quinoline}}$ ); 133.33 ( $\text{C}_{\text{quinoline}}$ ); 136.73 ( $\text{C}_{\text{quinoline}}$ ); 138.09 ( $\text{C}_{\text{quinoline}}$ ); 143.52 ( $\text{C}_{\text{quinoline}}$ ); 143.73 ( $\text{C}_{\text{pyrazine}}$ ); 144.06 ( $\text{C}_{\text{pyrazine}}$ ); 148.22 ( $\text{C}_{\text{pyrazine}}$ ); 149.37 ( $\text{C}_{\text{pyrazine}}$ ); 160.76 ( $\text{C}=\text{O}$ ). FT-IR ( $\text{cm}^{-1}$ ):  $\nu(\text{N-H})_{\text{amide}} = 3303$ ;  $\nu(\text{C}=\text{O})_{\text{amide}} = 1674$ . HR-MS (ESI):  $m/z$  Calcd for  $\text{C}_{15}\text{H}_{13}\text{N}_4\text{O}$ ; 265.1089, Found: 265.1082 [ $\text{M}$ ] $^{+}$ .

### 2.6.3. 5-Chloro-*N*-(quinolin-8-yl)pyridine-2-carboxamide (HL9)

8-aminoquinoline (1.44 g, 10.00 mmol), 5-chloro-pyridine-2-carboxylic acid (1.24 g, 10.00 mmol), triphenyl phosphite (TPPO) (2.80 mL, 10.00 mmol). and tetrabutylammonium tetrafluoroborate (3.29 g, 10.0 mmol). Light brown solid: Yield: 0.92 g (94%).  $^1\text{H}$  NMR (400 MHz, DMSO- $d_6$ ):  $\delta_{\text{H}}$  (ppm); 11.85(s,  $\text{H}_{\text{amide}}$ ), 9.03 (d,  $^3J_{\text{HH}} = 12$ ,  $\text{H}_{\text{pyridine}}$ ); 9.89 (d,  $^3J_{\text{HH}} = 12$ ,  $\text{H}_{\text{pyridine}}$ ); 8.48 (s,  $\text{H}_{\text{pyridine}}$ ); 8.27 (d,  $^3J_{\text{HH}} = 4$ ,  $\text{H}_{\text{quinoline}}$ ) 8.25 (d,  $^3J_{\text{HH}} = 4$ ,  $\text{H}_{\text{quinoline}}$ ); 8.18 (dd,  $^3J_{\text{HH}} = 4$ ,  $\text{H}_{\text{quinoline}}$ ); 7.88 (dd,  $^3J_{\text{HH}} = 12$ ,  $\text{H}_{\text{quinoline}}$ ); 7.86 (m,  $^3J_{\text{HH}} = 12$ ,  $\text{H}_{\text{quinoline}}$ );  $^{13}\text{C}$  NMR ( $d_6$ -DMSO):  $\delta_{\text{C}}$  (ppm): 116.06 ( $\text{C}_{\text{quinoline}}$ ); 122.42 ( $\text{C}_{\text{quinoline}}$ ); 122.73 ( $\text{C}_{\text{quinoline}}$ ); 127.02 ( $\text{C}_{\text{quinoline}}$ ); 127.85 ( $\text{C}_{\text{quinoline}}$ ); 133.33 ( $\text{C}_{\text{quinoline}}$ ); 136.73 ( $\text{C}_{\text{quinoline}}$ ); 138.09 ( $\text{C}_{\text{quinoline}}$ ); 143.52 ( $\text{C}_{\text{quinoline}}$ ); 143.73 ( $\text{C}_{\text{pyrazine}}$ ); 144.06 ( $\text{C}_{\text{pyrazine}}$ ); 148.22 ( $\text{C}_{\text{pyrazine}}$ ); 149.37 ( $\text{C}_{\text{pyrazine}}$ ); 160.76 ( $\text{C}=\text{O}$ ). FT-IR ( $\text{cm}^{-1}$ ):  $\nu(\text{N-H})_{\text{amide}} = 3315$ ;  $\nu(\text{C}=\text{O})_{\text{amide}} = 1678$ . HR-MS (ESI):  $m/z(\%)$ ; Calcd for  $\text{C}_{15}\text{H}_{10}\text{ClN}_3\text{O}$ ; 284.0591, Found: 284.0581 [ $\text{M} + \text{H}$ ] $^{+}$ .

## 2.7. Synthesis and characterisation of carbonyl-ruthenium(II) complexes of pyrazine-carboxamide ligands (Ru1-Ru4)

### 2.7.1. [Ru(L1)(CO)Cl(PPh<sub>3</sub>)<sub>2</sub>] (Ru1)

A prefabricated [RuHCl(CO)(PPh<sub>3</sub>)<sub>3</sub>] precursor (0.10 g, 0.10 mmol) in ethanol (15 ml) was added to a suspension of carboxamide ligand, **HL1** (0.03 g, 0.10 mmol), and the resulting mixture was refluxed at 110 °C to obtain a deep red solution. The crude solution was reduced in *vacuo* to about 3 mL and diethyl ether (25 mL) was added, and the yellow product was collected by filtration and dried in *vacuo*. Single crystals suitable for single crystal X-ray analysis were obtained by diffusion of diethyl ether into a saturated solution of the complex in dichloromethane. A yellow solid was obtained. Yield: 0.08 g (85%). <sup>1</sup>H NMR (400 MHz, CDCl<sub>3</sub>) δ<sub>H</sub>: 9.15 (d, <sup>3</sup>J<sub>HH</sub> = 4.0 Hz, H<sub>pyrazine</sub>), 8.24 (dd, <sup>3</sup>J<sub>HH</sub> = 4.0 Hz, H<sub>pyrazine</sub>), 7.88 (d, <sup>3</sup>J<sub>HH</sub> = 3.0 Hz, H<sub>pyrazine</sub>), 7.69 (d, <sup>3</sup>J<sub>HH</sub> = 8.0 Hz, H<sub>benzothiole</sub>), 7.63 (d, <sup>3</sup>J<sub>HH</sub> = 7.3 Hz, 2H<sub>benzothiole</sub>), 7.45-7.43 (m, 14H), 7.36 – 7.32 (m, 2H), 7.17 (s, 3H), 7.13-7.15(m, 2H), 7.04 - 7.00 (m, 13H). <sup>13</sup>C{<sup>1</sup>H} NMR (101 MHz, CDCl<sub>3</sub>) δ: 166.9(C-carbonyl), 148.2(C-benzothiole), 147.8(C-pyrazine), 147.4(C-pyrazine), 145.7(C-pyrazine), 143.9(C-pyrazine), 134.9(C-benzothiole), 133.7(C-benzothiole), 131.3(C-benzothiole), 131.1(C-benzothiole), 130.7(C-benzothiole), 129.6(C-benzothiole), 128.8(C-PPh<sub>3</sub>), 127.8(C-PPh<sub>3</sub>), 124.8(C-PPh<sub>3</sub>), 122.4(C-PPh<sub>3</sub>), 120.9(C-PPh<sub>3</sub>), 120.6(C-PPh<sub>3</sub>). <sup>31</sup>P{<sup>1</sup>H} NMR (162 MHz, CDCl<sub>3</sub>) δ 29.4 (s). FT-IR spectrum (Zn-Se ATR cm<sup>-1</sup>): 1935 (νC≡O)<sub>Ru-CO</sub>, 1629 (νC=O)<sub>amidate</sub>, and 1565 (νC=N)<sub>pyrazine</sub>. LC-MS: m/z(%); Calcd 944.08; Found 912.15 [M<sup>+</sup> - Cl, 100]. Anal. Calcd; for: C<sub>49</sub>H<sub>37</sub>ClN<sub>4</sub>O<sub>2</sub>P<sub>2</sub>RuS: C, 64.51; H, 4.09; N, 6.14; S, 3.40. Found: C, 64.26; H, 4.01; N, 6.13; S, 3.36.

Complexes **Ru2-Ru4** were synthesised following the protocol described for **Ru1**.

### 2.7.2. [Ru(L1)(CO)H(PPh<sub>3</sub>)<sub>2</sub>] (Ru2)

[RuH<sub>2</sub>(CO)(PPh<sub>3</sub>)<sub>3</sub>] (0.10 g, 0.10 mmol) and ligand **HL1** (0.03 g, 0.10 mmol). A crystal suitable for single crystal X-ray analysis was afforded by diffusion of pentane into a solution of the complexes in dichloromethane. A reddish orange solid compound was obtained. Yield: 0.06 g (65%). <sup>1</sup>H NMR (400 MHz, CDCl<sub>3</sub>): δ<sub>H</sub>: -13.26 (t, <sup>2</sup>J<sub>H-P</sub> = 20.3 Hz, H<sub>Ru-H</sub>), 8.96 (s, H<sub>pyrazine</sub>), 8.06 (d, <sup>3</sup>J<sub>HH</sub> = 7.9 Hz, H<sub>pyrazine</sub>), 7.82 (d, <sup>3</sup>J<sub>HH</sub> = 7.8 Hz, H<sub>pyrazine</sub>), 7.51 (m, 14H), 7.32 (t, <sup>3</sup>J<sub>HH</sub> = 7.5 Hz, H), 7.24 (t, <sup>3</sup>J<sub>HH</sub> = 7.4 Hz, 6H), 7.17 (d, <sup>3</sup>J<sub>HH</sub> = 2.9 Hz, 1H<sub>bz</sub>), 7.10 (m, 12H). <sup>13</sup>C{<sup>1</sup>H} NMR (101 MHz, CDCl<sub>3</sub>) δ: 166.8(C<sub>carbonyl</sub>), 166.3 (C<sub>benzothiole</sub>), 149.6(C<sub>pyrazine</sub>), 149.2(C<sub>pyrazine</sub>), 147.9(C<sub>pyrazine</sub>), 145.7(C<sub>pyrazine</sub>), 134.9(C<sub>benzothiole</sub>), 133.7(C<sub>benzothiole</sub>), 132.9 (C<sub>benzothiole</sub>), 132.7 (C<sub>benzothiole</sub>), 132.4 (C<sub>benzothiole</sub>), 129.7(C<sub>benzothiole</sub>), 127.9(C-PPh<sub>3</sub>), 125.0 (C-PPh<sub>3</sub>), 122.2(C-PPh<sub>3</sub>), 121.1(C-PPh<sub>3</sub>), 120.6(C-PPh<sub>3</sub>). <sup>31</sup>P{<sup>1</sup>H} NMR (162 MHz, CDCl<sub>3</sub>) δ 48.2 (s). FT-IR spectrum (Zn-Se ATR, cm<sup>-1</sup>): 1946 (νC≡O)<sub>Ru-CO</sub>, 1626 (νC=O)<sub>amidate</sub>, and 1567 (νC=N)<sub>pyrazine</sub>. LC-MS: m/z(%); Calcd. 912.12; Found 911.08 [M<sup>+</sup> - H, 100]. Anal. Calcd. for: C<sub>49</sub>H<sub>38</sub>N<sub>4</sub>O<sub>2</sub>P<sub>2</sub>RuS: C, 64.68; H, 4.21; N, 6.16; S, 3.52%. Found: C, 64.41; H, 4.30; N, 6.01; S, 3.46%.

### 2.7.3. [Ru(L2)(CO)Cl(PPh<sub>3</sub>)<sub>2</sub>] (Ru3)

[RuClH(CO)(PPh<sub>3</sub>)<sub>2</sub>] (0.100 g, 0.110 mmol) and **HL2** (0.025 g, 0.110 mmol). An orange compound was obtained. Yield: 0.091 g (88%). <sup>1</sup>H NMR (400 MHz, CDCl<sub>3</sub>): δ 9.08 (s, H<sub>pyrazine</sub>), 8.37 (s, H<sub>pyrazine</sub>), 8.26 (dd, <sup>3</sup>J<sub>HH</sub> = 4.0 Hz, H<sub>pyrazine</sub>), 7.56 (t, <sup>3</sup>J<sub>HH</sub> = 3.0 Hz, H<sub>pyrazine</sub>), 7.52 (s, 2H<sub>benzothiole</sub>), 7.29 (d, <sup>3</sup>J<sub>HH</sub> = 8.0 Hz, 2H<sub>benzothiole</sub>), 7.25-7.23 (m, 13H), 7.18 – 7.14 (m, 12H). <sup>13</sup>C{<sup>1</sup>H} NMR (101 MHz, CDCl<sub>3</sub>) <sup>13</sup>C{<sup>1</sup>H} NMR (101 MHz, CDCl<sub>3</sub>): δ; 198.1(C<sub>Ru≡CO</sub>), 168.2(C<sub>pyrazine</sub>), 165.5(C<sub>benzoimidazole</sub>), 149.7(C<sub>pyrazine</sub>), 148.7(C<sub>pyrazine</sub>), 148.4(C<sub>pyrazine</sub>), 147.2 (C<sub>benzoimidazole</sub>), 146.9 (C<sub>benzoimidazole</sub>), 133.8(C<sub>benzoimidazole</sub>), 126.0(C<sub>PPh<sub>3</sub></sub>), 123.1(C<sub>PPh<sub>3</sub></sub>), 121.8(C<sub>PPh<sub>3</sub></sub>), 120.4(C<sub>PPh<sub>3</sub></sub>). <sup>31</sup>P{<sup>1</sup>H} NMR (162 MHz, CDCl<sub>3</sub>) δ: 42.7 (s). FT-IR spectrum (Zn-

Se ATR,  $\text{cm}^{-1}$ ): 1935 ( $\nu\text{C}\equiv\text{O}$ )<sub>Ru-CO</sub>, 1629 ( $\nu\text{C}=\text{O}$ )<sub>amidate</sub>, 1562 ( $\nu\text{C}=\text{N}$ )<sub>pyrazine</sub>. LC-MS:  $m/z(\%)$ ; Calcd. 927.12; Found 894.09 [ $\text{M}^+-\text{Cl}$ , 100%]. Anal. Calcd. for:  $\text{C}_{49}\text{H}_{38}\text{ClN}_5\text{O}_2\text{P}_2\text{Ru}$ : C, 63.47; H, 4.13; N, 7.55. Found: C, 63.96; H, 4.07; N, 6.65.

#### 2.7.4. [Ru(L2)(CO)H(PPh<sub>3</sub>)<sub>2</sub>] (Ru4)

[RuH<sub>2</sub>(CO)(PPh<sub>3</sub>)<sub>3</sub>] (0.100 g, 0.110 mmol) and the corresponding ligand (**HL2**) (0.026 g, 0.110 mmol). Single crystals viable for single crystal X-ray analysis were obtained by slow diffusion of diethyl ether into solution of **Ru4** in CH<sub>2</sub>Cl<sub>2</sub>. A yellow compound was obtained. Yield: 0.072 g (75%). <sup>1</sup>H NMR (400 MHz, CDCl<sub>3</sub>)  $\delta_{\text{H}}$ : -13.12 (t, <sup>2</sup> $J_{\text{H-P}}$  = 20.1 Hz, H<sub>Ru-H</sub>), 11.71 (s, H), 9.08 (s, H<sub>pyrazine</sub>), 8.37 (s, H<sub>pyrazine</sub>), 8.25 (d, <sup>3</sup> $J_{\text{HH}}$  = 2.9 Hz, H<sub>pyrazine</sub>), 7.54 (m, 13H), 7.29 (s, 2H), 7.28 – 7.21 (m, 12H), 7.19 – 7.13 (m, 7H). <sup>13</sup>C{<sup>1</sup>H} NMR (126 MHz, CDCl<sub>3</sub>)  $\delta$ : 167.1(C<sub>carbonyl</sub>), 155.7(C<sub>benzimidazole</sub>), 150.5(C<sub>pyrazine</sub>), 149.5(C<sub>pyrazine</sub>), 149.0(C<sub>pyrazine</sub>), 147.7(C<sub>pyrazine</sub>), 146.9(C<sub>benzimidazole</sub>), 145.0(C<sub>benzimidazole</sub>), 144.3(C<sub>benzimidazole</sub>), 126.8(2C<sub>benzimidazole</sub>), 125.9(2C<sub>benzimidazole</sub>), 124.5(C<sub>PPh3</sub>), 123.4(C<sub>PPh3</sub>), 122.4(C<sub>PPh3</sub>), 121.3(C<sub>PPh3</sub>). <sup>31</sup>P{<sup>1</sup>H} NMR (162 MHz, CDCl<sub>3</sub>)  $\delta$  23.2 (s). FT-IR spectrum (Zn-Se ATR,  $\text{cm}^{-1}$ ): 1946 ( $\nu\text{C}\equiv\text{O}$ )<sub>Ru-CO</sub>, 1622 ( $\nu\text{C}=\text{O}$ )<sub>amidate</sub>, 1569 ( $\nu\text{C}=\text{N}$ )<sub>pyrazine</sub>. LC-MS:  $m/z(\%)$ , Calcd 893.11; Found 892.12 [ $\text{M}^+-\text{H}$ , 100]. Anal. Calcd. for:  $\text{C}_{49}\text{H}_{38}\text{ClN}_5\text{O}_2\text{P}_2\text{Ru}$ : C, 63.46; H, 4.13; N, 7.55. Found: C, 62.91; H, 4.48; N, 6.37.

### 2.8. Synthesis and characterisation of carbonyl-ruthenium(II) complexes of phenyl-dipicolinamide ligands, (Ru5-Ru7)

#### 2.8.1. [Ru<sub>2</sub>(H<sub>2</sub>L3)(PPh<sub>3</sub>)<sub>4</sub>(CO)<sub>2</sub>][2Cl] (Ru5)

To a solution of [RuHCl(CO)(PPh<sub>3</sub>)<sub>3</sub>] (0.10 g, 0.11 mmol) in methanol (30 ml) a solution of **H<sub>2</sub>L3** (0.02 g, 0.05 mmol) was added, and the suspension was refluxed for 18 h to obtain an orange solution. The resulting solution was evaporated, and the crude compound was dissolved

in dichloromethane (30 mL), filtered over a bed of celites and then concentrated to about 3 mL. Diethyl ether (3x 10 mL) was added to afford a yellow suspension which was filtered, and washed with diethyl ether (15 mL) and dried in a vacuum to obtain a pale-yellow compound. Recrystallisation in the combination of dichloromethane and diethyl ether (1/2) afforded a yellow crystal suitable for single-crystal X-ray crystallography. Yield: 0.05 g (55%).  $^1\text{H}$  NMR (400 MHz,  $\text{CDCl}_3$ ): 11.78 (s,  $\text{H}_{\text{amide}}$ ), 11.70 (s,  $\text{H}_{\text{amide}}$ ), 8.65 (m,  $^3J_{\text{HH}} = 5.6$  Hz,  $2\text{H}_{\text{pyridine}}$ ), 8.44 (dd,  $^3J_{\text{HH}} = 6.4$  Hz,  $2\text{H}_{\text{pyridine}}$ ), 8.19 (t,  $^3J_{\text{HH}} = 6.4$  Hz,  $\text{H}_{\text{pyridine}}$ ), 8.09 (d,  $^3J_{\text{HH}} = 6.4$  Hz,  $\text{H}_{\text{pyridine}}$ ), 8.09 (d,  $^3J_{\text{HH}} = 6.4$  Hz,  $\text{H}_{\text{pyridine}}$ ), 7.94 (d,  $^3J_{\text{HH}} = 10$  Hz,  $2\text{H}_{\text{benzene}}$ ), 7.69-7.27 (cluster of 45H  $\text{PPh}_3$ ), 7.19-7.16 (multiplets,  $4\text{H}_{\text{benzene}}$ ).  $^{13}\text{C}$  NMR (101 MHz,  $\text{CDCl}_3$ )  $\delta$ : 166.2 ( $\text{C}_{\text{carbonyl}}$ ), 149.6 ( $\text{C}_{\text{pyridine}}$ ), 149.9 ( $\text{C}_{\text{pyridine}}$ ), 149.0 ( $\text{C}_{\text{pyridine}}$ ), 138.6 ( $\text{C}_{\text{pyridine}}$ ), 137.2 ( $\text{C}_{\text{pyridine}}$ ), 134.3 ( $\text{C}_{\text{benzene}}$ ), 133.6 ( $\text{C}_{\text{benzene}}$ ), 133.2- ( $\text{C}_{\text{benzene}}$ ), 132.5 ( $\text{C}_{\text{PPh}_3}$ ), 131.9 ( $\text{C}_{\text{PPh}_3}$ ), 130.4 ( $\text{C}_{\text{PPh}_3}$ ), 129.2 ( $\text{C}_{\text{PPh}_3}$ ), 127.6 ( $\text{C}_{\text{PPh}_3}$ ), 126.1 ( $\text{C}_{\text{PPh}_3}$ ), 125.7 ( $\text{C}_{\text{PPh}_3}$ ), 122.69 ( $\text{C}_{\text{PPh}_3}$ ).  $^{31}\text{P}$  NMR (162 MHz,  $d_6$ -DMSO): 45. (s). FT-IR ( $\text{cm}^{-1}$ ): ( $\nu_{\text{N-H}}$ ) $_{\text{amide}} = 3418$ ; ( $\nu_{\text{C=O}}$ ) $_{\text{amide}} = 1608$ . ESI LC-MS:  $m/z$  (%): 813 [ $\text{M}^+$ , 30], 813 [ $\text{M}^+ - (3\text{PPh}_3 + \text{CO})$ , 100]. Anal. Calcd for  $\text{C}_{90}\text{H}_{74}\text{Cl}_2\text{N}_4\text{O}_2\text{P}_4\text{Ru}_2$ : C, 65.41; H, 4.43; N, 5.21. Found: C, 65.36; H, 4.28; N, 4.98.

Complexes **Ru6** and **Ru7** were synthesised by following similar protocols as described for **Ru5**.

### 2.8.2. [ $\text{Ru}_2(\text{HL4})(\text{CO})_2\text{Cl}_2(\text{PPh}_3)_3$ ] (**Ru6**)

A solution of  $\text{RuHCl}(\text{CO})(\text{PPh}_3)_3$  (0.100 g, 0.105 mmol) and **H<sub>2</sub>L4** (0.02 g, 0.05 mmol). Yellow solid. Yield = 0.02 g (78%).  $^1\text{H}$  NMR (400 MHz,  $\text{CDCl}_3$ ): 11.39 (s,  $\text{H}_{\text{amide}}$ ), 11.21 (s,  $\text{H}_{\text{amide}}$ ), 10.83 (d,  $^3J_{\text{HH}} = 5.6$  Hz,  $\text{H}_{\text{pyridine}}$ ), 8.82 (t,  $^3J_{\text{HH}} = 6.4$  Hz,  $\text{H}_{\text{pyridine}}$ ), 8.46 (t,  $^3J_{\text{HH}} = 6.4$  Hz,  $\text{H}_{\text{pyridine}}$ ), 8.26 (d,  $^3J_{\text{HH}} = 6.4$  Hz,  $\text{H}_{\text{pyridine}}$ ), 8.14 (dd,  $^3J_{\text{HH}} = 10$  Hz,  $2\text{H}_{\text{pyridine}}$ ), 7.63-7.25 (m, 45H  $\text{PPh}_3$ ), 7.10-7.04 (m,  $4\text{H}_{\text{benzene}}$ ).  $^{13}\text{C}\{^1\text{H}\}$  NMR (101 MHz,  $\text{CDCl}_3$ )  $\delta$ :  $^{13}\text{C}\{^1\text{H}\}$  NMR (101



MHz, CDCl<sub>3</sub>)  $\delta$ (ppm): 197.8(C<sub>C=O</sub>), 195.9(C<sub>C $\equiv$ O</sub>), 167.0(C<sub>carbonyl</sub>), 165.1(C<sub>carbonyl</sub>), 147.8(C<sub>pyridine</sub>), 146.4(C<sub>pyridine</sub>), 145.4(C<sub>pyridine</sub>), 133.8(C<sub>pyridine</sub>), 133.7(C<sub>pyridine</sub>), 132.8(C<sub>benzene</sub>), 132.6(C<sub>benzene</sub>), 128.6(C<sub>benzene</sub>), 128.4(C<sub>PPh<sub>3</sub></sub>), 122.1(C<sub>PPh<sub>3</sub></sub>), 120.8 (C<sub>PPh<sub>3</sub></sub>). <sup>31</sup>P{<sup>1</sup>H} NMR (101 MHz, CDCl<sub>3</sub>)  $\delta$ : 45 (s). ESI LC-MS: m/z (%) at 971[M-Cl<sup>+</sup>, 70%]. FT-IR (cm<sup>-1</sup>): (ν<sub>N-H</sub>)<sub>amide</sub> = 3334; (ν<sub>C=O</sub>)<sub>amide</sub> = 1646. ESI-MS: m/z (%) at 971 [M<sup>+</sup>- Cl, 70]. FT-IR (cm<sup>-1</sup>): (ν<sub>N-H</sub>)<sub>amide</sub> = 3334; (ν<sub>C=O</sub>)<sub>amide</sub> = 1646. Anal. Calcd for C<sub>54</sub>H<sub>44</sub>ClN<sub>4</sub>O<sub>2</sub>P<sub>2</sub>Ru: C, 62.52; H, 4.22; N, 3.17. Found: C, 61.26; H, 4.96; N, 3.13.

### 2.8.3. [Ru(HL4)Cl{(CO)(PPh<sub>3</sub>)<sub>2</sub>}]<sub>2</sub> (Ru7)

A solution of [RuHCl(CO)(PPh<sub>3</sub>)<sub>3</sub>] (0.10 g, 0.11 mmol) in ethanol (15 mL) and **H<sub>2</sub>L4** (0.02 g, 0.11 mmol) were refluxed for 18 h. A yellow solution was obtained. To the yellow solution [RuHCl(CO)(PPh<sub>3</sub>)<sub>3</sub>] (0.10 g, 0.11 mmol) was added and allowed to reflux for the next 18 h. A green compound was obtained. Yield = 0.08 g (85%). <sup>1</sup>H NMR (400 MHz, (*d*-CDCl<sub>3</sub>, 25 °C),  $\delta$  (ppm): <sup>1</sup>H NMR (400 MHz, CDCl<sub>3</sub>)  $\delta$ (ppm): 13.07 (s, 1H<sub>amide</sub>), 12.89 (s, H<sub>amide</sub>), 11.00 (m, <sup>3</sup>J<sub>HH</sub> = 5.6 Hz, H<sub>pyridine</sub>), 9.51 (d, <sup>3</sup>J<sub>HH</sub> = 6.4Hz, H<sub>pyridine</sub>), 8.66(t, <sup>3</sup>J<sub>HH</sub> = 5.6Hz, H<sub>pyridine</sub>) 8.47(d, <sup>3</sup>J<sub>HH</sub> = 7.2Hz, H<sub>pyridine</sub>), 8.35 (d, <sup>3</sup>J<sub>HH</sub> = 6.4Hz, H<sub>pyridine</sub>), 8.23 (d, <sup>3</sup>J<sub>HH</sub> = 7.2Hz, H<sub>pyridine</sub>), 7.83-7.26 (m, 45H PPh<sub>3</sub>), 7.19-7.16 (m, 4H<sub>benzene</sub>). <sup>13</sup>C{<sup>1</sup>H} NMR spectrum (101 MHz, CDCl<sub>3</sub>-*d*, 25 °C):  $\delta$ (ppm): <sup>13</sup>C{<sup>1</sup>H} NMR (101 MHz, CDCl<sub>3</sub>)  $\delta$ : 164.6(C<sub>carbonyl</sub>), 161.2(C<sub>carbonyl</sub>), 156.8(C<sub>pyridine</sub>), 153.8(C<sub>pyridine</sub>), 148.1(C<sub>pyridine</sub>), 147.8(C<sub>pyridine</sub>), 145.4(C<sub>pyridine</sub>), 144.5(C<sub>pyridine</sub>), 143.1(C<sub>pyridine</sub>), 137.1(C<sub>pyridine</sub>), 133.8(C<sub>pyridine</sub>), 133.5(C<sub>pyridine</sub>), 132.8(C<sub>pyridine</sub>), 132.2(C<sub>benzene</sub>), 131.5(C<sub>benzene</sub>), 129.3(C<sub>benzene</sub>), 128.9(C<sub>benzene</sub>), 127.3(C<sub>benzene</sub>), 127.5(C<sub>benzene</sub>), 127.1(C<sub>PPh<sub>3</sub></sub>), 122.7(C<sub>PPh<sub>3</sub></sub>), 122.1(C<sub>PPh<sub>3</sub></sub>), 121.5(C<sub>PPh<sub>3</sub></sub>), 120.5(C<sub>PPh<sub>3</sub></sub>). <sup>31</sup>P{<sup>1</sup>H} NMR spectrum (160 MHz, *d*-CDCl<sub>3</sub>, 25 °C): 23.2. ESI -MS: m/z (%) (+ve mode): 1073 [M<sup>+</sup>-Cl, 100]<sup>+</sup>. Anal. Calcd for C<sub>54</sub>H<sub>44</sub>ClN<sub>4</sub>O<sub>2</sub>P<sub>2</sub>Ru: C, 62.06; H, 4.01; N, 3.91. Found: C, 62.11; H, 4.13; N, 3.87.

#### 2.8.4. [(RuHCO{PPh<sub>3</sub>})<sub>2</sub>(H<sub>2</sub>L5)][2Cl] (Ru5b)

To a solution of **Ru5** (0.10 g, 0.06 mmol) in isopropoxide (10 ml), potassium *tert*-butoxide (0.01 g, 0.01 mmol) mixed and refluxed for 6 h to obtain a lemon green solution. The resulting solution was evaporated, and the crude product was dissolved in dichloromethane (30 mL), filtered over a bed of celites and then concentrated to about 3 mL. Diethyl ether (10 mL) was added to afford a yellow suspension, filtered, washed with diethyl ether (15 mL) and dried in a vacuum. A lemon green compound was afforded. Recrystallisation in dichloromethane/diethyl ether solution gave crystals suitable for single crystal X-ray analyses. Yield: 0.06 g (62%). <sup>1</sup>H NMR (400 MHz, CDCl<sub>3</sub>, 25 °C), δ (ppm): 13.68 (s, 1H<sub>amide</sub>), 13.53(s, 1H<sub>amide</sub>), 9.57 (d, <sup>3</sup>J<sub>HH</sub> = 5.6 Hz, 2H<sub>pyridine</sub>), 8.66 (dd, <sup>3</sup>J<sub>HH</sub> = 6.4Hz, 2H<sub>pyridine</sub>), 8.47(t, <sup>3</sup>J<sub>HH</sub> = 6.4H, 1H<sub>pyridine</sub>), 8.35(d, <sup>3</sup>J<sub>HH</sub> = 6.4Hz, 1H<sub>pyridine</sub>), 8.23 (d, <sup>3</sup>J<sub>HH</sub> = 6.4H, 1H<sub>pyridine</sub>), 7.48 (d, <sup>3</sup>J<sub>HH</sub> = 10 Hz, 2H<sub>benzene</sub>), 7.14 (d, <sup>3</sup>J<sub>HH</sub> = 10 Hz, 2H<sub>benzene</sub>), 6.96-6.43 (m, 60H, PPh<sub>3</sub>), 10.21(t, <sup>2</sup>J<sub>P-H</sub> = 11.6 Hz, H<sub>Ru-H</sub>) and 15.97(t, <sup>2</sup>J<sub>P-H</sub> = 14.8 Hz, H<sub>Ru-H</sub>). <sup>13</sup>C{<sup>1</sup>H} NMR (101 MHz, CDCl<sub>3</sub>) δ(ppm): 163.2(C<sub>carbonyl</sub>); 149.8(C<sub>pyridine</sub>); 148.2(C<sub>pyridine</sub>); 137.4(C<sub>pyridine</sub>); 134.3(C<sub>benzene</sub>); 133.6(C<sub>benzene</sub>); 133.7 (C<sub>benzene</sub>); 133.5(C<sub>PPh<sub>3</sub></sub>); 132.4(C<sub>PPh<sub>3</sub></sub>); 131.9(C<sub>PPh<sub>3</sub></sub>); 130.4(C<sub>PPh<sub>3</sub></sub>); 129.2(C<sub>PPh<sub>3</sub></sub>); 127.6(C<sub>PPh<sub>3</sub></sub>); 126.1 (C<sub>PPh<sub>3</sub></sub>); 125.7(C<sub>PPh<sub>3</sub></sub>); 122.7(C<sub>PPh<sub>3</sub></sub>). <sup>31</sup>P{<sup>1</sup>H} NMR (162 MHz, *d*-CDCl<sub>3</sub>), δ (ppm): 46.0 (s). LR ESI -MS *m/z* (%) (+ve mode): 1627 [M-H, 100%]<sup>+</sup>. Anal. Calcd. for C<sub>92</sub>H<sub>78</sub>N<sub>4</sub>O<sub>4</sub>P<sub>4</sub>Ru<sub>2</sub>·0.5CH<sub>2</sub>Cl<sub>2</sub>: C, 66.44; H, 4.76; N, 3.35. Found: C, 66.69; H, 4.65; N, 3.75.

#### 2.8.5. [{Ru(η<sup>6</sup>-*p*-cymene)<sub>2</sub>-μ-Cl]<sub>2</sub>L4] [RuCl<sub>3</sub>(η<sup>6</sup>-*p*-cymene)] (Ru8)

To solution of dichloro-ruthenium *p*-cymene dimer, [Ru(η<sup>6</sup>-*p*-cymene)Cl<sub>2</sub>]<sub>2</sub> (0.10 g, 0.16 mmol) in the mixed methanol and chloroform (1/1, 10/10 mL), **H<sub>2</sub>L4** (0.06 g, 0.16 mmol) and sodium methoxide, NaOMe (0.02 g, 0.32 mmol) were added, and the mixture was allowed to react at room temperature for 18 h. The resultant orange suspension was evaporated, and the

crude was dissolved and dichloromethane and filtered over celite. The filtrate is then concentrated, diethyl ether (20 mL) was added, filtered, and dried in vacuum. An orange compound was obtained. Yield: 0.16 g (86%).  $^1\text{H}$  NMR (400 MHz,  $\text{CDCl}_3$ )  $\delta$ : 9.40 (d,  $^3J_{\text{HH}} = 5.6$ ,  $2\text{H}_{\text{pyridine}}$ ), 8.28(t,  $^3J_{\text{HH}} = 7.6$ ,  $2\text{H}_{\text{pyridine}}$ ), 8.11(d,  $^3J_{\text{HH}} = 7.6$ ,  $2\text{H}_{\text{pyridine}}$ ), 7.88(t,  $^3J_{\text{HH}} = 8.0$ ,  $2\text{H}_{\text{pyridine}}$ ), 7.56(dd,  $^3J_{\text{HH}} = 3.6$ ,  $2\text{H}_{\text{benzene}}$ ), 7.27(dd,  $^3J_{\text{HH}} = 3.6$ ,  $2\text{H}_{\text{benzene}}$ ), 5.62(d,  $^3J_{\text{HH}} = 4.4$  Hz,  $2\text{H}_{\text{pcymene}}$ ), 5.52(d,  $^3J_{\text{HH}} = 4.4$  Hz,  $2\text{H}_{\text{pcymene}}$ ), 5.30(d,  $^3J_{\text{HH}} = 4.4$  Hz,  $2\text{H}_{\text{pcymene}}$ ), 5.05(d,  $^3J_{\text{HH}} = 4.4$  Hz,  $2\text{H}_{\text{pcymene}}$ ), 2.12(m,  $^3J_{\text{HH}} = 6.8$  Hz,  $2\text{H}_{\text{pcymene}}$ ), 1.19 (s,  $6\text{-H}_{\text{pcymene}}$ ), 0.98 (d,  $^3J_{\text{HH}} = 6.8$  Hz,  $6\text{H}_{\text{pcymene}}$ ), 0.81 (d,  $^3J_{\text{HH}} = 6.8$ ,  $6\text{H}_{\text{pcymene}}$ ).  $^{13}\text{C}\{^1\text{H}\}$  NMR (101 MHz,  $\text{CDCl}_3$ )  $\delta$ : 162.8, 154.1, 143.7, 139.2, 130.1, 128.9, 125.8, 124.9, 89.1, 81.4, 30.6, 22.1, 18.5. ESI-MS ( $m/z$ ) at 852 [ $\text{M}^+$ , 100%]. HR-MS (ESI):  $m/z$  823.0958 [ $\text{M}^+$ ], calcd for  $\text{C}_{38}\text{H}_{40}\text{N}_4\text{O}_2\text{ClO}_2\text{Ru}_2$  823.0927. FT-IR ( $\text{cm}^{-1}$ ): ( $\nu_{\text{C=O}}$ )<sub>amide</sub> = 1617.97; Anal. Calcd for  $\text{C}_{48}\text{H}_{54}\text{Cl}_4\text{N}_4\text{O}_2\text{Cl}_4\text{Ru}_3$ : C, 49.53; H, 4.68; N, 4.81. Found: C, 49.33.; H, 4.71; N, 4.57.

#### 2.8.6. [ $\{\text{Ru}(\eta^6\text{-}p\text{-cymene})_2\text{-}\mu\text{-Cl}\}_2\text{L4}\}\text{[PF}_6\text{]} (\text{Ru9})$

To solution of dichloro-ruthenium *p*-cymene dimer,  $[\text{Ru}(\eta^6\text{-}p\text{-cymene})\text{Cl}_2]_2$  (0.10 g, 0.16 mmol) in the mixed methanol and chloroform (1/1, 10/10 mL), **H<sub>2</sub>L4** (0.06 g, 0.16 mmol) and sodium methoxide, NaOMe (0.01 g, 0.32 mmol) were added, and the mixture was allowed to react at room temperature for 12 h.  $\text{KPF}_6$  (0.03 g, 0.16 mmol) was added and solution was stirred for 6 h. The resultant orange suspension was evaporated, and the crude was dissolved and dichloromethane and filtered over celite. The filtered is then concentrated, diethyl ether (20 mL) was added, filtered, and dried in vacuum. An orange compound was obtained. An orange compound was obtained. Yield: 0.14 g (88%).  $^1\text{H}$  NMR (400 MHz,  $\text{CDCl}_3$ )  $\delta$ : 9.40 (d,  $^3J_{\text{HH}} = 5.6$ ,  $2\text{H}_{\text{pyridine}}$ ), 8.28(t,  $^3J_{\text{HH}} = 7.6$ ,  $2\text{H}_{\text{pyridine}}$ ), 8.11(d,  $^3J_{\text{HH}} = 7.6$ ,  $2\text{H}_{\text{pyridine}}$ ), 7.87(t,  $^3J_{\text{HH}} = 8.0$ ,  $2\text{H}_{\text{pyridine}}$ ), 7.56(dd,  $^3J_{\text{HH}} = 3.6$ ,  $2\text{H}_{\text{benzene}}$ ),

7.26(dd,  $^3J_{\text{HH}} = 3.6$ , 2H<sub>benzene</sub>), 5.61(d,  $^3J_{\text{HH}} = 4.4$  Hz, 2H<sub>pcymene</sub>), 5.52(d,  $^3J_{\text{HH}} = 4.4$  Hz, 2H<sub>pcymene</sub>), 5.34(d,  $^3J_{\text{HH}} = 4.4$  Hz, 2H<sub>pcymene</sub>), 5.05(d,  $^3J_{\text{HH}} = 4.4$  Hz, 2H<sub>pcymene</sub>), 2.12(m,  $^3J_{\text{HH}} = 6.8$  Hz, 2H<sub>pcymene</sub>), 1.49 (s, 6-H<sub>pcymene</sub>), 0.98(d,  $^3J_{\text{HH}} = 6.8$ , 6H<sub>pcymene</sub>), 0.80 (d,  $^3J_{\text{HH}} = 6.8$ , 6H<sub>pcymene</sub>).  $^{13}\text{C}\{^1\text{H}\}$  NMR (101 MHz, CDCl<sub>3</sub>)  $\delta$ : 162.6, 154.1, 143.7, 139.2, 130.2, 128.9, 125.8, 124.9, 81.6, 30.6, 22.1, 18.7. ESI-MS (m/z); 823 [M<sup>+</sup>, 100%]. HR-MS (ESI): m/z 823.0958 [M<sup>+</sup>], calcd for C<sub>38</sub>H<sub>40</sub>N<sub>4</sub>O<sub>2</sub>ClO<sub>2</sub>Ru<sub>2</sub> 823.0927. FT-IR (cm<sup>-1</sup>): (ν<sub>C=O</sub>)<sub>amidate</sub> = 1618.76. Anal. Calcd for C<sub>38</sub>H<sub>40</sub>ClN<sub>4</sub>O<sub>2</sub>Ru<sub>2</sub>PF<sub>6</sub>: C, 47.18; H, 4.17; N, 5.79. Found: C, 47.31; H, 3.94; N, 5.42.

#### 2.8.7. [{Ru(η<sup>6</sup>-p-cymene)<sub>2</sub>-μ-Cl]<sub>2</sub>L5][PF<sub>6</sub>] (Ru10)

A [Ru(η<sup>6</sup>-p-cymene)Cl<sub>2</sub>]<sub>2</sub> (0.10 g, 0.16 mmol), methanol and chloroform (1/1, 10/10 mL), **H<sub>2</sub>L5** (0.06 g, 0.16 mmol), sodium methoxide, (0.009 g, 0.16 mmol). and KPF<sub>6</sub> (0.02 g, 0.16 mmol). An orange compound was obtained. Yield: 0.13 g (88%).  $^1\text{H}$  NMR (400 MHz, CDCl<sub>3</sub>)  $\delta$ : 9.40 (d,  $^3J_{\text{HH}} = 5.2$  Hz, 2H<sub>pyridine</sub>), 8.28(t,  $^3J_{\text{HH}} = 7.2$  Hz, 2H<sub>pyridine</sub>), 8.08(d,  $^3J_{\text{HH}} = 7.6$  Hz, 2H<sub>pyridine</sub>), 7.80(t,  $^3J_{\text{HH}} = 8.0$  Hz, 2H<sub>pyridine</sub>), 7.30(s, 2H<sub>benzene</sub>), 5.61(d,  $^3J_{\text{HH}} = 4.4$  Hz, 2H<sub>p-cymene</sub>), 5.49(d,  $^3J_{\text{HH}} = 4.4$  Hz, 2H<sub>p-cymene</sub>), 5.38(d,  $^3J_{\text{HH}} = 4.4$  Hz, 2H<sub>p-cymene</sub>), 5.05(d,  $^3J_{\text{HH}} = 4.4$  Hz, 2H<sub>p-cymene</sub>), 2.12(m,  $^3J_{\text{HH}} = 6.6$  Hz, 2H<sub>p-cymene</sub>), 3.31 (s, CH<sub>3</sub>), 2.32 (s, 6H<sub>p-cymene</sub>), 0.98(d,  $^3J_{\text{HH}} = 6.6$ , 6H<sub>p-cymene</sub>), 0.80 (d,  $^3J_{\text{HH}} = 6.6$ , 6H<sub>p-cymene</sub>).  $^{13}\text{C}\{^1\text{H}\}$  NMR (101 MHz, CDCl<sub>3</sub>)  $\delta$ : 162.5, 154.5, 141.0, 139.3, 133.3, 130.5, 129.0, 126.4, 125.9, 81.3, 36.4, 31.4, 24.1, 19.6. ESI-MS: m/z(%); 851 [M<sup>+</sup>, 100]. HR-MS (ESI): m/z(%); 851.127 [M<sup>+</sup>, 100], calcd for C<sub>40</sub>H<sub>44</sub>N<sub>4</sub>O<sub>2</sub>ClO<sub>2</sub>Ru<sub>2</sub> 81.1240. FT-IR (cm<sup>-1</sup>): (ν<sub>C=O</sub>)<sub>amidate</sub> = 1620. Anal. Calcd for C<sub>40</sub>H<sub>44</sub>ClN<sub>4</sub>O<sub>2</sub>Ru<sub>2</sub>PF<sub>6</sub>: C, 46.61; H, 4.30; N, 5.44. Found: C, 46.28; H, 4.42; N, 5.37.

### 2.8.8. [ $\{\text{Ru}(\eta^6\text{-p-cymene})_2\mu\text{-Cl}\}_2\text{L6}\}\text{[PF}_6\text{]}$ (**Ru11**)

A [ $\text{Ru}(\eta^6\text{-p-cymene})\text{Cl}_2$ ]<sub>2</sub> (0.10 g, 0.16 mmol), methanol and chloroform (1/1, 10/10 mL), **H<sub>2</sub>L6** (0.06 g, 0.16 mmol), sodium methoxide, (0.009 g, 0.16 mmol) and KPF<sub>6</sub> (0.02 g, 0.16 mmol). An orange compound was obtained. Yield: 0.13 g (88%). <sup>1</sup>H NMR (400 MHz, CDCl<sub>3</sub>) δ: 9.41 (m, 2H<sub>pyridine</sub>), 8.26(m, 2H<sub>pyridine</sub>), 8.13(m, 2H<sub>pyridine</sub>), 7.78(m, 2H<sub>pyridine</sub>), 7.46(d, <sup>3</sup>J<sub>HH</sub> = 4.6 Hz, 2H<sub>benzene</sub>), 7.08(d, <sup>3</sup>J<sub>HH</sub> = 4.6 Hz, 2H<sub>benzene</sub>), 7.06(s, 1H<sub>benzene</sub>), 5.61(d, <sup>3</sup>J<sub>HH</sub> = 4.6Hz, 2H<sub>p-cymene</sub>), 5.49(d, <sup>3</sup>J<sub>HH</sub>=4.4 Hz, 2H<sub>p-cymene</sub>), 5.38(d, <sup>3</sup>J<sub>HH</sub> = 4.4 Hz, 2H<sub>p-cymene</sub>), 5.05(d, <sup>3</sup>J<sub>HH</sub> = 4.4 Hz, 2H<sub>p-cymene</sub>), 2.12(m, <sup>3</sup>J<sub>HH</sub> = 6.6 Hz, 2H<sub>p-cymene</sub>), 3.31 (s, OCH<sub>3</sub>), 2.32 (s, 6H<sub>p-cymene</sub>), 0.98(d, <sup>3</sup>J<sub>HH</sub> = 6.6, 6H<sub>p-cymene</sub>), 0.80 (d, <sup>3</sup>J<sub>HH</sub> = 6.6, 6H<sub>p-cymene</sub>). <sup>13</sup>C{<sup>1</sup>H} NMR (101 MHz, CDCl<sub>3</sub>) δ: 169.5, 155.4, 141.0, 154.2, 144.8, 140.6, 137.4, 129.3, 128.4, 126.6, 115.09, 110.7, 86.8, 82.8, 81.3, 55.6, 20.7, 23.1, 20.9, 18.1. ESI-MS: m/z(%); 823 [M<sup>+</sup>, 100]. FT-IR (cm<sup>-1</sup>): (ν<sub>C=O</sub>)<sub>amide</sub> = 1619.11. Anal. Calcd for C<sub>40</sub>H<sub>44</sub>Cl<sub>2</sub>N<sub>4</sub>O<sub>3</sub>Ru<sub>2</sub>PF<sub>6</sub>: C, 46.97; H, 4.24; N, 5.62. Found: C, 46.21; H, 4.38; N, 5.81.

## 2.9. Synthesis and characterisation of dinuclear Ru(II) complexes of *N*-pyrazyl/Pyridyl(quinolin-8-yl)pyrazine-2-carboxamide ligands (**Ru12-Ru15**)

Complexes **Ru12-Ru15** were synthesised by following the synthetic procedure described for complex **Ru8**.

### 2.9.1. [ $\{\text{Ru}(\eta^6\text{p-cymene})\text{Cl}\}_2(\text{L10})\}$ (**Ru12**)

To a solution of [ $\text{Ru}(\eta^6\text{-p-cymene})\text{Cl}_2$ ]<sub>2</sub> (0.05 g, 0.08 mmol) in the mixed methanol and chloroform (1/1, 10/10 mL), pyrazine-2-carboxylic acid (**HL10**) (0.01 g, 0.08 mmol) and sodium methoxide, (0.004 g, 0.08 mmol) were added, and the suspension was allowed to react

at room temperature for 12 h. The resulting solution was filtered over celite then filtrate was concentrated, and diethyl ether (30 mL) was added. The suspension was filtered and dried in vacuum. An orange compound was obtained. Yield: 0.05 g (86%).  $^1\text{H}$  NMR (400 MHz,  $\text{CDCl}_3$ )  $\delta$ : 9.43(dd,  $^3J_{\text{HH}} = 1.2$  Hz,  $\text{H}_{\text{pyrazine}}$ ), 8.98(d,  $^3J_{\text{HH}} = 3.2$  Hz,  $\text{H}_{\text{pyrazine}}$ ), 8.92(d,  $^3J_{\text{HH}} = 1.2$  Hz,  $\text{H}_{\text{pyrazine}}$ ), 5.91(d,  $^3J_{\text{HH}} = 6.4$  Hz,  $2\text{H}_{p\text{-cymene}}$ ), 5.83(d,  $^3J_{\text{HH}} = 6.4$  Hz,  $2\text{H}_{p\text{-cymene}}$ ), 2.78(m,  $^3J_{\text{HH}} = 6.8$  Hz,  $2\text{H}_{p\text{-cymene}}$ ), 2.16(s,  $3\text{H}_{\text{methyl}}$ ), 2.09(s,  $3\text{H}_{\text{methyl}}$ ), 1.21(d,  $^3J_{\text{HH}} = 7.0$  Hz,  $3\text{H}_{\text{methyl}}$ ), 1.16(d,  $^3J_{\text{HH}} = 7.0$  Hz,  $3\text{H}_{\text{methyl}}$ ).  $^{13}\text{C}$  NMR (101 MHz,  $\text{CDCl}_3$ )  $\delta$ : 169.7(s,  $1\text{C}_{\text{carbonyl}}$ ), 149.2(s,  $1\text{C}_{\text{pyrazine}}$ ), 148.5(s,  $\text{C}_{\text{pyrazine}}$ ), 146.7 (s,  $\text{C}_{\text{pyrazine}}$ ), 144.8(s,  $\text{C}_{\text{pyrazine}}$ ), 143(s,  $\text{C}_{\text{pyrazine}}$ ), 106(s,  $\text{C}_{p\text{-cymene}}$ ), 102.3(s,  $\text{C}_{p\text{-cymene}}$ ), 100.5(s,  $\text{C}_{p\text{-cymene}}$ ), 86.8(s,  $2\text{C}_{p\text{-cymene}}$ ), 83.2(s,  $2\text{C}_{p\text{-cymene}}$ ), 81.1(s,  $4\text{C}_{p\text{-cymene}}$ ), 79.6(s,  $4\text{C}_{p\text{-cymene}}$ ), 30.9(s,  $2\text{C}_{p\text{-cymene}}$ ), 22.0(s,  $4\text{C}_{p\text{-cymene}}$ ), 18.4(s,  $2\text{C}_{p\text{-cymene}}$ ). ESI-MS:  $m/z(\%)$ ; 664[ $\text{M}^+ - \text{Cl}$ , 100]. HR-MS:  $m/z(\%)$ ; 662 [ $\text{M}^+ - \text{Cl}$ , 100], FT-IR ( $\text{cm}^{-1}$ ): ( $\nu_{\text{C=O}}$ ) $_{\text{Carboxylic}}$  = 1652. Anal. Calcd. for  $\text{C}_{25}\text{H}_{31}\text{Cl}_3\text{N}_2\text{O}_2\text{Ru}_2\cdot\text{CHCl}_3$ : C, 34.54; H, 3.54; N, 3.29. Found: C, 33.96; H, 2.97; N, 3.40.

## 2.9.2. [ $\{\text{Ru}(\eta^6 p\text{-cymene})\text{Cl}\}_2(\text{L7})\text{][PF}_6\text{]} (\text{Ru13})$

$[\text{RuCl}_2(\eta^6 p\text{-cymene})]_2$  (0.05 g, 0.08 mmol), *N*-(quinolin-8-yl)pyrazine-2-carboxamide (**H2L7**), (0.02 g, 0.08 mmol), and sodium methoxide (0.004 g, 0.08 mmol). A yellow compound was obtained. Yield: 0.05 g (77%).  $^1\text{H}$  NMR (400 MHz,  $\text{CDCl}_3$ )  $\delta$ : 9.28(s,  $\text{H}_{\text{pyrazine}}$ ), 9.17(d,  $^3J_{\text{HH}} = 5.2$  Hz,  $\text{H}_{\text{pyrazine}}$ ), 8.84 (d,  $^3J_{\text{HH}} = 5.6$  Hz,  $\text{H}_{\text{pyrazine}}$ ), 8.44(s,  $\text{H}_{\text{quinoline}}$ ), 8.25(d,  $^3J_{\text{HH}} = 7.6$  Hz,  $\text{H}_{\text{quinoline}}$ ), 7.81 (d,  $^3J_{\text{HH}} = 7.4$  Hz,  $\text{H}_{\text{quinoline}}$ ), 7.56 (t,  $^3J_{\text{HH}} = 6.3$  Hz,  $\text{H}_{\text{quinoline}}$ ), 7.46 (d,  $^3J_{\text{HH}} = 7.6$  Hz,  $\text{H}_{\text{quinoline}}$ ), 5.82(d,  $^3J_{\text{HH}} = 6.4$  Hz,  $2\text{H}_{p\text{-cymene}}$ ), 5.76(d,  $^3J_{\text{HH}} = 6.4$  Hz,  $2\text{H}_{p\text{-cymene}}$ ), 2.33(s,  $6\text{H}_{\text{methyl}}$ ), 2.86(m,  $^3J_{\text{HH}} = 6.7$  Hz,  $2\text{H}_{p\text{-cymene}}$ ), 1.21(s,  $3\text{H}_{\text{methyl}}$ ).  $^{13}\text{C}$  NMR (101 MHz,  $\text{CDCl}_3$ )  $\delta$ : 165.0(s,  $\text{C}_{\text{carbonyl}}$ ), 162.4(s,  $\text{C}_{\text{pyrazine}}$ ), 145.6(s,  $\text{C}_{\text{quinoline}}$ ), 144.8 (s,  $\text{C}_{\text{pyrazine}}$ ), 142.6(s,  $\text{C}_{\text{pyrazine}}$ ), 131.4(s,  $\text{C}_{\text{pyrazine}}$ ), 127.3(s,  $\text{C}_{\text{quinoline}}$ ), 127.1(s,  $\text{C}_{\text{quinoline}}$ ), 126.1(s,  $\text{C}_{\text{quinoline}}$ ), 125.9(s,  $\text{C}_{\text{quinoline}}$ ), 125.6(s,  $\text{C}_{\text{quinoline}}$ ), 101.2(s,  $\text{C}_{\text{quinoline}}$ ), 98.6(s,  $2\text{C}_{p\text{-cymene}}$ ), 86(s,  $2\text{C}_{p\text{-cymene}}$ ), 81(s,  $4\text{C}_{p\text{-cymene}}$ ),

30.6(s, 2C<sub>p-cymene</sub>), 22.1(s, 4C<sub>p-cymene</sub>), 18.9(s, 2C<sub>p-cymene</sub>). ESI-MS: m/z(%); 789 [M<sup>+</sup>, 100]. FT-IR (cm<sup>-1</sup>): (ν<sub>C=O</sub>)<sub>amide</sub> = 1615. Anal. Calcd for C<sub>50</sub>H<sub>52</sub>Cl<sub>5</sub>N<sub>8</sub>O<sub>2</sub>Ru<sub>3</sub>: C, 47.01; H, 4.10; N, 8.77. Found: C, 47.13; H, 4.19; N, 8.68

### 2.9.3. [RuCl(η<sup>6</sup> *p*-cymene)2(L8)][Ru(L8)Cl<sub>3</sub>] (Ru14)

[RuCl<sub>2</sub>(η<sup>6</sup> *p*-cymene)]<sub>2</sub> (0.05 g, 0.08 mmol), 5-methyl-*N*-(quinolin-8-yl)-picolinamide (**H<sub>2</sub>L8**) (0.02 g, 0.08 mmol), sodium methoxide (0.004 g, 0.08 mmol) and KPF<sub>6</sub> (0.01 g, 0.008 mmol). An orange compound was obtained. Yield: 0.06 g (88%). <sup>1</sup>H NMR (400 MHz, CDCl<sub>3</sub>) δ: 9.28(s, H<sub>pyrazine</sub>), 9.17(d, <sup>3</sup>J<sub>HH</sub> = 5.2 Hz H<sub>pyrazine</sub>), 8.84 (d, <sup>3</sup>J<sub>HH</sub> = 5.6 Hz, H<sub>pyrazine</sub>), 8.44(s, H<sub>quinoline</sub>), 8.25(d, <sup>3</sup>J<sub>HH</sub> = 7.6 Hz, H<sub>quinoline</sub>), 7.81 (d, <sup>3</sup>J<sub>HH</sub> = 7.4 Hz, H<sub>quinoline</sub>), 7.56 (t, <sup>3</sup>J<sub>HH</sub> = 6.3 Hz, H<sub>quinoline</sub>), 7.46 (d, <sup>3</sup>J<sub>HH</sub> = 7.6 Hz, H<sub>quinoline</sub>), 5.82(d, <sup>3</sup>J<sub>HH</sub> = 6.4 Hz, 2H<sub>p-cymene</sub>), 5.76(d, <sup>3</sup>J<sub>HH</sub> = 6.4 Hz, 2H<sub>p-cymene</sub>), 2.33(s, 6H C<sub>methyl</sub>), 2.86(m, <sup>3</sup>J<sub>HH</sub> = 6.7 Hz, 2H<sub>p-cymene</sub>), 1.21(s, 3H<sub>methyl</sub>). <sup>13</sup>C NMR (101 MHz, CDCl<sub>3</sub>) δ: 165.0(s, C<sub>carbonyl</sub>), 162.4(s, C<sub>pyrazine</sub>) 145.6(s, C<sub>quinoline</sub>), 144.8 (s, C<sub>pyrazine</sub>), 142.6(s, C<sub>pyrazine</sub>), 131.4(s, C<sub>pyrazine</sub>), 127.3(s, C<sub>quinoline</sub>), 127.1(s, C<sub>quinoline</sub>), 126.1(s, C<sub>quinoline</sub>), 125.9(s, C<sub>quinoline</sub>), 125.6(s, C<sub>quinoline</sub>), 101.2(s, C<sub>quinoline</sub>), 98.6(s, 2C<sub>p-cymene</sub>), 86(s, 2C<sub>p-cymene</sub>), 81(s, 4C<sub>p-cymene</sub>), 30.6(s, 2C<sub>p-cymene</sub>), 22.1(s, 4C<sub>p-cymene</sub>), 18.9(s, 2C<sub>p-cymene</sub>). ESI-MS: m/z(%); 789 [M<sup>+</sup>, 100]. FT-IR (cm<sup>-1</sup>): (ν<sub>C=O</sub>)<sub>amide</sub> = 1631; Anal. Calcd for C<sub>34</sub>H<sub>37</sub>Cl<sub>2</sub>N<sub>4</sub>ORu<sub>2</sub>PF<sub>6</sub>: C, 43.64; H, 3.99; N, 5.99. Found: C, 43.85; H, 3.79; N, 5.93.

### 2.9.4. [{RuCl(η<sup>6</sup> *p*-cymene)}<sub>2</sub>(L9)][PF<sub>6</sub>] (Ru15)

[RuCl<sub>2</sub> *p*-cymene]<sub>2</sub> (0.05 g, 0.08 mmol), methanol/chloroform (1/1, 10/10 mL), 5-chloro-*N*-(quinolin-8-yl)picolinamide (**H<sub>2</sub>L9**) (0.02 g, 0.08 mmol), sodium methoxide (0.004 g, 0.08 mmol) and KPF<sub>6</sub> (0.01 g, 0.008 mmol). An orange compound was obtained. Yield: 0.018 g (82%). <sup>1</sup>H NMR (400 MHz, CDCl<sub>3</sub>) δ: 8.43(dd, <sup>3</sup>J<sub>HH</sub> = 7.6 Hz, H<sub>pyridine</sub>), 8.12(d, <sup>3</sup>J<sub>HH</sub> = 7.6 Hz,

H<sub>pyridine</sub>), 8.09(d,  $^3J_{\text{HH}}=7.6$  Hz, H<sub>pyridine</sub>), 8.06(d,  $^3J_{\text{HH}}=7.6$  Hz, H<sub>pyridine</sub>), 7.98(d,  $^3J_{\text{HH}}=7.6$  Hz, H<sub>quinoline</sub>), 7.84(t,  $^3J_{\text{HH}}=7.4$  Hz, H<sub>quinoline</sub>), 7.64(d,  $^3J_{\text{HH}}=7.2$  Hz, H<sub>quinoline</sub>), 7.59(d,  $^3J_{\text{HH}}=7.6$  Hz, H<sub>quinoline</sub>), 7.12(d,  $^3J_{\text{HH}}=7.6$  Hz, H<sub>quinoline</sub>), 5.83(d,  $^3J_{\text{HH}}=6.4$  Hz, 2H<sub>*p*-cymene</sub>), 5.78(d,  $^3J_{\text{HH}}=6.4$  Hz, 2H<sub>*p*-cymene</sub>), 2.87(m,  $^3J_{\text{HH}}=6.8$  Hz, 2H<sub>*p*-cymene</sub>), 2.33(s, 6H<sub>*p*-cymene</sub>), 1.21(s, 3H<sub>*p*-cymene</sub>). ESI-MS:  $m/z(\%)$ : 825 [ $\text{M}^+$ , 100]. FT-IR ( $\text{cm}^{-1}$ ): ( $\nu_{\text{C=O}}$ )<sub>amide</sub> = 1634. Anal. Calcd for C<sub>34</sub>H<sub>36</sub>Cl<sub>3</sub>N<sub>4</sub>ORu<sub>2</sub>PF<sub>6</sub>: C, 42.09; H, 3.74; N, 5.78. Found: C, 42.16; H, 3.82; N, 5.69.

## 2.10. Synthesis and characterisation of dinuclear manganese(II) complexes of dipyridyl(phenylene)-dicarboxamides (Mn1-Mn4)

### 2.10.1. [Mn<sub>2</sub>(H<sub>2</sub>L3)<sub>2</sub>Cl<sub>4</sub>] (Mn1)

To a solution of MnCl<sub>2</sub>·4H<sub>2</sub>O (0.10 g, 0.51 mmol) in ethanol (15 mL), a solution of **H<sub>2</sub>L3** (0.10 g, 0.51 mmol) was added dropwise, and the resultant suspension was stirred at room temperature overnight. The crude product was filtered and washed with ethanol (15 mL) and diethyl (10 mL) ether. A light green compound was obtained. Yield = 0.40 g (90%). ESI-MS:  $m/z(\%)$ : 853 [ $\text{M}^+ - \text{Cl}$ , 100%]. FT-IR ( $\text{cm}^{-1}$ ): ( $\nu_{\text{C=O}}$ )<sub>amide</sub> = 1628. ( $\nu_{\text{N-H}}$ )<sub>amide</sub> = 3352.  $\mu_{\text{eff}}$  = 5.97 BM. Anal. Calcd for C<sub>38</sub>H<sub>28</sub>N<sub>8</sub>O<sub>4</sub>Mn<sub>2</sub>Cl<sub>4</sub>: C, 50.03; H, 3.09; N, 12.28. Found: C, 50.08; H, 3.11; N, 12.81.

### 2.10.2. [Mn<sub>2</sub>(H<sub>2</sub>L4)<sub>2</sub>Cl<sub>4</sub>] (Mn2)

MnCl<sub>2</sub>·4H<sub>2</sub>O (0.10 g, 0.51 mmol) and **H<sub>2</sub>L4** (0.16 g, 0.51 mmol). A yellow compound was obtained. Yield = 0.38 g (85%). ESI-MS:  $m/z(\%)$  852 [ $\text{M}^+ - \text{Cl}$ , 65]. FT-IR ( $\text{cm}^{-1}$ ): ( $\nu_{\text{C=O}}$ )<sub>amide</sub> = 1623. ( $\nu_{\text{N-H}}$ )<sub>amide</sub> = 3324.  $\mu_{\text{eff}}$  = 5.98 BM. Anal. Calcd for C<sub>38</sub>H<sub>28</sub>N<sub>8</sub>O<sub>4</sub>Mn<sub>2</sub>Cl<sub>4</sub>: C, 48.67; H, 3.18; N, 12.61. Found: C, 48.71; H, 3.22; N, 12.53.



### 2.10.3. [Mn<sub>2</sub>(H<sub>2</sub>L5)<sub>2</sub>Cl<sub>4</sub>] (Mn3)

MnCl<sub>2</sub>.4H<sub>2</sub>O (0.10 g, 0.51 mmol) and **H<sub>2</sub>L5** (0.18 g, 0.51 mmol). Yellow solid. Yield = 0.40 g (84%). ESI-MS: m/z(%); 907 [M<sup>+</sup> - Cl, 100]. FT-IR (cm<sup>-1</sup>): (νC=O)<sub>amide</sub>, = 1631. (νN-H)<sub>amide</sub> = 3402. μ<sub>eff</sub> = 5.97 BM. Anal. Calcd for C<sub>40</sub>H<sub>36</sub>N<sub>8</sub>O<sub>4</sub>Mn<sub>2</sub>Cl<sub>4</sub>.0.5(CH<sub>3</sub>)<sub>2</sub>O: C, 51.88; H, 4.55; N, 11.00. Found: C, 51.71; H, 4.78; N, 11.32.

### 2.10.4. [Mn<sub>2</sub>(H<sub>2</sub>L6)<sub>2</sub>Cl<sub>4</sub>] (Mn4)

MnCl<sub>2</sub>.4H<sub>2</sub>O (0.10 g, 0.51 mmol) and **H<sub>2</sub>L6** (0.17 g, 0.51 mmol). Yellow solid. Yield = 0.38 g (81%). ESI-MS: m/z(%); 911 [M<sup>+</sup> - Cl, 100]. FT-IR (cm<sup>-1</sup>): (νC=O)<sub>amide</sub>, = 3346. (νN-H)<sub>amide</sub> = 1638. μ<sub>eff</sub> = 5.95 BM. Anal. Calcd for C<sub>38</sub>H<sub>32</sub>N<sub>8</sub>O<sub>6</sub>Mn<sub>2</sub>Cl<sub>4</sub>: C, 48.13; H, 3.40; N, 11.82. Found: C, 48.21; H, 3.61; N, 12.13.

## 2.11. Typical procedure of the transfer hydrogenation of ketones

A mixture of acetophenone (1.00 mmol), K<sup>t</sup>BuO (1.0 mL of 0.4 M, 0.4 mmol) in 2.5 mL of 2-propanol, methoxybenzene (internal standard) (1.00 mmol) and **Ru1** (1.50 x 10<sup>-4</sup> mmol) was refluxed at 80 °C during which about 0.20 mL aliquot was taken at a regular time interval, cooled, and analysed for activity using <sup>1</sup>H NMR spectroscopic technique. The percentage conversions were calculated using the formula: [I<sub>a</sub>-I<sub>s</sub>]/[I<sub>a</sub>] x100%, while percentage yields were determined using: [I<sub>p</sub>]/[I<sub>a</sub>] x 100% where [I<sub>a</sub>] = integral value of OCH<sub>3</sub> signal at 3.78 ppm of the internal standard (methoxybenzene, anisole), [I<sub>s</sub>] = integral value of CH<sub>3</sub> protons of the substrate (*e.g.* acetophenone) at 2.50 ppm and [I<sub>p</sub>] = integral value of CH<sub>3</sub> proton of crude product (*e.g.* 1-phenylethanol) between 1.46 ppm and 1.50 ppm (**Figure 2.1**). Kinetic data were analysed using 64-bit Origin Pro 9.1. A standard nonlinear first-order monomolecular exponential growth model,  $y = e^{a(1-e^{(k(x-x_c))})}$ , where a = amplitude, x = time, x<sub>c</sub> = centre, and k = initial rate, was used to fit the kinetic data for **Ru6** or **Ru8** (**Figure 2.1**).

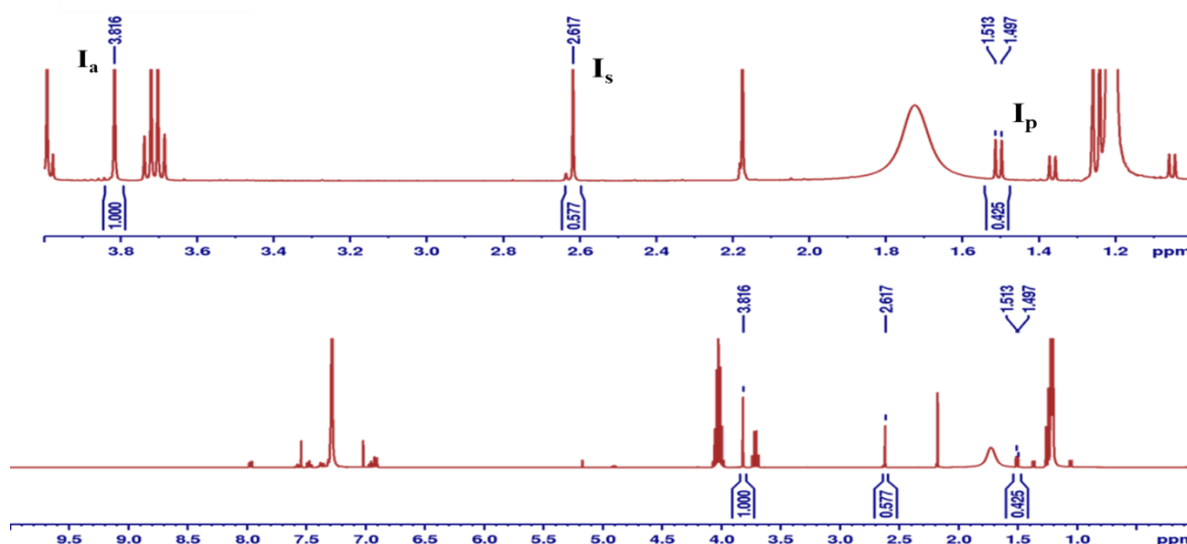


**Figure 2.1.**  $^1\text{H}$  NMR spectrum of the crude product of TH of acetophenone using complex **Ru8**, 0.0015 mol% (15ppm) as a catalyst. An aliquot was taken and analysed after 4 h of reaction. The integral values of methyl protons of acetophenone and 1-phenylethanol corresponding to percentage conversion and yield = 42%.

### 2.11.1. Isolation and characterisation of the TH products

To isolate the TH product of some selected ketones (*e.g.* acetophenone, 1-acetylnaphthanone, 2-pentanone and 4-chloroacetophenone, 1.0 mmol), a solution of  $\text{K}^t\text{BuO}$  (0.005 g, 2.5 mol%),  $^i\text{PrOH}$  (5.0 mL) and complex **Ru4** (0.93 mg, 0.001 mmol, 0.1 mol%). The crude product was cooled to room temperature, and the solvent was evaporated to give a brown crude product. The crude was further purified by column chromatography on silica gel using ethyl acetate/pentanes (5:95). The eluent was evaporated to obtain the pure product and identified using  $^1\text{H}$  NMR spectroscopy.

### 2.11.2. Mercury poisoning test

A mixture of acetophenone (1.00 mmol), K<sup>t</sup>BuO (1.0 mL of 0.4M, 0.4 mmol) in 2.5 mL of 2-propanol, methoxybenzene (internal standard) (1.00 mmol), 5 drops of Hg(0) and **Ru5** ( $1.50 \times 10^{-4}$  mmol) was refluxed at 80 °C for 6h. Percentage conversion and yield were determined using <sup>1</sup>H NMR spectroscopic technique.

### 2.11.3. Mechanistic studies of transfer hydrogenation

Mechanistic studies of the transfer hydrogenation of acetophenone catalysed by the complex **Ru1** was investigated using the low-resolution ESI-MS technique. Generally, a solution of the Ru complex (0.010 mol%, 100 ppm) in <sup>i</sup>PrOH, K<sup>t</sup>BuO (4.0 mol%), acetophenone (1.0 mmol) were mixed in 2.5 mL <sup>i</sup>PrOH. An aliquot of about 0.1 mL was withdrawn, dissolved in *d*<sub>8</sub>-toluene (0.50 mL), and analysed by <sup>31</sup>P NMR spectroscopic technique. The remaining solution was refluxed for 6 h at 82 °C. About 0.1 mL of the mixture was sampled at regular time intervals, cooled to about -4 °C and analysed using the ESI-MS technique to identify the respective mass fragments of the intermediates in the catalytic cycle.

## 2.12. References

1. Vogel, A., A Text-Book of Practical Organic Chemistry, 846. *ELBS and Longmann: London* **1989**.
2. Ogiwara, Y.; Miyake, M.; Kochi, T.; Kakiuchi, F., *Organometallics* **2017**, *36*, 159-164.
3. Zhang, J.; Wang, H.; Li, Z.; Wang, C., *Trans. Met. Chem.* **1995**, *20* (2), 118-119.
4. Berch, M. L.; Davidson, A., *J. Inorg. Nucl. Chem.* **1973**, *35*, 3763-3767.
5. APEX, B., SAINT and SADABS Bruker AXS Inc. *Madison, WI, USA* **2009**.

6. Sheldrick, G. M., Acta Crystallogr., Sect. A. A: *Found. Crystallogr* **2008**, 64 (1), 112.
7. Farrugia, L. J., WinGX and ORTEP for Windows: an update. *J. Appl. Crystallogr.* **2012**, 45, 849-854.
8. Farrugia, L., WinGX-A Windows Program for Crystal Structure Analysis. *J. Appl. Crystallogr* **2012**, 45, 849-854.
9. Reddyrajula, R.; Dalimba, U., *Bioorg. Med. Chem. Lett.* **2020**, 30, 126846.
10. Yadav, S.; Vijayan, P.; Yadav, S.; Gupta, R., *Dalton Trans.* **2021**, 50, 3269-3279.
11. Vijayan, P.; Yadav, S.; Yadav, S.; Gupta, R., *Inorg. Chim. Acta* **2020**, 502, 119285.
12. Vijayan, P.; Yadav, S.; Yadav, S.; Gupta, R., *Inorg. Chim. Acta* **2020**, 502, 119285.
13. Ramachandran, R.; Viswanathamurthi, P., *Spectrochimica Acta A: Mol. Biomol. Spectrosc.* **2013**, 103, 53-61.
14. Pachisia, S.; Kishan, R.; Yadav, S.; Gupta, R., *Inorg. Chem.* **2021**, 6, 2009-2022.

## CHAPTER 3

### CARBOXAMIDE CARBONYL-RUTHENIUM(II) COMPLEXES: DETAILED STRUCTURAL AND MECHANISTIC STUDIES IN THE TRANSFER HYDROGENATION OF KETONES

This chapter is adapted from the paper published in *New Journal of Chemistry*, 2022, **46**, 3146-3155 and is based on the experimental work of the first author, Robert Tettey Kumah. Copyright © 2022 Royal Society of Chemistry. The first author's contributions include syntheses of the complexes, transfer hydrogenation of ketones, and manuscript drafting.

#### 3.1. Introduction

The development of organometallic based complexes as catalysts in organic reactions is a major research field.<sup>1-3</sup> To date, a considerable number of novel catalysts have been designed to meet the high demands of valuable industrial and fine chemical products.<sup>4</sup> In the development of a catalyst for homogeneous reactions, an increasing impetus has been placed on ligand designs, which have the ability to modulate the electronic and steric parameters around the metal centre. This ultimately regulates the catalytic activity, stability and chemoselectivity in the organic transformation of interest.<sup>5-6</sup> As a result, many transition metal complexes supported on various ligands bearing well-defined donor atoms have been tailored to achieve the desired catalytic properties. *N*-heterocyclic carbenes (NHC),<sup>7</sup> imino-based, amino-phosphines,<sup>8</sup> imino-phosphines,<sup>9</sup> carboxamides,<sup>10-11</sup> thiosemicarbazone,<sup>12</sup> amino-alcohols,<sup>13</sup> phosphoramidites,<sup>14-15</sup> selenium-based ligands<sup>16</sup> among others<sup>17-18</sup> are among the common ligands, which have been utilised in the past few years.

A number of transition metals, including first- and second-row transition metals complexes<sup>19-20</sup> have been exploited for their potential catalytic properties in the transfer hydrogenation (TH) of ketones with varied outcomes. Notably, Ru(II),<sup>2</sup> Ir(II/III),<sup>21</sup> Os(II), Rh(I/II),<sup>22</sup> Fe(II),<sup>23</sup> Ni(II)<sup>24</sup> and Mn(I)<sup>25-26</sup> represent the broad spectrum of transition metals that have been studied for their prospective catalytic properties. Ruthenium(II) complexes are extensively studied and have proven to be the most active catalyst in transfer hydrogenation of ketones compared to Rh(I/II), Ir(I/III), and Os(II) complexes.<sup>2 27-28</sup> The chemistry and applications of carboxamide ligands have gained appreciable attention.<sup>29</sup> Carboxamide ligands are less expensive and can easily be synthesised using simple condensation methods compared to imine, amino-phosphines, imino-phosphines and phosphine-amidate ligand systems.<sup>8-10</sup> Neutral and anionic carboxamide ligands have the ability to improve the catalytic activity and stability in the TH reactions.<sup>11, 30</sup>

Recently, a number of Ru(II) carboxamide based complexes have been developed and utilised as potential catalysts in some organic transformations, including transfer hydrogenation reactions.<sup>31</sup> Notable among them is the Gupta's recently reported Ru(II)-phosphine-carboxamide complexes, which demonstrated catalytic activity, TON (Turnover number) up to 99 in TH of ketones.<sup>10</sup> Do and co-workers have also reported half-sandwich Ru(II) complexes bearing the pyridine-carboxamide backbone for TH of ketones and aldehydes and attained turnover frequency (TON up to 200).<sup>32</sup>

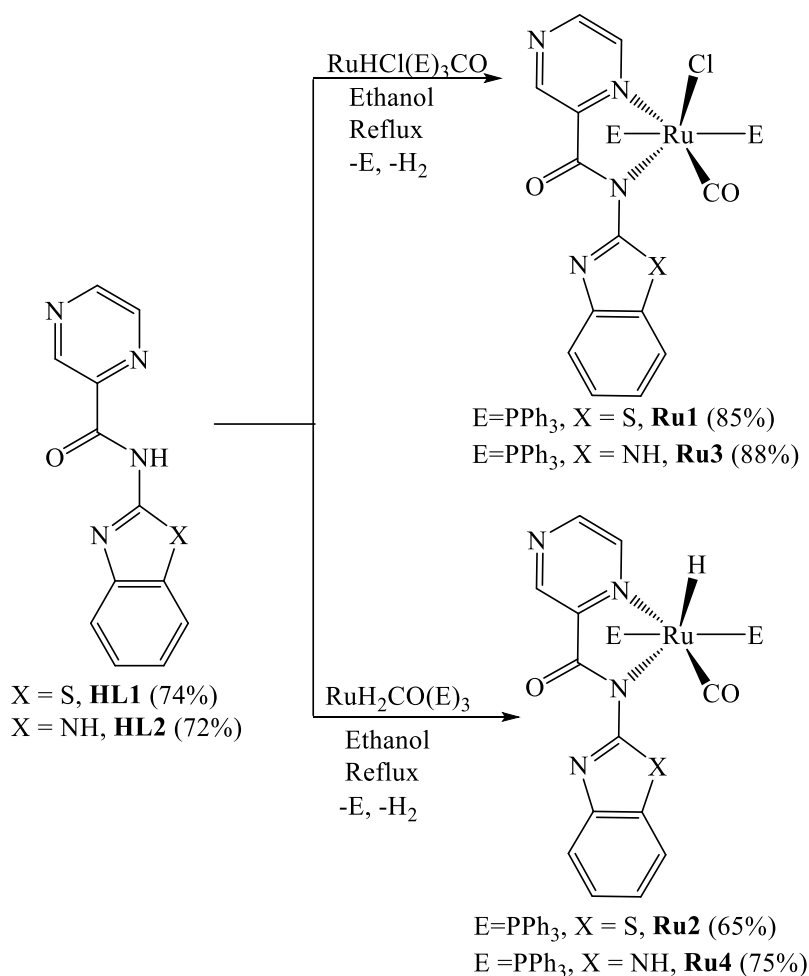
Heterocyclic compounds such as benzo[d]-thiazole and benzimidazole are known to alter the electron density at the metal centre, which could significantly impact on catalytic properties.<sup>33</sup> Benzo-[d]-thiazole and benzo-imidazole heterocyclic groups have been integrated with

pyridine moieties, and their influence on the corresponding metal complexes in terms of catalytic reactions have been studied. For example, Ru(II/III)-pyridyl benzo-imidazole/benzo-thiazole complexes and their propensity in TH of ketones have been reported with moderate catalytic activity (TON up to 540) by our group.<sup>34</sup> Therefore, the combination of pyrazine and benzo-[d]-imidazole/benzo-[d]-thiazole groups with the carboxamide functional group could impact significantly on the catalytic properties of the corresponding Ru(II) complexes. For these reasons, the development of Ru(II) complexes of pyrazine-benzo-[d]-thiozole/benzo-[d]-imidazole carboxamide has ignited our interest to prepare potential catalysts in the TH of ketones. Herein, we report the synthesis of new pyrazine-benzo-[d]-thiozole/benzo-[d]-imidazole carboxamide Ru(II) complexes with *co*-ligands; PPh<sub>3</sub>, Cl, CO, and hydride (H) and their potential applications as catalysts in the TH reaction of ketones. Detailed structural characterisation and mechanistic studies in the transfer hydrogenation of ketones have been carried out and are discussed.

## 3.2. Results and discussion

### 3.2.1. Synthesis and characterisation of compounds

The two carboxamide ligands, *N*-(benzo[d]thiazol-2-yl)pyrazine-2-carboxamide (**HL1**) and *N*-(1H-benzo[d]imidazol-2-yl)pyrazine-2-carboxamide (**HL2**), were prepared following literature procedures.<sup>35-36</sup> Detailed synthetic protocol and spectroscopic data of the ligands are provided in **Chapter 2**. The reactions of synthons **HL1** and **HL2** with [RuCl(CO)H (PPh<sub>3</sub>)<sub>3</sub>] and [RuH<sub>2</sub>(PPh<sub>3</sub>)<sub>3</sub>(CO)<sub>2</sub>] precursors afforded air-stable Ru(II) compounds (**Ru1-Ru4**) in good to high yields (65%-88%) as shown in **Scheme 3.1**.



**Scheme 3.1.** Synthesis of carboxamide Ru(II) complexes **Ru1-Ru4**.

The Ru(II) compounds were characterised by  $^1\text{H}$  NMR,  $^{13}\text{C}$  NMR and FT-IR spectroscopies, mass spectrometry, elemental analyses, and single-crystal X-ray analyses. The signals for the amide proton (N-H) in the  $^1\text{H}$  NMR spectra of the carboxamide ligands **HL1** and **HL2** were instrumental in the determination of the formation of the Ru(II) complexes. For instance, the  $^1\text{H}$  NMR spectrum of the carboxamide ligands, **HL2**, showed the signal for the  $\text{N-H}_{\text{amide}}$  proton at 12.68 ppm (**Figure 3.1**), and upon the formation of **Ru2**, this signal disappeared (**Figure 3.1**). This trend was observed in the  $^1\text{H}$  NMR spectra of the other complexes, **Ru2-Ru4**. The absence of the amide proton signal in the  $^1\text{H}$  NMR spectra of the Ru(II) complexes established the N-H deprotonation upon coordination as depicted in **Scheme 3.1**.<sup>36-37</sup> In addition, the new



triplet signals at  $\delta_{\text{H}}$  -13.08 ppm and -13.26 ppm, assigned to the Ru-H protons were observed (**Figure 3.1**) in the  $^1\text{H}$  NMR spectra of complexes **Ru2** and **Ru4**, respectively, and assigned to the P-H coupling ( $t, {}^2J_{\text{H-P}} = 20.3 \text{ Hz}, H_{\text{Ru-H}}$ ).<sup>36</sup>

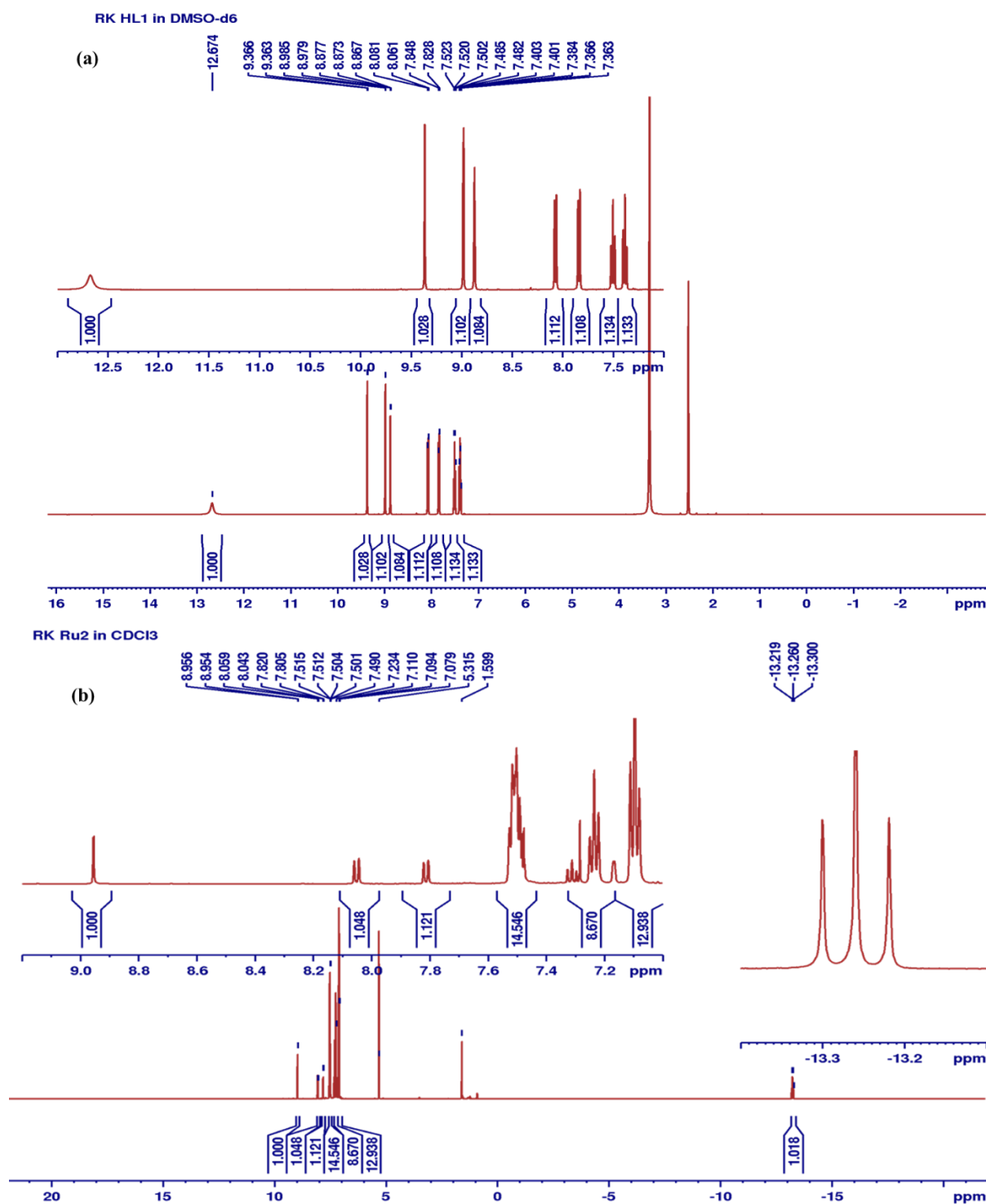


**Figure 3.1.** A comparison in chemical shifts in the  $^1\text{H}$  NMR spectra of **(a) HL1** ( $\text{N-H}_{\text{amide}}$  at 12.68 ppm) and **(b) Ru2** ( $\text{N-H}_{\text{amide}}$ : absent, Ru-H signal at  $\delta_{\text{H}}$ : -13.08 ppm).

$^{13}\text{C}\{^1\text{H}\}$  NMR spectroscopy was also relevant in establishing the successful formation of complexes **Ru1-Ru4**. For example,  $^{13}\text{C}\{^1\text{H}\}$  NMR spectrum of complex **Ru1** showed slight shifts in the  $\text{C}=\text{O}_{(\text{amidate})}$  signals (166.8 ppm) in relation to the free ligands **HL1** at 161.3 ppm (**Figure 3.2**). While the  $\text{O}_{\text{amidate}}$  -atom is expected to be non-coordinating (see molecular structures in **Figures 3.5-3.7**, these slight shifts could be attributed to electron flow from the **HL1** ligand to the Ru atom, causing a deshielding effect in the carbonyl moiety. Furthermore, the presence of the coordinated pi acceptor carbonyl ligand is expected to favour sigma-donation from the **HL1** ligand to the Ru atom.<sup>36-37</sup> Indeed, this argument is supported by the lower ( $-\text{Ru}-\text{C}\equiv\text{O}$ ) signals observed in the  $^{13}\text{C}$  NMR spectra, for instance, at 198.1 ppm for complex **Ru3** (typical range for terminal  $\text{C}\equiv\text{O}$  ligand is 200 – 210 ppm)<sup>31</sup> as shown in **Figure 3.2**.

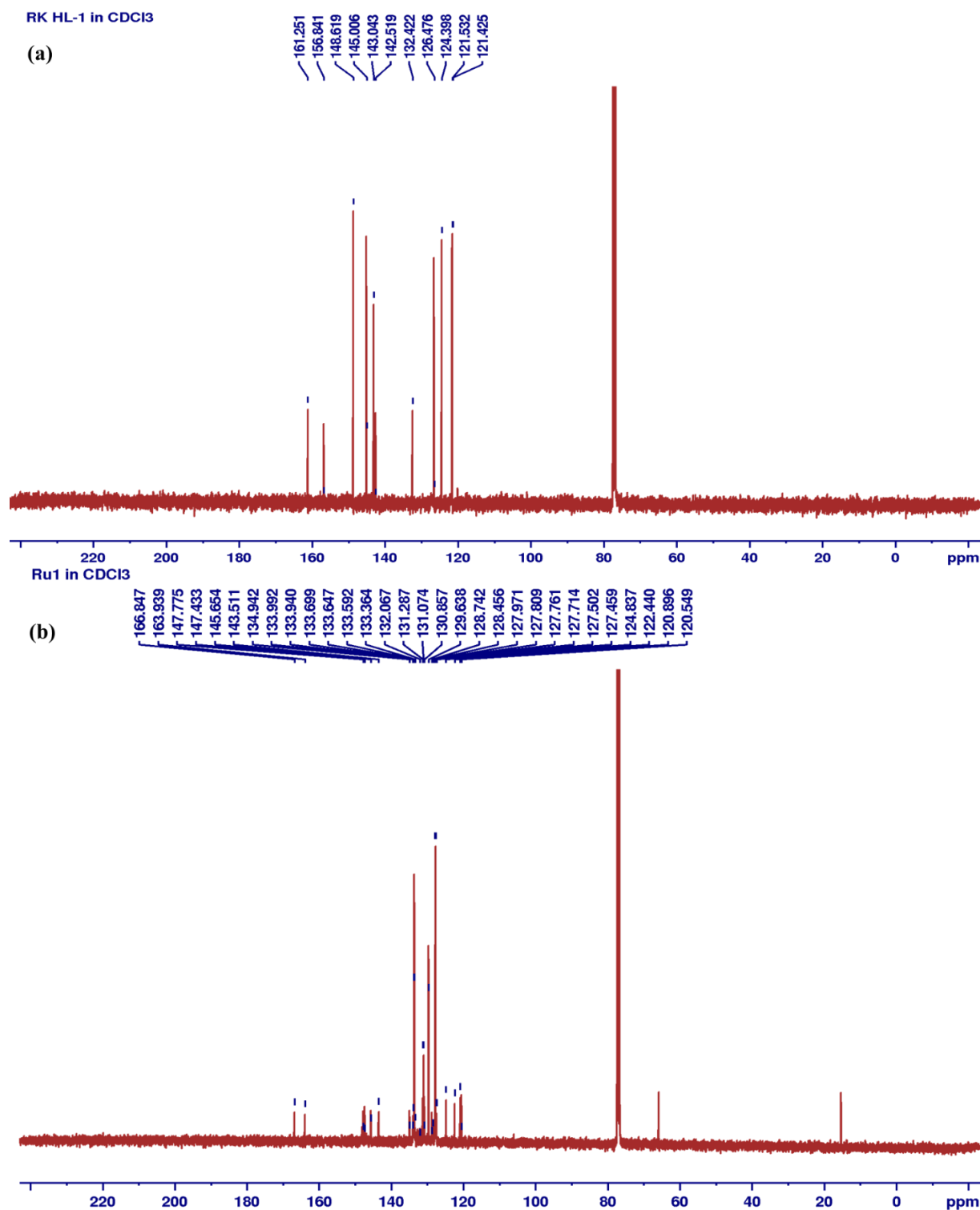


**Figure 3.2.** A comparison in chemical shifts in the  $^{13}\text{C}\{^1\text{H}\}$  NMR spectra of (a) **HL1** ( $-\text{C}=\text{O}$  at  $\delta$ : 161.3) and (b) complex **Ru1** ( $\text{C}=\text{O}$  signal at  $\delta$ : 166.9 ppm).

$^{31}\text{P}\{^1\text{H}\}$  NMR spectroscopy was also used to establish the identities of complexes **Ru1-Ru4**. For example, the  $^{31}\text{P}\{^1\text{H}\}$  NMR spectra displayed sharp singlets at  $\delta_{\text{P}}$  29.4 ppm (**Ru1**), 48.2 ppm (**Ru2**), 48.2 (**Ru3**) and 23.2 ppm (**Ru4**), consistent with the existence of two magnetically equivalent  $\text{PPh}_3$  groups in *trans* configurations (**Figure 3.3**).<sup>36</sup>

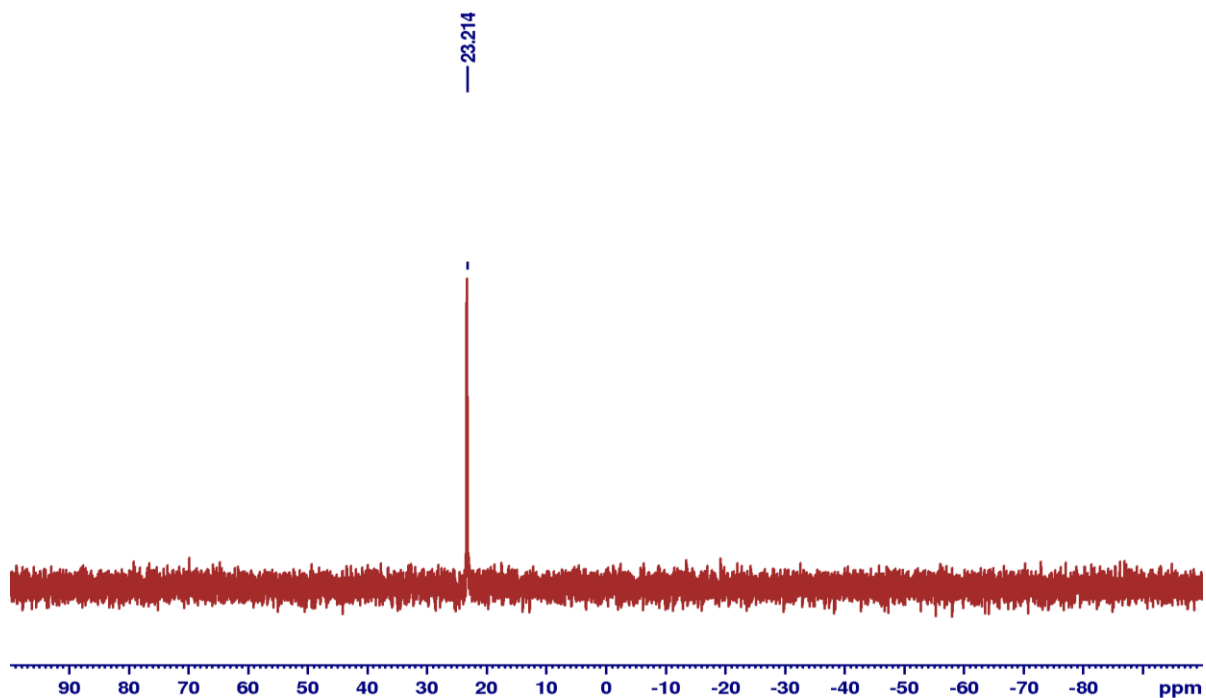


**Figure 3.3.**  $^{31}\text{P}\{^1\text{H}\}$  NMR spectrum of complex **Ru4** showing a signal at  $\delta$ : 23.2 ppm implicating the presence of two equivalent  $\text{PPh}_3$  *trans* to each other.

The successful coordination of the Ru(II) precursors to the carboxamide ligands **HL1-HL2** was further supported by FT-IR spectroscopy. In the FT-IR spectra of complexes **Ru1-Ru4**, the  $\nu(\text{C}=\text{O})$  absorption band shifted to lower frequencies between 1621-1629  $\text{cm}^{-1}$  in the complexes with respect to the free ligands of 1691  $\text{cm}^{-1}$  (**HL1**) and 1684  $\text{cm}^{-1}$  (**HL2**). This observation could be attributed to the resonance enhancement of the coordinated ligands leading to the weakening of the carbonyl bond.<sup>38</sup> In addition, the terminal carbonyl ( $-\text{Ru}-\text{C}\equiv\text{O}$ ) signals were recorded in the region of 1935-1947  $\text{cm}^{-1}$ . These values are relatively lower than

the values expected for terminal C≡O ligands (2000-2100 cm<sup>-1</sup>). The presence of sigma-donor spectator **HL1** and **HL2** ligands may account for this observation.<sup>36</sup> As reported in the <sup>1</sup>H NMR spectral data, the signals corresponding to N-H<sub>(amide)</sub> at 3251-3315 cm<sup>-1</sup> in the free ligand disappeared upon metalation (**Table 3.1**).<sup>39-40</sup>

**Table 3.1.** Selected FT-IR spectroscopic data of the complexes **Ru1-Ru4** and corresponding ligands **HL1-HL2**.

Entry	Complex	$\nu(\text{C=O})^{\text{a}}_{\text{amide}}$	$\nu(\text{C}\equiv\text{O})_{\text{terminal}}$	$\nu(\text{N-H})^{\text{a}}_{\text{amide}}$
1	Ru1	1629(1691)	1935	-(3324)
2	Ru2	1629(1684)	1987	- (3324)
3	Ru3	1612(1691)	1946	-(3251)
4	Ru4	1616(1684)	1956	-(3251)

<sup>a</sup>FT-IR spectroscopic data of the ligands are in brackets.

(-) - Not applicable

LC-MS spectra of the compounds gave the signals corresponding to their respective fragments; for example,  $m/z$  =909.12 [M - Cl]<sup>+</sup> (**Ru1**), 909.12 [M-H]<sup>+</sup> (**Ru2**), 892.15 [M - Cl]<sup>+</sup> (**Ru3**), and 892.15 [M - H]<sup>+</sup> (**Ru4**). Furthermore, the experimental and calculated isotopic mass distribution were in good agreement, as shown in **Figure 3.4**. Notably, the experimental elemental analysis data compared favourably with the proposed empirical formulae, thus establishing both the empirical formulae and purity of the complexes.

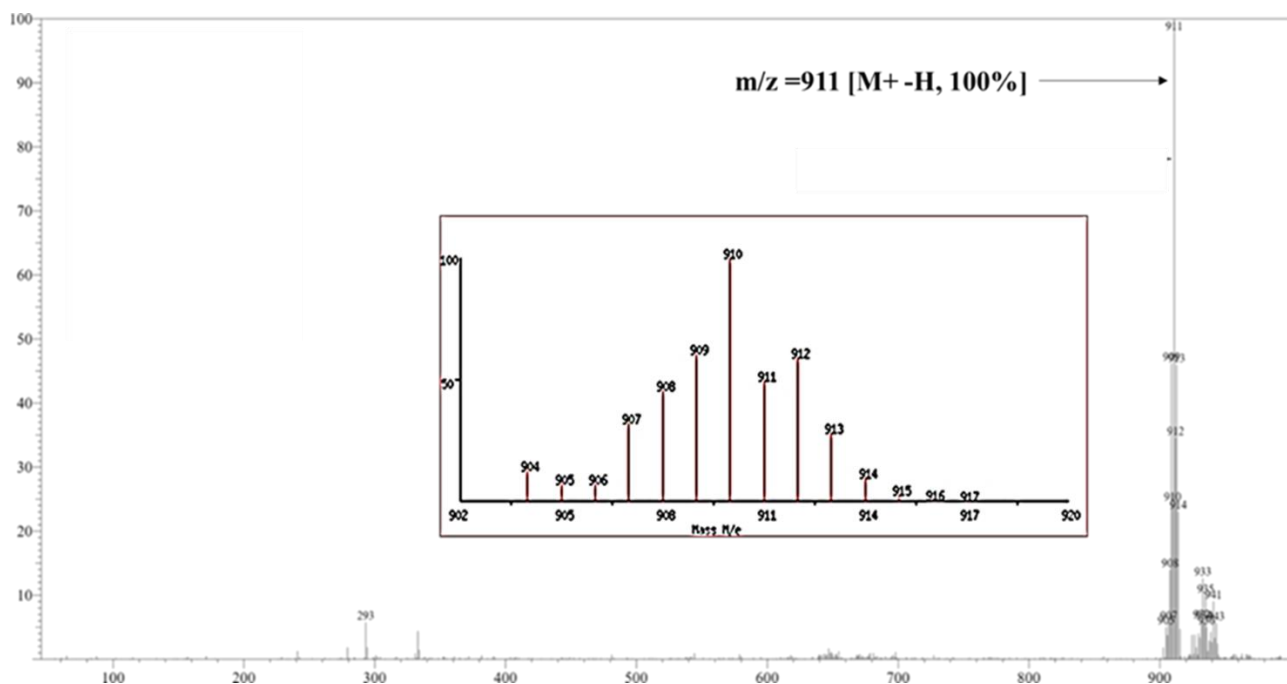


**Figure 3.4.** LC-MS spectrum of **Ru2** showing the  $m/z$  at 911,  $[M^+ + 100\%]$ . The simulated theoretical mass distribution plot (inset).

### 3.2.2. Solid-state structure of complexes **Ru1**, **Ru2**, and **Ru4**

Molecular structures of the complexes **Ru1**, **Ru2** and **Ru4** were confirmed by single-crystal X-ray crystallography analyses. The perspective views of their solid-state structures are shown in **Figures 3.5-3.7**, while the refinement data and selected bond parameters are presented in **Table 3.2**, respectively. The solid-state structures of complexes **Ru1**, **Ru2**, and **Ru4** have a distorted octahedral geometry around the Ru(II) centre. The carboxamide ligand is oriented nearly in the plane as defined by the Ru(II) centre and the two *trans* PPh<sub>3</sub> *co*-ligands. The fifth and sixth coordination sites are occupied by either CO, Cl or H *co*-ligands to complete the octahedral geometry. The solid-state structures of complexes **Ru1**, **Ru2**, and **Ru4** reveal that the Ru(II) atoms coordinate to the carboxamide ligands **HL1** and **HL2** *via* the pyrazine and amidate N-atoms to form five-membered metallocycles; N(1)-C(4)-C(5)-N(2)-Ru(1). The average bond distance of Ru(1)-N(2)<sub>amidate</sub> (2.114(3) Å), Ru-N<sub>pyrazine</sub> (2.118(12) Å), Ru-P (2.400(11) Å), Ru-Cl (2.390(10) Å) and Ru-CO (2.421(11) Å) in complexes **Ru1**, **Ru2** and

**Ru4**, respectively, are within the average bond lengths of Ru-N<sub>amidate</sub> (2.115(10) Å), Ru-N<sub>pyrazine</sub> (2.122(12) Å, Ru-P (2.383(12) Å), Ru-Cl (2.410(10) Å) and Ru-CO (1.819(15) Å) found in 8 similar Ru(II) structures deposited in the CCDC.<sup>41-42</sup> The bite angles of the three-membered chelating ring N(1)-Ru-N(2): 77.84(13)° (**Ru1**), 76.13(5)° (**Ru2**), and 76.63(8)° (**Ru4**) are within the mean bite angles of 76.48(5)° found in 8 similar Ru(II) complexes deposited in CCDC file.<sup>41</sup> The average P(1)-Ru-P(2) bond angles in complexes **Ru1**, **Ru2** and **Ru4** of 169.96(8)° deviate significantly from the ideal linearity, 180°. The slight deviation from the linearity of N(1)<sub>pyrazine</sub>-Ru-C(13)<sub>carbonyl</sub> 176.46(14)° in the complexes **Ru1**, **Ru2** and **Ru4** was also observed. It could originate from steric restrictions imposed by the bulkier PPh<sub>3</sub> groups on the five-membered ruthenacycle. In addition, the average N(1)<sub>pyrz</sub>-Ru-Cl(1) bond angles of 89.68(8)° and N(1)<sub>pyrz</sub>-Ru-H, 92.80(2)° in compounds **Ru2** and **Ru4** show slight deviations from the ideal bond angle of 90°.

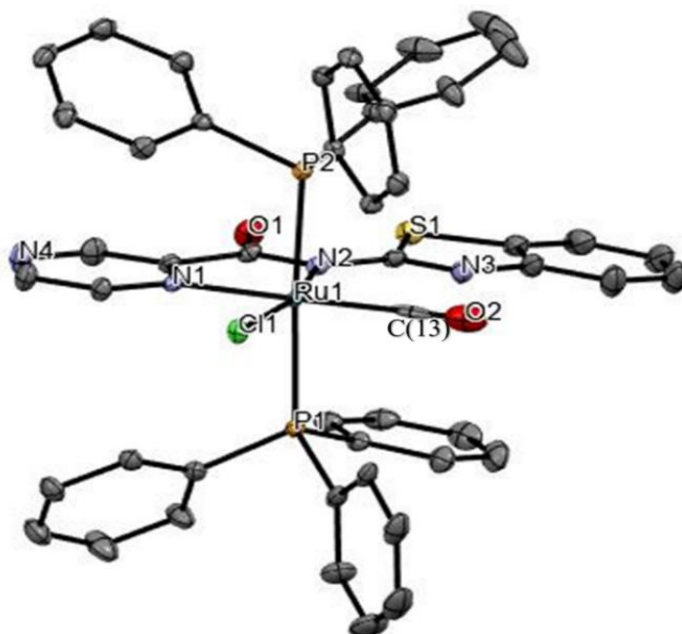


**Figure 3.5.** The ORTEP view of complex **Ru1** with thermal ellipsoids at a 50% probability level. All hydrogen atoms and  $\text{CH}_2\text{Cl}_2$  are omitted for clarity. Selected bond length ( $\text{\AA}$ ): Ru(1)-C(13), 1.984(7) Ru(1)-N(1), 2.113(3), Ru(1)-N(2), 2.115(3), Ru(1)-P(1), 2.400(11), Ru(1)-Cl(1), 2.426(10). Bond angle( $^\circ$ ): C(13)-Ru(1)-N(1), 176.32(16), N(1)-Ru(1)-N(2), 77.84(13), C(13)-Ru(1)-P(2), 89.04(13), N(1)-Ru(1)-P(2), 91.12(9), and P(2)-Ru(1)-P(1), 176.88(4).



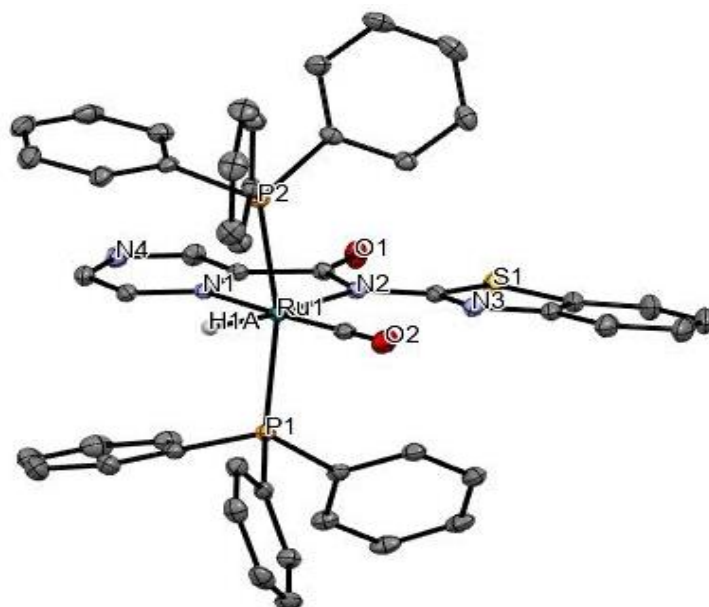


**Figure 3.6.** The ORTEP view of complex **Ru2** with thermal ellipsoids at a 50% probability level. All aromatic hydrogen atoms and CH<sub>2</sub>Cl<sub>2</sub> are omitted for clarity. Selected bond length (Å): Ru(1)-C(13), 1.984(7), Ru(1)-N(1), 2.118(14), Ru(1)-N(2), 2.116(15), Ru(1)-P(1), 2.364(4), Ru(1)-H(1A), 1.550(10). Bond angle(°): C(13)-Ru(1)-N(1), 177.73(7), N(1)-Ru(1)-N(2), 76.13(5), C(13)-Ru(1)-P(2), 90.76(5), N(1)-Ru(1)-P(2), 88.31(4), and P(2)-Ru(1)-P(1), 165.302(16).

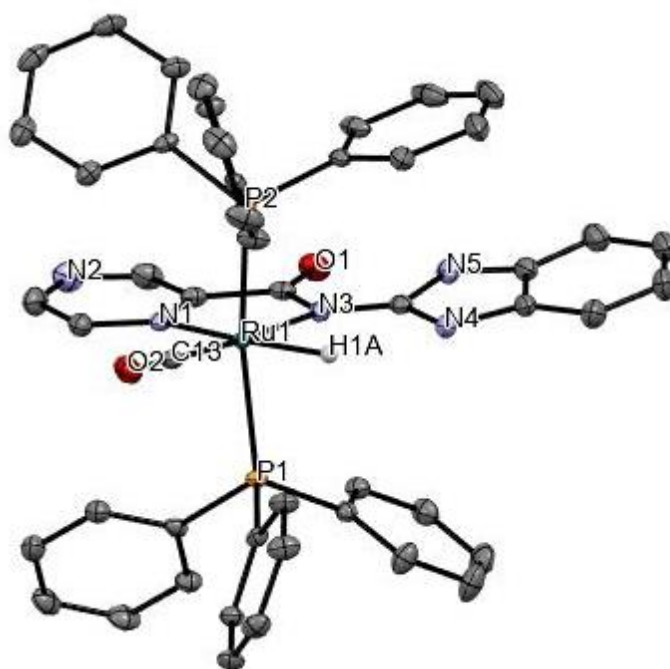


**Figure 3.7.** The ORTEP view of complex **Ru4** with thermal ellipsoids at a 50% probability level. All aromatic atoms and CH<sub>2</sub>Cl<sub>2</sub> are omitted for clarity. Selected bond length (Å): Ru(1)-C(13), 1.984(7), Ru(1)-N(1), 2.115(6), Ru(1)-N(2), 2.118(5), Ru(1)-P(1), 2.410(11), Ru(1)-H(1A), 1.967(10). Bond angle(°): C(13)-Ru(1)-N(1), 100.81(10), N(1)-Ru(1)-N(2), 76.24(8), C(13)-Ru(1)-P(2), 89.05(8), N(1)-Ru(1)-P(2), 95.06(6), and P(2)-Ru(1)-P(1), 168.60(2).

**Table 3.2.** Crystal data and structure refinement for complexes **Ru1**, **Ru2** and **Ru4**

Parameter	Ru1	Ru2	Ru4
Empirical formula	C <sub>99</sub> H <sub>75</sub> Cl <sub>4</sub> N <sub>8</sub> O <sub>4</sub> P <sub>4</sub> Ru <sub>2</sub> S <sub>2</sub>	C <sub>50</sub> H <sub>40</sub> Cl <sub>2</sub> N <sub>4</sub> O <sub>2</sub> P <sub>2</sub> RuS	C <sub>49</sub> H <sub>39</sub> Cl <sub>2</sub> N <sub>5</sub> O <sub>2</sub> P <sub>2</sub> Ru
Formula weight	1972.61	994.83	963.76
Temperature(K)	100(2)	100(2)	100(2)
Wavelength (Å)	0.71073	0.71073	0.71073
Crystal system	Monoclinic	Monoclinic	Monoclinic
Space group	P 2 <sub>1</sub> /c	P 2 <sub>1</sub> /n	P 2 <sub>1</sub> /n
Unit cell dimensions	a = 21.3269(17) Å b = 12.2526(10) Å c = 37.414(3) Å α = 90° β = 101.929(2)° γ = 90°	a = 12.1017(6) Å b = 13.8083(7) Å c = 27.2988(14) Å α = 90° β = 101.929(2)° γ = 90°	a = 9.8144(6) Å b = 18.5959(12) Å c = 23.1600(15) Å α = 90° β = 94.309(3)° γ = 90°
Volume (Å <sup>3</sup> )	9685.9(14)	4463.2(4)	4214.9(5)
Z	4	4	4
D <sub>calcd</sub> (mg/m <sup>3</sup> )	1.353	1.480	1.519
Absorption coefficient (mm <sup>-1</sup> )	0.585	0.636	0.623
F(000)	4020	2032	1968
Crystal size (mm <sup>3</sup> )	0.260×0.200×0.140	0.23×0.14×0.08	0.640×0.440×0.240
Index ranges	-28<=h<=28, -16<=k<=16, -49<=l<=49	-16<=h<=15 -18<=k<=16, -36<=l<=36	-13<=h<=13, -24<=k<=22, -30<=l<=30
Completeness to theta	100.0 %	100.0 %	99.9 %
Final R indices [I>2sigma(I)]	R1=0.0638, wR2= 0.1935	R1=0.0269, wR2=0.0627	R1= 0.0410, wR2=0.1157
Largest diff. peak and hole (e.Å <sup>-3</sup> )	1.897 and -2.779	0.645 and -0.664	1.803 and -1.997

### 3.2.3. Application of complexes **Ru1-Ru4** in the transfer hydrogenation of ketones

Preliminary investigations of the potential of the Ru(II) organo-carboxamide complexes (**Ru1-Ru4**) to catalyse the TH of ketones were carried out using complex **Ru3**, acetophenone as the model substrate, isopropyl alcohol as a source of hydrogen and KOH as a base. The conversion of the substrate to its respective products was followed and determined using  $^1\text{H}$  NMR spectroscopy (**Figures 3.1**). Percentage conversion of 53% was realised within 6 h at catalyst loadings of 0.10 mol% (**Table 3.3, entry 1**). Comparable percentage yields of crude products and conversions were realised; thus, percentage yields have been adopted in the entire discussion.

#### 3.2.3.1. Optimisation of catalyst loading using complex **Ru3**

Having established that the complex **Ru3** catalyse the TH of ketones, optimisation of reaction conditions was the next focus. First to be examined was the catalyst loading, which was investigated by varying catalyst **Ru3** loadings from 0.10 to 1.00 mol% (**Table 3.3**). It was noted that an increase in catalyst concentration from 0.100 mol% to 1.00 mol% led to an increase in percentage conversion from 53% to 98% (**Table 3.3, entries 1 and 5**). However, an increase in catalyst loading was followed by a decrease in TONs (**Table 3.3 and Figures 3.8**). For instance, TONs of 530 and 97 (maximum conversion after 6 h) were observed at catalyst loadings of 0.10 mol% and 1.00 mol%, respectively (**Table 3.3, entries 1 and 5**). From this trend, it is clear while the percentage conversions increased with catalyst loadings, this was not commensurate with the amount of catalyst added, possibly due to catalyst aggregation, and is in good agreement with the previous observation made by Ojwach and co-workers where a further increase in catalyst loading could not result in a significant increase in catalytic activity.<sup>34</sup>

**Table 3.3.** Optimisation of catalyst loading for effective TH of acetophenone using complex **Ru3**<sup>a</sup>

Entry	Catalyst loading/ mol%	<sup>b</sup> Conversion%	<sup>b</sup> Yield%	<sup>c</sup> TON	<sup>d</sup> TOF/h <sup>-1</sup>
1	0.10	53	52	530	88
2	0.15	59	58	393	65
3	0.25	68	66	272	34
4	0.50	79	79	158	20
5	1.00	98	97	97	16

<sup>a</sup>Reaction conditions: acetophenone, 1.00 mmol; KOH (0.100 mmol in 5 mL of <sup>i</sup>PrOH), Anisole (1.00 mmol) was used as internal standard 82 °C time, 6 h. <sup>b</sup>Determined by <sup>1</sup>H NMR spectroscopy (experiment repeated in triplicate to ensure reproducibility), <sup>c</sup>TON = moles of acetophenone converted per moles of **Ru3**. <sup>d</sup>TOF= (moles of acetophenone converted per moles of **Ru3** per hour).

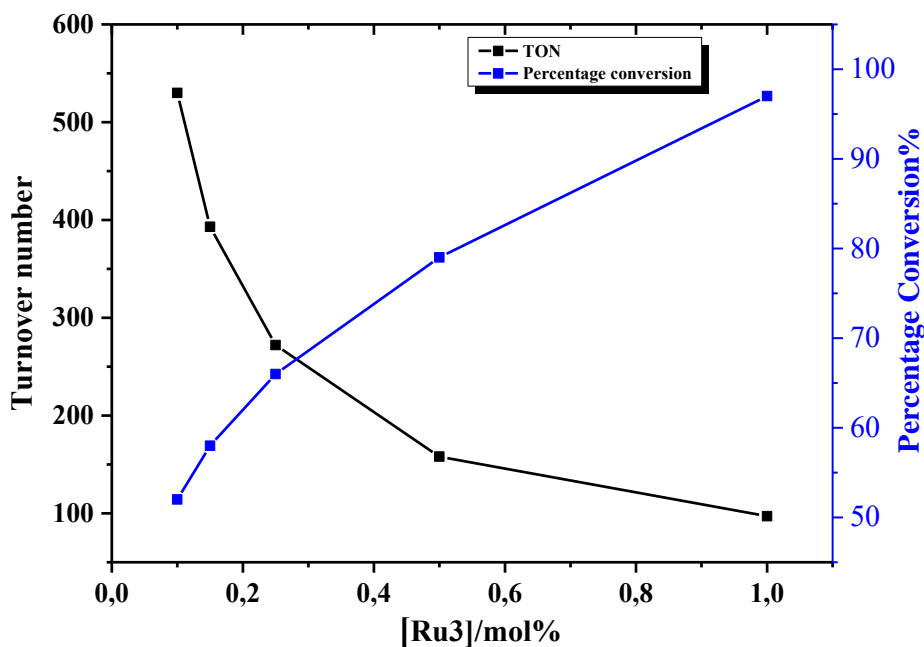


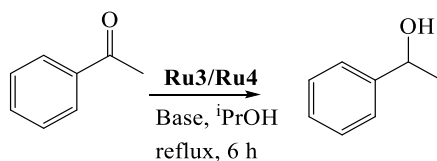
**Figure 3.8.** Plots of percentage conversion, turnover number (TON) vs time showing the effects of catalyst loading on the catalytic activity in the TH of acetophenone using complex **Ru3**.

### 3.2.3.2. Investigation of the effect of nature and concentration of base on the TH reactions

To fully understand the effect of the base in the TH of ketones, we carried out a number of control experiments. First, an experiment using KOH base alone without the ruthenium complex was conducted and afforded percentage conversions of 5% (6 h) and 16 % within 36 h (**Table 3.4, entries 1 and 2**) and are consistent with the findings reported by Polshettiwar *et al.*<sup>43-44</sup> This is much lower compared to the percentage conversions of 86% (6 h) reported using the **Ru3**/KOH system (**Table 3.4, entry 9**), thus confirming that the catalytic activities observed are due to the Ru(II) carboxamide complexes. In another control experiment, we used complexes **Ru3** and **Ru4** without adding any base. More significantly, percentage conversions of 39% in 6 h and 93% (18 h) were obtained for the hydride complex **Ru4** and 93% (36 h) for the non-hydride complex **Ru3** under base free conditions (**Table 3.4, entries 3-5**). The higher catalytic activities observed for the hydride complex **Ru4** compared to the non-hydride complex **Ru3** under base free conditions further reinforced the significance of the Ru-H moiety in the formation of the active intermediates.<sup>45</sup>

To establish the effects of the base loading on the rate of TH of acetophenone reaction, the concentration of KOH was varied from 0.025 mmol (2.5 mol%) to 1.00 mmol (100 mol%) at constant catalyst loading (0.10 mol%) using complex **Ru3** (**Table 3.4, entries 6-10**). From **Table 3.4**, it is evident that higher rates of the reactions were achieved at higher base loadings. For instance, TOF of up to 40 h<sup>-1</sup> and 120 h<sup>-1</sup> were obtained at base loadings of 2.5 mol% (0.025 mmol) and 7.5 mol% (0.075 mmol) as listed in **Table 3.4, entries 6 vs 8**. The nature of the base in controlling the catalytic activity of the complexes in the TH of acetophenone was also investigated using K<sub>2</sub>CO<sub>3</sub>, NaOH and K<sup>t</sup>BuO (**Table 3.4, entries 11-13**). Expectedly, K<sup>t</sup>BuO gave the highest catalytic activity, and the observed order of K<sup>t</sup>BuO > KOH > NaOH > K<sub>2</sub>CO<sub>3</sub> tally with the relative strengths of the bases.<sup>34</sup>

**Table 3.4.** Optimisation of base loading for effective TH of acetophenone using complexes **Ru3** and **Ru4**<sup>a</sup>



Entry	Base	Catalyst	Base loading mol%	Time/h	<sup>b</sup> Conversion%	<sup>c</sup> TOF/h <sup>-1</sup>
1	KOH	-	10.0	6	5	-
2 <sup>e</sup>	KOH	-	10.0	36	16 <sup>e</sup>	-
3 <sup>f</sup>	-	<b>Ru4</b>	-	6	39	65
4 <sup>g</sup>	-	<b>Ru4</b>	-	18	99	28
5 <sup>h</sup>	-	<b>Ru3</b>	-	36	93	51
6	KOH	<b>Ru3</b>	2.5	6	24	40
7	KOH	<b>Ru3</b>	5.0	6	61	102
8	KOH	<b>Ru3</b>	7.5	6	72	120
9	KOH	<b>Ru3</b>	10.0	6	86	143
10	KOH	<b>Ru3</b>	100.0	6	97	164
11	K <sup>t</sup> BuO	<b>Ru3</b>	10.0	6	91	152
12	K <sub>2</sub> CO <sub>3</sub>	<b>Ru3</b>	10.0	6	30	50
13	NaOH	<b>Ru3</b>	10.0	6	42	70

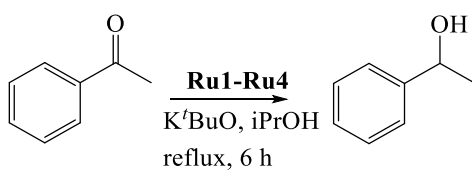
<sup>a</sup>Reaction condition: acetophenone, 1.00 mmol; [**Ru3**], 0.100 mol%; *i*PrOH, 5 ml; time, 6 h.

<sup>b</sup>Determined by NMR spectroscopy internal standard (methoxybenzene). <sup>c</sup>TOF (turnover frequency) = moles of substrate converted per moles of catalyst per hour. <sup>e</sup>Reaction without a catalyst, reaction time, 24 h. <sup>f</sup>Base-free reaction using **Ru4**, time, 6; <sup>g</sup>Base-free reaction using **Ru4**, time, 18 h. <sup>h</sup>Base-free reaction using **Ru3**, reaction = 36 h. All experiments were conducted in triplicate to ensure reproducibility.

### 3.2.3.3. Investigation of the role of complex structure on the TH of acetophenone

The optimised reaction conditions of catalyst (0.10 mol%) and K<sup>t</sup>BuO (10.0 mol%) loadings at 82 °C were then employed to investigate the role of the complex structure (**Ru1-Ru4**) in the TH of acetophenone (**Table 3.5**). From **Table 3.5** and **Figures 3.9**, it was evident that the ligand motif played a crucial role in regulating the catalytic activities of the complexes. For instance, complex **Ru3**, containing the *N*-(1H-benzo[d]imidazol-2-yl)pyrazine-2-carboxamide (**HL2**) ligand, displayed a higher TOF of 152 h<sup>-1</sup> (*k*<sub>obs</sub> of 2.02 x 10<sup>-1</sup> h<sup>-1</sup>) than complex **Ru1**, anchored on the *N*-(benzo[d]thiazol-2-yl)pyrazine-2-carboxamide ligand **HL1** (TOF of 118 h<sup>-1</sup> and *k*<sub>obs</sub> of 1.32 x 10<sup>-1</sup> h<sup>-1</sup>). This can be rationalised from the basicity of ligands **HL1** and **HL2**, where **HL2** is less basic. This increases the electrophilicity of the Ru metal atom in complex **Ru3** and is in good agreement with its higher catalytic activity.<sup>34, 46-48</sup> In terms of the role of the auxiliary ligands, the Ru-H complexes, **Ru2** and **Ru4** showed higher catalytic activities compared to the Ru-Cl analogues, **Ru1** and **Ru3**. This can be rationalised from a mechanistic perspective, where the Ru-H intermediate is considered the most active part of the catalytic cycle and requires less or no further activation in its reactions compared to the pre-catalysts **Ru1** and **Ru3**.<sup>10 36</sup> This trend is in tandem with the previous report by Gupta and co-workers where the Ru-hydride containing complexes demonstrated higher catalytic activity compared to the non-hydride Ru complexes.<sup>10</sup>



**Table 3.5.** Transfer hydrogenation of acetophenone data of complexes **Ru1-Ru4**<sup>a</sup>

Entry	Complex	<sup>b</sup> Conversion[%]	<sup>c</sup> TOF/h <sup>-1</sup> x 10 <sup>2</sup>	<i>k</i> <sub>obs</sub> x10 <sup>-1</sup>
1	<b>Ru1</b>	71	1.18	1.32(±0.01)
2 <sup>e</sup>	<b>Ru2</b>	94	1.46	2.02(±0.02)
3	<b>Ru3</b>	91	1.52	1.40(±0.04)
4 <sup>e</sup>	<b>Ru4</b>	99	1.52	2.08(±0.01)

<sup>a</sup>Condition: acetophenone, 1.00 mmol; K<sup>t</sup>BuO; [Ru], 0.100 mol%; iPrOH, 5ml; 82 °C, time, 6 h. <sup>b</sup>Determined by NMR spectroscopy (mean values of two independent runs) by employing methoxybenzene was used as internal standard. <sup>c</sup>TOF (Turn over frequency) = moles of acetophenone converted per moles of **Ru3** per hour). <sup>e</sup>Base loading of 2.5 mol%. (All experiments were carried out in triplicate to ensure reproducibility).

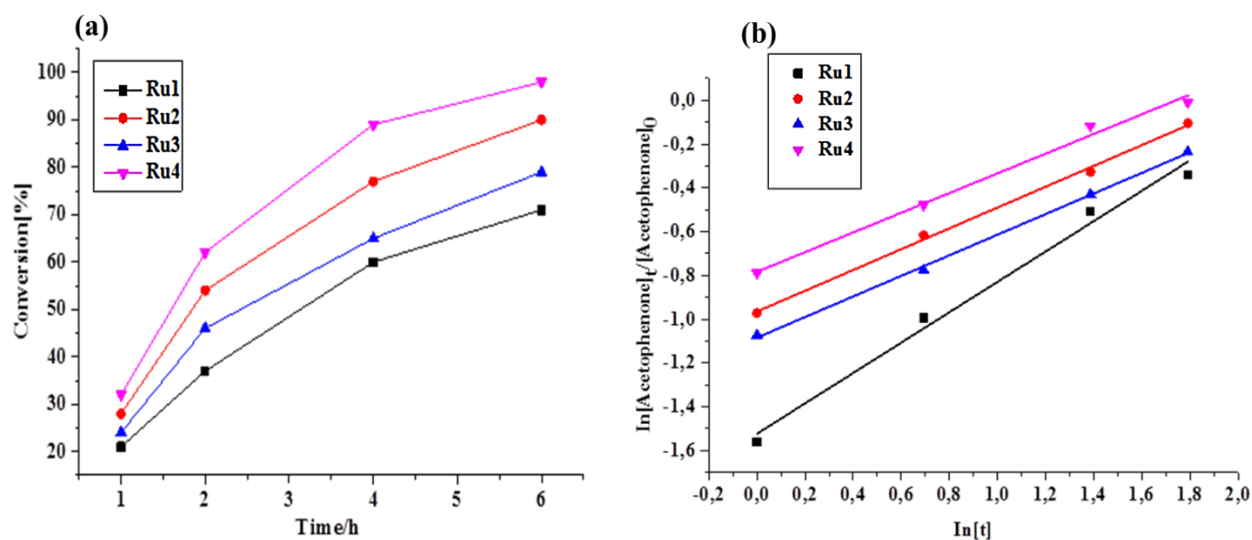


**Figure 3.9.** (a) A plot of percentage conversion vs time showing the effects of catalyst structure on the catalytic activity of TH of acetophenone reaction using complexes **Ru1-Ru4**. (b) a plot of  $\ln[\text{acetophenone}]_t/[\text{acetophenone}]_0$  vs  $\ln[t]$  for determination of the rate constants of each catalyst in TH of acetophenone reaction.

It is also instructive to note that the Ru-H complexes **Ru2** and **Ru4** required lower base loadings of 2.5 mol% compared to the 10 mol% used for the non-hydride complexes **Ru1** and **Ru3** (Table 3.5, entries 2 and 4). In comparison to literature reports, the catalytic activities achieved by **Ru1-Ru4** fall within the range of other related Ru(II)-PPh<sub>3</sub> complexes of TOF up to  $1.0 \times 10^2 \text{ h}^{-1}$ .<sup>49-57</sup> However, the catalytic activities of complexes **Ru1-Ru4** are lower compared to some of the highly active ruthenium(II) complexes where the TOFs between  $1.0 \times 10^4 - 1.0 \times 10^5 \text{ h}^{-1}$  were achieved.<sup>58-61</sup>

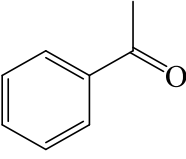
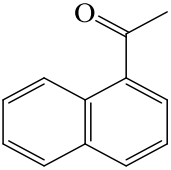
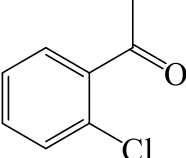
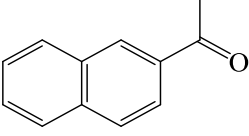
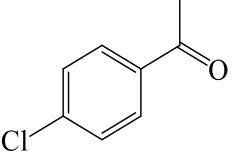
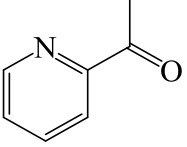
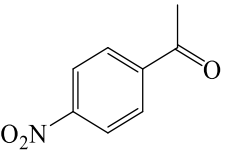
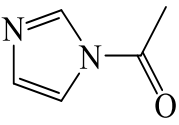
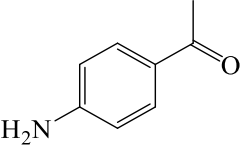
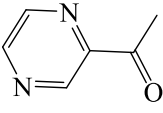
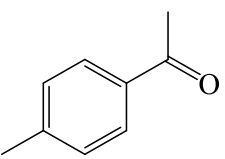
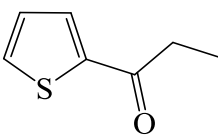
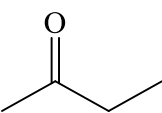
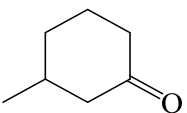
#### 3.2.3.4. Investigation of TH reactions using different ketone substrates

We next focused on investigating the substrate scope using complex **Ru4** (most active catalyst) under the optimised reactions (Table 3.6). It is significant to note that these complexes formed effective catalysts in the TH of a wide range of ketone substrates, with varied electronic and steric requirements. In general, electron-withdrawing substituents resulted in higher yields compared to those bearing electron-donating groups (Table 3.6, entries 2-6). For example, using complex **Ru4**, percentage yields of 91%, 97% and 61% were realised for acetophenone, 4-chloroacetophenone and 4-methyl-acetophenone, respectively (Table 3.6, entries 1, 3 and 6). This could be ascribed to the electronic effects of the substituents, where electron-withdrawing groups at the *para* position are known to activate the substrates.<sup>62</sup> Interestingly, no significant effect was observed by changing the position of the substituents. For instance, 4-chloroacetophenone and 2-chloroacetophenone gave yields of 95% and 97%, respectively, using catalyst **Ru4** (Table 3.6, entries 2 and 3), pointing to insignificant steric contributions of the *chlorido* substituents.<sup>63-64</sup>

The TH of fused acetophenone substrates as in 1'-acetonaphthone and 2'-acetonaphthone were also accomplished, albeit with lower percentage conversions of 86% and 74%, respectively.

Notably, complex **Ru4** was capable of reducing even the less reactive heterocyclic substrates (**Table 3.6, entries 10-13**). Interestingly, 1'-acetyl imidazole gave high percentage conversions of 97% (**Table 3.6, entry 11**). In contrast, the lower yields of 2-acetyl pyridine, 2-acetyl pyrazine and 1-(2-thienyl)-1-propanone of 55% (**Table 3.6, entries 11, 13 - 14**) could be ascribed to possible irreversible coordination of the nitrogen and sulphur atoms to the active sites of the catalyst.<sup>65-66</sup> The reactivity of the aliphatic ketones was also investigated using 2-propanone (70%) and 3-methyl -2- cyclohexanone (69%) substrates. The lower percentage conversions observed compared to acetophenone (91%) under similar reaction conditions (**Table 3.6, entries 1, 7 and 14**) could be ascribed to the electron-rich nature of the aliphatic ketones, thus reducing their reactivities.<sup>67</sup>

**Table 3.6.** Result of substrate scope studies using complex **Ru4**<sup>a</sup>

Entry	Substrate	<sup>b</sup> Yield%	Entry	Substrate	<sup>b</sup> Yield%
1		91	8		86(84) <sup>d</sup>
2		95	9		74
3		97	10		47
4		90	11		97
5		58	12		69
6		68	13		55
7		70	14		69

<sup>a</sup>General reaction conditions: Substrate, 1.00 mmol (1.10 mL); Internal standard methoxybenzene, 1.0 mmol (1.12 mL), **[Ru4]**, 0.10 mol% (0.93 mg); K<sup>t</sup>BuO, 2.5 mol% (0.025 mmol) in *isopropyl* alcohol, temperature 82 °C, reaction time; 6 h. <sup>b</sup>Determined by <sup>1</sup>H NMR spectroscopy. All experiments were conducted in triplicate to ensure reproducibility. Methoxy benzene was used as an internal standard.

### 3.2.3.5. Proposed mechanism of the transfer hydrogenation of ketones

To gain some insights into the TH reaction mechanism, an *in situ*  $^{31}\text{P}\{^1\text{H}\}$  NMR spectroscopy experiment was performed in deuterated toluene using catalyst **Ru4** at 60 °C over a period of 6 h (**Figure 3.10**). From the  $^{31}\text{P}\{^1\text{H}\}$  NMR spectral data (**Figure 3.10**), a new signal emerged at -5.28 ppm (assigned to the free  $\text{PPh}_3$  group) within 1 h, which implicates dissociation of one  $\text{PPh}_3$  co-ligands to give the intermediate **Ru4a** (**Scheme 3.2**).<sup>10, 34</sup> Subsequent coordination of acetophenone substrate to the **Ru4a** species results in the formation of Ru-acetophenone adduct, **Ru4b**. This is followed by the migration of the hydride [Ru-H] from the ruthenium centre to the substrate leading to the generation of intermediate **Ru4c**. Displacement of the protonated substrate from the ruthenium centre by 2-propyl oxide and  $\text{PPh}_3$  resulted in the formation of Ru-alkoxide **Ru4d** species, as depicted in **Scheme 3.2**. This further asserts that the role of the base in this TH mechanism is to assist the regeneration of Ru-alkoxide species.<sup>68</sup> Finally,  $\beta$ -hydride elimination and subsequent release of acetone from the Ru centre lead to regeneration of the active catalyst **Ru4a**.<sup>69 10, 70</sup>

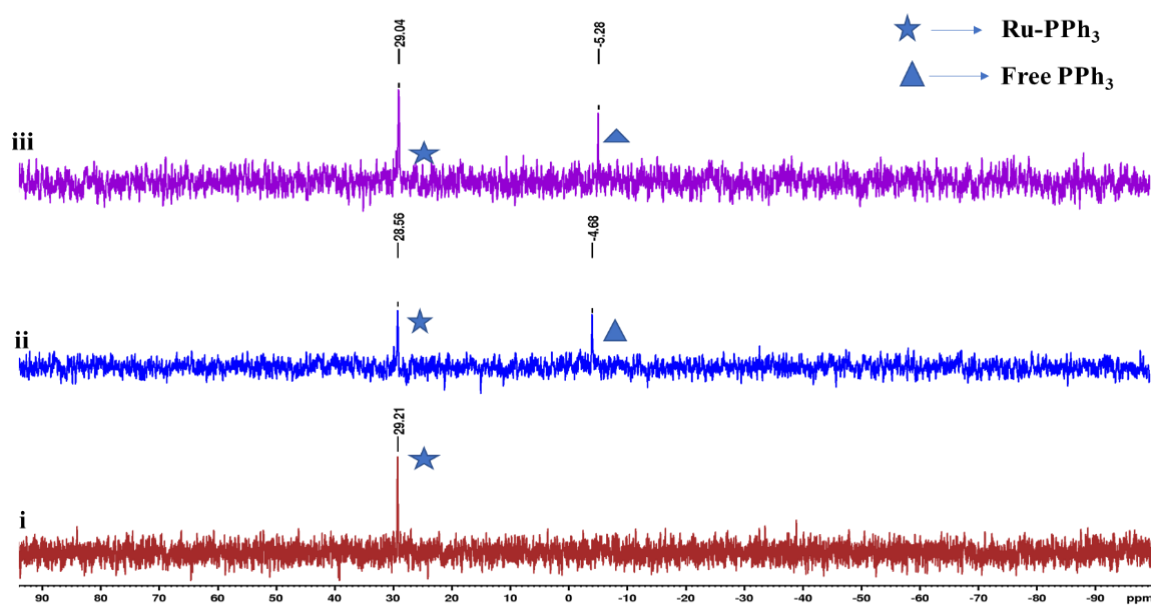
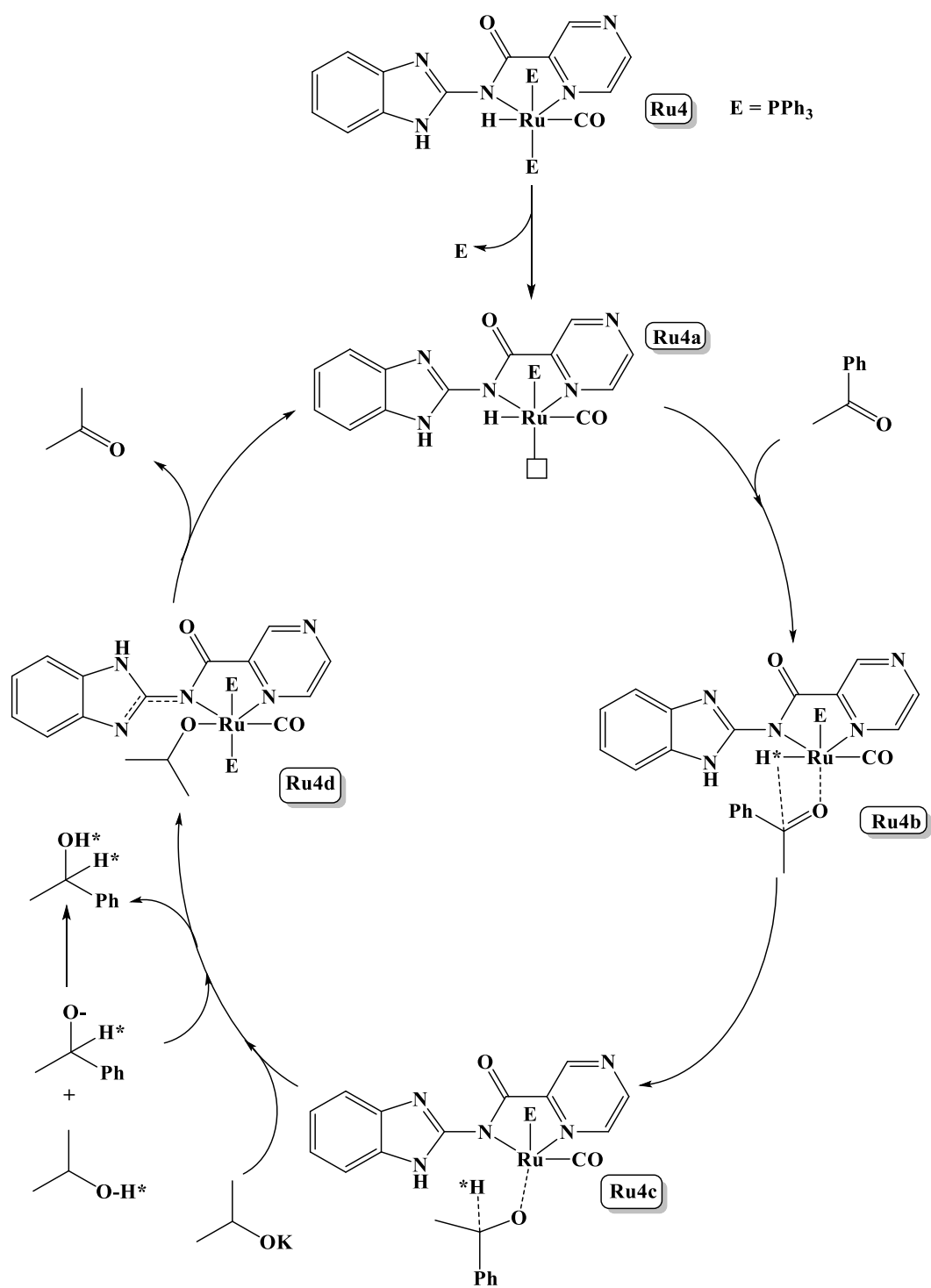


**Figure 3.10.**  $^{31}\text{P}\{^1\text{H}\}$  NMR spectral of complex  $[\text{RuHCO}(\text{L4})(\text{PPh}_3)_2]$ , **Ru4** in the presence of acetophenone,  $i\text{PrOH}$  and  $\text{K}^t\text{BuO}$  for 6 h. Spectrum, **i** shows a signal at  $\delta$  23.2 ppm corresponding to two equivalent  $\text{PPh}_3$  groups in the complex at  $t = 0$ . Spectra **ii** and **iii** show signals for the free  $\text{PPh}_3$  at  $\delta$  -4.7 and 5.28 ppm after 4 h and 6 h, respectively.



**Scheme 3.2.** A proposed monohydride reaction pathway for transfer hydrogenation of ketone catalysed by **Ru4**.

### 3.3. Conclusions

This work successfully demonstrated the synthesis and structural studies of carboxamide organo-ruthenium(II/III) complexes bearing PPh<sub>3</sub>/CO/Cl/H co-ligands and their applications as catalysts in the TH of ketones. The coordination nature of the Ru(II) complexes was established to consist of one bidentate anionic ligand and four co-ligands (PPh<sub>3</sub>/CO/Cl/H) to give distorted octahedral geometries. All the complexes showed good catalytic activities in the TH of a wide range of ketone substrates. More importantly, the Ru-H complexes are capable of promoting the TH reactions under base free conditions. The catalytic activities of the Ru(II) complexes were regulated by the ligand backbone and identity of the auxiliary ligands. Ru-H complexes generally displayed higher catalytic activities than the corresponding Ru-Cl analogues. An inner sphere monohydride mechanism involving dissociation of one PPh<sub>3</sub> group was proposed as derived from *in situ* <sup>31</sup>P{<sup>1</sup>H} NMR spectroscopy studies.

The next **Chapter 4** reports the synthesis and characterisation of dinuclear ruthenium(II) complexes supported on picolinamide. The dinuclear ruthenium complexes were evaluated as catalysts in the transfer hydrogenation of ketones and showed improvement in the catalytic activity compared to the mononuclear analogous. The effects of reaction conditions, catalyst structure, and substrate scope on the transfer hydrogenation of ketones were investigated, and a plausible mechanism was proposed.



### 3.4. References

1. Louie, J.; Bielawski, C. W.; Grubbs, R. H., *J. Am. Chem. Soc.* **2001**, *123*, 11312-11313.
2. Wang, D.; Astruc, D., *Chem. Rev.* **2015**, *115*, 6621-6686.
3. Widegren, J. A.; Finke, R. G., *J. Mol. Catal. A: Chem.* **2003**, *198*, 317-341.
4. Díez-González, S.; Nolan, S. P., *Angew. Chem. Int. Ed.* **2008**, *47*, 8881-8884.
5. Astruc, D.; Lu, F.; Aranzaes, J. R., *Angew. Chem. Int. Ed.* **2005**, *44*, 7852-7872.
6. Abbenhuis, H. C., *Chem. A Eur. J.* **2000**, *6*, 25-32.
7. Dragutan, V.; Dragutan, I.; Delaude, L.; Demonceau, A., *Coord. Chem. Rev.* **2007**, *251*, 765-794.
8. Milstein, D., *Top. Catal.* **2010**, *53*, 915-923.
9. Chu, W.-Y.; Richers, C. P.; Kahle, E. R.; Rauchfuss, T. B.; Arrigoni, F.; Zampella, G., *Organometallics* **2016**, *35*, 2782-2792.
10. Yadav, S.; Vijayan, P.; Yadav, S.; Gupta, R., *Dalton Trans.* **2021**, *50*, 3269-3279.
11. Yadav, S.; Vijayan, P.; Gupta, R., *J. Organomet. Chem.* **2021**, *954*, 122081.
12. Ramachandran, R.; Prakash, G.; Viswanathamurthi, P.; Malecki, J., *Inorg. Chim. Acta* **2018**, *477*, 122-129.
13. Everaere, K.; Mortreux, A.; Carpentier, J. F., *Adv. Synth. Catal.* **2003**, *345*, 67-77.
14. Widaman, A. K.; Rath, N. P.; Bauer, E. B., *New J. Chem.* **2011**, *35*, 2427-2434.
15. Huber, D.; Kumar, P. A.; Pregosin, P. S.; Mikhel, I. S.; Mezzetti, A., *Helv. Chim. Acta* **2006**, *89*, 1696-1715.
16. Zhang, Q.-F.; Cheung, F. K.; Wong, W.-Y.; Williams, I. D.; Leung, W.-H., *Organometallics* **2001**, *20*, 3777-3781.
17. Riedel, J. C. *PhD Thesis, Development and Design of Transition Metal-Catalyzed Transformations in Macrocyclizations and Carbon–Carbon Bond Formations*. California, UC Irvine, **2019**.

18. Choi, J.; Fu, G. C., *Science* **2017**, 356, eaaf7230.
19. Ohno, K.; Kataoka, Y.; Mashima, K., *Org. Lett.* **2004**, 6, 4695-4697.
20. Yan, P.; Nie, C.; Li, G.; Hou, G.; Sun, W.; Gao, J., *Appl. Organomet. Chem.* **2006**, 20, 338-343.
21. Rabten, W.; Åkermark, T.; Kärkäs, M. D.; Chen, H.; Sun, J.; Andersson, P. G.; Åkermark, B., A ruthenium water oxidation catalyst based on a carboxamide ligand. *Dalton Transactions* **2016**, 45 (8), 3272-3276.
22. He, L.; Ni, J.; Wang, L. C.; Yu, F. J.; Cao, Y.; He, H. Y.; Fan, K. N., *Chem. A Eur. J.* **2009**, 15, 11833-11836.
23. Zhang, Z.; Butt, N. A.; Zhou, M.; Liu, D.; Zhang, W., *Chin. J. Chem.* **2018**, 36, 443-454.
24. Li, Y.-Y.; Yu, S.-L.; Shen, W.-Y.; Gao, J.-X., *Acc. Chem. Res.* **2015**, 48, 2587-2598.
25. van Putten, R.; Filonenko, G. A.; Gonzalez De Castro, A.; Liu, C.; Weber, M.; Müller, C.; Lefort, L.; Pidko, E., *Organometallics* **2019**, 38, 3187-3196.
26. Perez, M.; Elangovan, S.; Spannenberg, A.; Junge, K.; Beller, M., *ChemSusChem* **2017**, 10, 83-86.
27. Qin, J.; Zhou, Z.; Cui, T.; Hemming, M.; Meggers, E., *Chem. Sci.* **2019**, 10, 3202-3207.
28. Liu, T.; Chai, H.; Wang, L.; Yu, Z., *Organometallics* **2017**, 36, 2914-2921.
29. Zotova, N.; Roberts, F. J.; Kelsall, G. H.; Jessiman, A. S.; Hellgardt, K.; Hii, K. K. M., *Green Chem.* **2012**, 14, 226-232.
30. Alam, R. M.; Keating, J. J., *Synth.* **2021**, 53, 4709-4722.
31. Melle, P.; Manoharan, Y.; Albrecht, M., *Inorg. Chem.* **2018**, 57, 11761-11774.
32. Ngo, A. H.; Do, L. H., *Inorg. Chem. Front.* **2020**, 7, 583-591.
33. Çetinkaya, B.; Özdemir, I.; Bruneau, C.; Dixneuf, P. H., *Eur. J. Inorg. Chem.* **2000**, 2000, 29-32.

34. Ogwen, A. O.; Ojwach, S. O.; Akerman, M. P., *Dalton Trans.* **2014**, 43, 1228-1237.
35. Reddyrajula, R.; Dalimba, U., *Bioorg. Med. Chem. Lett.* **2020**, 30, 126846.
36. Vijayan, P.; Yadav, S.; Yadav, S.; Gupta, R., *Inorg. Chim. Acta* **2020**, 502, 119285.
37. Aradhyula, B. P. R.; Kaminsky, W.; Kollipara, M. R., *J. Mol. Struct.* **2017**, 1149, 162-170.
38. Vijayan, P.; Yadav, S.; Yadav, S.; Gupta, R., *Inorg. Chim. Acta* **2020**, 502, 119285.
39. Bansal, D.; Kumar, G.; Hundal, G.; Gupta, R., *Dalton Trans.* **2014**, 43, 14865-14875.
40. Bansal, D.; Gupta, R., *Dalton Trans.* **2016**, 45, 502-507.
41. Groom, C. R.; Bruno, I. J.; Lightfoot, M. P.; Ward, S. C., *Acta Crystallogr. Sec. B: Struct. Sci., Cryst. Eng. Mat.* **2016**, 72, 171-179.
42. Bruno, I. J.; Cole, J. C.; Edgington, P. R.; Kessler, M.; Macrae, C. F.; McCabe, P.; Pearson, J.; Taylor, R., *Acta Crystallogr. Sec. B: Struct. Sci.* **2002**, 58, 389-397.
43. Polshettiwar, V.; Varma, R. S., *Green Chem.* **2009**, 11, 1313-1316.
44. Ramollo, G. K.; Strydom, I.; Fernandes, M. A.; Lemmerer, A.; Ojwach, S. O.; Van Wyk, J. L.; Bezuidenhout, D. I., *Inorg. Chem.* **2020**, 59, 4810-4815.
45. Hall, A. M.; Dong, P.; Codina, A.; Lowe, J. P.; Hintermair, U., *ACS Catal.* **2019**, 9, 2079-2090.
46. Noyori, R.; Yamakawa, M.; Hashiguchi, S., *J. Org. Chem.* **2001**, 66, 7931-7944.
47. Abdur-Rashid, K.; Lough, A. J.; Morris, R. H., *Organometallics* **2000**, 19, 2655-2657.
48. Clapham, S. E.; Hadzovic, A.; Morris, R. H., *Coord. Chem. Rev.* **2004**, 248, 2201-2237.
49. Altan, O.; Yilmaz, M. K., *J. Organomet. Chem.* **2018**, 861, 252-262.
50. Cho, C. S.; Kim, B. T.; Kim, T.-J.; Shim, S. C., *J. Org. Chem.* **2001**, 66, 9020-9022.
51. Aydemir, M.; Baysal, A., *Polyhedron* **2010**, 29, 1219-1224.
52. Nagalakshmi, V.; Nandhini, R.; Venkatachalam, G.; Balasubramani, K., *J. Coord. Chem.* **2020**, 73, 206-216.

53. Matveevskaya, V. V.; Pavlov, D. I.; Sukhikh, T. S.; Gushchin, A. L.; Ivanov, A. Y.; Tennikova, T. B.; Sharoyko, V. V.; Baykov, S. V.; Benassi, E.; Potapov, A. S., *ACS Omega* **2020**, *5*, 11167-11179.
54. Chowdhury, N. S.; GuhaRoy, C.; Butcher, R. J.; Bhattacharya, S., *Inorg. Chim. Acta* **2013**, *406*, 20-26.
55. Bala, M.; Ratnam, A.; Kumar, R.; Ghosh, K., *J. Organomet. Chem.* **2019**, *880*, 91-97.
56. Roy, P.; Sarkar, D.; Ghosh, P.; Manna, C. K.; Murmu, N.; Mondal, T. K., *J. Mol. Struct.* **2020**, *1204*, 127524.
57. Cavarzan, D. A.; Pinheiro, C. B.; de Araujo, M. P., *Trans. Met. Chem.* **2015**, *40*, 117-123.
58. Baratta, W.; Schütz, J.; Herdtweck, E.; Herrmann, W. A.; Rigo, P., *J. Organomet. Chem.* **2005**, *690*, 5570-5575.
59. Johnson, T. C.; Totty, W. G.; Wills, M., *Organic Lett.* **2012**, *14*, 5230-5233.
60. Baratta, W.; Da Ros, P.; Del Zotto, A.; Sechi, A.; Zangrando, E.; Rigo, P., *Angew. Chem. Int. Ed.* **2004**, *43*, 3584-3588.
61. Witt, J.; Pöthig, A.; Kühn, F. E.; Baratta, W., *Organometallics* **2013**, *32*, 4042-4045.
62. Maity, A.; Sil, A.; Patra, S. K., *Eur. J. Inorg. Chem.* **2018**, *2018*, 4063-4073.
63. Paul, B.; Chakrabarti, K.; Kundu, S., *Dalton Trans.* **2016**, *45*, 11162-11171.
64. Li, K.; Niu, J.-L.; Yang, M.-Z.; Li, Z.; Wu, L.-Y.; Hao, X.-Q.; Song, M.-P., *Organometallics* **2015**, *34*, 1170-1176.
65. Liu, T.; Wu, K.; Wang, L.; Fan, H.; Zhou, Y.-G.; Yu, Z., *Organometallics* **2019**, *39*, 93-104.
66. Kumah, R. T.; Tsaulwayo, N.; Xulu, B. A.; Ojwach, S. O., *Dalton Trans.* **2019**, *48*, 13630-13640.
67. Cao, Z.; Qiao, H.; Zeng, F., *Organometallics* **2019**, *38*, 797-804.

68. Kalsin, A. M.; Peganova, T. A.; Sinopalnikova, I. S.; Fedyanin, I. V.; Belkova, N. V.; Deydier, E.; Poli, R., *Dalton Trans.* **2020**, 49, 1473-1484.
69. Ohkuma, T.; Utsumi, N.; Tsutsumi, K.; Murata, K.; Sandoval, C.; Noyori, R., *J. Am. Chem. Soc.* **2006**, 128, 8724-8725.
70. Wettergren, J.; Buitrago, E.; Ryberg, P.; Adolfsson, H., *Chem. A Eur. J.* **2009**, 15, 5709-5718.

## CHAPTER 4

### MONONUCLEAR AND DINUCLEAR (BIPYRIDYL)-CARBOXAMIDE RUTHENIUM(II) COMPLEXES: LIGAND CONTROLLED COORDINATION DIVERSITY AND CATALYTIC TRANSFER HYDROGENATION OF KETONES

#### 4.1. Introduction

The successful development of more robust, efficient and less hazardous protocols for transforming organic feedstocks into more valuable fine-chemical has become an active field of research in the synthetic community.<sup>1-2</sup> Particularly, catalysis has provided a straightforward, atom-economic strategy for accessing valuable fine chemical products such as pharmaceuticals, and agrochemicals.<sup>2-3</sup> Ever since the seminal works of Noyori and Ikariya,<sup>4</sup> a number of transition metal-based, including mononuclear and multinuclear complexes, have been developed for transfer hydrogenation (TH) reactions.<sup>5-6</sup> The process of cooperating multiple catalytic units into single organic moieties provide an opportunity to enhance catalytic activity and chemoselectivity.<sup>7</sup> The development of new multinuclear complexes for catalytic reactions has emerged as an interesting topic in homogeneous catalysis.<sup>8</sup> Multinuclear complexes have a bright future in catalysis, more significantly due to their attractive catalytic activities and synergistic impacts compared to their monometallic analogues.<sup>9-10</sup> Recently, a number of multinuclear complexes (i.e. Ru(II),<sup>6, 8</sup> Ir(I/III),<sup>11-13</sup> and Rh(II)<sup>14</sup>) complexes have been reported with the potential to catalyse TH of ketones. Many of these complexes were supported on *N*-heterocarbene (NHC),<sup>12</sup> amino-phosphine, Schiff base,<sup>15</sup> and phosphinite- Schiff base organic ligands.<sup>16</sup> Generally, the electronic property and adaptability of a ligand are the key factors that determine the efficiency of a multinuclear complex for a particular catalytic reaction.<sup>16</sup> A ligand-framework bearing multi-coordinating sites often favours the

establishment of the polynuclear complex. Multinuclear complexes are made by following simple synthetic procedures. Sequential coordination of a metal salt to a single ligand framework has also been recognised as a possible route of accessing polynuclear complexes.<sup>17-</sup>  
<sup>18</sup> The Ir(III)-NHC complexes reported by Taylor and co-workers is a classic example of multinuclear complexes made by adopting sequential coordination protocol.<sup>13</sup> Another versatile method of synthesising a multinuclear complex is the one-pot coordination method.  
<sup>18</sup> The one-pot coordination method has been employed in the synthesis of a number of polynuclear complexes that are used as catalysts in TH of ketones.<sup>9</sup> For instance, Yu and co-workers have recently employed the one-pot method to synthesis of a number of highly active multinuclear Ru(II) catalysts for TH of ketones.<sup>8, 19</sup> Dinuclear Ru(II)-NNN complex with the 4,4'-(CH<sub>2</sub>)<sub>3</sub>- bipyridine linker have also been developed using similar coordination method.<sup>8</sup>

Recently, a number of highly active multinuclear Ru(II) complexes have been synthesised and applied as catalysts for TH of ketones. Among them are the tri- and hexanuclear Ru(II) complexes reported with TOF up to  $7.1 \times 10^6 \text{ h}^{-1}$  by Yu and co-workers.<sup>8, 19</sup> Inspired by the works of Yu and co-workers, we herein report the synthesis of dinuclear ruthenium complexes, coordination chemistry driven by both carboxamide ligands and ruthenium(II) precursors and transfer hydrogenation of ketones.

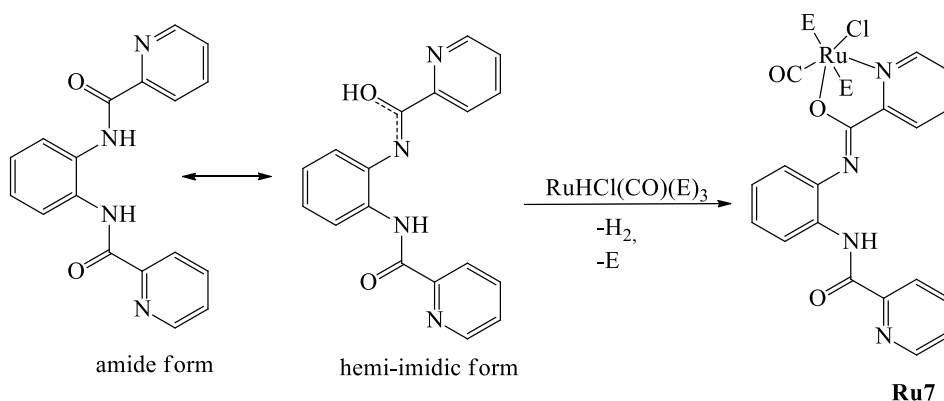
## 4.2. Results and discussion

### 4.2.1. Synthesis and characterisation of ligands and complexes

The *N, N*-(phenylene)-dipicolinamide ligands, **H<sub>2</sub>L3-H<sub>2</sub>L6**, were synthesised by simple condensation reactions between the appropriate phenylene-1,4-diamine/phenylene-1,2-diamine and picolinic acids following modified literature procedures.<sup>20-22</sup> Detailed synthetic

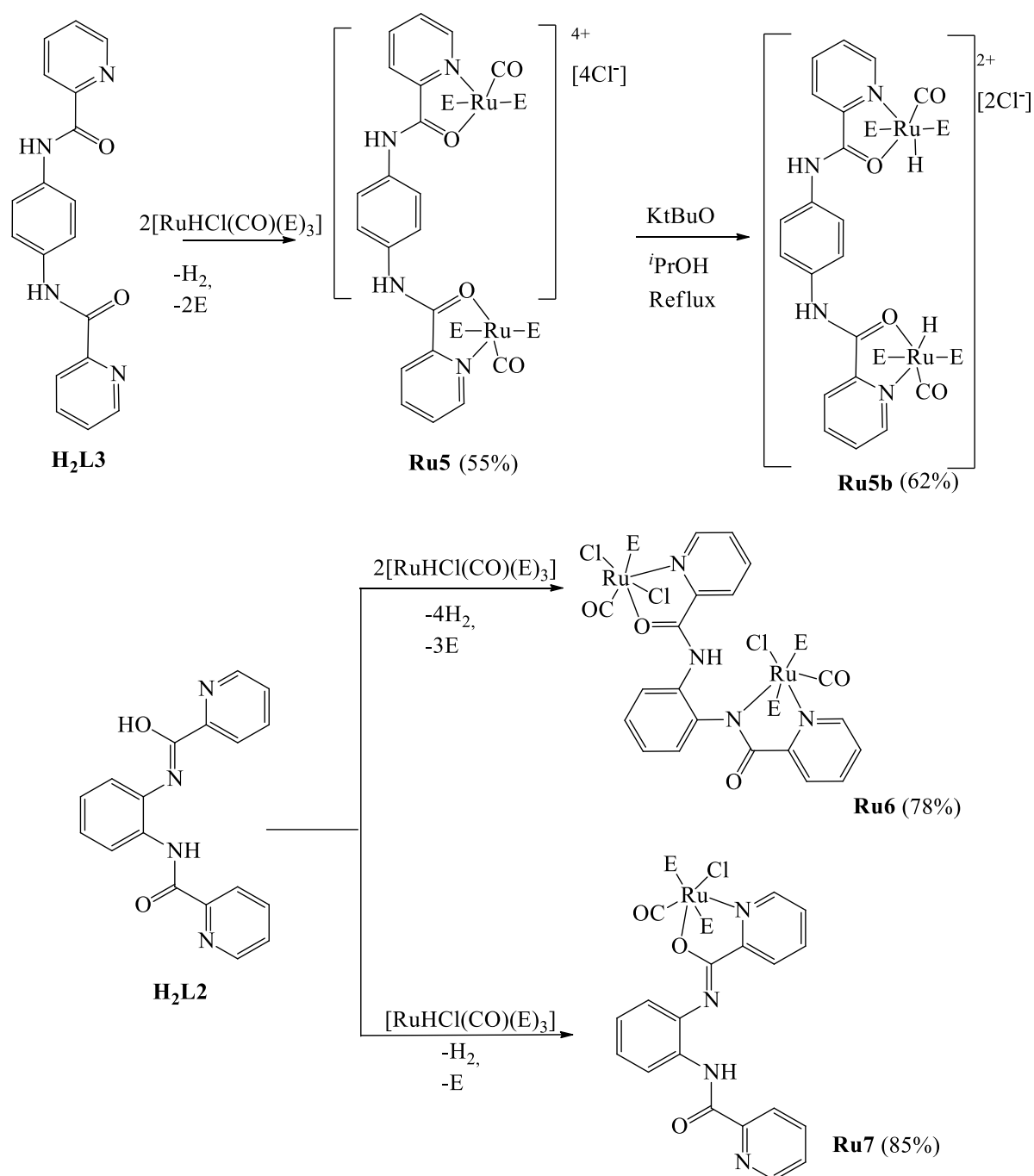
protocol, spectroscopic and analytical data are presented in **Chapter 2**. Treatment of *N,N*-(1,4-phenylene)-dipicolinamide (**H<sub>2</sub>L3**) with two molar equivalents of [RuHCl(CO)Cl(PPh<sub>3</sub>)<sub>3</sub>] afforded a dinuclear cationic Ru(II) complex **Ru5**, in which the ligand adopts an  $\kappa^1(\text{N})\text{-}\kappa^1(\text{O})$  coordination mode.

Interestingly, reactions of *N,N*-(1,2-phenylene)-dipicolinamide (**H<sub>2</sub>L4**) with two molar equivalents of [RuHCl(PPh<sub>3</sub>)<sub>3</sub>(CO)] gave a non-symmetrical **Ru6** complex (**Scheme 4.2**). As opposed to the N<sup>^</sup>O coordination mode in complex **Ru5**, in complex **Ru6**, both  $\kappa^1(\text{N})\text{-}\kappa^1(\text{O})$  and  $\kappa^1(\text{N})\text{-}\kappa^1(\text{N})$  binding modes are adopted. In addition, in complex **Ru6**, one Ru(II) atom is six-coordinate, bearing one PPh<sub>3</sub> and two Cl ligands in the coordination sphere, while the other Ru(II) atom is six-coordinate, containing two PPh<sub>3</sub> *co*-ligands. It is believed that this unique coordination behaviour witnessed in complex **Ru6** is driven by steric effects imposed by the rigid 1,2 substituted ligand (**H<sub>2</sub>L4**), as opposed to the less sterically demanding 1,4 substituted ligand **H<sub>2</sub>L3**. Separately, the use of one molar equivalent of [RuHCl(PPh<sub>3</sub>)<sub>3</sub>(CO)] with **H<sub>2</sub>L4** afforded the respective neutral mononuclear complex **Ru7**, containing one non-coordinating arm of the ligand (**Scheme 4.1**). This observation points to the reactions of the ligands and the [RuHCl(PPh<sub>3</sub>)<sub>3</sub>(CO)] as being more kinetically controlled than a thermodynamic phenomenon.



**Scheme 4.1.** Rearrangement reactions within the ligand prior to the formation of dinuclear Ru(II) complex **Ru7**.

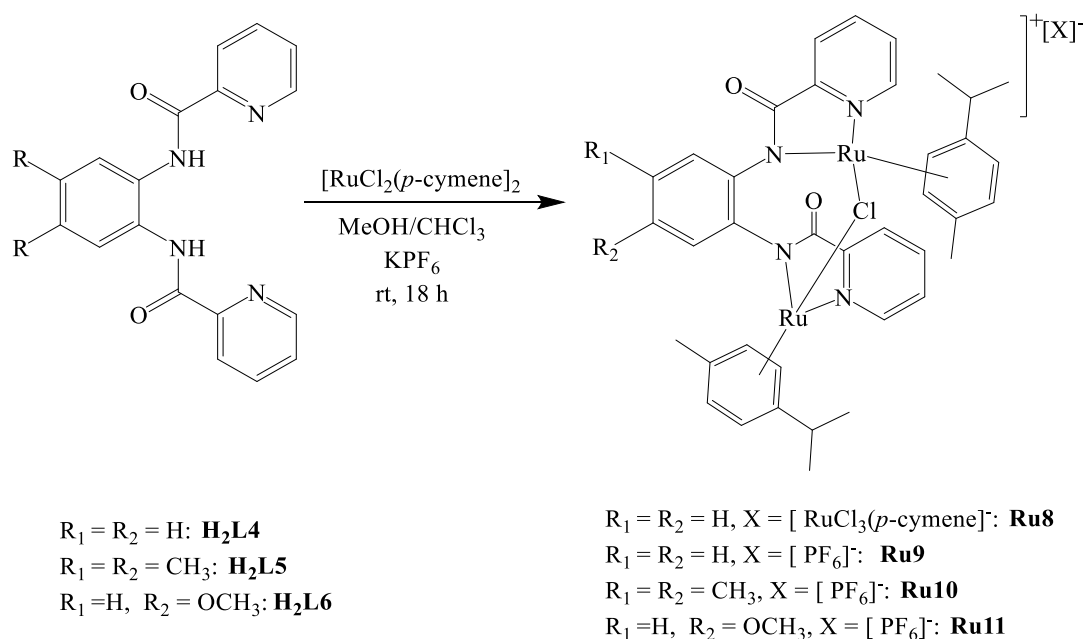




**Scheme 4.2.** Synthesis of carbonyl ruthenium(II) complexes, **Ru5** - **Ru7**.

The treatments of [Ru( $\eta^6$ -cymene)Cl<sub>2</sub>]<sub>2</sub> precursor with the *N,N*-(1,4-phenylene)-dipicolinamide ligand **H<sub>2</sub>L4** in the presence of sodium methoxide (NaOMe) resulted in the formation of the dinuclear half-sandwich ruthenium(II) complex [{Ru( $\eta^6$ -*p*-cymene)<sub>2</sub>- $\mu$ -

Cl}**L4**][Ru( $\eta^6$ -*p*-cymene)Cl<sub>3</sub>], (**Ru8**). An anionic exchange with KPF<sub>6</sub> resulted to the formation of corresponding complex [{Ru( $\eta^6$ -*p*-cymene)]<sub>2</sub>- $\mu$ -Cl}**L4**][PF<sub>6</sub>], (**Ru9**) as illustrated in **Scheme 4.3**. Reaction of [RuCl<sub>2</sub>( $\eta^6$ -cymene)]<sub>2</sub> precursor with the *N,N*-(phenylene)-dipicolinamide ligands **H2L5** and **H2L6** following similar protocol as described for **Ru2** gave the corresponding complexes [ {(Ru( $\eta^6$ -*p*-cymene)<sub>2</sub>- $\mu$ -Cl}**L5**][PF<sub>6</sub>], (**Ru1**) and [ {(Ru( $\eta^6$ -*p*-cymene)<sub>2</sub>- $\mu$ -Cl}**L6**][PF<sub>6</sub>], respectively (**Scheme 1**). The complexes **Ru5-Ru11** were soluble in dichloromethane, chloroform, methanol, dimethyl sulfone, ethanol, and isopropyl alcohol but insoluble in diethyl ether, hexane and THF. All complexes were characterised using FT-IR spectroscopy, ESI-MS spectrometry, <sup>1</sup>H and <sup>13</sup>C{<sup>1</sup>H}, <sup>31</sup>P{<sup>1</sup>H} and <sup>19</sup>F{<sup>1</sup>H} NMR spectroscopies, elemental analyses, and single-crystal X-ray analysis (**Ru5-Ru8** and **Ru11**).



**Scheme 4.3.** Synthesis of half-sandwich ruthenium(II) complexes **Ru8-Ru11**.

The successful formation of complexes **Ru5-Ru11** was established by comparing the <sup>1</sup>H NMR spectra of the complexes to the respective free ligands. For example, the <sup>1</sup>H NMR spectrum of complex **Ru5** showed the signal assigned to N-H proton shifted considerably to 11.78 ppm

relative to  $\delta$ : 10.07 ppm in the ligand, **H<sub>2</sub>L3** (**Figure 4.1**). The appearance of the two signals of the N-H<sub>amide</sub> group in **Ru1** could arise from the existence of two different fluxional isomers, which indicates restricted rotations in the complexes leading to the protons being subjected to different signal contributions on the NMR time scale. However, the signal separation ( $\Delta\delta = 0.079$  ppm) is rather unusual and indicates the increased restricted rotation from the arene linker groups, as shown in **Figure 4.9**. The shift in the signal of the N-H<sub>amide</sub> upon coordination suggests resonance enhancement in the amide functionality and involvement of O<sub>carbonyl</sub>-atom in the coordination, as revealed by the solid-state structure (**Figure 4.9**). It is consistent in the <sup>1</sup>H NMR spectra of complexes **Ru5-Ru7**.

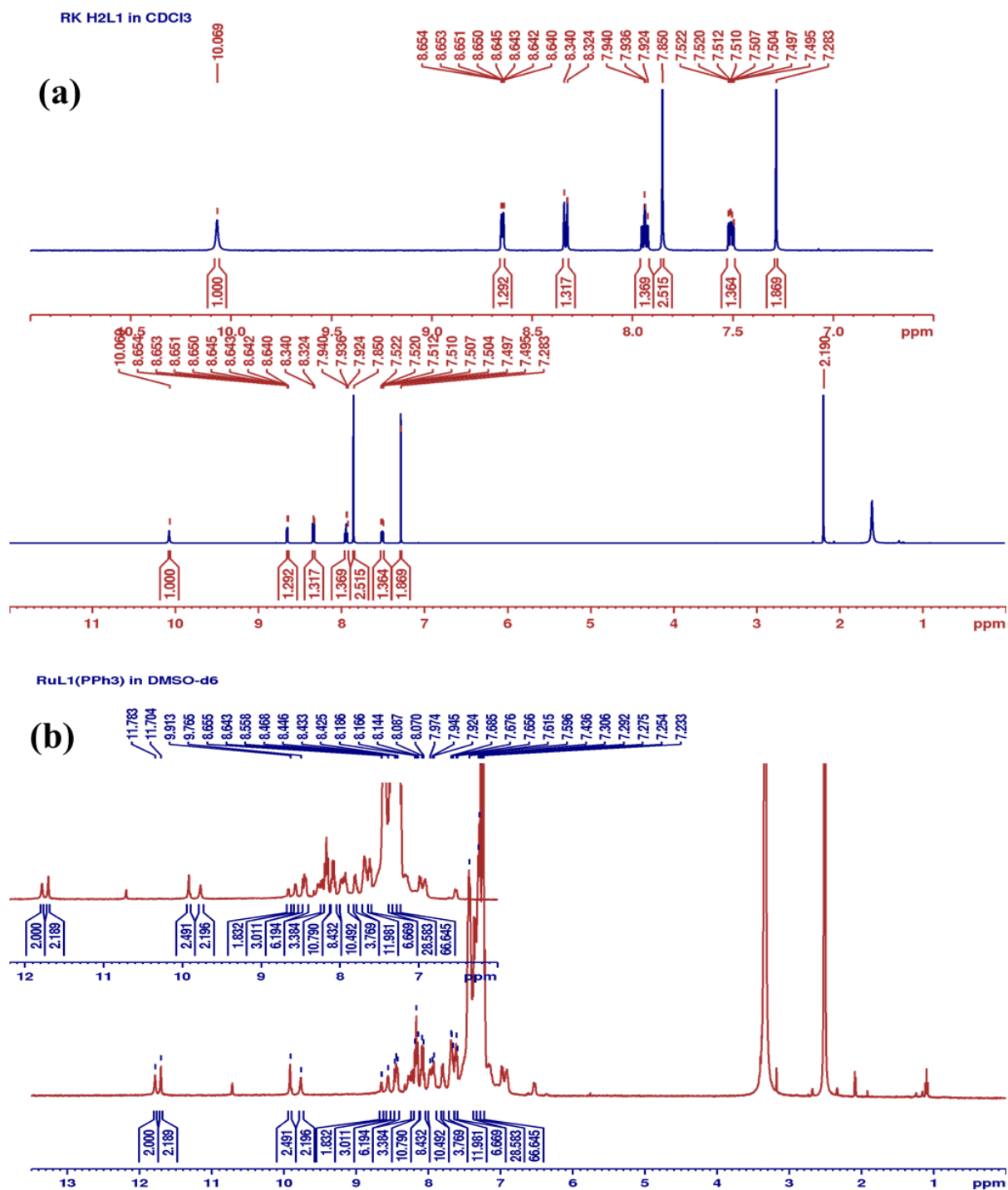


**Figure 4.1.** A comparison in chemical shifts in the <sup>1</sup>H NMR spectra of **(a) H<sub>2</sub>L3** (N-H<sub>amide</sub> at δ: 10.07 ppm) and **(b) Ru5** (N-H<sub>amide</sub> at δ: 11.07 ppm).

The formation of the [Ru-H<sub>2</sub>] species (**Ru5b**) from complex **Ru5** was easily deduced from the two triplets at -10.21 (t, <sup>2</sup>J<sub>H-P</sub>: 14.8 Hz, Ru-H) and -16.00 ppm (t, <sup>2</sup>J<sub>H-P</sub>: 12.8 Hz, Ru-H) assignable to the Ru-H protons (**Figure 4.2**). In contrast to the complex **Ru5**, the <sup>1</sup>H NMR spectrum of **Ru6**, displayed only one signal of the N-H<sub>amide</sub> proton was observed at 10.63 ppm (10.71 ppm for the ligand **H<sub>2</sub>L4**). This agrees with the molecular structure of complex **Ru6** (**Figure 4.10**), which confirms the deprotonation of one N-H proton to give the N<sup>-</sup>N coordination at one of the Ru(II) centre. In the <sup>1</sup>H NMR spectrum of the mononuclear complex **Ru7**, the N-H<sub>amide</sub> signal appeared at 12.52 ppm (compared to the free-ligand, **H<sub>2</sub>L4**, 10.71 ppm). This supports the coordination of ligand **H<sub>2</sub>L4** to the of Ru(II) atom on one arm as established from its molecular structure (**Figure 4.11**). The observation indicates the existence of one species in solution, which is assumed to be the same as the solid-state structure in **Figure 4.11**.

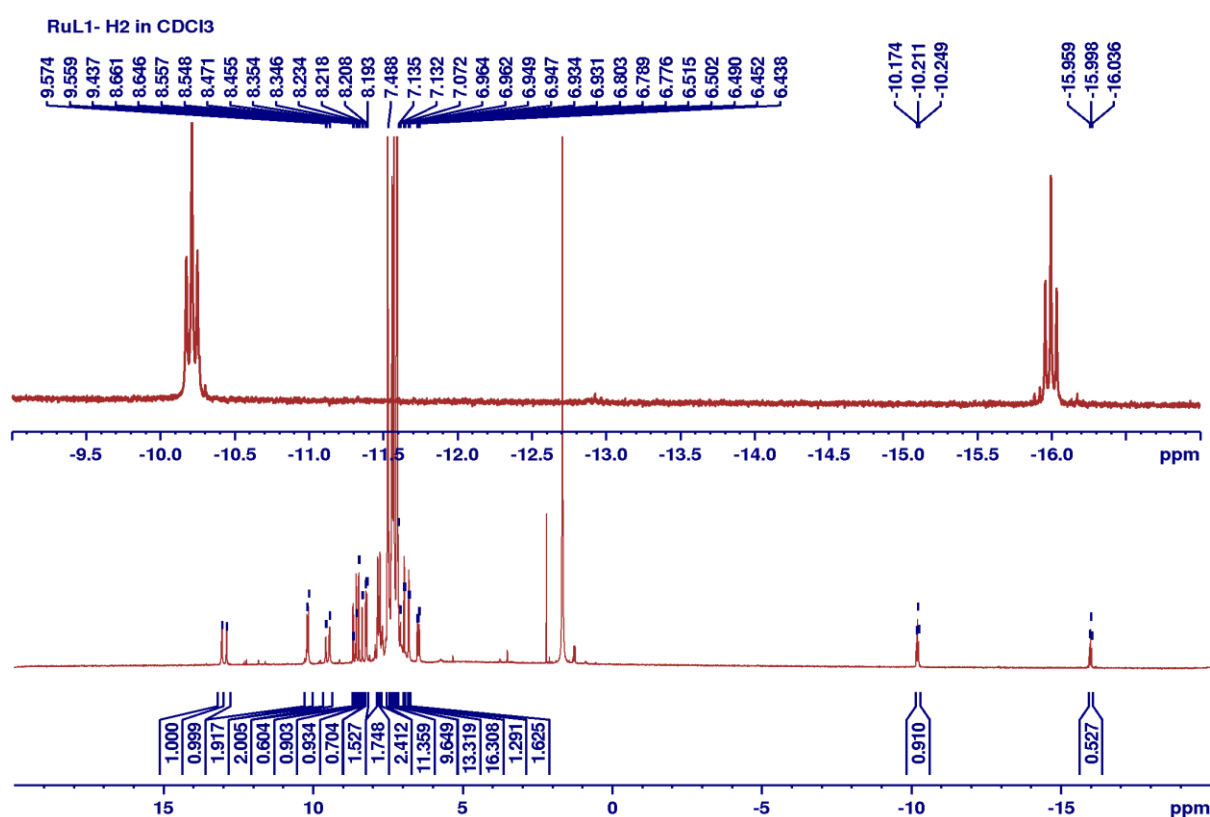


**Figure 4.2.** <sup>1</sup>H NMR spectrum of complex **Ru5b** obtained from **Ru5** showing two signals for N-H<sub>iminolate</sub> protons at 13.8 ppm and 13.6 ppm and Ru-H at -10.21 ppm and -16.03 ppm.

The half-sandwich complexes, **Ru8-Ru11**, exhibited different characteristic features from their analogous complexes, **Ru5-Ru7**. For instance, in the complex **Ru9**, amide proton (N-H) signals disappeared upon coordination (**Figures 4.3**). This observation is consistent in the  $^1\text{H}$  NMR spectroscopic data of **Ru8**, **Ru9-Ru11**, which is clear evidence of deprotonation and coordination of the metal precursor to the  $\text{N}_{\text{amide-atom}}$ .<sup>23-24</sup> In addition, the  $^1\text{H}$  NMR spectra of the complexes **Ru5-Ru11** also displayed a significant shift in the signals of the pyridyl protons (7.80-9.40 ppm) compared to the free ligands **H<sub>2</sub>L4-H<sub>2</sub>L6** (7.45 - 8.69 ppm). This could be attributed to the involvement of the  $\text{N}_{\text{pyridine-atom}}$ .<sup>23</sup> Noticeably, both the *p*-cymene and phenylene linker protons showed no considerable shift in the  $^1\text{H}$  NMR of the complexes **Ru8-Ru11** compared to the corresponding ligands (**H<sub>2</sub>L4-H<sub>2</sub>L6**).

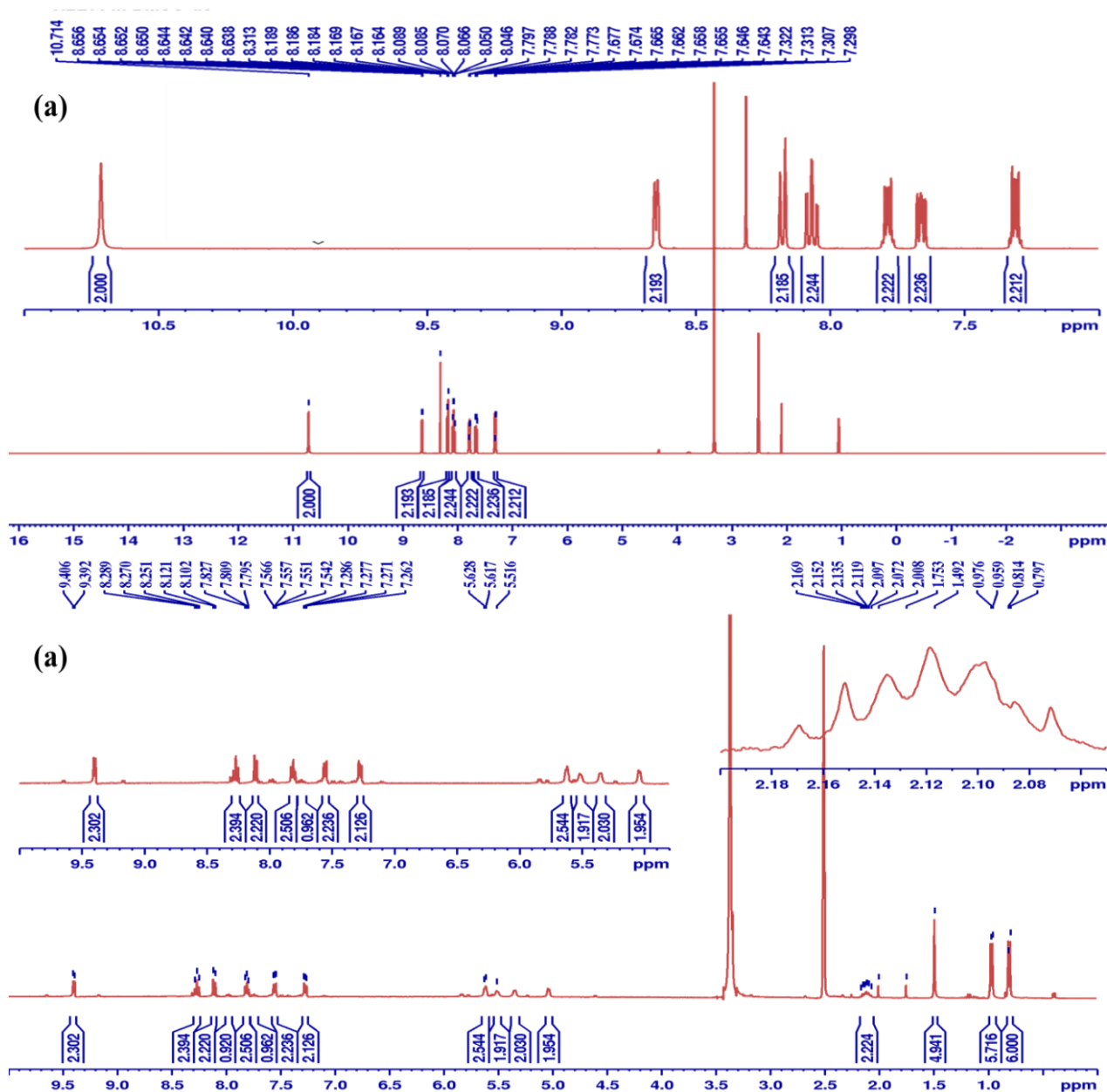


**Figure 4.3.** A comparison in chemical shifts in the  $^1\text{H}$  NMR spectra of (a) **H<sub>2</sub>L4** ( $\text{N-H}_{\text{amide}}$  at  $\delta$ : 10.07 ppm) and (b) **Ru9** ( $\text{N-H}_{\text{amide}}$ : absent).

$^{13}\text{C}\{^1\text{H}\}$  NMR spectroscopy was also helpful in establishing the formation of the Ru(II) complexes **Ru5-Ru11**. The  $^{13}\text{C}\{^1\text{H}\}$  NMR spectra of the complexes **Ru5-Ru7** showed carbonyl carbon ( $\text{C}_{\text{iminolate}}$ ) signal slightly shifted to the higher field (downfield) compared to the free ligands, **H<sub>2</sub>L3** and **H<sub>2</sub>L4**. For example, **Ru5** showed the carbonyl carbon ( $\text{C}_{\text{iminolate}}$ )

signal at  $\delta$ : 167 ppm compared to corresponding ligand **H<sub>2</sub>L3** (164 ppm). A similar observation was made in the  $^{13}\text{C}\{^1\text{H}\}$  NMR spectra of half-sandwich **Ru8-Ru11** complexes where the carbonyl carbon ( $\text{C}_{\text{amide}}$ ) shifted slightly downfield (168.7-169.6 ppm) compared to their corresponding free ligands, **H<sub>2</sub>L1-H<sub>2</sub>L3** (162.9-163.6 ppm). For example, complex **Ru10** showed a shift in carbonyl carbon ( $\text{C}_{\text{amide}}$ ) signal at  $\delta$ : 169.6 ppm relative to its corresponding ligand **HL4** ( $\delta$ : 162.9 ppm), as depicted in **Figure 4.4**.

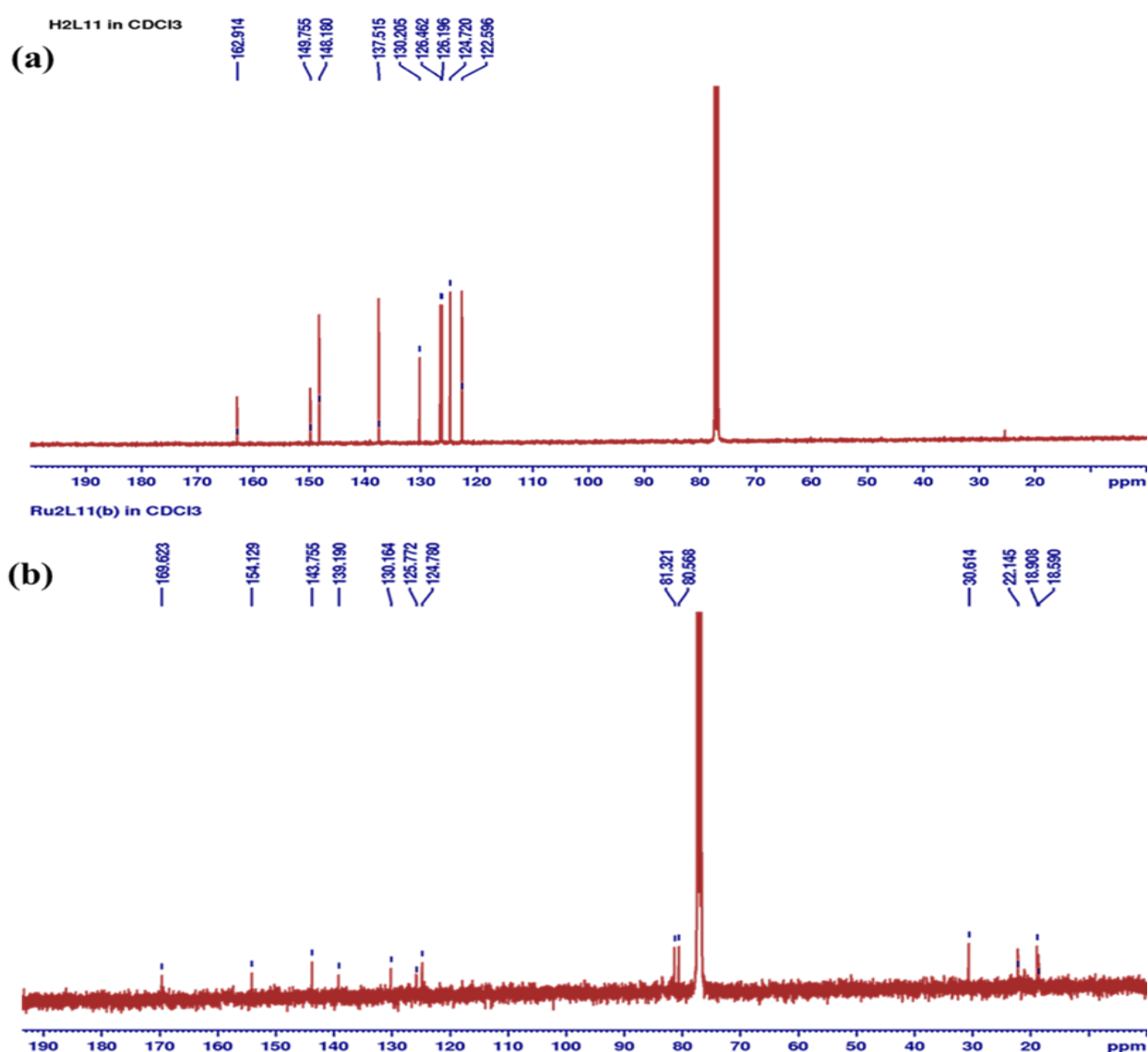


**Figure 4.4.** A comparison in chemical shifts between the  $^{13}\text{C}\{^1\text{H}\}$  NMR spectra of (a) **H<sub>2</sub>L4** ( $\text{C}_{\text{amide}}$  at  $\delta$ : 162.9 ppm) and (b)  $^1\text{H}$  NMR spectrum of **Ru9** ( $\text{C}_{\text{amide}}$  at  $\delta$ : 169.6 ppm).



$^{31}\text{P}\{^1\text{H}\}$  NMR spectra of the complexes of **Ru5** and **Ru7**, for instance, **Ru5** showed a singlet signal assigned to the  $\text{PPh}_3$  moiety at  $\delta$ : 44.5 ppm (**Figure 4.5**), which rationally suggests the presence of two equivalent phosphines oriented *trans* at each Ru(II) centres.<sup>25-26</sup> Interestingly, **Ru6** showed two peaks which resonance at 45 ppm signifying the presence of two sets of non-equivalent  $\text{PPh}_3$  in the compound. The  $^{31}\text{P}\{^1\text{H}\}$  NMR spectroscopy was also instrumental in confirming the presence of the counterion,  $[\text{PF}_6]^-$  in the complexes **Ru9-Ru11**. For instance, complex **Ru11** showed a septet signal between  $\sim 131$  and  $\sim 157$  ppm in the  $^{31}\text{P}\{^1\text{H}\}$  NMR spectrum.  $^{19}\text{F}\{^1\text{H}\}$  NMR spectroscopic data was also given doublets between  $\sim 69$  and ( $\sim 71$ ) ppm (**Figure 4.5** and **4.6**), which further support the presence of  $[\text{PF}_6]^-$ .

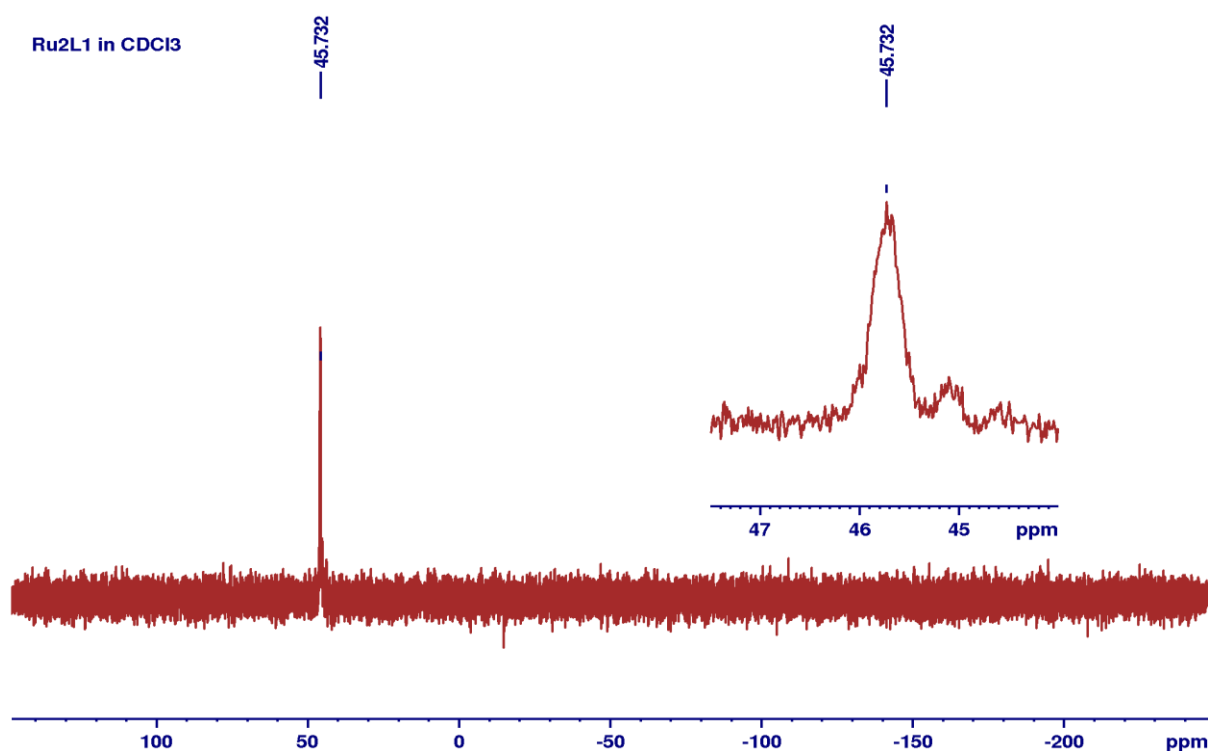


**Figure 4.5.**  $^{31}\text{P}\{^1\text{H}\}$  NMR spectrum of complex **Ru5** showing a typical septet signal at  $\delta$ : 44.6 ppm indicating the presence of two equivalent  $\text{PPh}_3$  *trans* to each other.

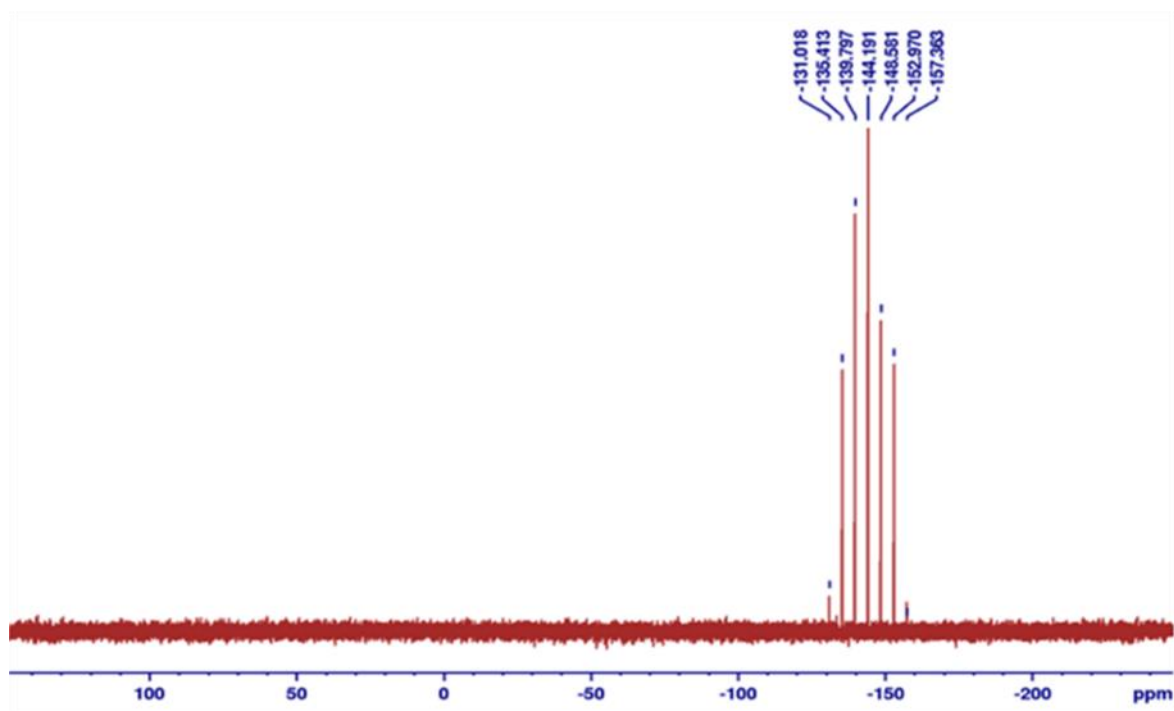


**Figure 4.6.**  $^{31}\text{P}\{^1\text{H}\}$  NMR of complex **Ru11** showing signal between 131 and 157 ppm confirming the presence of  $[\text{PF}_6]^-$  counterion.

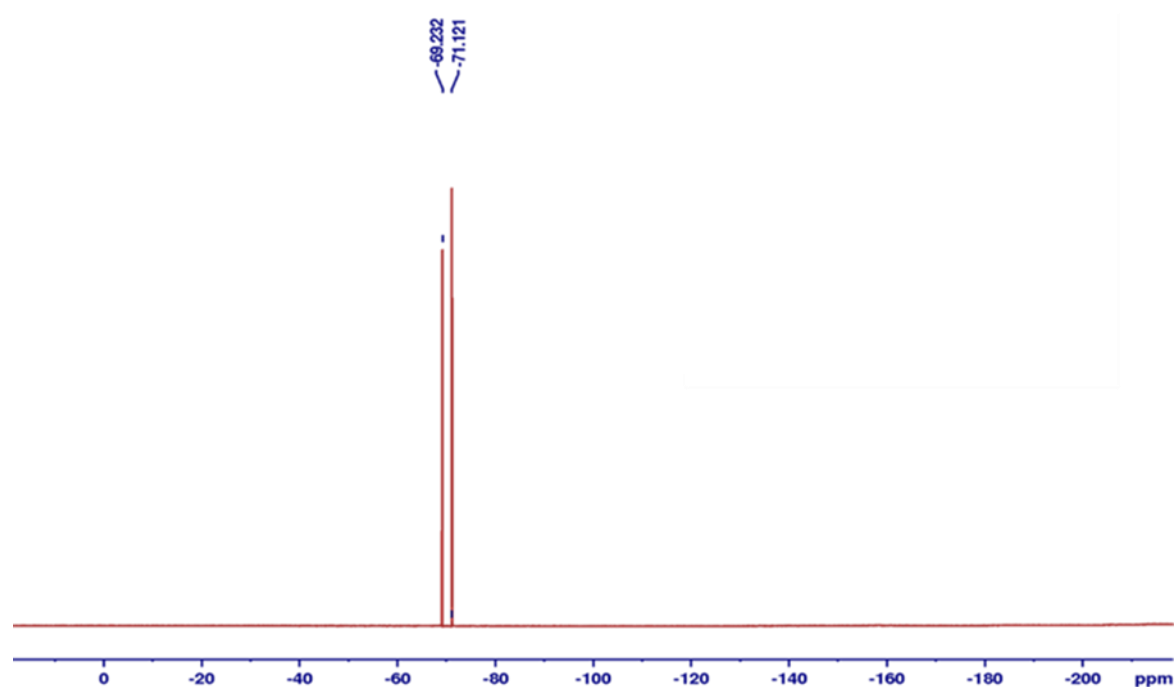


**Figure 4.7.**  $^{19}\text{F}$  NMR of complex **Ru11** showing a doublet signal between ~69 and ~79 ppm confirming the presence of  $[\text{PF}_6]^-$  counterion.

FT-IR spectra of complexes **Ru5-Ru11** were also used to decipher their identities. In general, the  $\nu(\text{N-H})$  stretching frequencies of the complexes **Ru5-Ru7** were recorded downfield (3257-3358  $\text{cm}^{-1}$ ), compared to the corresponding free-ligands **H2L3** and **H2L4** in the range of 3312-3331  $\text{cm}^{-1}$  (**Table 4.1**). In addition, the sharp  $\nu(\text{C=O})$  stretching band in **H2L3** at (1662) shifted slightly to lower frequencies (1578  $\text{cm}^{-1}$ ) in the respective complex **Ru5** (**Table 4.1**). This clearly, confirmed the established O-atom coordination to the Ru(II) atoms in **Ru5**. In the FT-IR spectrum of complexes **Ru6**, two stretching signals at 1620  $\text{cm}^{-1}$  and 1578  $\text{cm}^{-1}$  assigned to (C=O) groups respectively, were observed. The bathochromic shift in the carbonyl  $\nu(\text{C=O})$  signal to 1620  $\text{cm}^{-1}$  compared to the corresponding ligand, **H2L4** (1667  $\text{cm}^{-1}$ ) (**Table 4.1**) could be the consequence of resonance enhancement in of the amidate bond and also an indication of both  $\kappa 1(\text{N})-\kappa 1(\text{N})$  and  $\kappa 1(\text{N})-\kappa 1(\text{O})$  coordination modes.<sup>20</sup> Similarly, two stretching signals assigned to  $\nu(\text{C=O})$  and  $\nu(\text{C-O})$  appeared at 1678  $\text{cm}^{-1}$  and 1578  $\text{cm}^{-1}$  (**Table 4.1**) in the FT-IR spectrum of **Ru7** and supports the coordinated and non-coordinated arms as depicted in **Scheme 2** and molecular structure in **Figure 4.12**. The presence of the terminal CO *co*-ligand ( $\text{Ru-C}\equiv\text{O}$ ) in complexes **Ru5-Ru7** was also derived from the additional stretching frequencies at 1916  $\text{cm}^{-1}$  (**Ru5**), 1930  $\text{cm}^{-1}$  (**Ru6**) and 1930  $\text{cm}^{-1}$  (**Ru7**) as showed in **Table 4.1**. These values compare well with the frequencies of 1939-1949  $\text{cm}^{-1}$  reported by Gupta *et al.*<sup>20, 22, 25</sup>

However, the stretching signal of  $\nu(\text{N-H})_{\text{amide}}$  recorded between 3322-3325  $\text{cm}^{-1}$  in the ligand **H2L4-H2L6** disappeared in the spectroscopic data of the corresponding complexes **Ru8-Ru11**, which is consistent with the  $^1\text{H}$  NMR data of the complexes **Ru8-Ru11** as discussed *vide supra*. Furthermore, the FT-IR spectroscopic data of the complexes **Ru8-Ru11** (**Table 4.1**) showed an absorption band for the  $\nu(\text{C=O})_{\text{amide}}$  at lower frequencies (1618-1620  $\text{cm}^{-1}$ ) compared to their corresponding free ligands **H2L4-H2L6** (1664-1688  $\text{cm}^{-1}$ ), which could be interpreted in terms

of resonance-enhancement in the ligand backbone as observed in the  $^1\text{H}$  NMR spectroscopic data of the complexes **Ru8-Ru11**.

**Table 4.1.** Selected FT-IR spectroscopic data of the complexes **Ru5-Ru11** and corresponding ligands **H<sub>2</sub>L3-H<sub>2</sub>L6**.

Entry	Complex	$\nu(\text{C}=\text{O})^{\text{a}}_{\text{amide}}$	$\nu(\text{C}\equiv\text{O})_{\text{terminal}}$	$\nu(\text{N}-\text{H})^{\text{a}}_{\text{amide}}$
1	<b>Ru5</b>	1578(1660)	1960	3418(3331)
2	<b>Ru6</b>	1620 and 1578(1664)	1953	3334(3312)
3	<b>Ru7</b>	1678 and 1578(1664)	1948	3364(3312)
4	<b>Ru8</b>	1618(1664)	-	-
5	<b>Ru9</b>	1619(1664)	-	-
6	<b>Ru10</b>	1620(1663)	-	-
7	<b>Ru11</b>	1619(1664)	-	-

<sup>a</sup>FT-IR spectroscopic data of the ligands are in brackets.

(-) - Not applicable

The ESI-MS spectra of complexes of the complexes **Ru5-Ru11** were recorded in positive mode to establish the molecular composition. For instance, complex **Ru5** exhibited a base peak at  $m/z = 1626$  (**Ru5**) corresponding to the fragment,  $[\text{M}, 100]^+$  (**Figure 4.8**), while complexes **Ru6** and **Ru7** showed a base peak at  $m/z = 1365$  (**Ru6**) and  $972$  (**Ru7**) corresponding to molecular fragment ions,  $[\text{M}-\text{Cl}, 100]^+$ . Similarly, **Ru8-Ru11** showed their base peak corresponding to the cationic species,  $[\text{M}]^+$ . For instance, complex, **Ru10** showed its base peak at  $m/z = 825$   $[\text{M}, 100]^+$  corresponding to the cationic complex. All experimental and theoretical calculated isotopic mass distributions were in good agreement, as illustrated in **Figures 4.8** and **4.9**. The elemental analysis data of complexes **Ru5-Ru12** were consistent with

one ligand motif and two metal centres, confirming empirical formulae of the complexes and the purity.

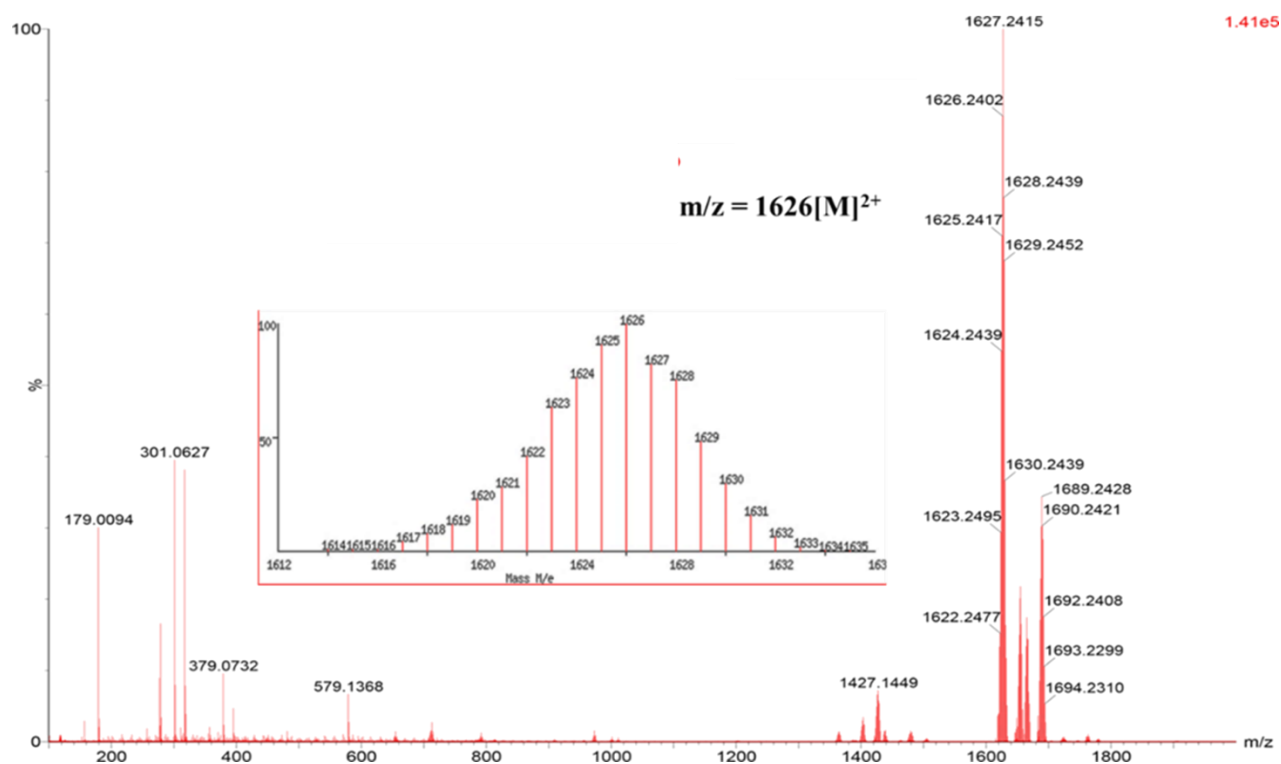


**Figure 4.8.** ESI -MS (positive mode) of complex **Ru5** showing the molecular ion peak at  $m/z = 1626 [M]^{2+}$ . Simulated isotopic mass distribution of the cationic species, **Ru5** (Inset).

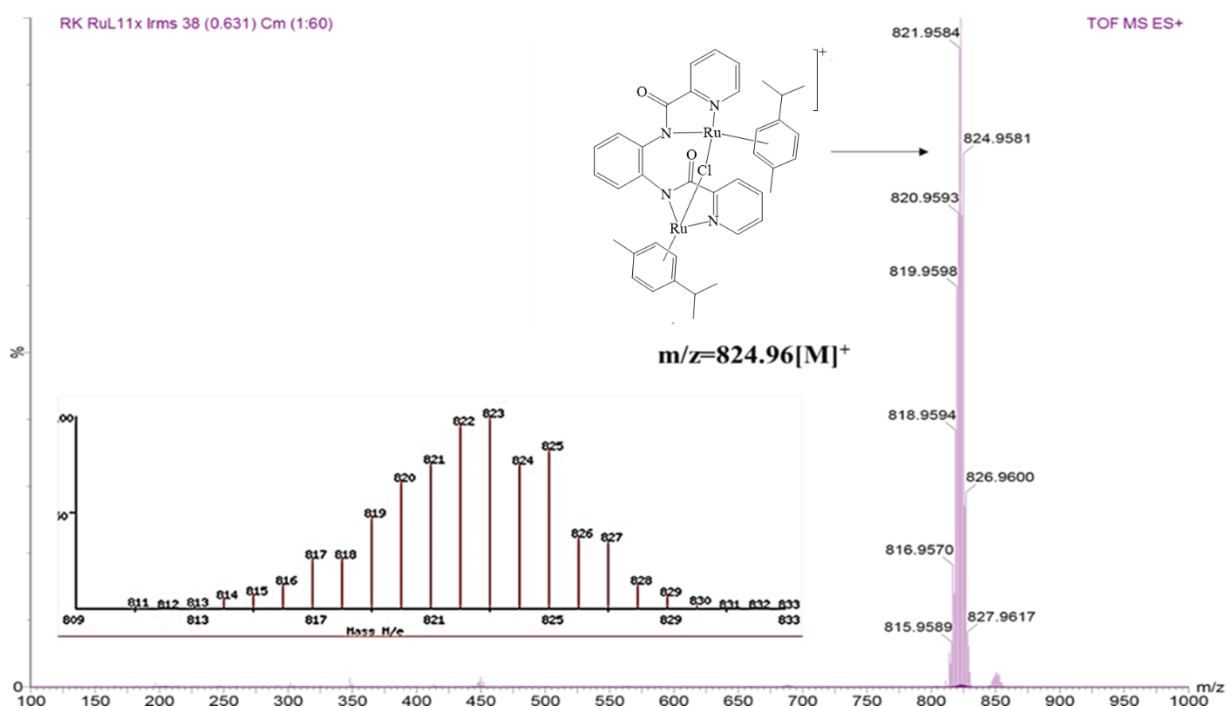


**Figure 4.9.** ESI -MS (positive mode) of complex **Ru9** showing the molecular ion peak at  $m/z = 825[M^+, 100]$  corresponding to the cationic species with formula,  $C_{92}H_{74}N_4O_4P_4Ru_2$ . Theoretical isotopic mass distribution of the cationic species of the complex, **Ru9** (inset).

#### 4.2.2. Molecular structure of the complexes **Ru5-Ru8** and **Ru11**

Single-crystal X-ray crystallography technique was used to confirm the coordination geometry around the Ru(II) atoms in complexes **Ru5-Ru8** and **Ru11**. The ORTEP view of the three complexes drawn at 50% thermal ellipsoid with atom labelling is depicted in **Figures 4.10-4.13**, while the summary of the crystallographic data is presented in **Tables 4.2** and **4.3**. The complexes **Ru5** and **Ru5b** belong to a monoclinic system with a space group of  $P2_1/n$ , while the remaining complexes **Ru6** and **Ru7** belong to the triclinic system with the  $P_1$  space group. In the compound, **Ru5**, the Ru(II) atoms coordinated to the dipyridine-dipicolinamide ligands, **H<sub>2</sub>L3** through the  $N_{pyridine}$ -atom and  $O_{amidate}$ -atom to form 5 membered ruthenium-cycles with bite angles of  $74.10(8)^\circ$  (**Figure 4.10**). However, the Ru(II) atoms in the complex **Ru6**, coordinated *via*  $N_{pyridine}$  and  $N_{amidate}$  atoms  $N_{pyridine}$  and  $O_{amidate}$  mode to form 5- and 6-

membered rings with bite angles of  $66.12(12)^\circ$  and  $69.21(11)^\circ$ , respectively (**Figure 4.11**). In the complex **Ru5**, two  $\text{PPh}_3$  and  $\text{C}\equiv\text{O}$  co-ligands occupy the three remaining coordinating sites of the two Ru(II) atoms to constitute a distorted trigonal bipyramidal geometry (**Figure 4.10**). However, the complex, **Ru6**, adopts both distorted octahedron and trigonal bipyramidal geometries around its Ru(II) atoms. The complex **Ru7** displays distorted octahedral geometry around its Ru(II) ion, with an additional Cl atom occupying the sixth axial coordinating site (**Figure 4.12**). In the complexes **Ru5- Ru7**,  $\text{PPh}_3$  are oriented *trans* to each other and while the  $\text{C}\equiv\text{O}$  groups reside in the same plane with the chelating sphere. This arrangement is favoured to minimise steric hindrance around the coordination spheres to enhance the complexes' stability and mutual  $\pi$ -interactions of atoms.<sup>27</sup> Notably, a slight torsional angle is observed for the planar orthometalated chelated rings  $\text{N}(1)\text{-C}(6)\text{-C}(7)\text{-O}(1)$ ,  $-6.8(3)^\circ$  in both complexes **Ru5** and **Ru7** compared to  $-10.41(8)^\circ$  observed in similar nine (9) complexes deposited in the CCDC file.<sup>28</sup> The net charge on complex **Ru5** is balanced by the presence of two chlorido co-ligands located outer-sphere of the coordination environment. In general, the average  $\text{Ru-N}_{\text{pyridine}}$ ,  $2.153(7) \text{ \AA}$ ,  $\text{Ru-O}_{\text{amidate}}$ ,  $2.153(4) \text{ \AA}$ , and  $\text{Ru-C}\equiv\text{O}$ ,  $1.866(6) \text{ \AA}$  in the complexes **Ru5 - Ru7** are found within the maximum range of  $2.155 \pm 0.073 \text{ \AA}$ ,  $2.158 \pm 0.045 \text{ \AA}$ , and  $1.984 \pm 0.053 \text{ \AA}$  respectively in 8-15 similar structures deposited in CSD file.<sup>28</sup> Similarly, the average  $\text{Ru-P}$  bond distance,  $2.338(7) \text{ \AA}$ , is within the average bond length,  $2.338 \pm 0.042 \text{ \AA}$  of 26 related Ru(II) complexes containing similar two *trans*  $\text{PPh}_3$  co-ligands found in CSD.<sup>28</sup> The bond angles subtended by the ruthenium centres, namely;  $\text{N}(1)\text{-Ru}(1)\text{-O}(1)$ ,  $74.10(8)^\circ$ ;  $\text{P}(1)\text{-Ru}(1)\text{-O}(1)$ ,  $85.68(5)^\circ$ ; and  $\text{N}(1)\text{-Ru}(1)\text{-P}(1)$ ,  $93.12^\circ$  deviate from the idealised  $90^\circ$  of the perfect trigonal bipyramidal in the complexes **Ru5-Ru7**. In addition, the average *trans* angles of  $\text{P}(1)\text{-Ru}(1)\text{-P}(2)$ ,  $165.68(5)^\circ$  and  $\text{C}(1)\text{-Ru}(1)\text{-O}(1)$ ,  $175.80(13)^\circ$  to the coordinated  $\text{N}(1)$  and  $\text{O}(1)$  atom respectively deviate from linearity,  $180^\circ$  and consequently resulted to minimal the average  $\text{N}(1)\text{-Ru}(1)\text{-O}(1)$  bite angle,  $74.10(5)^\circ$ .<sup>28</sup>

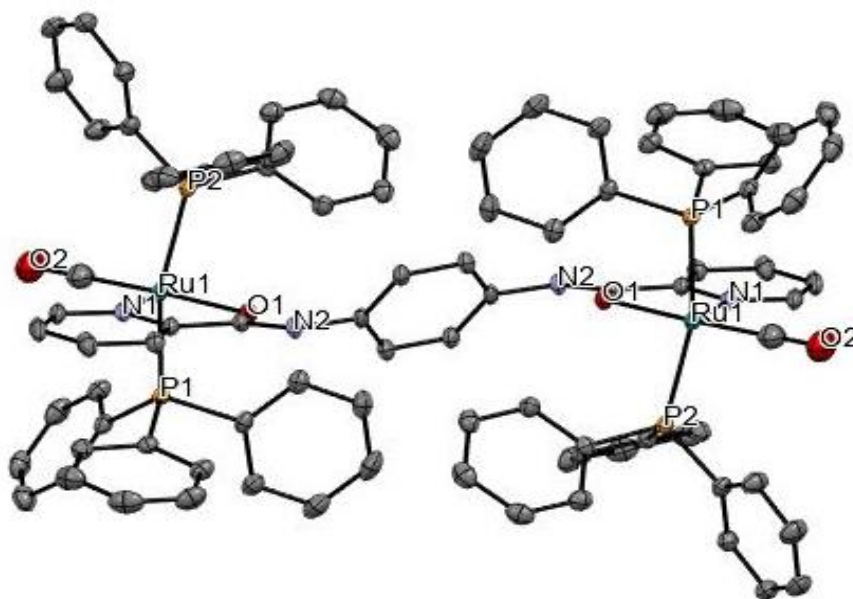


**Figure 4.10.** An ORTEP view of **Ru5** showing displacement ellipsoids represented at 50% and atom labelling. All hydrogen atoms, chloride ions and solvents are omitted for the purpose of clarity. Selected bond distances (Å): Ru(1)-N(1), 2.153(2); Ru(1)-O(1), 2.1530(18); Ru(1)-P(1), 2.3443(7); Ru(1)-P(2), 2.3728(7); Ru(1)-C(1), 1.833(8). Selected bond angles (°): N(1)-Ru(1)-O(1), 74.10(5); N(1)-Ru(1)-P(1), 93.12; N(1)-Ru(1)-P(2), 95.78(6); N(1)-Ru(1)-C(1), 101.84(13); C(1)-Ru(1)-O(1), 175.80(13); C(1)-Ru(1)-P(1), 93.12(2); C(1)-Ru(1)-P(2), 96.14(8), P(1)-Ru(1)-O(1), 85.68(5); P(1)-Ru(1)-P(2), 165.68(5).



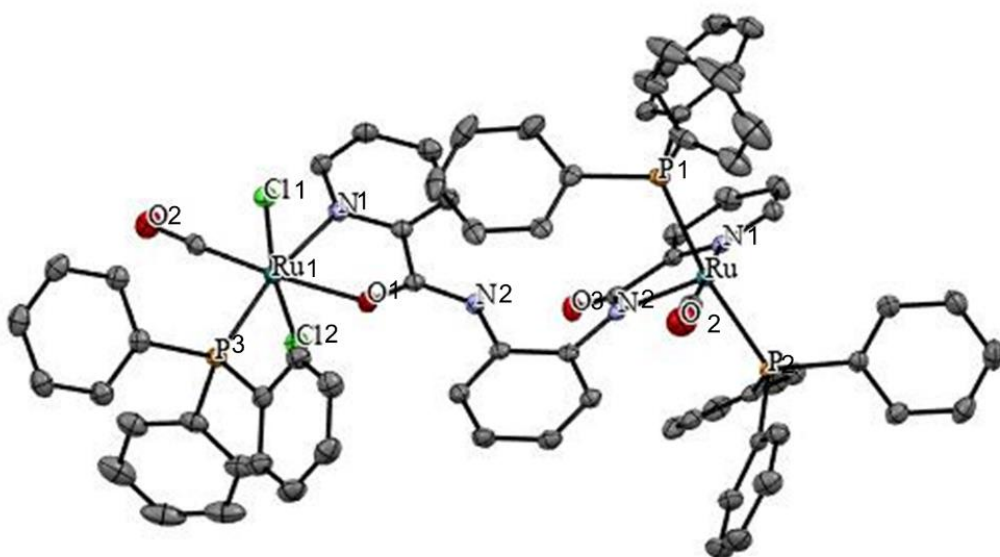


**Figure 4.11.** An ORTEP view of **Ru6** showing displacement ellipsoids represented at 50% and atom labelling. All hydrogen atoms and diethyl ether are omitted for clarity. Selected bond distances (Å): Ru(1)-N(1), 2.153(2); Ru(1)-O(1), 2.1530(18); Ru(1)-P(1), 2.3443(7); Ru(1)-P(2), 2.3728(7); Ru(1)-C(1), 1.833(8). Selected bond angles (°): N(1)-Ru(1)-O(1), 67.64(5); N(1)-Ru(1)-P(1), 93.12; N(1)-Ru(1)-P(2), 95.78(6); N(1)-Ru(1)-C(1), 101.84(13); C(1)-Ru(1)-O(1), 175.80(13); C(1)-Ru(1)-P(1), 93.12(2); C(1)-Ru(1)-P(2), 96.14(8), P(1)-Ru(1)-O(1), 85.68(5); P(1)-Ru(1)-P(2), 165.68(5).

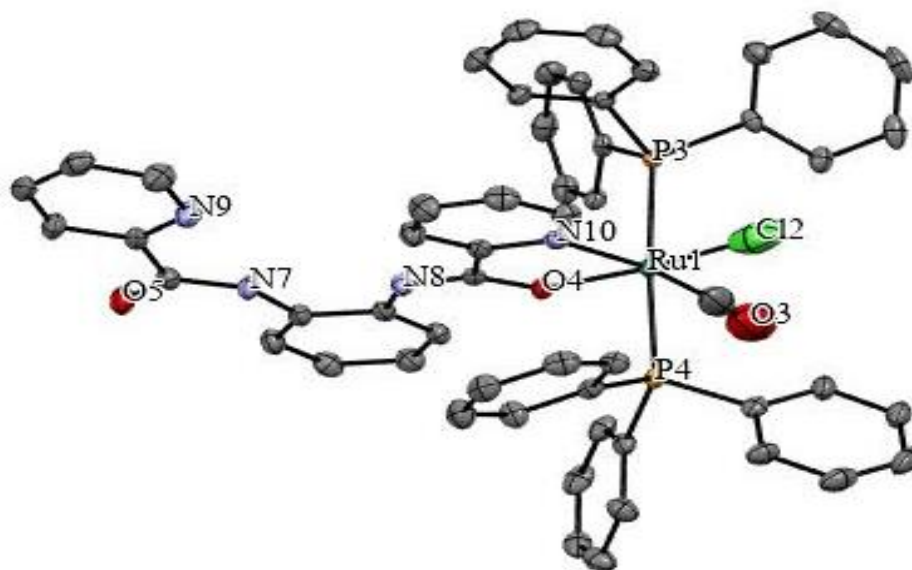


**Figure 4.12.** An ORTEP view of **Ru7** showing displacement ellipsoids represented at 50% and atom labelling. All hydrogen atoms and chloroform are omitted for clarity. Bond length (Å): N(1)-Ru(1), 2.151(7); O(1)-Ru(1), 2.094(5); Ru(1)-P(1), 2.3735(18); Ru(1)-C(55), 2.094(5); Ru-Cl(1), 2.367(6). Bond angles (°): N(1)-Ru(1)-P(1), 91.40(17); N(1)-Ru(1)-C(55), 168.3(7); N(1)-Ru(1)-Cl(1), 95.42(19); O(1)-Ru(1)-P(1), 91.03(15); O(1)-Ru(1)-N(1), 75.8(2), O(1)-Ru(1)-C(55), 92.5(6) and O(1)-Ru-Cl(1), 171.20(17); P(1)-Ru(1)-P(2), 175.07(6) and P(1)-Ru(1)-Cl(1), 88.72(9).

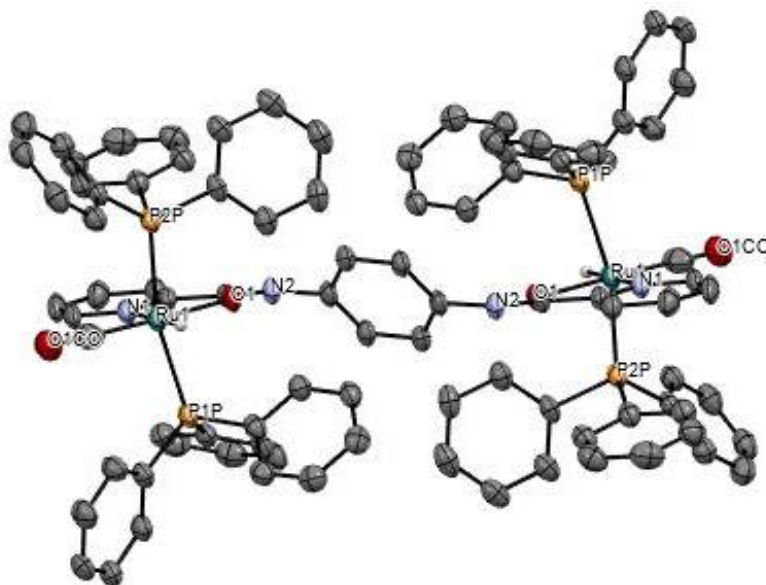


**Figure 4.13.** Solid state structure of complex **Ru5b** drawn at displacement 50% thermal ellipsoids. All aromatic and amide hydrogen atoms are omitted for clarity. Selected bond distances (Å): Ru(1)-N(1), 2.188(4); Ru(1)-O(1), 2.1510(3); Ru(1)-P(1), 2.3703(11); Ru(1)-P(2), 2.3421(10); Ru(1)-C(1)O, 1.833(5), O(1)-C(7), 1.840(4). Ru(1)-H, 1.54(3). Selected bond angles (°): N(1)-Ru(1)-O(1), 74.10(5); N(1)-Ru(1)-P(1), 95.85(9); N(1)-Ru(1)-P(2), 95.88(7); N(1)-Ru(1)-C(1)O, 101.46(19); OC(1)-Ru(1)-O(1), 175.55(19); OC(1)-Ru(1)-P(1), 95.80(15); P(1)-Ru(1)-O(1), 85.68(5); P(1)-Ru(1)-P(2), 164.79(4), N(1)-Ru(1)-H, 92.75(4).

The half-sandwich complexes **Ru8** and **Ru11** exhibited a three-legged piano stool geometry around their Ru(II) ion centres (**Figures 4.12** and **4.13**) which are typical of  $[\text{RuCl}(\eta^6\text{-cymene})(\text{L})]^+$  complexes with *p*-cymene rings forming the seat, whereas the Cl, N<sub>py</sub> and N<sub>amidate</sub> constitute the three legs of the piano stool. The two complexes, **Ru8** and **Ru11**, the Ru(II) ion coordinated to the anionic ligand via the N<sub>pyridine</sub> and N<sub>amidate</sub> atoms constituting five-membered chelating rings with the average bite angle, N<sub>pyridine</sub>-Ru-N<sub>amidate</sub> of 74.10(5) Å. Interestingly, the two metal centres in both complexes, **Ru8** and **Ru11**, share one bridged chlorine atom, which indicates the closeness of the two metal centres. In these complexes, the average Ru-

$N_{\text{pyridine}}$  and  $Ru-N_{\text{amidate}}$  are 2.093(2) Å and 2.109(2) Å and are within the average bond length;  $Ru-N_{\text{pyridine}} = 2.090(14)$  Å and  $Ru-N_{\text{amidate}}, 2.083(22)$  Å of similar 56 compounds deposited in CCDC database.<sup>28</sup> The *p*-cymene rings are almost planar with the Ru atoms at 3.205(11) Å from the centroid of the *p*-cymene rings, comparable to the average 3.182(18) Å calculated for 18 similar half sandwich structures found in the CCDC database.<sup>28</sup> The two Ru(II) centres are positioned *trans* to each other such that each Ru(II) centre and 3.0462 Å away from the arene plane. The net charge on the cationic species in **Ru8** and **Ru11** are balanced by counterion  $[RuCl_3(\eta^6 p\text{-cymene})]^-$  and  $[PF_6]^-$  respectively.

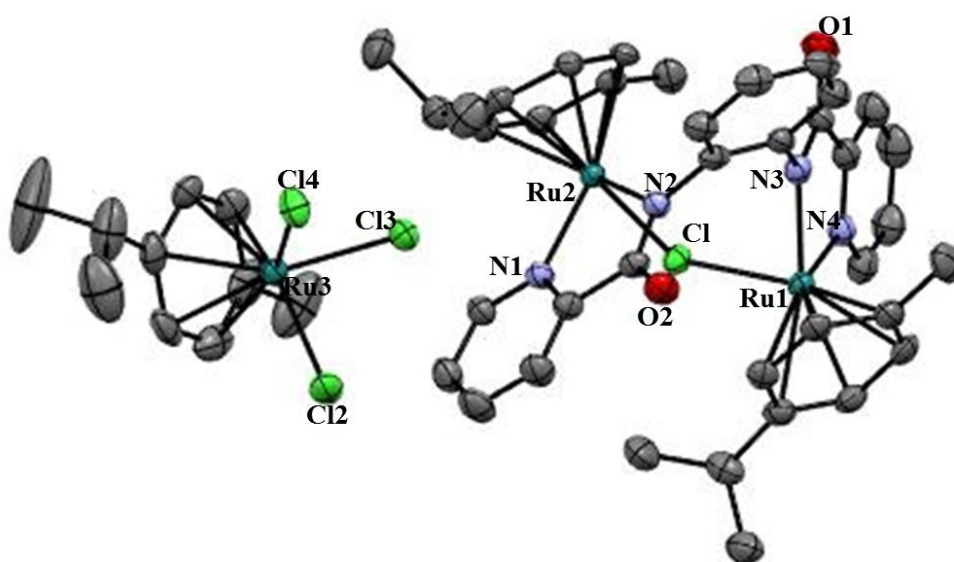


**Figure 4.14.** An ORTEP view of **Ru8** showing displacement ellipsoids represented at 50% and atom labelling. All hydrogen atoms are omitted for clarity. Bond lengths (Å): N(1)-Ru(1), 2.093(2); N(2)-Ru(1), 2.1090(2); Ru(1)-Cl(1), 2.460(6); Ru(3)-Cl(2), 2.392(3). Bond angles (°): N(1)-Ru(1)-N(2), 77.55(18); N(1)-Ru(1)-Cl(1), 85.39(14); N(2)-Ru(1)-Cl(1), 86.95(13); Cl(2)-Ru(3)-Cl(3), 87.65(5).

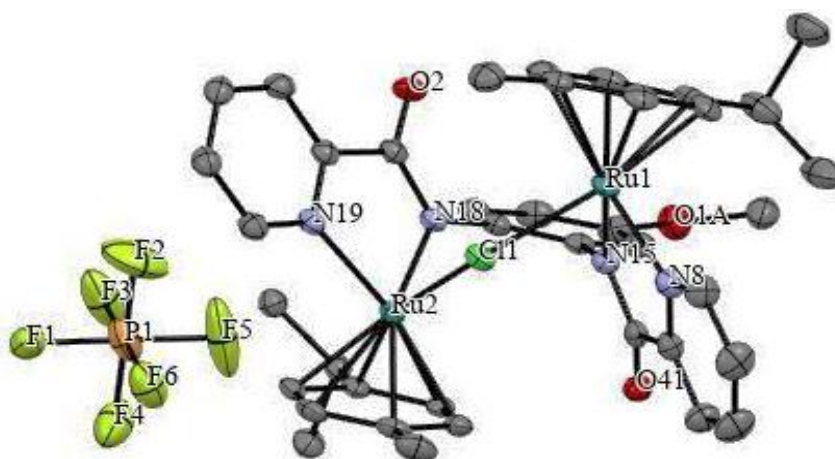


**Figure 4.15.** An ORTEP view of **Ru11** showing displacement ellipsoids represented at 50% and atom labelling. All hydrogen atoms are omitted for clarity. Bond lengths (Å): N(1)-Ru(1), 2.093(2); N(2)-Ru(1), 2.1090(2); Ru(1)-Cl(1), 2.460(6); Ru(3)-Cl(2), 2.392(3). Bond angles (°): N(1)-Ru(1)-N(2), 77.55(18); N(1)-Ru(1)-Cl(1), 85.39(14); N(2)-Ru(1)-Cl(1), 86.95(13); Cl(2)-Ru(3)-Cl(3), 87.65(5).

**Table 4.2.** A summary of crystallographic parameters and refinement data for complexes **Ru5-Ru7**.

Parameters	Ru5	Ru5b	Ru6 <sup>a</sup>	Ru7
Empirical formula	C <sub>92</sub> H <sub>74</sub> Cl <sub>4</sub> N <sub>4</sub> O <sub>4</sub> P <sub>4</sub> Ru <sub>2</sub> +2[CH <sub>3</sub> O H]	C <sub>92</sub> H <sub>76</sub> Cl <sub>2</sub> N <sub>4</sub> O <sub>4</sub> P <sub>4</sub> Ru <sub>2</sub> + [Solvent]	C <sub>74</sub> H <sub>58</sub> Cl <sub>2</sub> N <sub>4</sub> O <sub>4</sub> P <sub>3</sub> Ru <sub>2</sub> + [C <sub>4</sub> H <sub>10</sub> O]	C <sub>55</sub> H <sub>44</sub> ClN <sub>4</sub> O <sub>3</sub> P <sub>2</sub> Ru
Formula weight	1760.56	1627.58	1497.23	1007.44
Temperature/K	100(2)	104	100(2)	100(2)
Wavelength(Å)	1.5473	1.5478	1.54178	1.5418
Crystal system	Monoclinic	Monoclinic	Monoclinic	Triclinic
Space group	P2 <sub>1</sub> /n	P2 <sub>1</sub> /n	P <sub>1</sub>	P <sub>1</sub>
Unit cell dimensions;				
a	13.1759(8)Å	13.1360(2)	18.7581(4)Å	13.1287(3)
b	19.9842(12)Å	19.9853(4)	11.8817(2)Å	13.5068(3)
c	15.9805(10)Å	15.9303(3)	30.6450(6)Å	14.0669(3)
α	90°	90	90°	90.762(1)°
β	102.710(3)°	102.332(1)	91.240(1)°	95.264(1)°
γ	90°	90	90°	105.107(1)°
Volume	410.7(4)(Å) <sup>3</sup>	4085.63(13)	6828.5(2)Å <sup>3</sup>	2396.26(9)
Z	2	2	2	2
Density (calculated)/ Mg/m <sup>3</sup>	1.424	1.323	1.394	1.396
Absorption coefficient/ mm <sup>-1</sup>	0.569	4.149	11.186	5.038
F(000)	1808.0	1672.0	2916.0	1102.0
Reflections collected	79673	1672	11036	9403
Completeness to theta	99.6%	99.7%	98.3%	99%
Corrections method	MULTI-SCAN	MULTI-SCAN	MULTI-SCAN	MULTI-SCAN
Goodness-of-fit on F <sup>2</sup>	1.069	1.042	0.965	0.90
R indices (all data)	R <sub>1</sub> = 0.0508, wR <sub>2</sub> = 0.1241	R <sub>1</sub> =0.0531 wR <sub>2</sub> = 0.1438	R <sub>1</sub> =0.0616, wR <sub>2</sub> =0.186	R <sub>1</sub> =0.0665, wR <sub>2</sub> =0.1984

<sup>a</sup>A solvent mask was calculated, and 176 electrons were found in a volume of 800 Å<sup>3</sup> in 2 voids per unit cell. This is consistent with diethyl ether per Asymmetric Unit, which accounts for 168 electrons per unit cell.

**Table 4.3.** Summary of crystallographic parameters and refinement data of **Ru8** and **Ru11**.

Parameters	<b>Ru8</b>	<b>Ru11</b>
Empirical formula	C <sub>51</sub> H <sub>60</sub> Cl <sub>4</sub> N <sub>4</sub> O <sub>2</sub> Ru <sub>3</sub> + [CH <sub>2</sub> Cl <sub>2</sub> ]	C <sub>39</sub> H <sub>42</sub> ClN <sub>4</sub> O <sub>3</sub> Ru <sub>2</sub> PF <sub>6</sub>
Formula weight	1418.74	997.32
Temperature/K	100(2)	100(2)
Wavelength(Å)	1.54178	1.54170
Crystal system	Triclinic	Triclinic
Space group	P <sub>1</sub>	P2 <sub>1</sub> /C
Unit cell dimensions;		
a	13.121(2)Å	15.3868(4)
b	15.820(3)Å	19.3230(5)
c	16.506(4)Å	13.7638(4)
α	61.430(6)°	90
β	71.530(11)°	101.771(1)
γ	72.142(7)°	90
Volume	2803.9(10)Å <sup>3</sup>	4006.18(19)
Z	2	4
Density (calculated) / Mg/m <sup>3</sup>	1.680	1.654
Absorption coefficient/ mm <sup>-1</sup>	11.186	7.713
F(000)	1424.0	200080
Reflections collected	11036	7297
Completeness	95.6%	99.4%
Goodness-of-fit on F <sup>2</sup>	0.965	0.994
Final R indices [I>2sigma(I)]	R <sub>1</sub> =0.0628, wR <sub>2</sub> =0.1976	R <sub>1</sub> =0.0278, wR <sub>2</sub> =0.0785
R indices (all data)	R <sub>1</sub> =0.0616, wR <sub>2</sub> =0.1860	R <sub>1</sub> =0.0616, wR <sub>2</sub> =0.1860
Largest diff. peak and hole/eA <sup>-3</sup>	1.051/-0.50	1.421/-0.50

#### 4.2.3. Transfer hydrogenation of ketones

To study the catalytic efficiency of the pre-catalysts **Ru5–Ru11** in TH of ketones, acetophenone (model substrate) and potassium *tert*-butoxide K<sup>t</sup>BuO (base), respectively, were used. For the pre-catalyst, **Ru5**, a conversion of 95% (TON of  $6.30 \times 10^4$ ) was achieved (**Table 4.4, entry 5**) with catalyst loading of  $1.50 \times 10^{-2}$  mol% (150 ppm), which indicates that the complex is active in TH of acetophenone. A number of controlled experiments were conducted to confirm the performance of the catalysts (**Table 4.4**). Firstly, a catalyst-free experiment involving only K<sup>t</sup>BuO was carried out, and 2.0 % (6 h) conversion was achieved (**Table 4.4, entry 1**). A base free experiment involving only **Ru9** was also carried out, and lower conversion of 32 % (6 h) was obtained (**Table 4.4, entry 2**), which compared well with the literature reported by Tenorio *et al.*<sup>29</sup>

##### 4.24.1. Optimisation of reaction conditions for transfer hydrogenation

Inspired by the catalytic activities (TONs) obtained in the preliminary screening, we sought to establish the optimum reaction conditions by varying the catalyst concentrations and base. The effect of catalyst concentration was studied by varying the catalyst concentration from 0.0025 to 0.055 mol% (**Table 4.4, entries 3-9**). From the results, an increase in the catalyst concentration resulted in higher percentage conversions but lower (TONs). For instance, an increase in catalyst loading from 0.0025 mol% to 0.055 mol% was accompanied by an increase in the percentage conversion from 41 to 99% but a decrease in TON from  $1.56 \times 10^4$  to  $1.3 \times 10^3$  (**Table 4.4, entries 3 vs 8**). A similar trend was observed when complex **Ru9** was used under the same reaction conditions. For example, increasing catalyst loading from 150 ppm to 550 ppm for **Ru9** leads to the TON decreasing from  $3.60 \times 10^4$  to  $1.69 \times 10^4$  (**Table 4.4, entries 6 to 9**), although the percentage conversions increased significantly from 54 % to 93 %. The reduction in catalytic activity (TON) due to an increase in catalyst concentration suggests



catalyst aggregation, which subsequently led to the deactivation of the catalysts.<sup>8</sup> This observation is in good agreement with the previous work by Yu and co-workers, where Ru(II) complexes were more efficient at very low catalyst loading.<sup>8</sup>

The nature of the base used has a pronounced influence on the performance of the catalyst, **Ru1b**. Noticeably, K<sub>2</sub>CO<sub>3</sub> appeared to impede the reaction progress and demonstrate a sign of reaction incompleteness in 6 h, although an integral TON up to  $5.8 \times 10^3$  was achieved. (**Table 4.4, entry 11**). The reaction in the presence of KOH gave catalytic activity, TON up to  $1.71 \times 10^4$ , comparable to the integral TON of  $1.94 \times 10^4$  obtained by K<sup>t</sup>BuO under similar reaction conditions (**Table 4.4, entries 4 vs 10**). The order of reactivity was K<sub>2</sub>CO<sub>3</sub> < KOH < K<sup>t</sup>BuO, consistent with the relative basicity of the bases and highlighting their strengths of forming a sufficient amount of isopropoxide required for generating Ru-hydrides.<sup>10</sup>

**Table 4.4.** Effects of catalyst concentration and base on TH of acetophenone using complexes **Ru5** and **Ru9** as a catalysts.<sup>a</sup>

Entry	catalyst	Catalyst loading/ x10 <sup>-3</sup> mol% (ppm)	Base	<sup>b</sup> Conversion[%].	Yield%	<sup>c</sup> TON x10 <sup>4</sup>
1	<b>Ru5</b>	-	K <sup>t</sup> BuO	2	1	-
2 <sup>d</sup>	<b>Ru5</b>	5(50)	-	32	30	6.4
3	<b>Ru5</b>	2.5(25)	K <sup>t</sup> BuO	41	39	1.56
4	<b>Ru5</b>	5(50)	K <sup>t</sup> BuO	86	86	1.94
5	<b>Ru5</b>	15(150)	K <sup>t</sup> BuO	95	94	6.30
6 <sup>e</sup>	<b>Ru9</b>	15(150)	K <sup>t</sup> BuO	54	53	3.69
7	<b>Ru5</b>	25(250)	K <sup>t</sup> BuO	97	95	0.26
8	<b>Ru5</b>	55(550)	K <sup>t</sup> BuO	99	98	1.36
9 <sup>f</sup>	<b>Ru9</b>	55(550)	K <sup>t</sup> BuO	93	93	1.69
10	<b>Ru5</b>	5(50)	KOH	76	76	1.71
11	<b>Ru5</b>	5(50)	K <sub>2</sub> CO <sub>3</sub>	29	28	0.58
12	<b>Ru5</b>	5(50)+Hg(0)	K <sup>t</sup> BuO	80	79	1.78

<sup>a</sup>Conditions: 1.0 mmol acetophenone, 0.4 mol%, K<sup>t</sup>BuO in 1.00 ml <sup>1</sup>PrOH, temperature 80 °C, time = 6 h. <sup>b</sup>Determined by <sup>1</sup>H NMR spectroscopy. Methoxybenzene was used as an internal standard. <sup>c</sup>Turn Over Number(TON) = moles of product formed/moles of catalyst used. <sup>d</sup>**Ru5** without base and time = 32 h was and <sup>e and f</sup> **Ru9** was used. All experiments were carried out in duplicate to ensure reproducibility.

#### 4.2.4.2. Effects of catalyst structure on TH of ketones

Having established the optimum reaction conditions, we sought to investigate the effects of the catalyst structure on the TH of ketones. In general, all the complexes showed high catalytic activity owing to the carboxamide ligands, which can provide a wide range of stability and steric influence that significantly impact the performance of complexes.<sup>25</sup> To effectively evaluate the effect of catalyst structure on the rate of TH of ketone, a plot of  $\ln[\text{Ac.}]_0/[\text{Ac.}]_t$  vs time/h, where  $[\text{Ac.}]$  = concentration of acetophenone (**Figure 4.14**) was employed to determine the observed rate constants,  $k_{\text{obs}}$  for each complex with respect to the acetophenone substrate. A *pseudo*-first order with respect to the acetophenone substrate was deduced from the plots (**Figure 4.14**) as illustrated in **Equation 1**.<sup>30</sup> The rate constants ( $k_{\text{ob}}$ ) are in tandem with the corresponding catalytic activities TONs exhibited by the complexes **Ru5–Ru11** (**Table 4.5**).

$$-d[\text{Ac.}]_t/dt = k_{\text{ob}}[\text{Ac.}]_0 \dots\dots\dots \text{Equation 1.}$$

**Table 4.5** and **Figure 4.14** show that the dinuclear complexes **Ru5** and **Ru6** demonstrated similar catalytic activities, regardless of their structural difference. The complexes **Ru5** and **Ru6** demonstrated higher catalytic activity compared to the mononuclear complex **Ru7**. For example, complex **Ru5** showed an integral TON of  $5.46 \times 10^4$  corresponding to the initial rate constant of  $2.48(\pm 0.21) \times 10^{-1} \text{ h}^{-1}$  compared to the TON of  $3.60 \times 10^4$  ( $1.47(\pm 0.24) \times 10^{-1} \text{ h}^{-1}$ ) recorded for **Ru7** and is in good agreement with the findings of Liu *et al.*<sup>8</sup> This could be assigned to better cooperativity from the two metal centres with enhanced catalytic activity exhibited by the two complexes compared to the mononuclear complex **Ru7**.<sup>8, 31</sup>

**Table 4.5.** Effects of catalyst structure on the transfer hydrogenation of acetophenone catalysed by complexes **Ru5 – Ru11**.<sup>a</sup>

Entry	Catalyst	<sup>b</sup> Conversion[%]	<sup>b</sup> Yield[%]	<sup>c</sup> TON x10 <sup>4</sup>	TOF/h <sup>-1</sup> x10 <sup>3</sup>	<i>k</i> <sub>obs</sub> /h <sup>-1</sup> x10 <sup>-1</sup>
1	<b>Ru5</b>	81	82	1.43	4.98	2.48(±0.21)
2 <sup>d</sup>	<b>Ru5b</b>	98	97	3.54	8.82	2.55(±0.41)
3	<b>Ru6</b>	78	78	1.36	4.72	1.86(±0.24)
4	<b>Ru7</b>	54	54	0.94	3.03	1.47(±0.24)
5	<b>Ru5b</b>	35	33	2.21	3.62	
6	<b>Ru5b</b>	99	99	6.6	4.13	
7	<b>Ru5</b>	15	14	1.3	1.56	
8	<b>Ru8</b>	99	98	1.71	2.83	1.97(±0.12)
9	<b>Ru9</b>	86	86	1.49	2.48	1.69(±0.31)
10	<b>Ru10</b>	92	92	1.66	2.77	1.73(±0.24)
11	<b>Ru11</b>	96	94	1.57	2.62	1.76(±0.24)
12	<b>[RuCl<sub>2</sub>(η<sup>6</sup>-<i>p</i>-cymene)]<sub>2</sub></b>	12	11	0.19	3.16	-
13	<b>Ru5</b> +Hg(0)	78	76	1.36	2.27	-
14	<b>Ru9</b> +Hg(0)	88	87	1.52	2.53	-

<sup>a</sup>Conditions: acetophenone: 1.00 mmol; [**Ru**]: 5.00 x10<sup>-3</sup> mol% (50 ppm); K<sup>t</sup>BuO: 4.00 mol% in 2.5 mL and diluted with 1.00 mL <sup>i</sup>PrOH, temperature 80 °C, 6 h. <sup>b</sup>Determined by <sup>1</sup>H NMR spectroscopy. Methoxybenzene was used as an internal standard. <sup>c</sup>Turn Over Number(TON) = moles of product formed/moles of catalyst, <sup>d</sup>Time = 5 h. [**Ru**] = concentration of the catalyst. Experiments were carried outs in duplicate to ensure reproducibility).

Similarly, the role of the carboxamide ligand was more pronounced in the complexes **Ru8** - **Ru11**. In addition, the aryl *p*-cymene and the counterion,  $[\text{PF}_6]^-$  in the complexes **Ru8** – **Ru11** appeared to enhance the stability and render the complexes less prone to catalytic deactivation and change in oxidation state. From plots of (c) percentage conversion vs time/h and (d)  $\ln[\text{Ac.}]_t/[\text{Ac.}]_0$  vs time/h, the complexes **Ru10** and **Ru11** bearing electron-donating groups, methyl and methoxy substituents showed slightly higher catalytic activity than the unsubstituted **Ru9** (**Figure 4.14** and **Table 4.5**). For example, the complex **Ru11** bearing the methoxy substituent on the linker showed higher catalytic activity of  $1.57 \times 10^4$  corresponding to  $k_{\text{ob}}$  of  $1.73 \times 10^{-1} (\pm 0.12) \text{ h}^{-1}$  compared to the analogues **Ru9** which gave integral TON  $1.49 \times 10^4$  ( $k_{\text{ob}}$  of  $1.69 \times 10^{-1} (\pm 0.03) \text{ h}^{-1}$ ) (**Table 4.5, entries 11 vs 9**). This observation could be assigned to the electronic effect of methyl and methoxy groups, resulting in increasing electrophilicity of the metal centre. In addition, complex **Ru8** demonstrated higher catalytic activity compared to its analogues, **Ru9-Ru11** (**Table 4.5, entries 8 vs 11**). The presence of the counterion,  $[\text{RuCl}_3 \text{ } p\text{-cymene}]$ , which is capable of mediating the reaction to some extent (**Table 4.5, entry 12**), could be responsible for this catalytic activity. In general, no induction period was observed at the initial stage of the reaction under the described reaction conditions and indicating the homogeneity of the novel catalytic system. (**Figure 4.14**). Compared to the most highly active multinuclear catalysts reported in the literature, the complexes **Ru5-Ru11** demonstrated lower catalytic activities.<sup>8, 10, 19</sup> For instance, Ru(II) catalyst reported by Yu and co-workers with TOF up to  $1.0 \times 10^7 \text{ h}^{-1}$  compared to  $2.9 \times 10^3 \text{ h}^{-1}$  showed by the complexes **Ru5-Ru11**.<sup>8</sup> The carboxamide ligands generally stabilise complexes, enhance the robustness and render its metal complexes less prone to catalysts deactivation.<sup>22, 32</sup> However, this effect could be less pronounced in the newly synthesised complexes **Ru5-Ru11** (**Figure 4.14**). More importantly, the proximity of the two Ru(II) centres has the tendency to minimise the catalytic

activity and cooperativity between two metal centres *via* the arene linker and chlorido bridged atom.

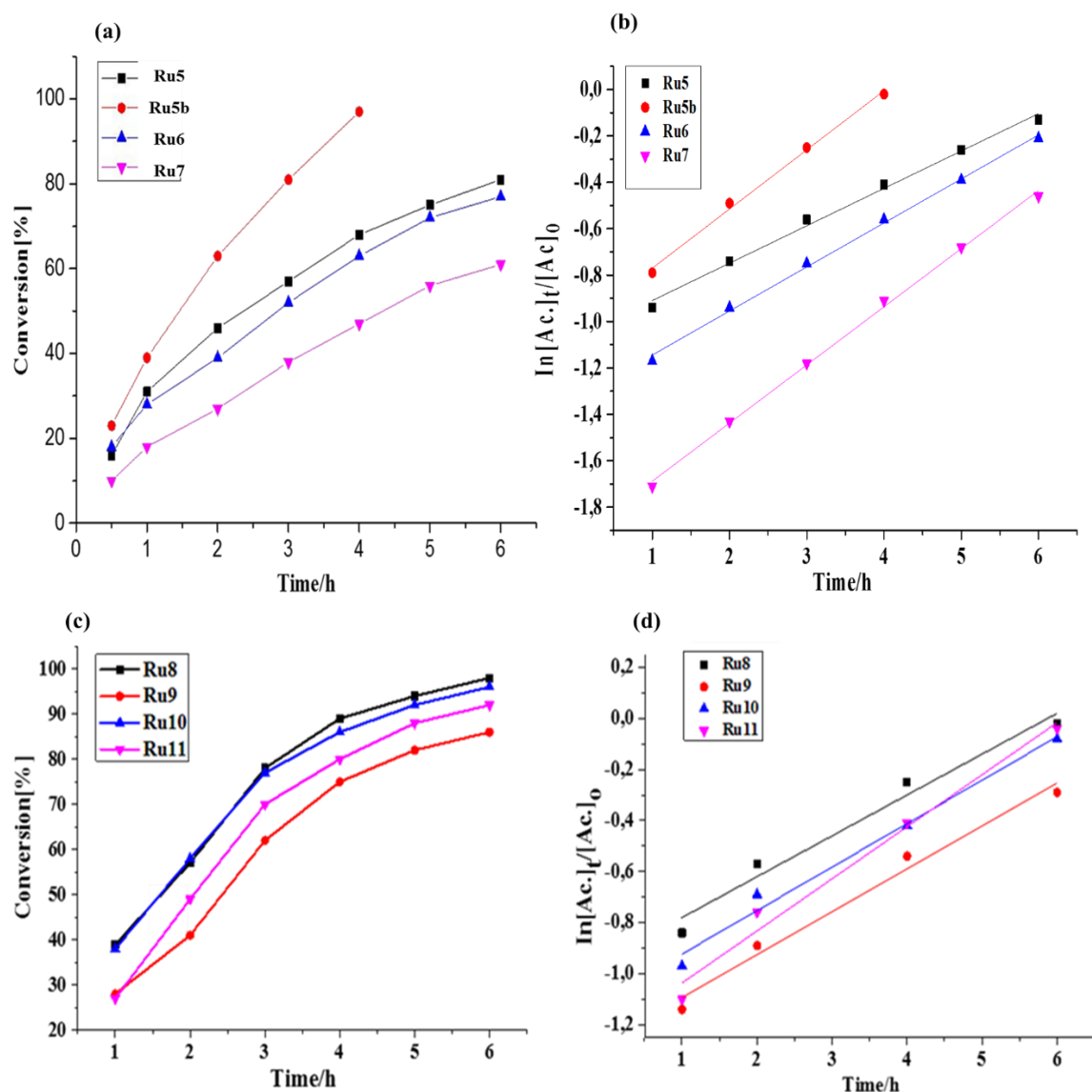


**Figure 4. 16.** Time-dependent transfer hydrogenation reaction of acetophenone catalysed by **Ru5-Ru11**:  $5.00 \times 10^{-3}$  mol% (50 ppm);  $K^tBuO$ : 4.0 mol%; temperature 82 °C. (a) and (c) Conversion[%] vs time plots, (b) and (d)  $-\ln[Ac.]_t/[Ac.]_0$  vs time plot of the **Ru9-Ru11** catalysts in the TH of acetophenone.

A mercury poisoning test was conducted to confirm the homogeneous nature of the complexes in the TH of acetophenone reaction. The addition of the Hg(0) did not result in a significant reduction of catalytic activity of the complex **Ru9** in comparison to the mercury-free reactions. (**Table 4.5 entries 9 and 14**). This supports the kinetic profile of the response (**Figure 4.14**) and confirms the homogeneous nature of this catalytic system.<sup>33-34</sup>

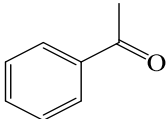
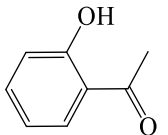
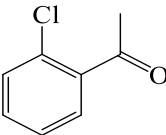
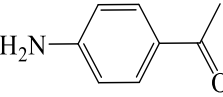
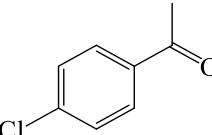
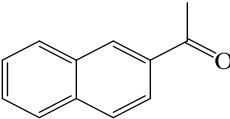
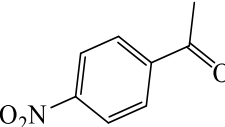
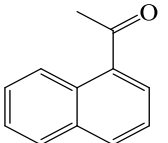
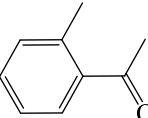
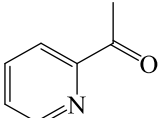
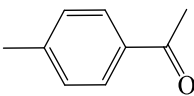
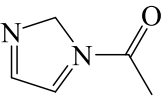
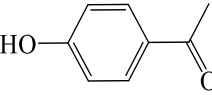
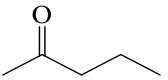
#### 4.2.4.3. Investigation of ketone substrate scope

Having established the optimum reaction conditions, we extended the scope of the substrate to a number of ketones, including heteroaromatic and aliphatic ketones using **Ru5** and **Ru9**. The results are summarised in **Table 4.6**. Acetophenone derivatives bearing electron-withdrawing substituents showed higher reactivity compared to acetophenone without a substituent under similar reaction conditions. For example, while 2-chloroacetophenone and 4-chloroacetophenone furnished a 97% and 99% conversion, acetophenone could only achieve up to 82% under similar reaction conditions. A similar trend was observed when **Ru5** was employed under the reaction conditions. The electronic effect could reduce the electron density on the carbonyl carbon of the substrates and ultimately enhance the reactivity.<sup>10, 35</sup> The position of the electron-withdrawing groups on the arene ring appeared to have little effect on the catalytic efficiency of the catalyst **Ru5** and **Ru9**. For instance, 4-chloroacetophenone and its analogous 2-chloroacetophenone demonstrated almost the same activity under similar reaction conditions (**Table 4.6, entries 1 vs 2 and 3**), which is in line with the findings reported by Yu and co-workers using the *NNN* diruthenium(II) pincer complex where both 2-chloroacetophenone and 4-chloroacetophenone gave conversions of 98% and 99% respectively.<sup>31</sup> The introduction of electron-donating groups on the arene ring of the substrates has significantly affected the reactivity. For instance, 4-amino acetophenone exhibited a lower conversion of 78% compared to 86% recorded for acetophenone using **Ru9** under similar

reaction conditions (**Table 4.6, entries 1 vs 9**). Furthermore, the position of the electron-donating substituents on the arene ring of acetophenone derivatives in relation to the acetyl group plays a role in determining the reactivity of the substrates. The *ortho*-substituted substrates appeared to show relatively lower percentage yields than the *para*-substituted acetophenone derivatives, suggesting that the electronic effect is more pronounced in the *para*-substituted acetophenones.<sup>31</sup> For example, 4-methyl acetophenone gave a higher reactivity of 81% compared to 2-methyl acetophenone (81%) under similar reaction conditions using **Ru9**. In addition, bulkier polyaromatic ketones such as 1-acetylnaphthalene and 2-acetylnaphthalene underwent the TH reaction to produce the corresponding alcohols. Higher percentage conversions were achieved for 1-acetylnaphthalene (94%) and 2-acetylnaphthalene (98%), respectively, compared to the acetophenone (86%) under similar reaction conditions (**Table 4.6, entries 1 vs 10 and 11**). This observation contradicts the earlier finding reported by Chai *et al.*, where similar reactivity was observed for both 2-acetylnaphthalene (97%) and acetophenone (98%).<sup>31</sup> 2-Acetylpyridine and 1-acetyl imidazole were also reacted, and percentage conversions of 68% and 73% were obtained under similar reaction conditions, respectively (**Table 4.6, entries 12 and 13**). The lower catalytic activity of the hetero-aromatic substrates compared to acetophenone could allude to irreversible coordination of N- donor atoms of the hetero-aryl group of the substrate to the active site centre of the catalysts, which could lower the catalytic reactivities.<sup>8</sup> Aliphatic ketones such as 2-pentanone and 2-methyl cyclohexanone were also transformed to their respective secondary alcohols with moderate to good catalytic activities. For example, 2-pentanone was reacted to give the targeted alcohol product with 68% and 52% conversions under similar reaction conditions (**Table 4.6, entry 14**) and is consistent with the literature reported by Liu *et al.*, where aliphatic ketones showed lower catalytic activities compared to acetophenone under similar reaction conditions.<sup>36</sup>



**Table 4.6.** Result of substrate scope studies using complexes **Ru5** and **Ru9** as catalysts.<sup>a</sup>

Entry	Substrate	Conversion (%) <sup>b</sup>	Entry	Substrate	Conversion(%) <sup>b</sup>
1		86 82 <sup>b</sup>	8		75 67 <sup>b</sup>
2		97 92 <sup>b</sup>	9		78 70 <sup>b</sup>
3		99 97 <sup>b</sup>	10		98 82 <sup>b</sup>
4		70 68 <sup>b</sup>	11		94 83 <sup>b</sup>
5		79 72 <sup>b</sup>	12		68 78 <sup>b</sup>
6		81 68 <sup>b</sup>	13		73 74 <sup>b</sup>
7		78 70 <sup>b</sup>	14		68 52 <sup>b</sup>

<sup>a</sup>Conditions: 1.0 mmol acetophenone, <sup>t</sup>KBuO (4.00 mol%) in 2.5 mL and diluted with 1.00 mL <sup>i</sup>PrOH, **Ru9**, 5.00 x10<sup>-3</sup> mol% (50 ppm) temperature 80 °C, 6 h. Percentage conversion was determined by <sup>1</sup>H NMR spectroscopy. <sup>b</sup>Complex **Ru5** (50 ppm) was used. Methoxybenzene was used as an internal standard. \*Reaction time = 4 h. All experiments were carried out in duplicate to ensure reproducibility, S.D = ±1.0.

#### 4.2.4.4. Elucidating of the mechanism of the transfer hydrogenation catalysed by **Ru5** and **Ru9**

Finally, we focused on understanding the possible mechanistic pathway of these transfer hydrogenation reactions using complex **Ru5** using a combination of *in situ*  $^1\text{H}$  and  $^{31}\text{P}$  NMR spectroscopies and structural elucidation of the isolated intermediates. Based on observed high catalytic activity of the Ru-H species, **Ru5b**, we are now in a position to propose that the transfer hydrogenation of ketone using complex **Ru5** begins with the solvation of **Ru5** by *isopropoxide* to form a Ru(II) alkoxide intermediate (**Ru5a**) as shown in **Scheme 4.4**. Subsequent  $\beta$ -hydride elimination in **Ru5a** adduct, gives the Ru-H intermediate (**Ru5b**), presumed to be the active species. This was confirmed by the isolation and determination of the molecular structure of this intermediate (**Figure 4.13**). The formation of **Ru5b** in the catalytic cycle was further elucidated using  $^1\text{H}$  NMR spectroscopy by analysing the catalytic reaction mixture at regular intervals. For example, the  $^1\text{H}$  NMR spectra showed two triplets at -10.21 (t,  $^2J_{\text{H-P}}$ : 14.8 Hz, Ru-H) and -15.99 ppm (t,  $^2J_{\text{H-P}}$ : 12.8 Hz, Ru-H) confirming the formation of ruthenium(II)-hydride (**Figure 4.17**). Based on the lability of the  $\text{PPh}_3$  ligand in such complexes, we propose dissociating of one  $\text{PPh}_3$  group prior to the coordination of the ketone substrate to form species **Ru5c** (**Scheme 4.4**). This hypothesis was further supported by *in-situ* time-dependent  $^{31}\text{P}$  NMR spectral data showing the signal at -4.9 ppm, corresponding to the presence of free  $\text{PPh}_3$  (**Figure 4.18**).<sup>22, 37</sup> Coordination of the acetophenone substrate to the species (**Ru5b**) species leads to the formation of the Ru-acetophenone adduct, **Ru5d**. This is followed by hydride migration<sup>26</sup> to give the coordinated alcohol complex (**Ru5e**) as depicted in **Scheme 4.4**. Finally, elimination of the product is followed by concomitant regeneration of the active species (**Ru5a**) to complete the catalytic cycle.

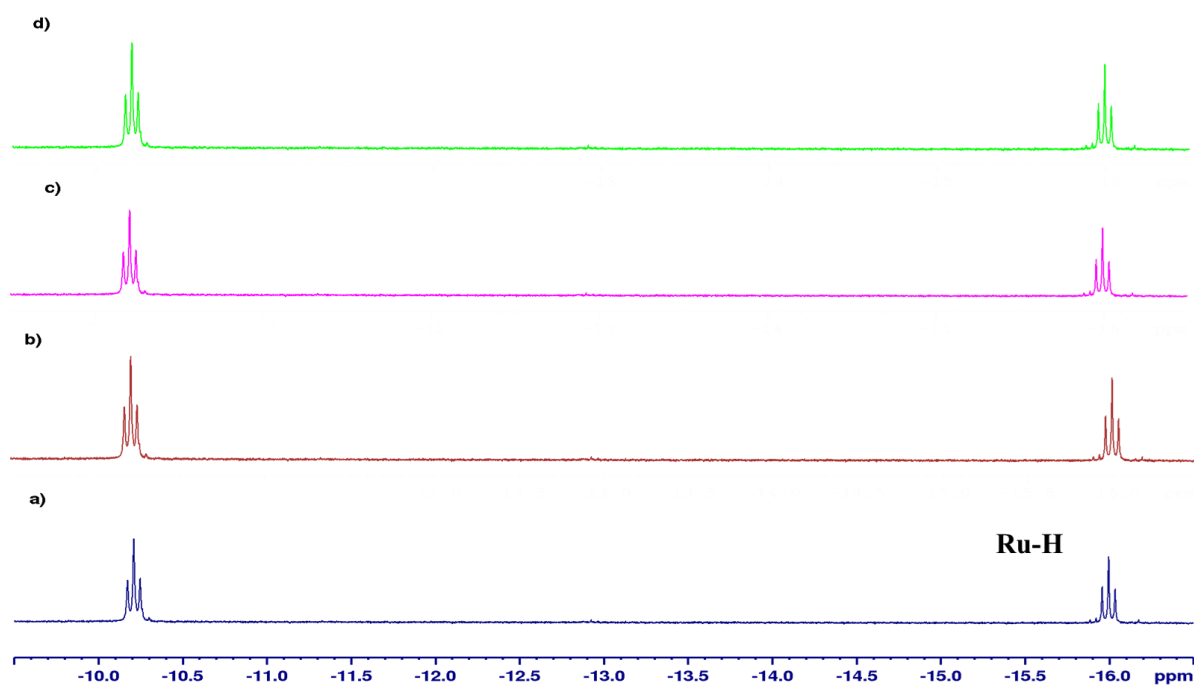


**Figure 4.17.** Hydride region of  $^1\text{H}$  NMR spectra of the Ru-H species (**Ru1b**), obtained from the reactions of **Ru5** with  $[\text{iPrOH}/^t\text{BuOK}]$  at  $80\text{ }^\circ\text{C}$  in (a) 30 min, (b) 1 h, (c) 1: 30 min and (d) 2 h.

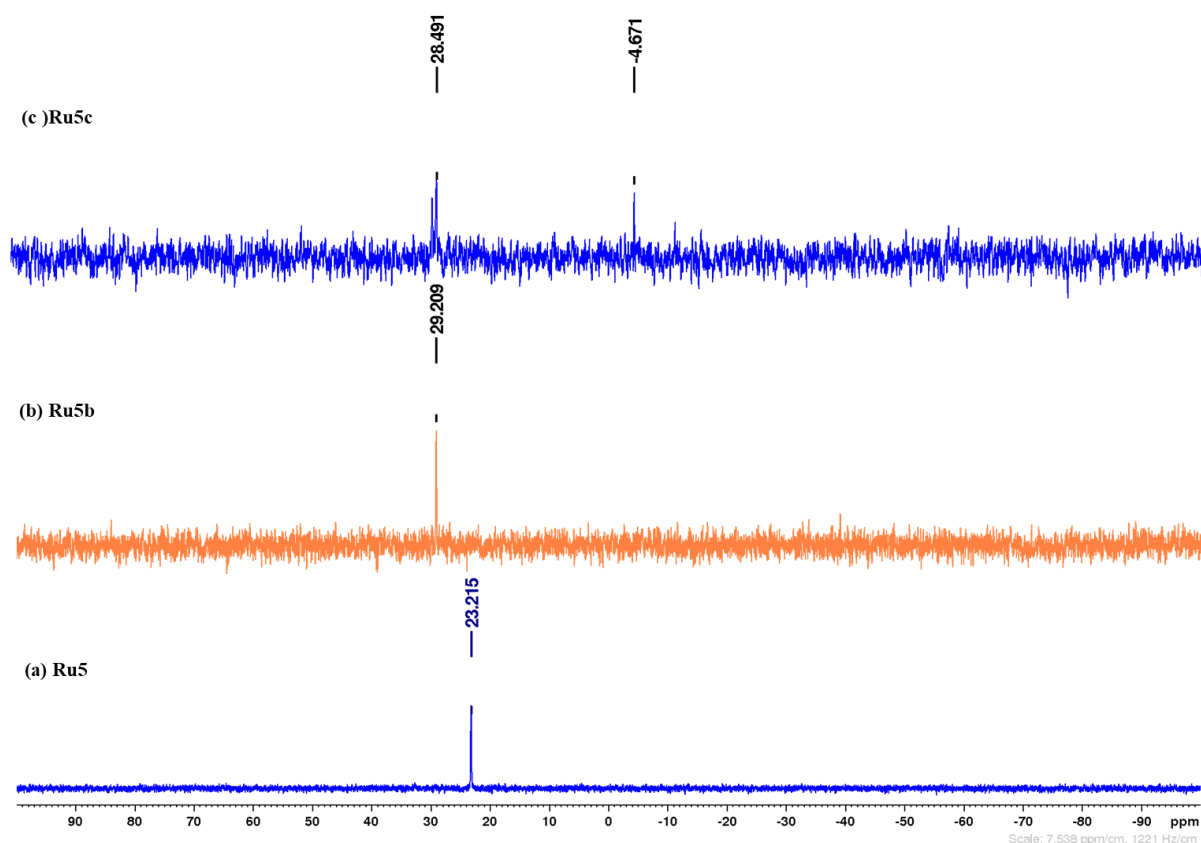
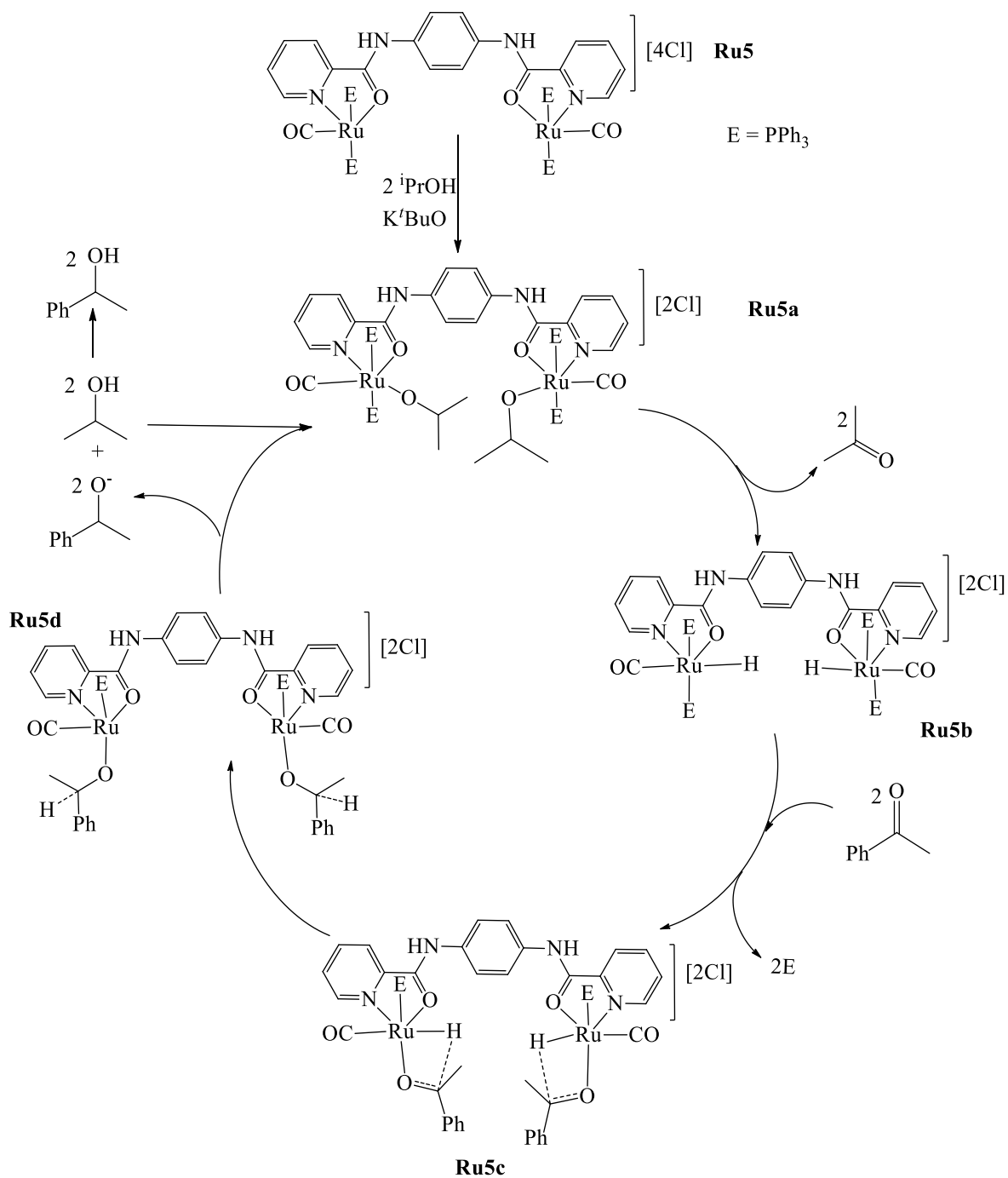


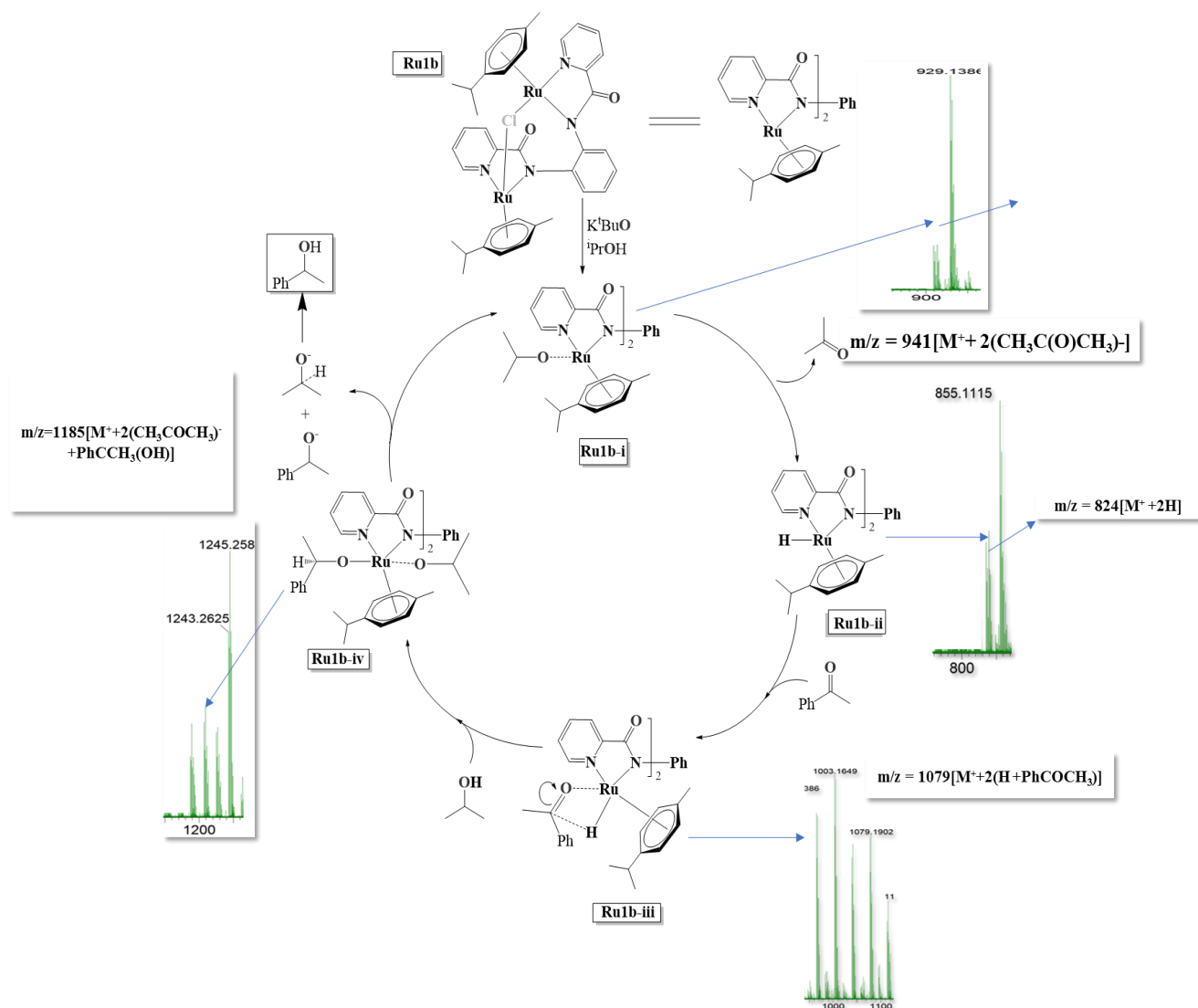
**Figure 4.18.**  $^{31}\text{P}$  NMR spectra of original complex **Ru5** (a) showing the signal at 23.2 ppm corresponding to the two  $\text{PPh}_3$  groups in **Ru5** and (b) showing the signals at 29.2 ppm corresponding two  $\text{PPh}_3$  of group in **Ru5b**, (c) intermediates showing the signals at  $\sim 4.7$  ppm and 28.5 ppm corresponding dissociated  $\text{PPh}_3$  and coordinated  $\text{PPh}_3$  of intermediate Ru5c respectively at 80  $^\circ\text{C}$  after 6 h.



**Scheme 4.4.** Proposed monohydride mechanism for the transfer hydrogenation of acetophenone catalysed by **Ru5** as deduced from NMR spectroscopy and structural characterisation of the Ru-H intermediate.

A classical inner-sphere monohydride mechanistic route was proposed for transfer hydrogenation reactions of ketones catalysed by the half-sandwich Ru(II) complex **Ru9**. Low-

resolution mass spectral data obtained from the analyses of the aliquots of TH of the acetophenone reaction withdrawn at regular time intervals were used to support the deduced reactive intermediates. From the data obtained, the mechanism is believed to begin with the coordination of isopropoxide to the metal centre to give the intermediate **Ru9-i**, which could be hypothesised from the signal at  $m/z = 929$  (**Scheme 4.5**).<sup>38-39</sup> The active species **Ru9-ii** was formed as the result of  $\beta$ -hydride elimination, which occurred within the intermediate, **Ru9-i**, and could be deduced from the signal at  $m/z = 824$  (**Scheme 4.5**).<sup>40</sup> Several attempts to capture the Ru-H species using the  $^1\text{H}$  NMR spectroscopic technique did not materialise. By reversible slippage of the Ru- $\text{C}_{p\text{-cymene}}$  ring from  $\eta^6$  to  $\eta^4$  to generate a  $16e^-$  Ru centre, a vacant site is created for acetophenone to coordinate and form the adduct, **Ru9-iii**,<sup>41-42</sup> which is confirmed by the signal at  $m/z = 1069$ . The catalytic cycle was then accompanied by the hydride migration from the Ru(II) centre to the coordinated acetophenone leading to the formation of **Ru9-iv** as supported by the signal at  $m/z = 1069$  (**Scheme 4.5**). The reaction pathway was terminated by eliminating the end-product, 1-phenyl ethanol, from the metal centre and subsequent reverse slippage of the Ru- $\text{C}_{p\text{-cymene}}$  bonding from  $\eta^4$  to  $\eta^6$  (**Ru9-iv**). Regeneration of the solvated species **Ru9-i** indicates the commencement of a new cycle.



**Scheme 4.5.** A plausible mechanism for transfer hydrogenation of acetophenone catalysed by **Ru9**. The reactive intermediates were identified by low-resolution ES-MS analysis.

### 4.3. Conclusions

In summary, new mononuclear and dinuclear ruthenium(II) complexes anchored on carboxamide ligand were synthesised and fully characterised. The coordination chemistry of the complexes was controlled by the nature of the ligand and reaction conditions to give dinuclear and mononuclear N-O/N-N compounds. The ruthenium(II) complexes demonstrated good catalytic activities in the transfer hydrogenation of ketones. The catalytic activities of the

complexes were primarily controlled by the nuclearity of the complexes, where the dinuclear complexes displayed higher catalytic activities than the mononuclear analogues. Significantly, the catalysts showed the potential to reduce a wide range of ketone substrates. The catalytic activity of complex **Ru5-Ru11** was of the substrates was controlled by the electronic and steric factors of the ketone substrates, where substrates bearing electron withdrawing giving higher percentage yields. Using  $^1\text{H}$ ,  $^{31}\text{P}$  NMR spectroscopies and single-crystal X-ray crystallography, a monohydride inner-sphere mechanistic route was proposed for **Ru5** in the transfer hydrogenation of ketones. A similar monohydride outers-sphere mechanisms were proposed for the reaction catalysed by the **Ru9** and were supported with ESI-MS analysis of TH of acetophenone reaction crude mixture.

#### 4.4 References

1. Saint-Denis, T. G.; Zhu, R.-Y.; Chen, G.; Wu, Q.-F.; Yu, J.-Q., *Science* **2018**, 359 (6377).
2. Cornils, B.; Herrmann, W. A., *J. Catal.* **2003**, 216, 23-31.
3. Wang, L.; Yang, Q.; Chen, H.; Li, R.-X., *Inorg. Chem. Commun.* **2011**, 14, 1884-1888.
4. Noyori, R.; Hashiguchi, S., *Acc. Chem. Res.* **1997**, 30, 97-102.
5. Foubelo, F.; Najera, C.; Yus, M., *Tetrahedron: Asymmetry* **2015**, 26, 769-790.
6. Aydemir, M.; Durap, F.; Baysal, A.; Meric, N.; Buldağ, A.; Gümgüm, B.; Özkar, S.; Yıldırım, L. T., *J. Mol. Catal. A: Chem.* **2010**, 326, 75-81.
7. Pye, D. R.; Mankad, N. P., *Chem. Sci.* **2017**, 8, 1705-1718.
8. Liu, T.; Chai, H.; Wang, L.; Yu, Z., *Organometallics* **2017**, 36, 2914-2921.
9. Wang, D.; Astruc, D., *Chem. Rev.* **2015**, 115, 6621-6686.
10. Chai, H.; Wang, Q.; Liu, T.; Yu, Z., *Dalton Transactions* **2016**, 45, 17843-17849.



11. Yoshida, K.; Kamimura, T.; Kuwabara, H.; Yanagisawa, A., *Chem. Commun.* **2015**, 51, 15442-15445.
12. Volpe, A.; Baldino, S.; Tubaro, C.; Baratta, W.; Basato, M.; Graiff, C., *Eur. J. Inorg. Chem.* **2016**, 2016, 247-251.
13. Ashley, J. M.; Farnaby, J. H.; Hazari, N.; Kim, K. E.; Luzik Jr, E. D.; Meehan, R. E.; Meyer, E. B.; Schley, N. D.; Schmeier, T. J.; Tailor, A. N., *Inorg. Chim. Acta* **2012**, 380, 399-410.
14. Madern, N.; Talbi, B.; Salmain, M., *Appl. Organomet. Chem.* **2013**, 27, 6-12.
15. Dayan, O.; Çetinkaya, B., *J. Mol. Catal. A: Chem.* **2007**, 271, 134-141.
16. Nath, B. D.; Takaishi, K.; Ema, T., *Catal. Sci. Technol.* **2020**, 10, 12-34.
17. Maity, A.; Sil, A.; Patra, S. K., *Eur. J. Inorg. Chem.* **2018**, 2018, 4063-4073.
18. Bratko, I.; Gomez, M., *Dalton Trans.* **2013**, 42, 10664-10681.
19. Liu, T.; Wu, K.; Wang, L.; Fan, H.; Zhou, Y.-G.; Yu, Z., *Organometallics* **2019**, 39, 93-104.
20. Vijayan, P.; Yadav, S.; Yadav, S.; Gupta, R., *Inorg. Chim. Acta* **2020**, 502, 119285.
21. Ramachandran, R.; Viswanathamurthi, P., *Spectrochim. Acta A: Mol. Biomol. Spectrosc.* **2013**, 103, 53-61.
22. Pachisia, S.; Kishan, R.; Yadav, S.; Gupta, R., *Inorg. Chem.* **2021**, 60, 2009-2022.
23. Aradhyula, B. P. R.; Kaminsky, W.; Kollipara, M. R., *J. Mol. Struct.* **2017**, 1149, 162-170.
24. Almodares, Z.; Lucas, S. J.; Crossley, B. D.; Basri, A. M.; Pask, C. M.; Hebden, A. J.; Phillips, R. M.; McGowan, P. C., *Inorg. Chem.* **2014**, 53, 727-736.
25. Yadav, S.; Vijayan, P.; Yadav, S.; Gupta, R., *Dalton Trans.* **2021**, 50, 3269-3279.
26. Wang, L.; Liu, T., *Chin. J. Catal.* **2018**, 39, 327-333.

27. Vijayan, P.; Viswanathamurthi, P.; Sugumar, P.; Ponnuswamy, M. N.; Balakumaran, M. D.; Kalaichelvan, P. T.; Velmurugan, K.; Nandhakumar, R.; Butcher, R. J., *Inorg. Chem. Front.* **2015**, *2*, 620-639.
28. Allen, F. H., *Acta Crystallogr. Sec. B: Struct. Sci.* **2002**, *58*, 380-388.
29. Botubol-Ares, J. M.; Córdón-Ouahhabi, S.; Moutaoukil, Z.; Collado, I. G.; Jiménez-Tenorio, M.; Puerta, M. C.; Valerga, P., *Organometallics* **2021**, *40*, 792-803..
30. Kumah, R. T.; Tsaulwayo, N.; Xulu, B. A.; Ojwach, S. O., *Dalton Trans.* **2019**, *48*, 13630-13640.
31. Chai, H.; Wang, Q.; Liu, T.; Yu, Z., *Dalton Trans.* **2016**, *45*, 17843-17849.
32. Yadav, S.; Vijayan, P.; Gupta, R., *J. Organomet. Chem.* **2021**, *954*, 122081.
33. Sonnenberg, J. F.; Morris, R. H., *Catal. Sci. Technol.* **2014**, *4*, 3426-3438.
34. Sonnenberg, J.; Morris, R., *ACS Catal.* **2013**, *3*, 1092-1102.
35. Martins, J. E.; Clarkson, G. J.; Wills, M., *Org. Lett.* **2009**, *11*, 847-850.
36. Wang, Q.; Chai, H.; Yu, Z., *Organometallics* **2017**, *36*, 3638-3644.
37. Chai, H.; Liu, T.; Zheng, D.; Yu, Z., *Organometallics* **2017**, *36*, 4268-4277.
38. Hall, A. M.; Dong, P.; Codina, A.; Lowe, J. P.; Hintermair, U., *ACS Catal.* **2019**, *9*, 2079-2090.
39. Noyori, R.; Yamakawa, M.; Hashiguchi, S., *J. Org. Chem.* **2001**, *66*, 7931-7944.
40. Clapham, S. E.; Hadzovic, A.; Morris, R. H., *Coord. Chem. Rev.* **2004**, *248*, 2201-2237.
41. Samec, J. S.; Bäckvall, J.-E.; Andersson, P. G.; Brandt, P., *Chem. Soc. Rev.* **2006**, *35*, 237-248.
42. Carrión, M. C.; Jalón, F. A.; Manzano, B. R.; Rodríguez, A. M.; Sepúlveda, F.; Maestro, M., (Arene) ruthenium (II) Complexes Containing Substituted Bis (pyrazolyl) methane

Ligands—Catalytic Behaviour in Transfer Hydrogenation of Ketones. Wiley Online Library:  
2007.

## CHAPTER 5

### PIANO-STOOL DIRUTHENIUM(II) COMPLEXES OF QUINOLINYL-CARBOXAMIDE: STRUCTURAL, MECHANISTIC STUDIES AND TRANSFER HYDROGENATION OF KETONES

#### 5.1. Introduction

Ruthenium-based catalysts have attracted considerable attention due to their efficiency and robustness in multiple reactions.<sup>1-4</sup> A number of ruthenium catalysed reactions, including hydrogenations, oxidations,<sup>5</sup> N-alkylation of amines,<sup>6</sup> olefin metathesis,<sup>7-8</sup> dimerisation of alkynes,<sup>9</sup> among others, have been reported in the last two decades. Ruthenium complexes are also efficient catalysts for asymmetric and catalytic tandem reactions, for a example, transfer hydrogenation-epoxidation reactions. The development of ruthenium-based catalysts has led to the transformation of many organic molecules essential for pharmaceuticals and agrochemicals.<sup>10-12</sup> Despite the advances made toward the developments of mononuclear complexes for the effective transformation of organic molecules, the application of multinuclear metal catalysts has been less explored.<sup>13-15</sup> In recent years, a number of multinuclear complexes with exceptionally high catalytic activities have been developed and reported.<sup>16-19</sup> Liu *et al.* have reported a number of highly active dinuclear ruthenium(II) complexes supported on bis(pyrazolyl-imidazolyl-pyridine) ligand for TH of ketones.<sup>20</sup>

Half-sandwich ruthenium complexes are relatively inert toward rapid oxidation and decomposition and are considered suitable for tuning the electrophilicity of the metal centre.<sup>21</sup> Half-sandwich ruthenium complexes have proven to be an efficient catalyst for transfer

hydrogenation owing to its enhanced stability and ability to withstand catalyst deactivation.<sup>22-</sup>

23

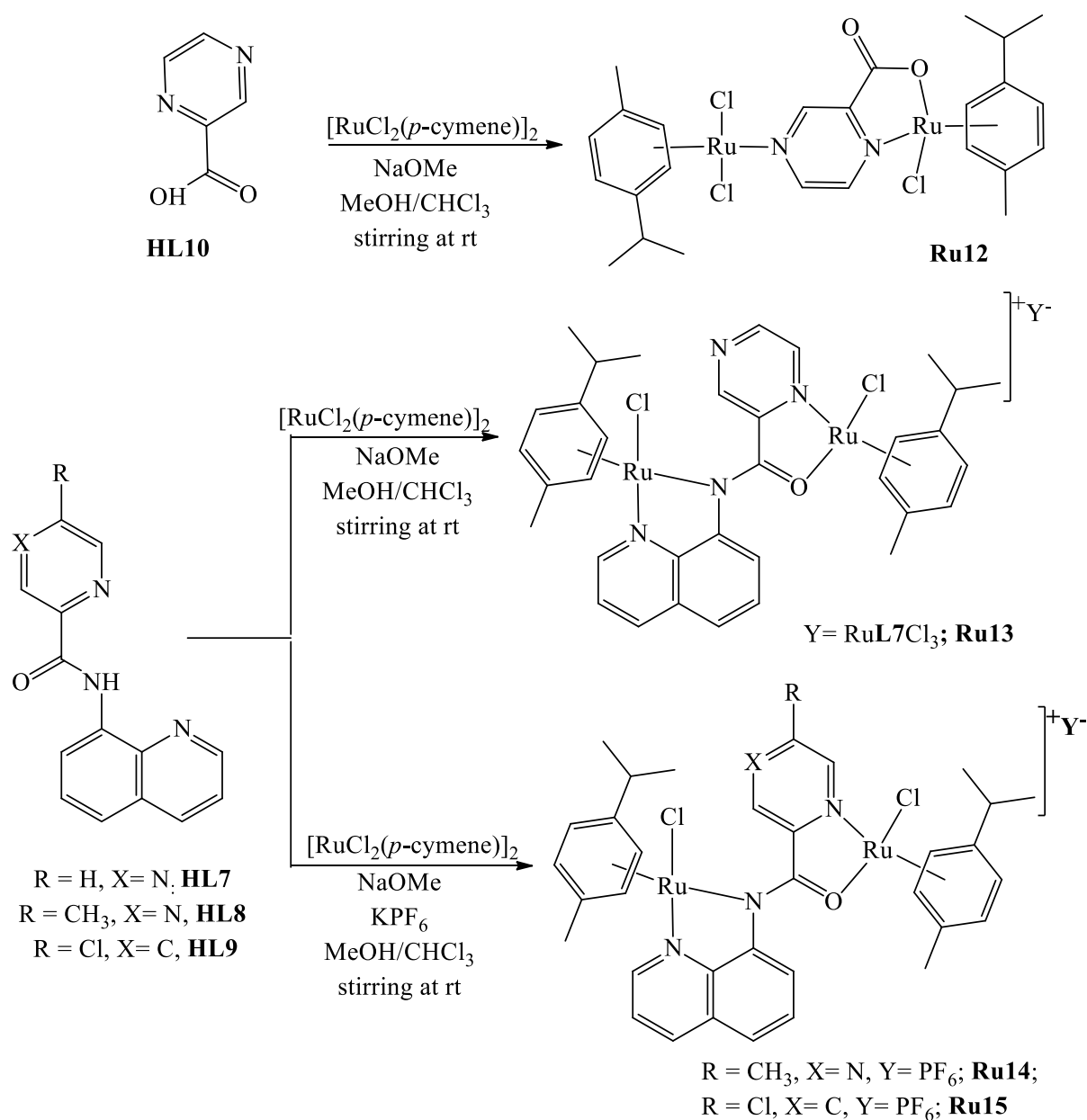
Carboxamide ligands have proven to be promising for designing transition metal complexes for effective homogeneous catalysis, possibly due to their ease of synthesis, steric and electronic properties suitable for enhancing catalytic properties of the resulting catalyst.<sup>24</sup> For example, dinuclear Ru(II) complexes supported on pyridine-2,6-dicarboxamide ligands have been reported with good catalytic activity in the nitrobenzene reduction reaction by Gupta and co-workers.<sup>25</sup> Albeit a number of multinuclear Ru(II) complexes have been developed for effective TH reactions, the demand for a new catalyst with high activity and stability has been quite a task in recent years. Inspired by the results of the previous studies in **Chapter 4** using the dinuclear complexes **Ru5-Ru11**, this chapter, presents the preparation, structural elucidation, and application of a new series of half-sandwich Ru(II) complexes **Ru12-Ru15** supported on quinoline-carboxamide ligands as catalysts for TH of ketones and aldehydes. Uniquely, these catalytic systems achieved better catalytic activity and cooperativity in the TH of ketones and aldehydes compared to **Ru5-Ru11** discussed in **Chapter 4**.

## 5.2. Results and discussion

### 5.2.1 Synthesis and characterisation of complexes Ru12-Ru15

The *N*-(quinoline-8-yl)-carboxamide ligands, **HL7-HL9**, were synthesised by condensation reactions between 8-aminoquinoline and respective carboxylic acids following modified literature procedures.<sup>25-27</sup> Detailed synthetic protocols, spectroscopic and analytical data of the ligands (**HL7-HL9**) are reported in **Chapter 2**. The dinuclear half-sandwich Ru(II) complexes **Ru12-Ru13** were synthesised by reacting [RuCl<sub>2</sub>-*p*-cymene)]<sub>2</sub> with the ligands, namely, *N*-

(quinoline 8-yl) pyrazine-2-carboxamide (**HL7**), and Pyrazine-2-carboxylic acid (**HL10**), in the presence of a stoichiometric amount of sodium methoxide (NaOMe) (**Scheme 5.1**). On the contrary, reactions of  $[\text{RuCl}_2(\eta^6\text{-}p\text{-cymene})]_2$  precursor with the dipicolamide ligands, 5-methyl-*N*-(quinoline-8-yl) pyrazine-2 carboxamide (**HL8**), and 5-chloro-*N*-(quinoline-8-yl) pyrazine-2-carboxamide (**HL9**) in the presence of  $\text{KPF}_6$  afforded the cationic complexes  $[\{\text{Ru}(\eta^6\text{-}p\text{-cymene})\}_2\text{-}\mu\text{-Cl}\}\text{L8}][\text{PF}_6]$ , (**Ru14**) and  $[\{\text{Ru}(\eta^6\text{-}p\text{-cymene})\}_2\text{-}\mu\text{-Cl}\}\text{L9}][\text{PF}_6]$ , (**Ru15**) respectively as shown in **Scheme 5.1**. The new half-sandwich Ru(II) complexes were air-stable, non-hygroscopic and soluble in methanol, ethanol, acetone, dimethyl sulfoxide, 2,5-dimethylfuran, and 2-propanol.



**Scheme 5.1.** Synthesis of half-sandwich dinuclear Ru(II) complexes **Ru12-Ru15**.

The Ru(II) complexes **Ru12-Ru15** were characterised by  $^1\text{H}$  NMR spectroscopy,  $^{13}\text{C}$  NMR spectroscopy, FT-IR spectroscopy, ESI-mass spectrometry, and single-crystal X-ray crystallography technique (**Ru12** and **Ru14**). The molecular identity of the complexes **Ru12 - Ru15** is established by comparing the  $^1\text{H}$  NMR spectroscopic data to their corresponding free ligands **HL7-HL10**. For example, in the  $^1\text{H}$  NMR spectrum of complex **Ru12**, the signal of the pyrazine protons shifted downfield to 9.40 ppm, 8.98 ppm and 8.92 ppm when compared

to the  $^1\text{H}$  NMR spectrum of **HL10** (9.18 ppm, 8.85 ppm and 8.79 ppm respectively) as shown in **Figure 5.1**. The downfield shift in the signals of pyrazine protons,  $\text{H}_{\text{pyrazine}}$  in the **Ru12** compared to **HL10**, indicates the successful coordination of the ruthenium precursor to the  $\text{N}_{\text{pyrazine}}$ -atoms of the ligand.<sup>28-29</sup> In addition, a slight downfield shift in the signal of carbonyl the carbon (**Ru12**) to  $\delta$ : 169.7 ppm compared to the corresponding free ligand **HL10** (165.5 ppm) as illustrated in **Figure 5.2**, confirmed the coordination of the  $\text{RuCl-}p\text{-cymene}$  precursor to the O-atoms of the carboxylate group. The metalation of the carboxamide ligands, **HL7- HL9**, gave similar characteristic features as observed in **Ru12**. For instance, the signal of N-H disappeared in the **Ru15** upon coordination, as depicted in the overlaid spectra in **Figure 5.2**. Similarly,  $^{13}\text{C}\{^1\text{H}\}$  NMR spectrum of the **Ru15** showed carbonyl carbon shifted downfield to 167.9 ppm compared to the corresponding free ligand **HL9** (162.8 ppm) as shown in **Figure 5.4**. The absence of the characteristic N- $\text{H}_{\text{amide}}$  signal in the  $^1\text{H}$  NMR and reasonably downfield shifted signal of  $\text{C}_{\text{carbonyl}}$ -atom in  $^{13}\text{C}\{^1\text{H}\}$  NMR spectroscopic data suggest coordination of the half-sandwich Ru(II) precursor to the  $\text{O}_{\text{amidate-}}$  and  $\text{N}_{\text{amidate-}}$  atoms.<sup>30</sup> The  $^{13}\text{C}$  NMR spectra of complexes **Ru12-Ru15** also showed signals corresponding to  $\text{C}_{p\text{-cymene}}$  between 79.6 ppm-106.9 ppm, which are comparable to other related ruthenium(II) complexes bearing  $p\text{-cymene}$  moiety.<sup>31-37</sup>



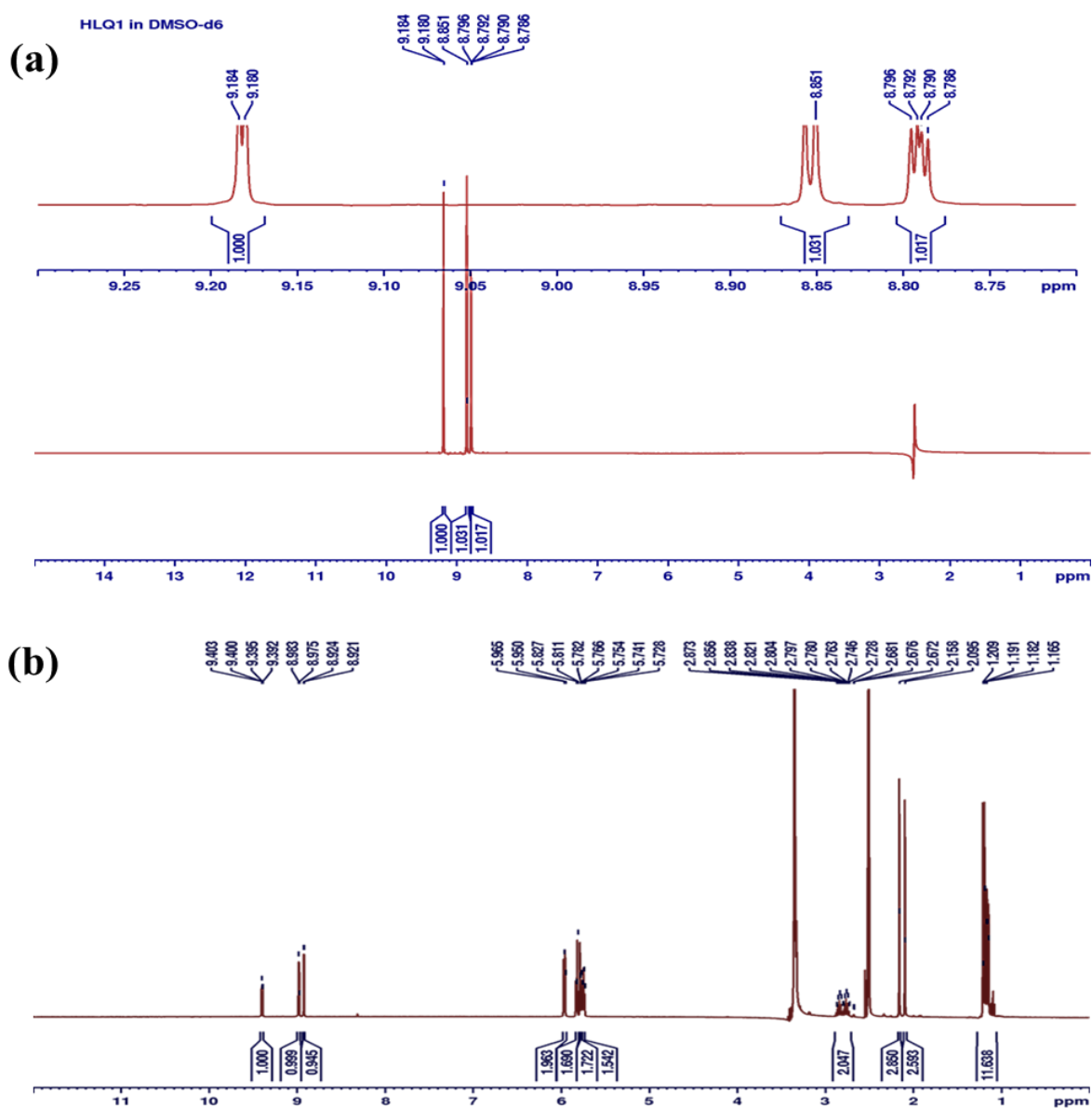


**Figure 5.1.** A comparison in chemical shifts in the  $^1\text{H}$  NMR spectra of (a) **HL10** ( $H_{\text{prazine}}$ : 9.18-8.79 ppm) and (b) **Ru12** ( $H_{\text{prazine}}$  : 9.40-8.92 ppm).

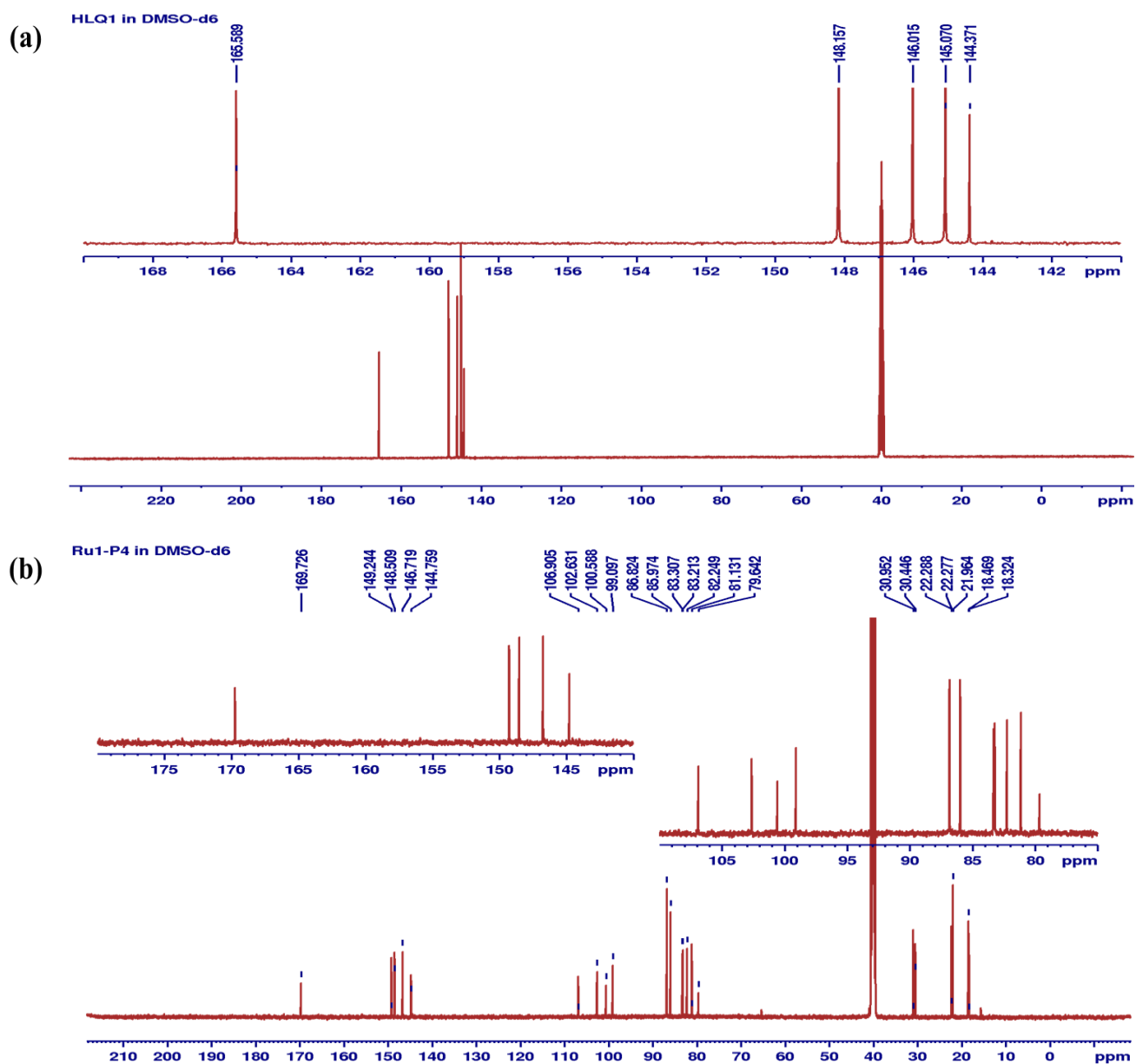


**Figure 5.2.** A comparison in the chemical shifts in the  $^{13}\text{C}\{^1\text{H}\}$  NMR spectra of (a) **HL10** ( $\text{C}=\text{O}_{\text{amide}}$  at  $\delta$ : 166.5 ppm) and (b) **Ru12** ( $-\text{C}=\text{O}_{\text{amide}}$  at  $\delta$ : 169.7 ppm).

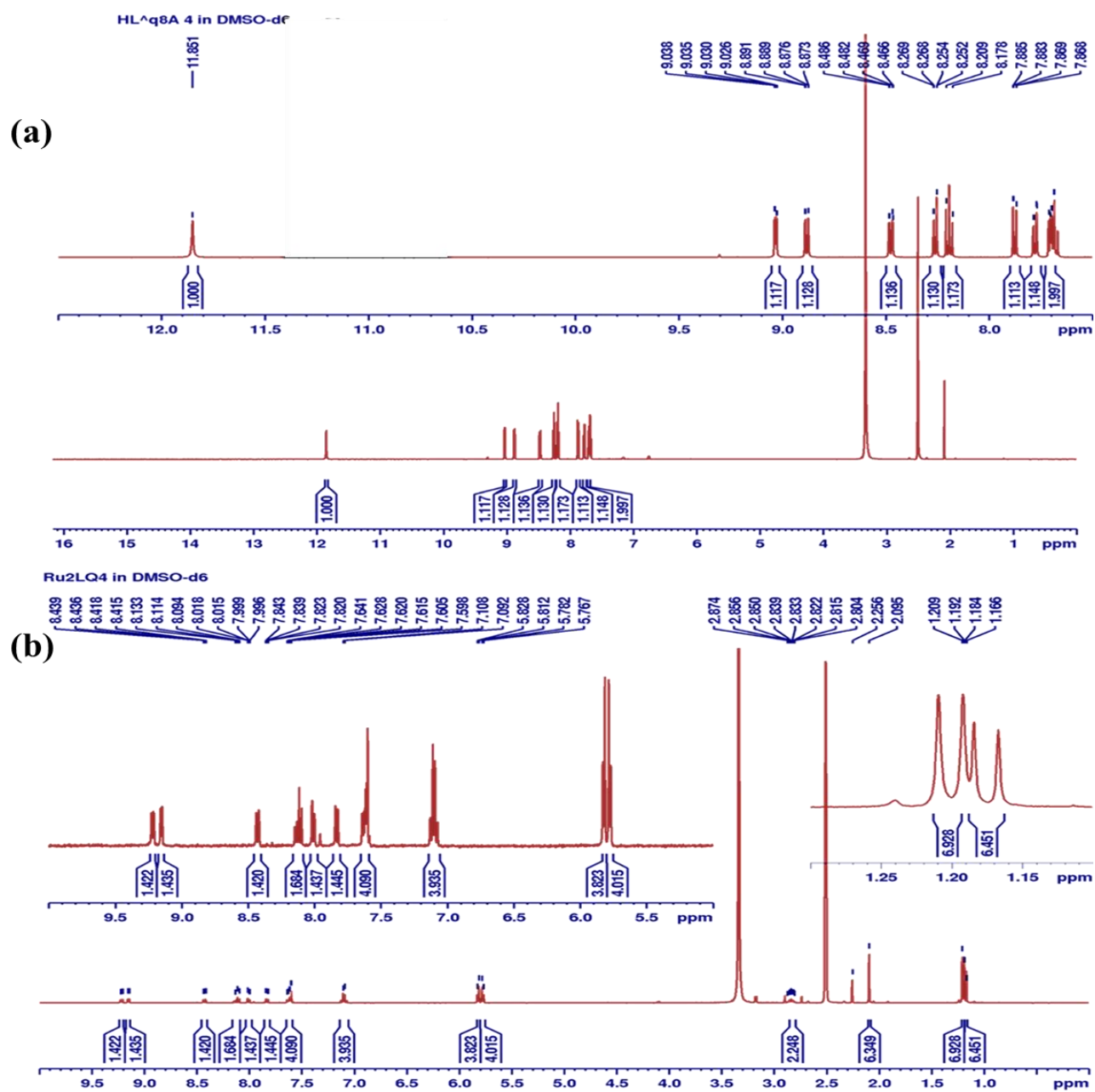


**Figure 5.3.** A comparison in the chemical shifts in the <sup>1</sup>H NMR spectra of (a) **HL9** (N-H<sub>amide</sub> at  $\delta$ : 11.65 ppm) and (b) **Ru15** (N-H<sub>amide</sub> absent).

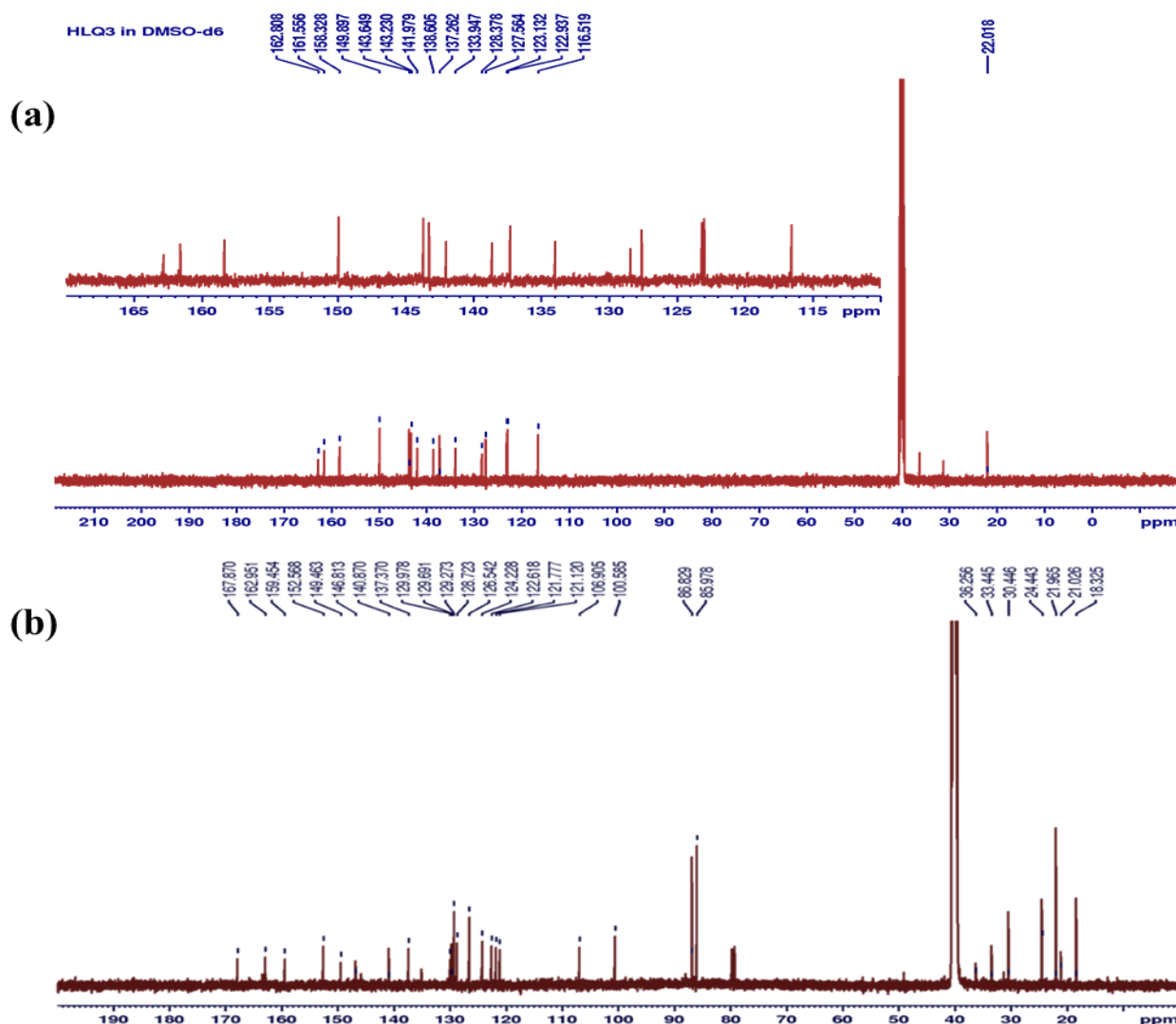


**Figure 5.4.** A comparison in the chemical shifts in the  $^{13}\text{C}\{^1\text{H}\}$  NMR spectra of (a) **HL9** (-C=O<sub>amide</sub> at  $\delta$ : 162.8 ppm) and (b) **Ru15** (-C=O<sub>amide</sub> at  $\delta$ : 167.9 ppm).

The formation of complexes **Ru12-Ru15** was further supported by comparing the FT-IR spectra of the complexes and their corresponding carboxamide ligands (**HL7- HL10**). For instance, the N-H<sub>amide</sub> absorption band in **Ru15** disappeared upon complexation, and it correlates well with the  $^1\text{H}$  NMR data. In addition, the sharp carbonyl,  $\nu(\text{C-O})$  stretching band at  $1628\text{ cm}^{-1}$  in **HL9** shifted to a lower frequency ( $1589\text{ cm}^{-1}$ ) upon formation of **Ru15** and consistent in the FT-IR spectra of complexes **Ru12-Ru14** (Table 5.1). These observations could be assigned to the resonance enhancement of the deprotonated amide and

participation of the O-atom of carbonyl in the coordination resulting in the weaker carbonyl bond.<sup>28, 38-39</sup> The  $^{31}\text{P}\{^1\text{H}\}$  and  $^{19}\text{F}$  NMR spectroscopies were also used to confirm the presence of the counterion,  $[\text{PF}_6]^-$  in the complexes **Ru14** and **Ru15**. For instance, complex **Ru14** showed septet signal between  $\sim 132$  and  $\sim 158$  ppm in the  $^{31}\text{P}\{^1\text{H}\}$  NMR spectrum (**Figure 5.5**).  $^{19}\text{F}$  NMR spectroscopic data, for example **Ru14**, also gave doublets between  $\sim 69$  and ( $\sim 71$ ) ppm (**Figure 5.6**) which pointed to the presence of  $[\text{PF}_6]^-$  as the counterion.

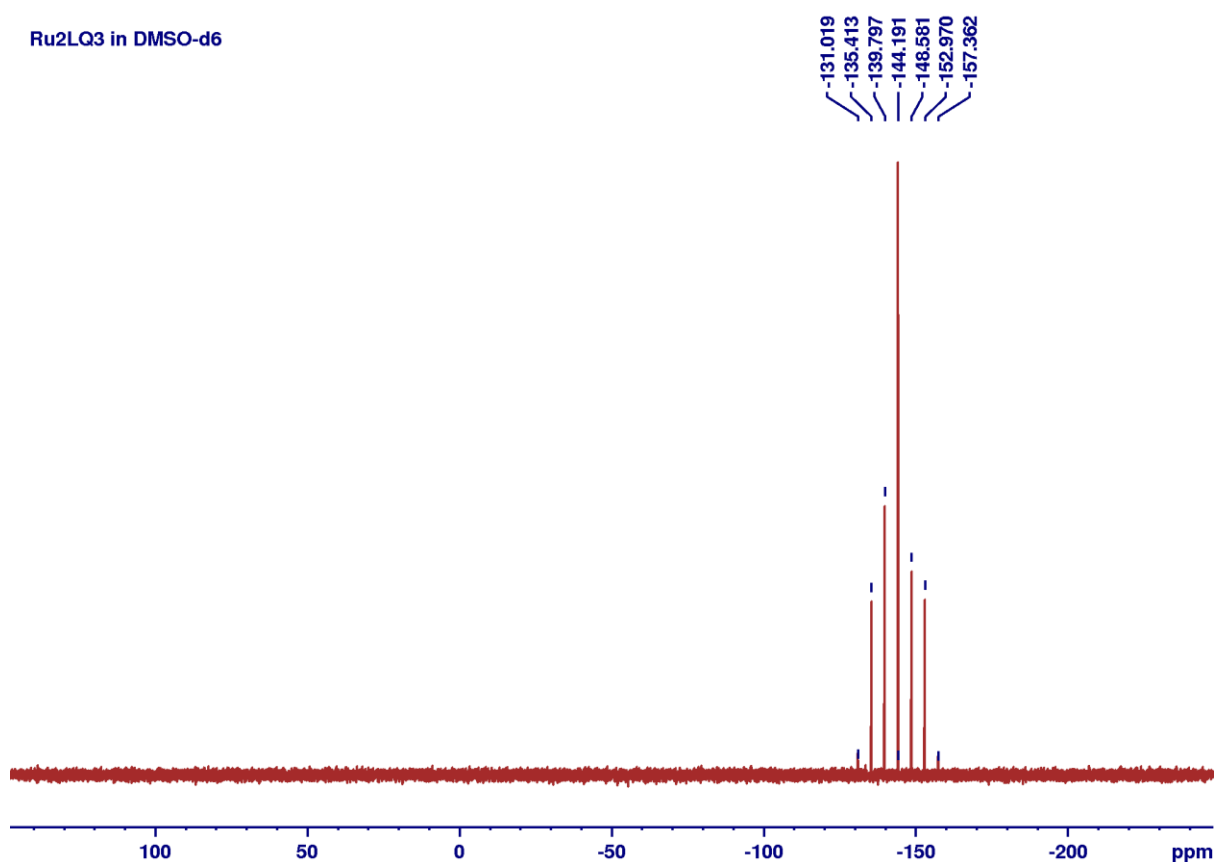


**Figure 5.5.**  $^{31}\text{P}\{^1\text{H}\}$  NMR of complex **Ru14** showing signal between  $\sim 131$  and  $\sim 157$  ppm confirming the presence of  $[\text{PF}_6]^-$  counterion.

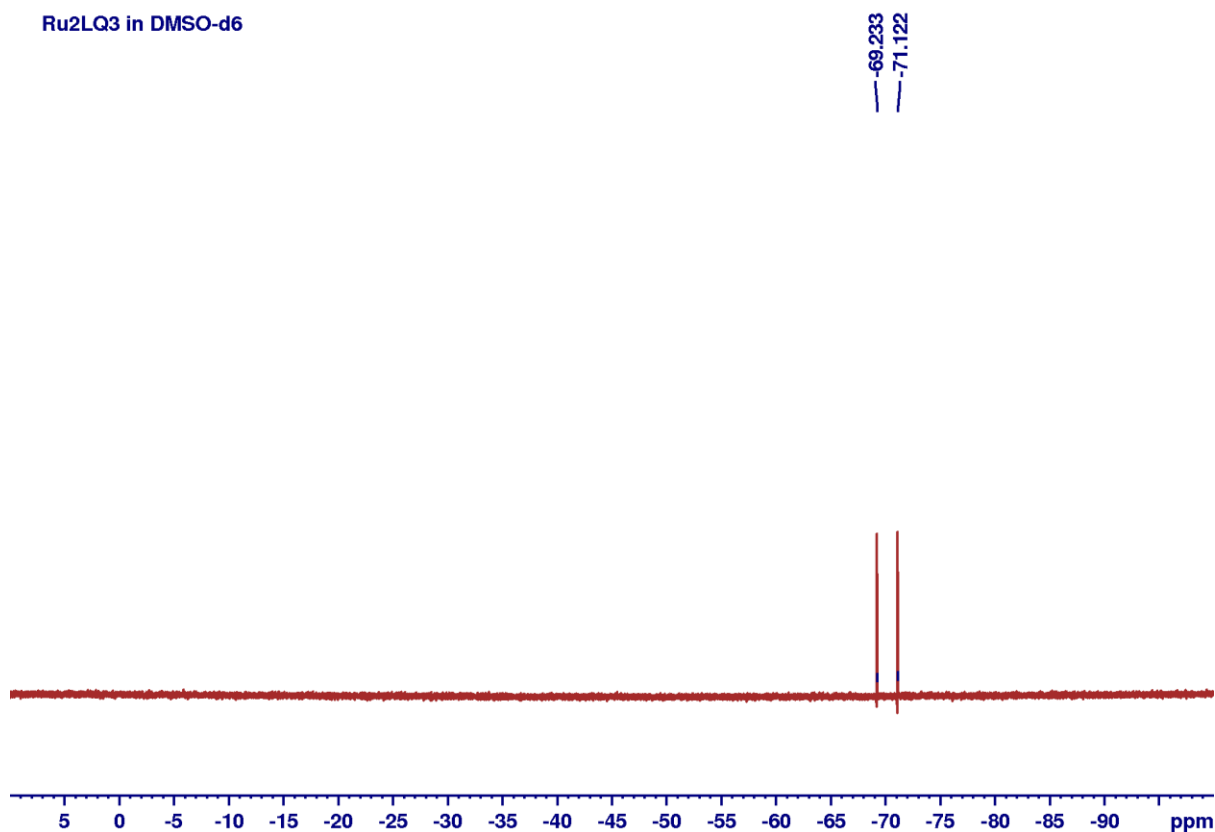


**Figure 5. 6.**  $^{19}\text{F}$  NMR of complex **Ru14** showing a doublet signal between ~69 and ~79 ppm confirming the presence of  $[\text{PF}_6]^-$  counterion.

**Table 5. 1.** Selected FT-IR spectroscopic data of the complexes **Ru12-Ru15** and corresponding ligands **HL7-HL10**.

Entry	Complex	$\nu(\text{C-O})^{\text{a}}_{\text{hemi-mide}}$	$\nu(\text{N-H})^{\text{a}}_{\text{amide}}$
1	<b>Ru12</b>	1615(1720)	
2	<b>Ru13</b>	1598(1675)	- (3313)
3	<b>Ru14</b>	1578(1678)	- (330.3)
4	<b>Ru15</b>	1589(1628)	- (3315)

<sup>a</sup>FT-IR spectroscopic data of the ligands are in brackets.

(-) - disappeared

ESI mass spectrometry of complexes **Ru12-Ru15** further confirmed their composition, molecular masses and formulae. In general, low-resolution ESI-MS data of complexes **Ru12-Ru15** showed  $m/z$  signals corresponding to the cationic species, containing two Ru(II) metal atoms and one ligand unit. For instance, the mass spectra of the complexes showed peaks at  $m/z$  730 (**Ru12**), 791(**Ru13**), 805(**Ru14**), and 826 (**Ru15**), corresponding to molecular formulae of the dinuclear species  $[(\text{Ru-}p\text{-cymene})_2(\text{L})\text{Cl}_3]^+$  for **Ru12** and  $[(\text{Ru-}p\text{-cymene})_2(\text{L})\text{Cl}_2]^+$  for **Ru2-Ru4**, respectively. More significantly, the experimental and simulated isotopic mass distributions showed good correlations (**Figure 4.5**). Elemental analysis data of complexes **Ru12-Ru15** were consistent with the proposed structures (**Scheme 5.1**) and established the purity of the bulk materials.

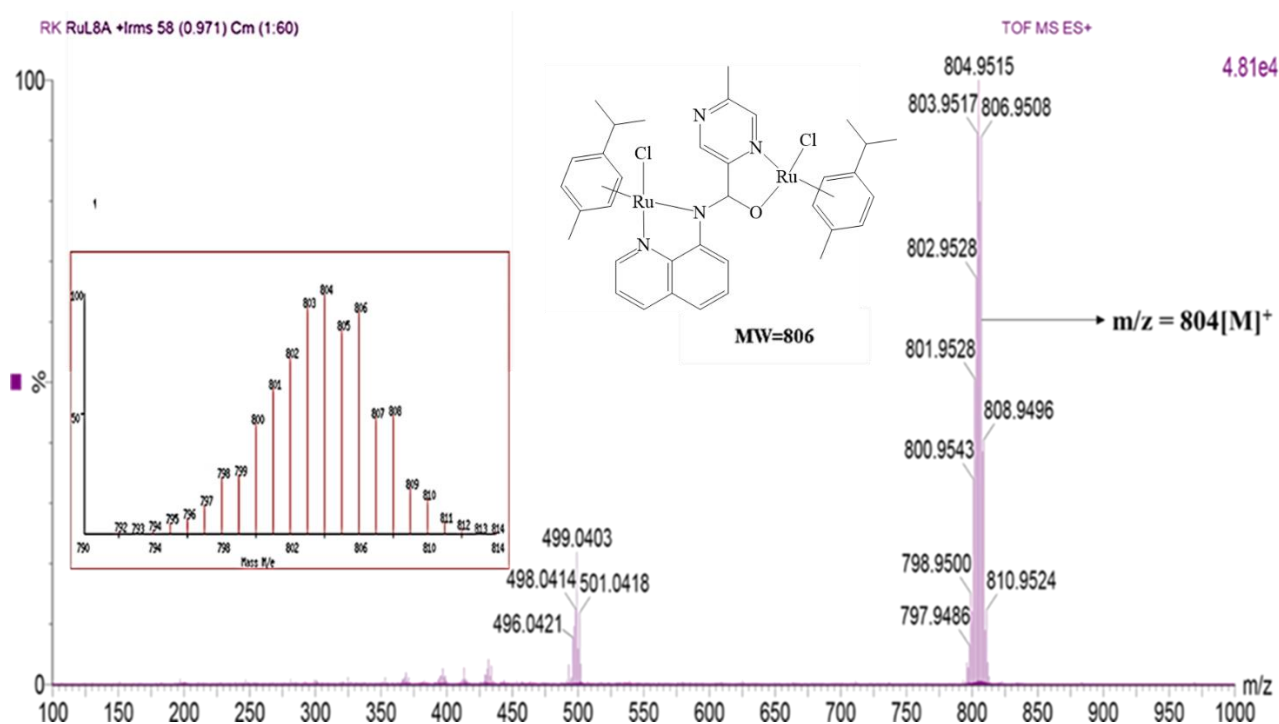


**Figure 5.7.** ESI-MS spectrum of **Ru14**, showing  $m/z = 804.95$  [ $\text{M}^+$ , 100%] and consistent with theoretical isotopic mass distribution (inset).

### 5.2.2. Solid-state structures of the dinuclear half-sandwich complexes **Ru12** and **Ru14**

Single-crystal X-ray crystallographic technique was used to establish the molecular structures and coordination geometry around the ruthenium(II) ions of the dinuclear Ru(II) complexes, **Ru12** and **Ru14**. The perspective views of the two complexes, **Ru12** and **Ru14**, are displayed in **Figures 5.8** and **5.9**, respectively. A summary of the crystallographic data and details of refinement are summarised in **Table 5.2**. The complexes **Ru12** and **Ru14** crystallise in the monoclinic system with the space group  $P2_1/c$  and  $P2_1/n$ , respectively. The ruthenium(II) ions in the two complexes **Ru12** and **Ru14** adopt a typical three-legged piano-stool (*pseudo-octahedral*) geometry with the  $\eta^6$ -bonded *p*-cymene constituting the base and the Ru-N<sub>pyrazine</sub>, Ru-O<sub>iminolate</sub>, and chlorido ligand forming the three legs. As shown in **Figure 5.8**, the Ru-atom in complex **Ru12** is coordinated to the 2,4 pyrazine-carboxylate ligand (**HL7**) *via* the N<sub>pyrazine</sub> and its geometry is completed by the two chlorido co-ligand while the Ru(II) ion coordinates to the ligand **HL7** *via* the N<sub>pyrazine</sub>, N(2) and O<sub>carboxylate</sub>-atom, and is surrounded by the  $\eta^6$  bonded *p*-cymene and one chlorido co-ligand. However, **Ru14** crystallised with a counterion containing a Ru(III) anion in which the anionic ligand **L7** is tridentately bound to the Ru(IV) atom [Ru<sup>(III)</sup>Cl<sub>3</sub>(**L7**)]. The formation of the Ru(III) anionic species could be attributed to the presence of excess [Ru( $\eta^6$ -*p*-cymene)Cl<sub>2</sub>]<sub>2</sub> and **HL7** solvent at room temperature. In the structure of **Ru14** (**Figure 5.9**), the Ru(II) precursor coordinated to the N<sub>pyrazine</sub>-, N<sub>amidate</sub>-, N<sub>quinoline</sub>- and O<sub>amidate</sub>- atoms of the chelating, 5-methyl-*N*-(quinoline-8-yl) pyrazine-2-carboxamide (**HL9**) ligand. The chlorido auxiliary ligand completes the coordination geometry of the Ru-atom. The observed bond distance Ru(1)-N(1), 2.117(3) (Å) in **Ru12** and **Ru14** [2.089(4) (Å)] are within the average bond distance of 2.104(12) (Å) of similar half-sandwich Ru(II) compounds deposited in CCDC file.<sup>40</sup> The bond length of Ru(1)-O(1), 2.091(2) (Å) in **Ru12** is slightly shorter compared to **Ru14** [2.120(3) (Å)] and is within the average bond length of 2.116(15) Å of 16 similar Ru(II) compounds deposited in CCDC file.<sup>40</sup> The two Ru(II) ions



in **Ru12** and **Ru14** exhibit dihedral angles of -N(2)-C(3)-C(5)-O(2)  $-1.18(13)^\circ$  is comparable to  $-1.35(11)^\circ$  and observed in **Ru14**, and are in good agreement with 18 related half-sandwich Ru(II) complexes deposited in the CDCC file.<sup>40</sup> The bond angles of N(1)-Ru(1)-O(1),  $77.83(10)^\circ$  **Ru12** and **Ru14** [ $84.03(12)^\circ$ ] are also found to be within the average bond angle of  $78.13(24)^\circ$ , exhibited by 56 similar compounds deposited in CCDC.<sup>40</sup>

However, the bond length of Ru(1)-N(1),  $2.117(3)$  Å in complex **Ru12** is appreciably longer than the bond length for Ru(1)-N(1) of  $2.089(4)$  Å for **Ru14** and could be as the result of the  $\pi$  electron-donating property of quinoline moiety in complex **Ru14**. The average bond distances for Ru- $C_{p\text{-cymene}}$  of  $2.182(3)$  Å (**Ru12**) and  $2.196(6)$  Å (**Ru14**) are slightly longer compared to the average Ru- $C_{p\text{-cymene}}$  bond length of  $2.166(1)$  Å reported for the dimeric  $[\text{RuCl}_2(\eta^6\text{-}p\text{-cymene})]_2$  precursor.<sup>41</sup> This could be attributed to a strong sigma-electron donating and accepting interactions between  $p\text{-cymene}$  *co*-ligand and Ru(II) centre.<sup>42</sup> Nonetheless, the average Ru- $C_{p\text{-cymene}}$  bond distance (**Ru12** and **Ru14**) is comparable to 6 compounds bearing Ru-N bond deposited in CDCC.<sup>43</sup> The distance from the Ru(II) atom to the  $p\text{-cymene}$  ring centroid is  $2.34$  Å and  $1.892$  Å (**Ru12**) and  $1.864(4)$  Å and  $1.871(3)$  Å (**Ru14**), respectively. Both complexes **Ru12** and **Ru14** adopt an intermediate conformation between eclipsed and staggered with respect to the  $p\text{-cymene}$  ring and the Ru(II) centres.

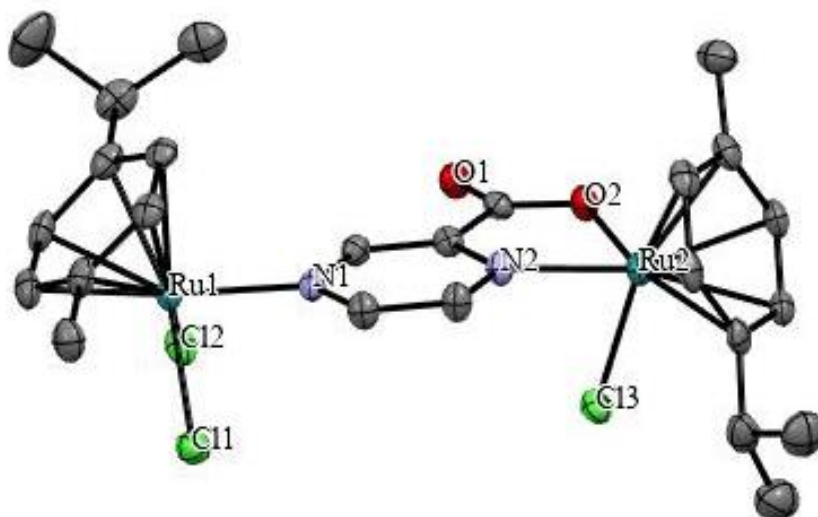


**Figure 5.8.** ORTEP representation of **Ru12** at 50% probability thermal ellipsoids level. Hydrogen atoms and solvent,  $\text{CHCl}_3$  have been removed for clarity. Bond length( $\text{\AA}$ ): Ru(1)-N(1), 2.117(3) Ru(2)-N(2), 2.097(3), Ru(1)-Cl(1), 2.173(4), Ru(1)-O(2), 2.091(2). Bond angle( $^\circ$ ): N(1)-Ru(1)-Cl(1), 86.95(8), O(2)-Ru(1)-N(1), 77.83(10), N(2)- Ru(1)-Cl(3), 81.24(8), and O(1)- Ru(1)-Cl(3), 84.76(7).

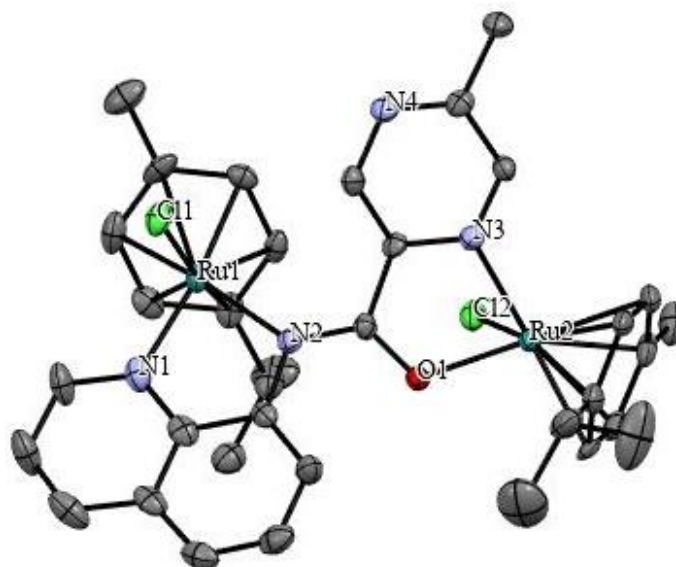


**Figure 5.9.** ORTEP representation of **Ru14** at 50% probability thermal ellipsoids level. Hydrogen atoms and counterion of **Ru3**,  $\text{RuCl}_3(\text{L}^3)$  have been removed for clarity. Bond length ( $\text{\AA}$ ): Ru(1)-N(1), 2.089(4), Ru(2)-N(2), 2.173(4), Ru(1)-Cl(1), 2.391(14), Ru(2)-N(3), 2.173(4), Ru(1)-O(2), 2.120(3). Bond angle ( $^\circ$ ): N(1)-Ru(1)-Cl(1), 93.83(13), O(2)-Ru(1)-N(1), 84.03(12), N(2)-Ru(1)-Cl(3), 77.75(16), and O(1)-Ru(1)-Cl(3), 86.04(10).

**Table 5.2.** Summary of crystallographic data and structural refinement data for complexes **Ru12** and **Ru14**.

Parameters	Ru12	Ru14
Chemical formula	C <sub>25</sub> H <sub>31</sub> O <sub>2</sub> N <sub>2</sub> Ru <sub>2</sub> Cl <sub>3</sub> + CHCl <sub>3</sub>	C <sub>36</sub> H <sub>40</sub> Cl <sub>2</sub> N <sub>4</sub> ORu <sub>2</sub> + [C <sub>16</sub> H <sub>12</sub> Cl <sub>3</sub> N <sub>2</sub> ORu]
Formula weight	819.37	1273.45
Temperature/K	102	100
Crystal system	monoclinic	monoclinic
Space group	P2 <sub>1</sub> /c	P 2 <sub>1</sub> /n
a(Å)	17.0442(4)	19.6266(5)
b(Å)	17.2349(4)	13.9931(3)
c(Å)	10.5921(2)	20.1531(6)
α(°)	90	90
β(°)	94.129(1)	117.705(1)
γ(°)	90	90
Volume (Å <sup>3</sup> )	3103.41(12)	4900.2(2)
Z	4	4
ρ	1.754	1.796
μ(CuKα)	12.857	10.290
F(0 0 0)	1632.0	2556
Crystal size(mm)	0.11 x 0.105 x 0.035	0.260 x 0.0042 x 0.035
Tmin. and Tmax	0.547, 0.754	0.480, 0.753
Absorption coefficient/mm <sup>-1</sup>	12.857	10.290
Goodness-of- fit on F <sup>2</sup>	1.017	1.048
R <sub>1</sub> , wR <sub>2</sub> [I> 2(I)]	R <sub>1</sub> = 0.0320, wR <sub>2</sub> = 0.0746	R <sub>1</sub> = 0.0412, wR <sub>2</sub> = 0.0959
Data completeness	0.993	0.997
R <sub>1</sub> , wR <sub>2</sub> (all data)	0.0778(6063)	0.9412(7230),
Largest diff. peak and hole (e.Å <sup>-3</sup> )	1.181 and -1.14	0.041 and -1.161

### 5.2.3. Transfer hydrogenation of ketones and aldehydes

#### 5.2.3.1. Optimisation of reaction conditions of transfer hydrogenation of ketones

Preliminary catalyst screening was performed using acetophenone as a model substrate, **Ru13** as a pre-catalyst and  $K^tBuO$  as a promoter. The results are presented in **Table 5.3**. Initially, the catalytic transfer hydrogenation of ketone was conducted using **Ru13** [0.0010 mol% (10 ppm)] in the presence of  $K^tBuO$  (0.4 mol%) to give a conversion of 21% corresponding to a TON of  $2.10 \times 10^4$  was obtained (**Table 5.3, entry 3**). A blank experiment without a catalyst was carried out, and catalytic activity of 2% after 6 h was obtained. Another controlled experiment was conducted without a base to establish that the pre-catalyst is responsible for the catalytic activity recorded in **Table 5.3**. However, only 10% conversion corresponding to  $9.0 \times 10^3$  TON was achieved in 6 h (**Table 5.3, entry 2**). These results show that a base is required to activate these catalysts to promote the reaction. Therefore, two critical parameters, viz; the effects of catalyst concentration and the nature of base for effective transfer hydrogenation of ketones were investigated. To optimise, different catalyst loading ranging from 0.0010 mol% (10 ppm) to 0.100 mol% (1000 ppm) were employed, and the results are listed in **Table 5.3**. From the result, it can be concluded that increasing catalyst loading resulted in higher percentage conversions. Although higher yields were achieved at higher catalyst concentrations, lower TONs were achieved. For example, a catalyst loading of 0.0010 mol %, a percentage conversion of 21 % corresponding to a TON of  $2.10 \times 10^4$  compared to 88% yield (TON up to 8800) achieved using 0.010 mol% (100 ppm) catalyst loading (**Table 5.3, entry 3 vs 6**). From **Figure 5.10**, a catalyst loading of 0.0020 mol% (20 ppm) could be considered ideal since a higher TON value of  $3.25 \times 10^4$  was achieved compared to the TON value of  $8.8 \times 10^4$  achieved by 0.100 mol% (1000 ppm) under similar reaction conditions.

**Table 5.3.** Optimisation of reaction conditions for transfer hydrogenation of acetophenone using **Ru13**<sup>a</sup>.

Entry	Catalyst loading/mol%(ppm)	Base	<sup>b</sup> Conversion[%]	Yield%	TON x 10 <sup>4</sup>	TOF/h <sup>-1</sup> x10 <sup>3</sup>
1	0.0010(10 ppm)	K <sup>t</sup> BuO	12	10	1.00	1.67
2	0.0015(15 ppm)	K <sup>t</sup> BuO	27	24	1.60	2.67
3	0.0020(20 ppm)	K <sup>t</sup> BuO	68	65	3.25	5.42
4	0.0040(40 ppm)	K <sup>t</sup> BuO	72	70	1.75	2.92
5	0.0060(60 ppm)	K <sup>t</sup> BuO	88	87	1.45	2.42
6	0.0100(100 ppm)	K <sup>t</sup> BuO	91	88	8.80	1.47
7	0.0020(20 ppm)	KOH	32	30	0.16	0.26
8	0.0020(20 ppm)	K <sub>2</sub> CO <sub>3</sub>	22	19	0.95	0.16
9 <sup>c</sup>	-	K <sup>t</sup> BuO	5	5	---	---
10	0.010(100 ppm)	-	10	9	0.90	1.50

<sup>a</sup>Reaction conditions: Acetophenone (1.0 mmol), **Ru2** as catalyst, base (0.4 mol%), refluxed in <sup>i</sup>PrOH (2.5 mL) at 82 °C for 6 h, <sup>b</sup>Determined by <sup>1</sup>H NMR spectroscopy (Anisole was used as an internal standard). <sup>c</sup>Reaction time = 16 h. TON (Turnover number) = mmol of product x mmol of substrate/catalyst loading. TOF(Turnover frequency) = mmol of product x mmol of substrate/catalyst loading/time/h. All experiments were conducted in triplicate to ensure reproductivity and averaged (SD ±1.0).

The effects of inorganic bases such as KOH and K<sub>2</sub>CO<sub>3</sub> were studied under similar reaction conditions. From Table 5.3, the reactivities of the bases are in the order K<sup>t</sup>BuO > KOH > K<sub>2</sub>CO<sub>3</sub>. This trend could be ascribed to the basicity and solubility of the bases in isopropanol. This observation is in good agreement with the earlier reports by Chai and co-workers.<sup>20</sup>

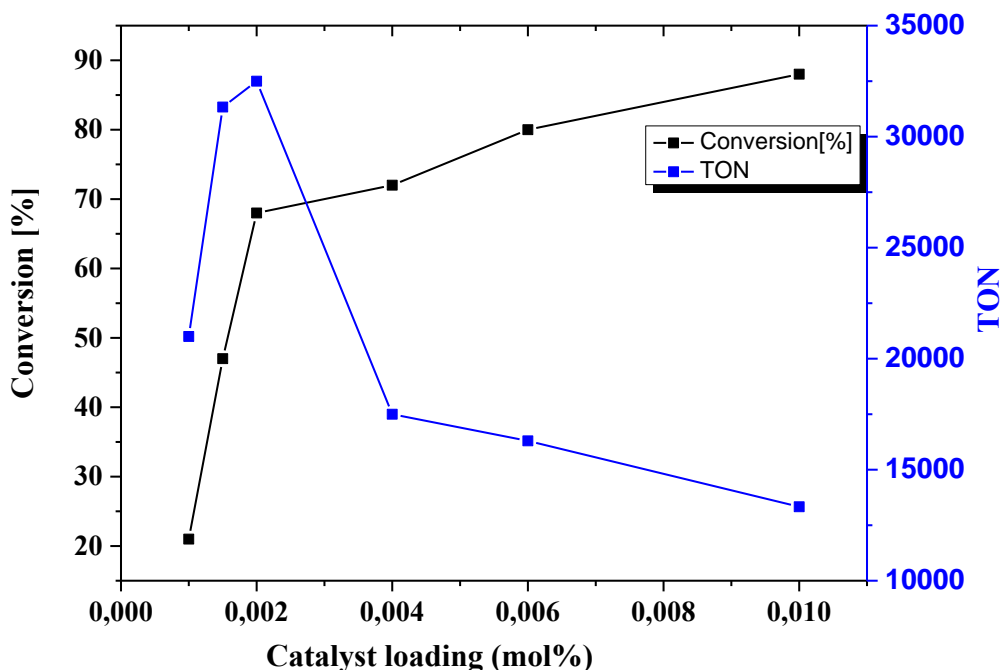


**Figure 5.10.** A plot of catalysts loading (mol%) vs conversion [%] and TON was used to determine optimised catalyst loading.

#### 5.2.3.2. Effects of catalyst structure on the transfer hydrogenation of acetophenone

To investigate the impact of the catalyst structure on the TH of acetophenone, we sought to screen the pre-catalysts **Ru12-Ru15** under the optimised reaction conditions, and the results are summarised in Table 5.11. The plot of  $\ln[\text{Ac.}]_t / [\text{Ac.}]_0$  vs time was also employed to determine the observed rate constant,  $k_{\text{obs}}$  (Figure 5.8). From Table 5.4, the catalytic activity of the complexes follows the order **Ru12** < **Ru13** < **Ru14** < **Ru15**. The complexes **Ru13-Ru15** supported on the quinoline- carboxamide ligands, **HL7-HL9** demonstrated superior catalytic

activity compared to **Ru12** bearing *carboxylate* ligand (**HL10**). For example, **Ru13** supported *N*-(quinoline-8-yl) pyrazine-2-carboxamide (**HL7**) showed a higher percentage conversion of 95 %, corresponding to  $k_{\text{obs}}$  0.232( $\pm$ 0.003) h<sup>-1</sup> compared to **Ru12** supported on the pyrazine-carboxylate ligand (**HL10**), which gave a lower percentage conversion of 78 % ( $k_{\text{ob}}$  of 0.211( $\pm$ 0.001) h<sup>-1</sup>), hitting to the significant of the quinoline moiety, which participated in coordination and rendered the complexes **Ru13- Ru15** more robust and less prone to deactivation than **Ru12**.

The introduction of substituents on the pyridyl and pyrazyl groups of the ligand backbone has shown marginal effects on the performance of the complexes. For instance, **Ru15** supported on 5-chloro-*N*-(quinoline-8-yl) pyrazine-2-carboxamide (**HL9**) showed higher percentage conversion of 97% corresponding to  $k_{\text{ob}}$  of 0.293( $\pm$  0.040) h<sup>-1</sup> compared to its analogous complex **Ru13** anchored unsubstituted on *N*-(quinoline-8-yl) picolinamide (**HL8**) ligand backbone which attained conversion of 95 % ( $k_{\text{ob}}$  = 0.232( $\pm$  0.030) h<sup>-1</sup>). The introduction of an electron-withdrawing substituent such as chlorine atom on the pyridyl group could enhance the electrophilicity of the Ru(II) centre and promotes better catalytic activity than the complex supported on the unsubstituted ligand. In contrast, the methyl group on the **Ru14** turned to minimise the electrophilicity of the Ru atoms and gave lower activity compared to **Ru15**. . This might be explained from the remote proximity of the methyl substitutes in **HL8**; hence does not significantly affect the Ru(II) metal centre. **Ru15** showed higher catalytic activity owing to the combined effect of the  $\pi$ -acceptor ability of pyridine and the chlorine electron-withdrawing group of the ligand backbone.



In comparison with the earlier reported dinuclear Ru(II) complexes in literature, our Ru(II) complexes supported on the carboxamide-quinoline ligands displayed higher catalytic activity, TON, although much lower catalyst loading was employed.<sup>44-45</sup> However, the complexes **Ru12-Ru15** showed relative lower catalytic activity compared to recently reported dinuclear Ru(II) complexes which demonstrated exceptionally higher TOF between  $1.0 \times 10^5$  -  $2.1 \times 10^6$  h<sup>-1</sup>.<sup>20, 46</sup> The Ru(II)-Ru(II) interaction thus appears to affect the performance of the new catalyst (**Ru12-Ru15**). Multinuclear complexes with less metal-metal interactions showed good catalytic activities and compared to those with strong metal-metal interactions.<sup>14, 17</sup>

**Table 5.4.** Effects of catalyst structure on transfer hydrogenation of acetophenone<sup>a</sup>.

Entry	Catalyst	% Conversion <sup>b</sup>			TON <sub>6h</sub>	<i>k</i> <sub>obs</sub> /h <sup>-1</sup>
		2h	4h	6h		
1	<b>Ru12</b>	34	59	78	39000	0.211(±0.001)
2	<b>Ru13</b>	44	68	95	46500	0.232(±0.003)
3	<b>Ru14</b>	42	61	94	46000	0.213(±0.04)
4	<b>Ru15</b>	48	73	97	48500	0.293(0.040)
5	<b>Ru15+Hg(0)</b>	NA	NA	91	45500	N/A

<sup>a</sup>Reaction conditions: Acetophenone (1.0 mmol), catalyst (0.0020 mol%(20 ppm), base (0.4 mol%), refluxed in <sup>1</sup>PrOH (2.5 mL) at 82 °C for 6 h, <sup>b</sup>Determined by <sup>1</sup>H NMR spectroscopy. Anisole was used as an internal standard. TON<sub>6h</sub> = Turnover number at 6 h. All experiments were conducted in triplicate to ensure reproductivity.

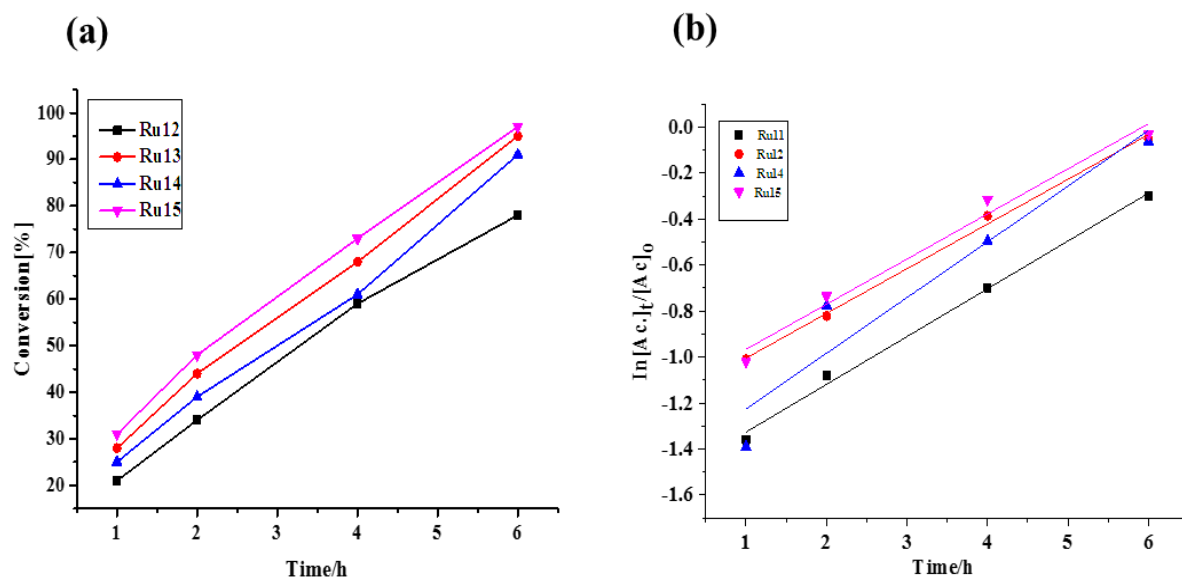


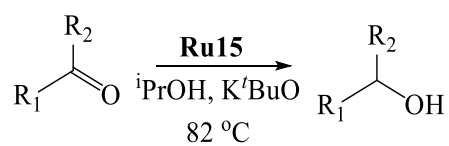
**Figure 5.11.** Time-dependence plots of the TH of acetophenone reactions catalysed by **Ru12-Ru15**. (a) Percentage conversion vs time/h, (b)  $\ln[Ac.]_t/[Ac.]_o$  vs time/h.

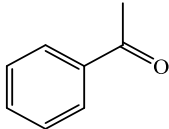
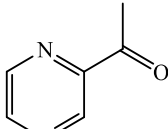
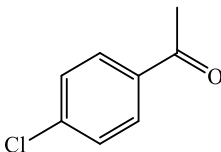
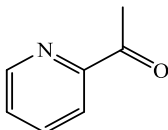
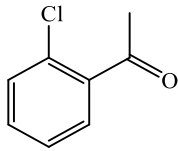
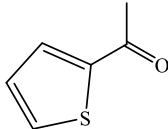
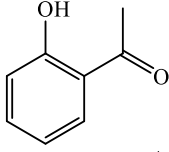
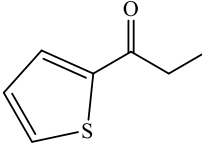
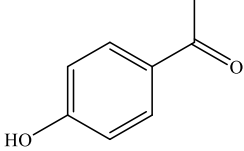
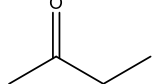
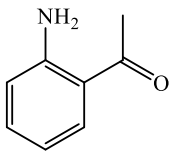
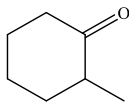
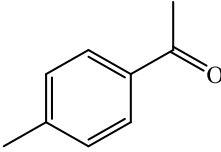
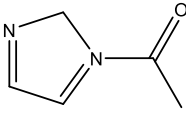
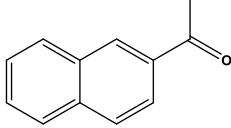
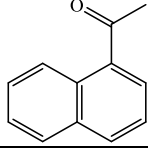
### 5.2.3.3. Investigation of the ketone substrate scope in the transfer hydrogenation reactions

To investigate the effects of substrate variation, a number of ketones were reacted using the best-performing pre-catalyst, **Ru15**, and the results are presented in **Table 5.5**. Acetophenone derivatives bearing electron-donating and electron-withdrawing substituents were reacted to give corresponding products under similar reaction conditions. Acetophenone derivatives bearing electron-withdrawing groups showed higher percentage conversions compared to unsubstituted acetophenone. For example, 2-chloroacetophenone demonstrated a percentage yield of 91% higher than acetophenone (**Table 5.5, entries 1 vs 2**). This observation could be attributed to the electronic effect, which reduced electron density on the carbonyl centre of the substrate and ultimately promoted higher reactivity. This trend is in good agreement with previous work reported by Aydemir and co-workers, where similar dinuclear half-sandwich Ru(II) supported on N^N ligands gave a higher conversion of 92 % for 2-chloroacetophenone compared to acetophenone (89%).<sup>45</sup>

The position of the electron-withdrawing substituent on the phenyl group of acetophenone also appeared to affect the reactivity of the substrates significantly. The electron-withdrawing group present at the *para*-position of acetophenone showed higher catalytic activity compared to those at the *ortho*-position. For example, 4-chloroacetophenone gave a percentage yield of 99 % compared to its analogue 2-chloroacetophenone (91%) and it is line with the previous findings by Wang *et al.*<sup>47</sup> In contrast, the electron-donating substituent on the acetophenone played a significant role in regulating the catalytic activity of the complex, **Ru15**. For instance, 4-methyl and 2- amino substituents on the acetophenone derivatives showed lower reactivities of 61 % and 56 %, respectively, compared to acetophenone under similar reactions (**Table 5.5, entries 1 vs 6 and 7**). The *para*-substituted electron-donating group on the phenyl group turned to give lower catalytic activity compared to *ortho*- and electron-donating groups as reported by Chai *et al.*<sup>20</sup> For example, 4-hydroxy acetophenone showed lower catalytic activity of 68 % compared to 2-hydroxy acetophenone (65 %) under similar reaction conditions (**Table 5.5, entries 4 and 5**). This trend could be interpreted in terms of the electronic effect of the substituents on the reactivity of the substrate. In addition, bulkier substrates such as 1-acetylnaphthone and 2-acetylnaphone (**Table 5.5, entries 8 and 9**) were also compatible with the TH reaction conditions and exhibited reactivities of 67% and 71%, respectively, compared to acetophenone. Furthermore, the complex, **Ru15**, displayed moderate to good catalytic activity for TH of heteroaromatic ketones including 2-acetylpyridine, 1-(thiophen-2-yl)ethan-1-one, 1-(thiophen-2-yl)propan-1-one and 1-(pyrazin-2-yl)ethan-1-one (**Table 5.5, entries 10-13**). The lower reactivity of the heteroaromatic ketones compared to acetophenone could be alluded to the possible irreversible binding of the heteroaromatic S- and N-atoms to the active site of the catalysts and thereby reducing the catalytic activity of the catalyst.<sup>20, 46</sup> Aliphatic ketones were also transformed into corresponding alcohols under similar reaction conditions.

For example, 2-propanone and 1-methylcyclopentanone reacted under similar reaction conditions and gave 79% and 56% reactivity, respectively (**Table 5.5, entries 14 and 15**).

**Table 5.5.** Substrate scope investigation using the dinuclear complex **Ru15**.<sup>a</sup>

Entry	Substrate	<sup>b</sup> Yield %	Entry	Substrate	<sup>b</sup> Yield %
1		68	10		65
2		99	11		49
3		91	12		52
4		68	13		47
5		65	14		79
6		56	15		56
7		61	16		76
8		67			
9		71			

<sup>a</sup>Reaction conditions: Substrate (1.0 mmol), **Ru15** as catalyst (20 ppm), base (0.4 mol%), refluxed in <sup>i</sup>PrOH (2.5 mL) at 82 °C for 6 h. <sup>b</sup>Determined by <sup>1</sup>H NMR spectroscopy. Anisole was used as an internal standard. All experiments were repeated in triplicate to ensure reproducibility and averaged (SD ±1.0).

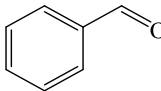
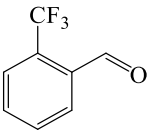
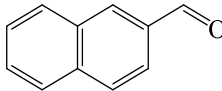
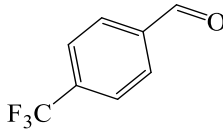
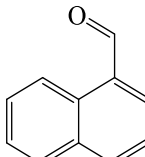
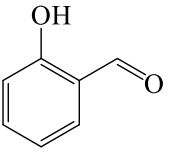
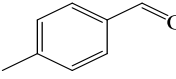
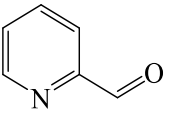
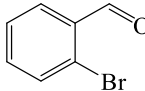
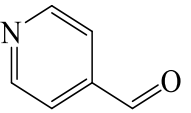
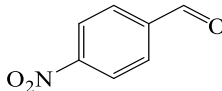
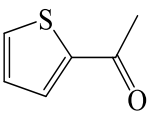
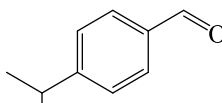
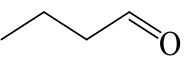
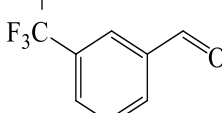
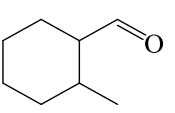
#### 5.2.3.4. Transfer hydrogenation of aldehydes using complex **Ru15**

Impressed by the performance of the dinuclear complex **Ru15** in the TH of ketones, we then explored the TH of a number of aldehydes (**Table 5.6**), which were reacted under an ideal reaction condition of 2.5 mmol of aldehyde, 0.0025 mol% (25 ppm) of catalyst loading, and 1.0 mol % of K<sup>t</sup>BuO. Benzaldehyde and its derivatives were effectively transformed into their corresponding primary alcohols without side products. In general, the use of benzaldehyde as a model substrate, excellent percentage yields of 89% in 3 h were obtained. Benzaldehyde derivatives bearing electron-donating substituents on the phenyl group showed lower reactivity compared to unsubstituted benzaldehyde, which gave a percentage conversion of 89% under similar reaction conditions. For instance, 4-isopropylbenzaldehyde showed lower reactivity of 78% compared to benzaldehyde (**Table 5.6, entry 1 vs 7**). Benzaldehyde derivatives bearing electron-withdrawing substituents were also explored, and a higher percentage conversion was afforded compared to benzaldehyde under similar reaction conditions. For instance, 4-trifluoromethyl benzaldehyde, 3-trifluoromethyl benzaldehyde and 4-bromobenzaldehyde (**Table 5.6, entries 5,8 -10**) were reacted, and exceptionally higher percentage conversions between 97% and 99% were obtained. The trends in the reactivity of the aldehyde derivatives bearing electron-donating and withdrawing substituents could be attributed to electronic effects as previously established by Segizbayev *et al.*<sup>48</sup> However, the heteroaromatic aldehydes showed slightly lower reactivity in comparison with benzaldehyde. For instance, 2-pyridine carboxaldehyde could only attain a percentage conversion of 68% lower than benzaldehyde under similar conditions, consistent with the earlier observation (**Table 5.5, entries 1 vs 12**).

In addition, **Ru15** effectively transformed aliphatic aldehydes to their corresponding alcohols. Higher catalytic activities were recorded for the aliphatic aldehydes compared to benzaldehydes. For example, pentanal was reacted to give the desired product and furnished

the conversion of 99% under similar conditions. A similar finding has been reported by Abdelaziz and co-workers, where higher yields were achieved for aliphatic aldehydes compared to aromatic aldehydes.<sup>49</sup> Nevertheless, the new Ru(II) system performed considerably better in catalysing aldehydes compared to the ketone substrates. For instance, benzaldehyde demonstrated a percentage conversion of 89%, corresponding to the initial TON of 89000. This is much higher than the 97% (TON of 48500) achieved by acetophenone.

**Table 5.6.** Result of transfer hydrogenation of aldehydes catalysed by complex **Ru15**.<sup>a</sup>

Entry	Substrate	Yield% (TON)	Entry	Substrate	Yield% (TON)
1		89 (89000)	9		91 (91000)
2		99 (99000)	10		96 (96000)
3		99 (99000)	11		63 (63000)
4		65 (65000)	12		68 (68000)
5		99 (99000)	13		72 (72000)
6		67 (67000)	14		86 (86000)
7		78 (78000)	15		99 (99000)
8		98 (98000)	16		91 (91000)

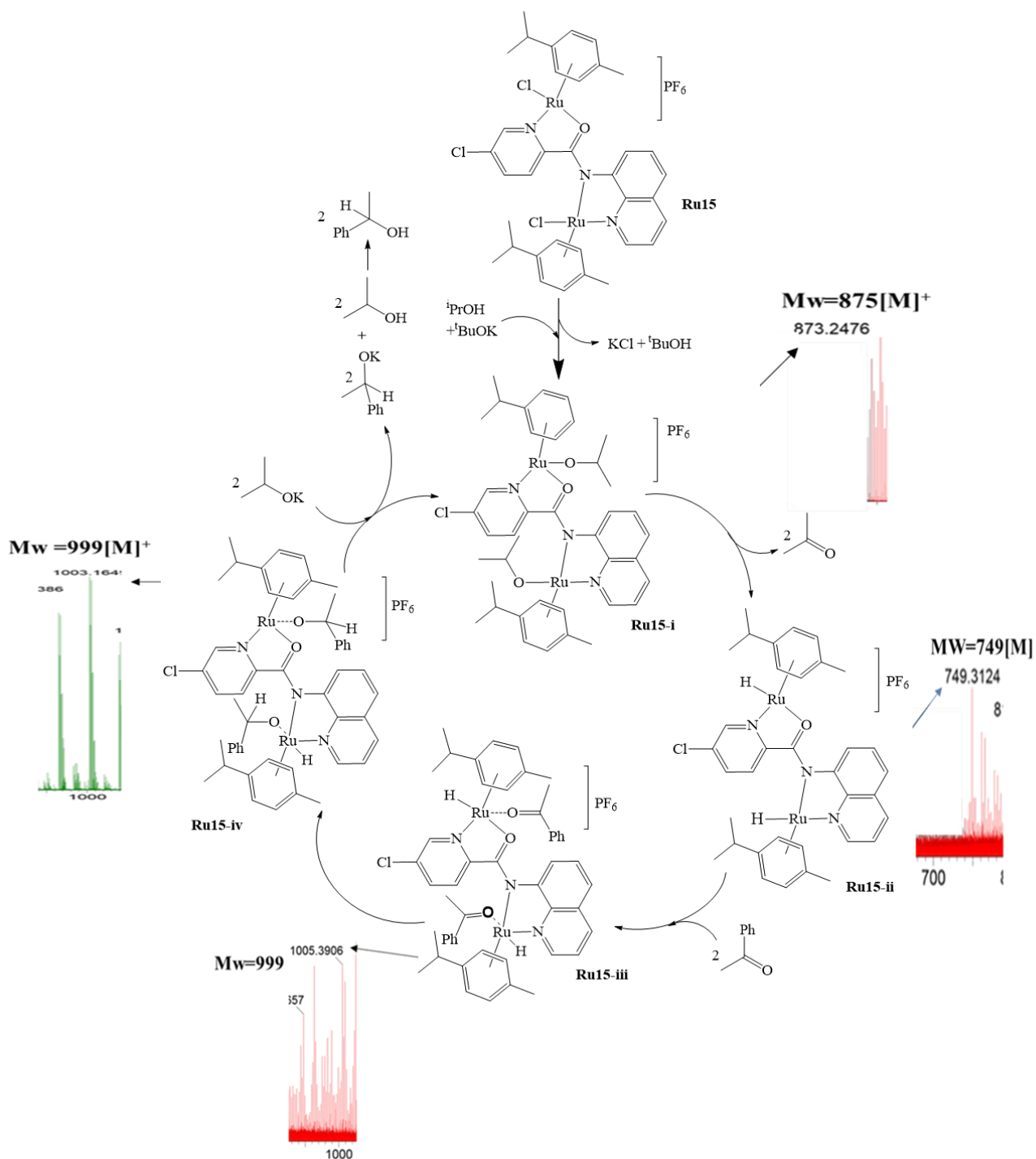
<sup>a</sup>Reaction conditions: Substrate (2.50 mmol), **Ru15** as catalyst, 0.0025 mol%, base (0.4 mol%), refluxed in <sup>i</sup>PrOH (2.5 mL) at 82 °C for 3 h, <sup>b</sup>Determined by <sup>1</sup>H NMR spectroscopy (Methoxybenzene was used as an internal standard). Experiments were repeated in triplicate to ensure reproductivity and averaged (SD ±1.0).

#### 5.2.3.5. Proposed mechanism of the transfer hydrogenation of ketones catalysed by complex **Ru15**.

A classical monohydride catalytic cycle is proposed for the transfer hydrogenation of ketones using **Ru15** as the model catalyst and supported with low-resolution mass spectrometry data



<sup>50</sup>(**Scheme 5.2**). It is reasonable to propose that the mechanism involves the two active Ru(II) sites. This mechanistic study was accomplished by subjecting the aliquots of the reaction mixture to the ESI-MS analyses. From the data, we can assume that the first step of the mechanism involves the displacement of chlorido co-ligands to allow the coordination of isopropoxide to the Ru(II) centres, as detected from the signal at  $m/z = 875$ . This step is followed by  $\beta$ -hydride elimination from the isopropoxide leading to the formation of Ru-H intermediates as the active species (**Scheme 5.2**). The generation of Ru-H as the active species could be established from the signal at  $m/z = 749$  corresponding to  $[(M^+ - 2Cl^-) + 2H^+]$  (**Scheme 5.2**). The reversible slippage of the Ru-C<sub>p-cymene</sub> ring from  $\eta^6$  to  $\eta^4$  generates a vacant site for acetophenone to bind, as demonstrated by Canivet *et al.*<sup>51</sup> Insertion of acetophenone into the metal to form the adduct **Ru15-iii**, and subsequent migration of the hydride to the acetophenone, resulting in the intermediate **Ru15-iv** with the functionalised alkoxide (evident from the signal at  $m/z = 1003$ ), as shown in **Scheme 5.2**. The substitution of the product with isopropoxide leads to the termination and the commencement of new catalytic cycles. The further reaction of the alkoxide with the isopropoxide leads to the formation of the desired product, 1-phenylethanol.



**Scheme 5.2.** Monohydride mechanism proposed for TH of acetophenone catalysed by **Ru15**.

### 5.3. Conclusions

In summary, the dinuclear Ru(II) complexes have been synthesised and characterised. The complexes were explored as catalysts for the transfer hydrogenation of ketones and aldehydes.

The catalytic activity of the complexes was influenced by the identity of the ligand backbone of the catalysts. The half sandwich dinuclear Ru(II) complexes supported on quinoline-carboxamide backbones outperformed the analogue complex anchored on pyrazine-carboxylate ligands in the TH reactions. As a result, the catalysts demonstrated a large substrate scope ranging from aldehydes to ketones with good quantitative yields using relatively low catalyst loadings. The monohydride pathway was proposed for the TH of ketone catalysed by the dinuclear Ru(II) complexes and was supported with *in situ* LR ESI-MS analysis of crude mixture.

The next chapter reports the preparation and structural studies of dinuclear Mn(II) complexes supported on dipicolinamide ligands. The dinuclear Mn(II) complexes were explored as catalysts in transfer hydrogenation of ketones. The effects of the catalyst structures and reaction conditions were investigated.

#### 5.4. References

1. Duca, G., *Homogeneous catalysis with metal complexes: fundamentals and applications*. Springer Science & Business Media: 2012; Vol. 102.
2. Dyker, G., *Angew. Chem. Int. Ed.* **2000**, *39*, 4237-4239.
3. Herrmann, W. A.; Cornils, B., *Angew. Chem.Int. Ed.* **1997**, *36*, 1048-1067.
4. Cornils, B.; Herrmann, W. A., *J. Catal.* **2003**, *216*, 23-31.
5. Di Giovanni, C.; Vaquer, L.; Sala, X.; Benet-Buchholz, J.; Llobet, A., *Inorg. Chem.* **2013**, *52*, 4335-4345.
6. Cherepakhin, V.; Williams, T. J., *ACS Catal.* **2019**, *10*, 56-65.
7. Ogba, O.; Warner, N.; O'leary, D.; Grubbs, R., *Chem. Soc. Rev.* **2018**, *47*, 4510-4544.

8. Morvan, J.; Mauduit, M.; Bertrand, G.; Jazzar, R., Cyclic (alkyl)(amino) carbenes (CAACs) in ruthenium olefin metathesis. *ACS Catalysis* **2021**, *11*, 1714-1748.
9. Kuramochi, A.; Komine, N.; Kiyota, S.; Hirano, M., *Bull. Chem. Soc. Jpn* **2021**, *94*, 2113-2132.
10. Van Leeuwen, P. W., *Homogeneous catalysis: understanding the art*. Springer Science & Business Media: 2006.
11. Belete B, B., Advances in Organometallic Chemistry, Volume 71. *Comments on Inorganic Chemistry* **2020**, *40* (6), 304-306.
12. Van Leeuwen, P. W., *Supramolecular catalysis*. John Wiley & Sons: 2008.
13. Maraval, V.; Laurent, R.; Caminade, A.-M.; Majoral, J.-P., *Organometallics* **2000**, *19*, 4025-4029.
14. Matsuzawa, A.; Harvey, J. N.; Himo, F., *Top. Catal.* **2021**, 1-9.
15. Mankad, N. P., Catalysis with multinuclear complexes. In *Non-Noble Metal Catalysis: Molecular Approaches and Reactions*, Wiley-VCH: 2019; pp 49-68.
16. Xiao, W.; Li, S.; Zhao, Y.; Ma, Y.; Li, N.; Zhang, J.; Chen, X., *Dalton Trans.* **2021**, *50*, 8690-8695.
17. Nath, B. D.; Takaishi, K.; Ema, T., *Catal. Sci. Technol.* **2020**, *10*, 12-34.
18. Bolitho, E. M.; Worby, N. G.; Coverdale, J. P.; Wolny, J. A.; Schünemann, V.; Sadler, P. J., *Organometallics* **2021**, *40*, 3012-3023.
19. Rendón-Nava, D.; Vásquez-Pérez, J. M.; Sandoval-Chávez, C. I.; Alvarez-Hernández, A.; Mendoza-Espinosa, D., *Organometallics* **2020**, *39*, 3961-3971.
20. Chai, H.; Wang, Q.; Liu, T.; Yu, Z., *Dalton Trans.* **2016**, *45*, 17843-17849.
21. Kumar, P.; Gupta, R. K.; Pandey, D. S., *Chem. Soc. Rev.* **2014**, *43*, 707-733.
22. Botubol-Ares, J. M.; Córdón-Ouahhabi, S.; Moutaoukil, Z.; Collado, I. G.; Jiménez-Tenorio, M.; Puerta, M. C.; Valerga, P., *Organometallics* **2021**, *40*, 792-803.

23. Jia, W.-G.; Zhi, X.-T.; Li, X.-D.; Zhou, J.-P.; Zhong, R.; Yu, H.; Lee, R., *Inorg. Chem.* **2021**, *60*, 4313-4321.
24. Yadav, S.; Vijayan, P.; Gupta, R., *J. Organomet. Chem.* **2021**, *954*, 122081.
25. Pachisia, S.; Kishan, R.; Yadav, S.; Gupta, R., *Inorg. Chem.* **2021**, *60*, 2009-2022.
26. Vijayan, P.; Yadav, S.; Yadav, S.; Gupta, R., *Inorg. Chim. Acta* **2020**, *502*, 119285.
27. Ramachandran, R.; Viswanathamurthi, P., *Spectrochim. Acta A: Mol. Biomol. Spectrosc.* **2013**, *103*, 53-61.
28. Ngo, A. H.; Do, L. H., *Inorg. Chem. Front.* **2020**, *7* (3), 583-591.
29. Poljarević, J. M.; Gál, G. T.; May, N. V.; Spengler, G.; Dömötör, O.; Savić, A. R.; Grgurić-Šipka, S.; Enyedy, É. A., *J. Inorg. Biochem.* **2018**, *181*, 74-85.
30. Almodares, Z.; Lucas, S. J.; Crossley, B. D.; Basri, A. M.; Pask, C. M.; Hebden, A. J.; Phillips, R. M.; McGowan, P. C., *Inorg. Chem.* **2014**, *53*, 727-736.
31. Bhattacharjee, J.; Bockfeld, D.; Tamm, M., *J. Org. Chem.* **2022**, *87*, 1098-1109.
32. Zhao, J.; Li, S.; Wang, X.; Xu, G.; Gou, S., *Inorg. Chem.* **2019**, *58*, 2208-2217.
33. Kasim, M. S. M.; Sundar, S.; Rengan, R., *Inorg. Chem. Front.* **2018**, *5*, 585-596.
34. Mashima, K.; Nakamura, T.; Matsuo, Y.; Tani, K., *J. Organomet. Chem.* **2000**, *607*, 51-56.
35. Stringer, T.; Therrien, B.; Hendricks, D. T.; Guzgay, H.; Smith, G. S., *Inorg. Chem. Commun.* **2011**, *14*, 956-960.
36. Cheung, K.-C.; Wong, W.-L.; So, M.-H.; Zhou, Z.-Y.; Yan, S.-C.; Wong, K.-Y., *Chem. Commun.* **2013**, *49*, 710-712.
37. Sija, É.; Hartinger, C. G.; Keppler, B. K.; Kiss, T.; Enyedy, É. A., *Polyhedron* **2014**, *67*, 51-58.
38. Meghdadi, S.; Mereiter, K.; Shams Mohammadi, N.; Amiri, A., *Inorg. Chem. Res.* **2017**, *1*, 69-78.

39. Meghdadi, S.; Amirnasr, M.; Kiani, M.; Fadaei Tirani, F.; Bagheri, M.; Schenk, K. J., *J. Coord. Chem.* **2017**, *70*, 2409-2424.
40. Allen, F. H., *Acta Crystallogr. Sec. B: Struct. Sci.* **2002**, *58*, 380-388.
41. Allardyce, C. S.; Dyson, P. J.; Ellis, D. J.; Salter, P. A.; Scopelliti, R., *J. Organomet. Chem.* **2003**, *668*, 35-42.
42. Małecki, J., *Struct. Chem.* **2012**, *23*, 461-472.
43. Allen, F. H.; Davies, J. E.; Galloy, J. J.; Johnson, O.; Kennard, O.; Macrae, C. F.; Mitchell, E. M.; Mitchell, G. F.; Smith, J. M.; Watson, D. G., *J. Chem. Inf. Comput. Sci.* **1991**, *31*, 187-204.
44. Viji, M.; Tyagi, N.; Naithani, N.; Ramaiah, D., *New J. Chem.* **2017**, *41*, 12736-12745.
45. Aydemir, M.; Durap, F.; Baysal, A.; Meric, N.; Buldağ, A.; Gümgüm, B.; Özkar, S.; Yıldırım, L. T., *J. Mol. Catal. A: Chem.* **2010**, *326*, 75-81.
46. Liu, T.; Chai, H.; Wang, L.; Yu, Z., *Organometallics* **2017**, *36*, 2914-2921.
47. Wang, L.; Yang, Q.; Chen, H.; Li, R.-X., *Inorg. Chem. Commun.* **2011**, *14*, 1884-1888.
48. Segizbayev, M.; Öztöpcü, Ö.; Hayrapetyan, D.; Shakhman, D.; Lyssenko, K. A.; Khalimon, A. Y., *Dalton Trans.* **2020**, *49*, 11950-11957.
49. Ajjou, A. N.; Pinet, J.-L., *J. Mol. Catal.: Chem.* **2004**, *214*, 203-206.
50. Müller, C. A.; Markert, C.; Teichert, A. M.; Pfaltz, A., *Chem. Commun.* **2009**, 1607-1618.
51. Canivet, J.; Labat, G.; Stoeckli-Evans, H.; Süss-Fink, G., Water-soluble arene ruthenium complexes containing a trans-1, 2-diaminocyclohexane ligand as enantioselective transfer hydrogenation catalysts in aqueous solution. Wiley Online Library: 2005.

## CHAPTER 6

### DINUCLEAR MANGANESE(II) COMPLEXES OF DIPYRIDYL-CARBOXAMIDES: STRUCTURAL STUDIES AND TRANSFER HYDROGENATION OF KETONES

#### 6.1. Introduction

One of the fundamental research goals in green chemistry is to develop sustainable, efficient, and cost-effective chemical transformations for accessing fine chemical products.<sup>1-2</sup> Catalysis is considered one of the best approaches for achieving this goal.<sup>2-4</sup> More especially, catalysts made from earth-abundant transition metals are the most successful examples of practical catalysts and are continuously receiving considerable attention.<sup>4-5</sup> The use of ruthenium-, iridium-, rhodium-, and palladium-based catalysts have remained the most studied and predominated in the field of homogeneous catalysis despite their scarcity, high cost of establishment and toxicity.<sup>6-8</sup>

Manganese is the third most abundant element in earth's crust and has been known to exist in multiple oxidation states ranging from -3 to +7.<sup>3</sup> Manganese ions are capable of forming complexes with coordination numbers up to 7, making them a suitable candidate for catalysis.<sup>7</sup> Over the years, manganese catalysis has been confined only to water oxidation using hypervalent manganese complexes.<sup>9</sup> Recently, the focus has been directed towards the use of well-defined manganese complexes with lower valency for organic transformation, such as hydrogenation, dehydrogenation, alkylation of amines and amides, among others.<sup>9-10</sup> In recent years, well-defined Mn(I) complexes have emerged as important players in the sustainable catalytic transfer hydrogenation of ketones.<sup>11-13</sup> Mn(II)-based catalysts demonstrated high catalytic efficiency in the reduction of a number of carbonyl compounds, olefins, nitriles,

imines, and heterocycles, among others.<sup>6, 14-15</sup> Manganese(I) catalysed transfer hydrogenation reactions have emerged as a subject of intense research since 2016, after the pioneering work of Beller and co-workers.<sup>11</sup> Inspired by the work of Beller and co-workers, a number of Mn(I) complexes catalysed TH of ketones have been reported with promising catalytic activities.<sup>11</sup> For example, Kundu and his group have developed benzimidazole-amine Mn(I) tricarbonyl complexes which achieved conversions between 70-98% with 5.0 mol% in transfer hydrogenation of ketones and imines using isopropyl alcohol at relatively mild reaction conditions.<sup>16</sup> Thorough reviews of the literature show that most of the Mn(I) complexes used for TH of ketones contains N-H fragment which played significant roles in the determination of the catalytic activity of the Mn(I) complexes.<sup>15</sup> The application of Mn(II) analogues remained relatively unexplored in transfer hydrogenation of ketones although Mn(II) has favourable redox potentials compared to Mn(I). Mn(II) has been regarded as the most stable oxidation state. In addition, Mn(II) has excellent half-shell effects that breaks the trend of electronegativity and more electropositive compared to Mn(I) and Mn(IV).<sup>15</sup>

Multinuclear complexes in catalysis have witnessed rapidly increasing developments during the past decades. In recent years, considerable attention has been paid to the development of dinuclear complexes due to their high catalytic efficiency in catalysis.<sup>17</sup> For example, a number of bimetallic complexes supported on multifunctional ligands have been reported with exceptionally high catalytic activity and cooperativity in TH of ketones.<sup>18-20</sup> Notable among them are the diruthenium(II)-NNN complexes of 4,4'-(CH<sub>2</sub>)<sub>3</sub>- bipyridine ligands which demonstrated TOF values up to  $1.4 \times 10^7 \text{ h}^{-1}$  in TH of ketones.<sup>21</sup>

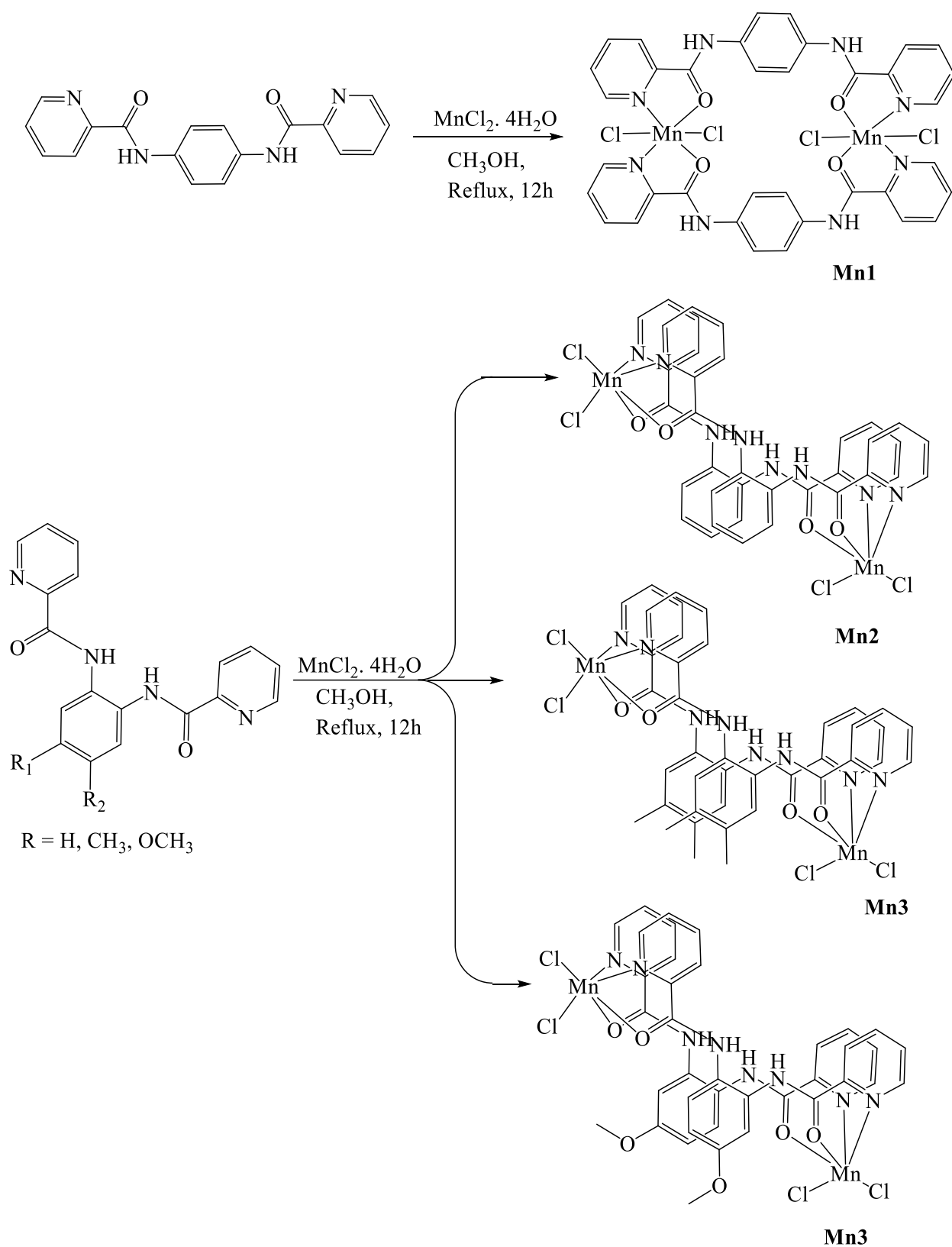


In the last two decades, carboxamide-based ligands have proven effective and considered smart organic moieties for designing transition metal catalysts for effective catalysis, including transfer hydrogenation of ketones, transamination of amides, and *N*-alkylation of amines.<sup>22-23</sup> Carboxamide-based ligands are relatively easy to synthesise and modifies to include other functional groups.<sup>24</sup> Carboxamide-based ligands are capable of fine-tuning the electronic and steric parameters and, undoubtedly, form strong metal-ligand bonds with a number of transition metals.<sup>24</sup> In addition, metal-complexes of carboxamides are typically robust and less prone to changes in oxidation states in solution.<sup>25</sup> In this Chapter, we present the synthesis and structural studies of bimetallic Mn(II) complexes supported on multifunctional dicarboxamide ligands and their applications in the transfer hydrogenation of ketones.

## 6.2. Results and discussion

### 6.2.1. Synthesis and characterisation of carboxamide Mn(II) complexes

Treatment of the carboxamide ligands, *N,N'*-(1,4-phenylene)dipicolinamide (**H<sub>2</sub>L3**), *N,N'*-(1,2-phenylene)dipicolinamide (**H<sub>2</sub>L4**), *N,N'*-(4,5-dimethyl-1,2-phenylene)dipicolinamide (**H<sub>2</sub>L5**) and *N,N'*-(4-methoxy-1,2-phenylene)dipicolinamide (**H<sub>2</sub>L6**) with MnCl<sub>2</sub> · 4H<sub>2</sub>O salt in a (1:1) molar ratio in methanol at 50 °C afforded the corresponding light-yellow Mn(II) complexes, **Mn1-Mn4** with the general formula [Mn<sub>2</sub>(**H<sub>2</sub>Ln**)<sub>2</sub>Cl<sub>4</sub>] (**Scheme 6.1**) and isolated in good to excellent yields (81% – 90%).



**Scheme 6.1.** Synthesis of bimetallic manganese(II) carboxamide complexes **Mn1-Mn4**.

The manganese complexes **Mn1-Mn4** were characterised by FT-IR spectroscopy, mass spectrometry, elemental analyses, magnetic moment measurement and single-crystal X-ray crystallography analysis (**Mn2**). The successful formation of the complexes was established by comparing FT-IR spectroscopic data of the complexes **Mn1-Mn4** to their corresponding free ligands **H<sub>2</sub>L3 - H<sub>2</sub>L6**. For instance, the FT-IR spectrum of complex **Mn2** showed the stretching signal of  $\nu(\text{C}=\text{O})$  at a higher frequency,  $1671\text{ cm}^{-1}$  with respect to the free ligand **H<sub>2</sub>L3** ( $1661\text{ cm}^{-1}$ ) upon complexation (**Table 6.1**). This observation was observed in the other complexes **Mn2-Mn4** as depicted in **Table 6.1**. The shift in the signals of the carbonyl to higher frequencies indicated the involvement of the carbonyl O-atom in the coordination.<sup>26-27</sup> In contrast, a slight shift occurs in the absorption band of  $\nu(\text{N-H})$  in FT-IR spectra of complexes **Mn1-Mn4** ( $3324 - 3331\text{ cm}^{-1}$ ) compared to the free ligands, **H<sub>2</sub>L3-H<sub>2</sub>L6** ( $3318\text{ cm}^{-1} - 3327\text{ cm}^{-1}$ ) (**Table 6.1**). This showed that the amide N-atoms were not involved in the coordination and in tandem with the similar report by Sutradhar *et al.*, where the N-H shifted slightly from  $3380\text{ cm}^{-1}$  (hydrazone-carboxamide ligand) to a higher frequency of  $3383\text{ cm}^{-1}$  in the complex upon coordination.<sup>28</sup> The slight shift in the signal of  $\nu(\text{NH})_{\text{amide}}$  could be assigned to resonance enhancement in the coordinated ligands leading to the strengthening of the N-H bonds.<sup>29</sup>

**Table 6.1.** Selected FT-IR spectroscopic data of the complexes **Mn1-Mn4** and corresponding ligands **H<sub>2</sub>L3-H<sub>2</sub>L6**.

Entry	Complex	$\nu(\text{C}=\text{O})^{\text{a}}/\text{cm}^{-1}$	$\nu(\text{N-H})^{\text{a}}/\text{cm}^{-1}$
1	<b>Mn1</b>	1669(1660)	3330(3321)
2	<b>Mn2</b>	1671(1661)	3324(3318)
3	<b>Mn3</b>	1675(1663)	3328(3327)
4	<b>Mn4</b>	1673(1663)	3331(3325)

<sup>a</sup>FT-IR spectroscopic data of the ligands are in brackets

In addition, ESI-MS spectrometry was employed to establish the molecular composition of the dinuclear complexes **Mn1–Mn2**. In general, ESI-MS (low resolution) data of complexes **Mn1–Mn4** showed  $m/z$  signals corresponding to with a neutral unit containing two ligands and Mn(II) centres as proposed in **Scheme 1**. For instance, the positive mode mass spectrum of complex **Mn1** showed a signal at  $m/z = 852$  amu, corresponding to the fragment ( $M^+ - Cl$ ) of the dinuclear species (**Figure 6.1**), respectively. In contrast, complex **Mn4** gave a signal at  $m/z = 804$  which corresponds to  $[M^+ - 3Cl, 100\%]$ . This is largely due to the instability of the cationic species,  $[M-Cl]$ , hence ease of fragmentation to give more stable cationic species,  $[M^+ - 3Cl]$ . Experimental and simulated isotopic mass distributions were correlated in all cases.

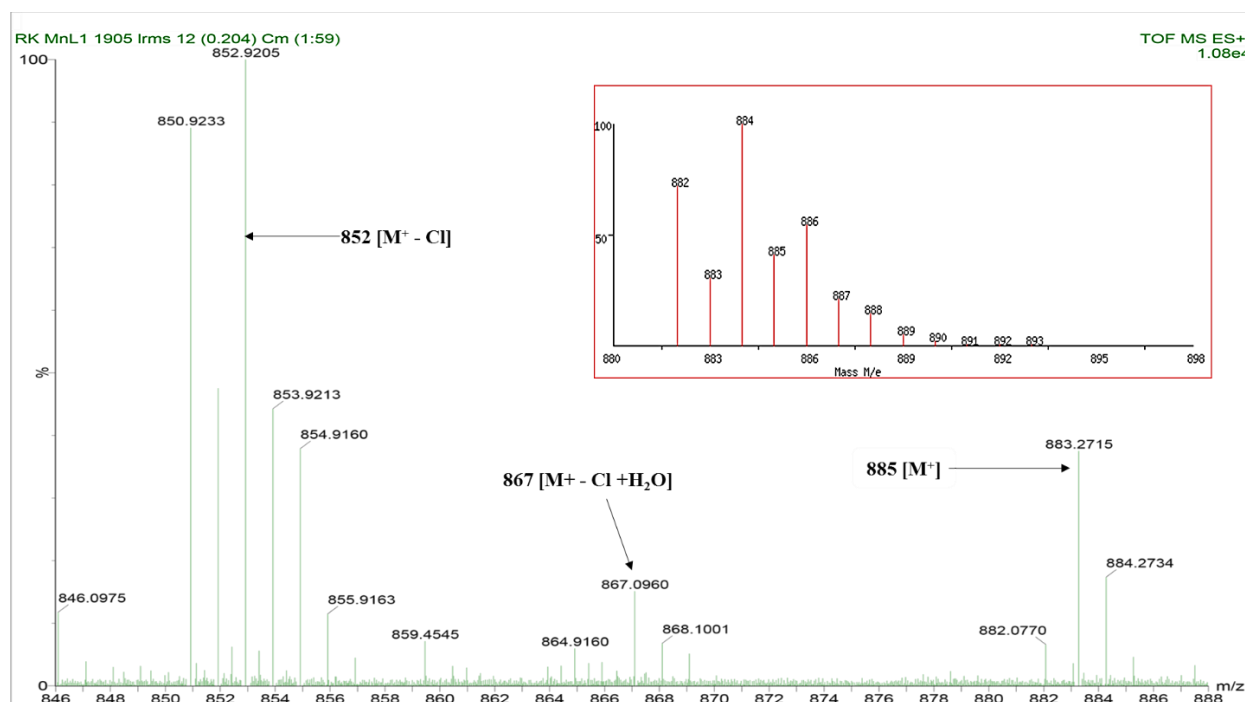


**Figure 6.1.** ESI-MS spectrum of complex **Mn1** showing the  $m/z = 852$   $[M^+ - Cl, 100]$  and 885  $[M^+, 40\%]$ . The simulated theoretical isotopic mass distribution pattern (inset).

Magnetic moment measurement was also performed to determine the magnetic property of complexes **Mn1–Mn4**. The  $\mu_{\text{eff}}$  values of the complexes were found in the range of 5.93 BM to 5.98 BM at room temperature and comparable to the anticipated spin-only magnetic moment of the Mn(II) ion (5.91 BM), which is indicative of the presence of the Mn(II) centres in a high-spin configuration.<sup>30-31</sup> Furthermore, all of the values were comparable and indicated similarity in the ligand-field splitting of ligands **H<sub>2</sub>L1–H<sub>2</sub>L4**. Furthermore, elemental analysis data of complexes **Mn1–Mn4** confirmed the purity and empirical formulae of the complexes and were in line with two ligand units per two manganese(II) atoms, as shown in **Scheme 6.1**.

#### 6.2.2. Molecular structure of the dinuclear Mn2 complex

The coordination geometry and structural configuration of the dinuclear complex **Mn2** were further confirmed by single-crystal X-ray crystallographic analysis. A single crystal suitable for X-ray crystallography was obtained by slow diffusion of diethyl ether into a solution of **Mn2** in methanol at room temperature. The compound crystallises in a triclinic system with space group **P-1**. **Table 6.2** presents the crystal data and structural refinement data, while the solid-state structure is depicted in **Figure 6.2**. The solid-state structure of the complex **Mn2** (a monomeric form of **Mn2**) showed a centrosymmetric fashion with the two Mn(II) ions residing in a distorted octahedral environment surrounded by two tetradentate ligands and chlorido co-ligands, respectively. Each Mn(II) ion coordinates to the ligands through the pyridine nitrogen ( $N_{\text{pyridine}}$ ) and carbonyl oxygen-atom ( $O_{\text{amide}}$ ) to form a 6-membered chelating ring with the remaining coordination sites occupied by the chlorido co-ligands. Mn(II) ions are hard acid, preferring to coordinate to the hard-base carbonyl O-atom of the amide group, thereby leaving the amide N-atom uncoordinated. The average bond distances,  $\text{Mn}-N_{\text{pyridine}} = 2.265(4) \text{ \AA}$ , and  $\text{Mn}-O_{\text{amide}} = 2.265(3) \text{ \AA}$ , are slightly longer than the average bond distances of 11 similar distorted octahedral Mn(II) compounds deposited in the CCDC file ( $\text{Mn}-O_{\text{amide}} = 2.210(60) \text{ \AA}$ )

and  $\text{Mn-N}_{\text{pyridine}} = 2.302(24)\text{\AA}$ .<sup>32-33</sup> The average bond distance of  $\text{Mn-Cl} = 2.403(11)\text{\AA}$  is slightly shorter than the uncoordinated  $\text{MnCl}_2 \cdot 4\text{H}_2\text{O}$  ( $\text{Mn-Cl} = 2.549\text{\AA}$ ), and it is comparable to the average bond distance of 19 similar Mn(II) complexes ( $\text{Mn-Cl} = 2.475(34)\text{\AA}$ ) deposited in CCDC file.<sup>32-34</sup> This observation could be assigned to the chelating effects imposed by the ligand.<sup>34</sup> The average bite angles,  $\text{N}_{\text{pyridine}}\text{-Mn-O}_{\text{amide}}$ ,  $73.08(12)^\circ$ ,  $\text{O}_{\text{amide}}\text{-Mn-O}_{\text{amide}} = 80.99(10)^\circ$ , and  $\text{N}_{\text{pyridine}}\text{-Mn-Cl}$ ,  $98.23(11)^\circ$  exhibit deviation from the ideal  $90^\circ$  of a regular octahedral angle suggesting a distorted octahedral geometry around the Mn(II) ions.

**Table 6.2.** Crystal and structural refinement data for complex **Mn2**.

Parameters	Mn2
Empirical formula	C <sub>18</sub> H <sub>14</sub> N <sub>4</sub> O <sub>2</sub> MnCl <sub>2</sub>
Formula weight	444.17
Temperature	100(2) K
Wavenumber	1.541 Å
Crystal system	Triclinic
Space group	P-1
a(Å)	8.0825(2)
b(Å)	11.4807(3)
c(Å)	11.7194(3)
α(°)	68.0886(10)
β(°)	88.641(10)
γ(°)	88.642(10)
Volume	1014.05(5)
Z	2
D <sub>calcd</sub> (mg.m <sup>-3</sup> )	1.455 Mg/m <sup>3</sup>
Absorption coefficient	7.891
F(000)	450
Crystal size/mm <sup>3</sup>	0.320x0.130x0.115
Max. and min. transmission	0.7536 and 0.5042
Completeness to theta	97.9%
Refinement method	Full matrix least-squares on $F^2$
Goodness of fit on $F^2$	1.003
Final R indices [I>2sigma(I)]	R <sub>1</sub> 0.00218, wR <sub>2</sub> = 0.0566,
Largest diff. peak and hole	0.233 and -0.218 eÅ <sup>-3</sup>

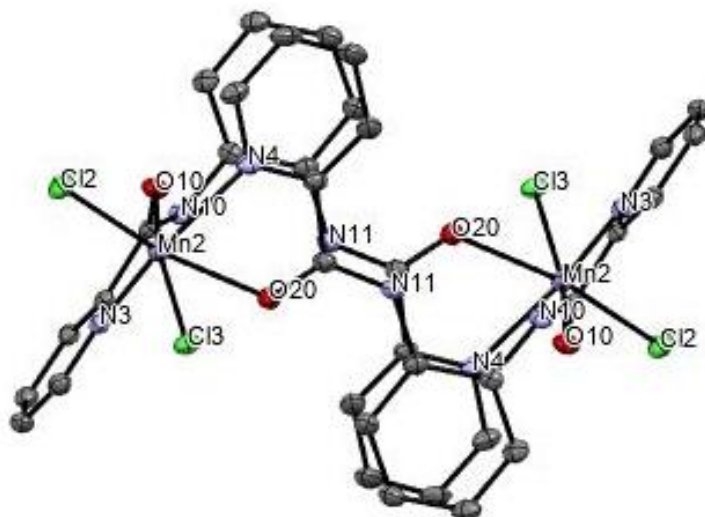


**Figure 6.2.** ORTEP plot of symmetric unit of complex **Mn2** (atomic displacement ellipsoid at 50% probability). All hydrogen atoms are omitted for clarity. Bond lengths (Å): Mn(1)-N(2), 2.266(4), Mn(2)-Cl(2), 2.4023(11), Mn(2)-O(10), 2.262(4). Bond angles (°): O(10)-Mn(2)-N(3), 73.04(12), O(10)-Mn(2)-O(20), 81.56(10), N(3)-Mn(2)-N(4), 143.92(13), N(4)-Mn(2)-Cl(2), 98.10(10).

### 6.2.3. Transfer hydrogenation of ketones

To investigate the catalytic efficiency of the new dinuclear Mn(II) complexes **Mn1-Mn4** in the transfer hydrogenation of ketones, a preliminary screening was carried out using acetophenone (1.00 mmol) as the model substrate, potassium *tert* butoxide ( $K^tBuO$ ) (8.0 mol%) as the co-catalyst, anisole (1.00 mmol) as the internal standard and isopropyl alcohol. The percentage conversion was determined by analysing an aliquot of the reaction mixture using  $^1H$  NMR spectroscopic technique. With **Mn2** (0.015 mol%) as the representative catalyst, a percentage conversion of 61% corresponding to a TOF of  $508\ h^{-1}$  was realised after 8 h of reaction (**Table 6.3**). Having been inspired by this catalytic activity, we proceeded with the optimisation of the reaction conditions for effective TH of ketones. To optimise the reaction condition, the TH of acetophenone was studied under different catalyst loadings ranging from 0.050 mol% to 0.100



mol%, and the results are summarised in **Table 6.3**. From **Table 6.3**, catalyst loadings have significant effects on the catalytic activity of the pre-catalyst. For instance, increasing the catalyst loading from 0.015 mol% to 0.025 mol% increase the percentage conversion from 61 % to 77%, although the TOF decreased from 508 h<sup>-1</sup> to 385 h<sup>-1</sup> (**Table 6.3, entries 4 and 5**). Further increase in the catalyst loading to 0.050 mol% led to improvement in the percentage conversion (85% corresponding to a lower TOF of 213 h<sup>-1</sup>). In addition, when higher catalyst loading of 1.00 mol% was employed, a percentage conversion of 99% was achieved with a decline in TOF (12.5 h<sup>-1</sup>) (**Table 6.3, entry 8**). This observation is in good agreement with the previous findings reported by Leitner and co-workers, where varying catalyst loading from 1.00 mol% to 5.0 mol% resulted in increased catalytic activity from 30 % to 90%, with a decline in TOF from 1.25 h<sup>-1</sup> to 0.83 h<sup>-1</sup>.<sup>35</sup> The decrease in TOF as a result of increasing catalyst loading could be assigned to aggregation of catalyst which eventually led to deactivation.<sup>36</sup> Also, the catalysts free reaction proceeded with poor percentage conversion of 5% in 8 h, thus necessitating the application of the pre-catalyst (**Table 6.3, entry 1**). As a result, catalyst loading of 0.015 mol% (15 ppm) is considered ideal the optimum catalyst loading for effective TH of ketone (**Table 6.3, entry 4**). Next, the effect of the base on the catalytic activity was investigated. While K<sup>t</sup>BuO was more effective (61%), potassium hydroxide (KOH) resulted in moderate conversion of (48%) under similar reaction conditions (**Table 6.3, entry 4 vs 9**).

**Table 6.3.** The results of reaction conditions optimisation for TH of ketones using **Mn2**<sup>a</sup>

Entry	Catalyst loading/mol%	Base	Percentage Conversion[%]	TON	TOF/h <sup>-1</sup>
1	-	K <sup>t</sup> BuO	5	-	-
2	0.100	-	18	184	23
3	0.010	K <sup>t</sup> BuO	36	3600	450
4	0.015	K <sup>t</sup> BuO	61	4064	508
5	0.025	K <sup>t</sup> BuO	77	3080	385
6	0.050	K <sup>t</sup> BuO	85	1704	213
7	0.10	K <sup>t</sup> BuO	98	992	124
8	1.00	K <sup>t</sup> BuO	99	96	12
9	0.015	KOH	48	3200	400

<sup>a</sup>Condition: Acetophenone (1.00 mmol, 0.100 mL), methoxybenzene (1.00 mmol, 0.11 mL), K<sup>t</sup>BuO (8.0 mol%) in 2.5 mL of isopropyl alcohol, time, 8 h, temperature, 82 °C, <sup>b</sup>Determined by using <sup>1</sup>H NMR spectroscopy technique using anisole as internal standard. <sup>c</sup>TOF (Turnover Frequency) = mmol of acetophenone consumed/mmol of catalyst used/time/h. All experiments were performed in triplicate to ensure reproducibility.

#### 6.2.4. Effect of catalyst structure on the transfer hydrogenation of acetophenone

Having optimised the reaction conditions, we proceeded to study the effects of catalyst structure on the performance of the complexes **Mn2-Mn4** in the transfer hydrogenation of acetophenone (**Table 6.4**). From the result, it was clear that the ligand architecture played a significant role in the determination of the catalytic efficiency of the complexes. For example, complex **Mn1**, supported on a carboxamide ligand, showed a higher TOF of 567 h<sup>-1</sup> compared to the precursor, MnCl<sub>2</sub>.4H<sub>2</sub>O, which attained TOF up to 0.88 h<sup>-1</sup> (**Table 6.4, entries 1 and 2**) under similar reaction conditions. The Mn(II)-Mn(II) interaction in a close proximity thus appears to affect the performance of the pre-catalyst. Dinuclear complexes with weak metal-metal interactions provide favourable conditions for enhancing catalytic activity and

cooperativity compared to those in closed proximity.<sup>18, 20-21, 37-38</sup> For example, **Mn1** supported on *N,N'*-(1,4-phenylene)dipicolinamide ligands (TOF of 567 h<sup>-1</sup>) showed higher catalytic activity compared to **Mn2** bearing *N,N'*-(1,2-phenylene)dipicolinamide (TOF = 508 h<sup>-1</sup>). This observation could be assigned to the effect of metal-metal interactions and cooperativity between the two Mn(II) centres.<sup>17, 39</sup>

In addition, the presence of electron-donating substituents appeared to influence the catalytic activity of the pre-catalysts. For example, the complex **Mn4**, bearing the methoxy substituent on its aryl linker, furnished a TOF of 658 h<sup>-1</sup>, compared to the complex **Mn2**, supported on the unsubstituted ligand which achieved TOF up to 508 h<sup>-1</sup> (**Table 6.4, entries 3 and 5**) under similar reaction conditions. In comparison to the previously reported Mn(I) catalysts, the complexes **Mn1–Mn2** showed higher catalytic efficiency, although lower catalyst loading was employed.<sup>40-46</sup> This could be attributed to good cooperativity between the Mn(II) centres. For instance, the pre-catalysts **Mn1–Mn4** gave conversion of 98% (corresponding to TOF of 658 h<sup>-1</sup>) in 8 h, while bipyridine -Mn(I) tricarbonyl complexes reported by Khusnutdinova's group gave conversion of 98% with catalyst loading of 5.0 mol% in 24 h.<sup>40</sup>

**Table 6.4.** Investigation of effects of catalyst structure in the transfer hydrogenation of acetophenone.<sup>a</sup>

Entry	Pre-catalyst	<sup>b</sup> Conversion[%] Time /h		TON	<sup>c</sup> TOF/h <sup>-1</sup> at 8 h
		4	8		
1	<b>MnCl<sub>2</sub>·4H<sub>2</sub>O (1 mol%)</b>	2	7	7.04	0.88
2	<b>Mn1</b>	48	72	4536	567
3	<b>Mn2</b>	37	61	4064	508
4	<b>Mn3</b>	44	69	4800	600
5	<b>Mn4</b>	41	79	5264	658

<sup>a</sup>Conditions: Acetophenone (1.00 mmol, 0.100 mL), methoxybenzene (1.00 mmol, 0.11 mL), K<sup>t</sup>BuO (8.0 mol%) in 2.5 mL of isopropyl alcohol, pre-catalyst( time, 8 h, temperature, 82 °C, <sup>b</sup>Determined by using <sup>1</sup>H NMR spectroscopy technique using anisole as internal standard. <sup>c</sup>TOF (Turnover Frequency) = mmol of acetophenone consumed/mmol of catalysts used/ time in hours. All experiments were carried out in triplicate to ensure reproducibility.

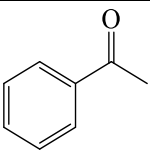
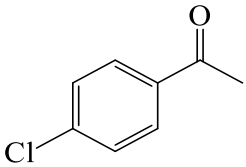
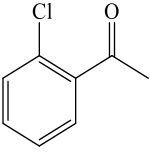
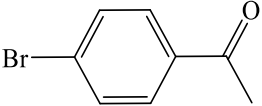
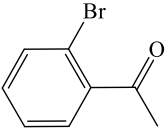
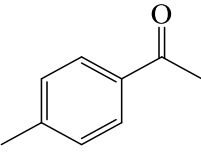
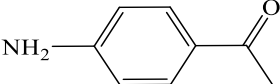
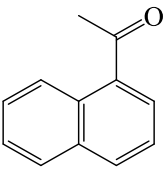
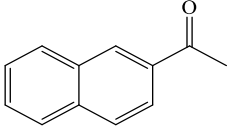
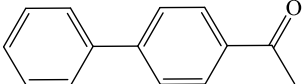
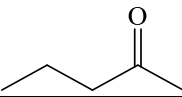
### 6.2.5. Substrate scope studies using complex Mn4

The applicability of the optimised reaction conditions has been extended to a few ketone substrates using **Mn4** (Table 6.5). For instance, acetophenone derivatives bearing an electron-withdrawing group, 4-chloroacetophenone was reacted to give higher conversions of 90% compared to acetophenone (79%) (Table 6.5, entries 1 vs 2). This could be assigned to the electronic effects of the substituent on the carbonyl carbon. In addition, the position of the electron-withdrawing substituents on the arene group has a pronounced effect on the catalytic activity. Substrates with the electron-withdrawing groups at the *para* position showed higher percentage conversions compared to those at the *ortho* position. For example, while 4-bromo acetophenone gave a percentage conversion of 86%, 2-bromo acetophenone gave only 80% (Table 6.5, entries 4 vs 5). A similar observation has been reported by Sortais and co-workers where the 2-chloroacetophenone showed a lower conversion of 56% compared to 4-acetophenone (96%) using *in-situ* generated Mn(I) carbonyl diamine complexes.<sup>47</sup> On the other hand, substrates bearing electron-donating groups were less reactive, and lower percentage conversions were recorded compared to acetophenone. For example, 4-methyl acetophenone witnessed lower reactivity affording conversion of 70% compared to acetophenone (Table 6.5, entries 1 vs 6).

Ketones bearing bulkier aromatic groups were also reacted, and good to excellent percentage conversions were obtained. For instance, 1-acetylnaphthalene was reacted to give a conversion of 81% comparable to acetophenone (Table 6.5, entry 1 vs 8). However, a much lower percentage conversion of 58% was obtained for 4-acetyl biphenyl ketone compared to acetophenone (79%) (Table 6.5, entries 1 vs 10). This could be attributed to electronic effects in which the electron density on the carbonyl carbon makes it less reactive compared to acetophenone. In contrast, Jayaprakash and co-workers reported a slightly higher percentage

conversion of 86% for 4-acetyl biphenyl ketones compared to acetophenone (84%) under similar reaction conditions using chiral Mn(I) carbonyl complexes as catalysts.<sup>45</sup> In addition, a moderate reactivity has been observed for aliphatic ketone substrate such as 2-pentanone (63%) compared to acetophenone under similar reaction conditions. The results show that the new complexes are capable of reducing both electron-rich and deficient ketone substrates, and are in good agreement with the early findings reported by Sun *et al.* using amino-benzimidazole Mn(I)(CO)<sub>3</sub> based complexes which demonstrated good catalytic activities in TH ketones bearing electron-rich and deficient substituents.<sup>46</sup>

**Table 6.5.** Results of substrate scope studies using complex **Mn4**<sup>a</sup>

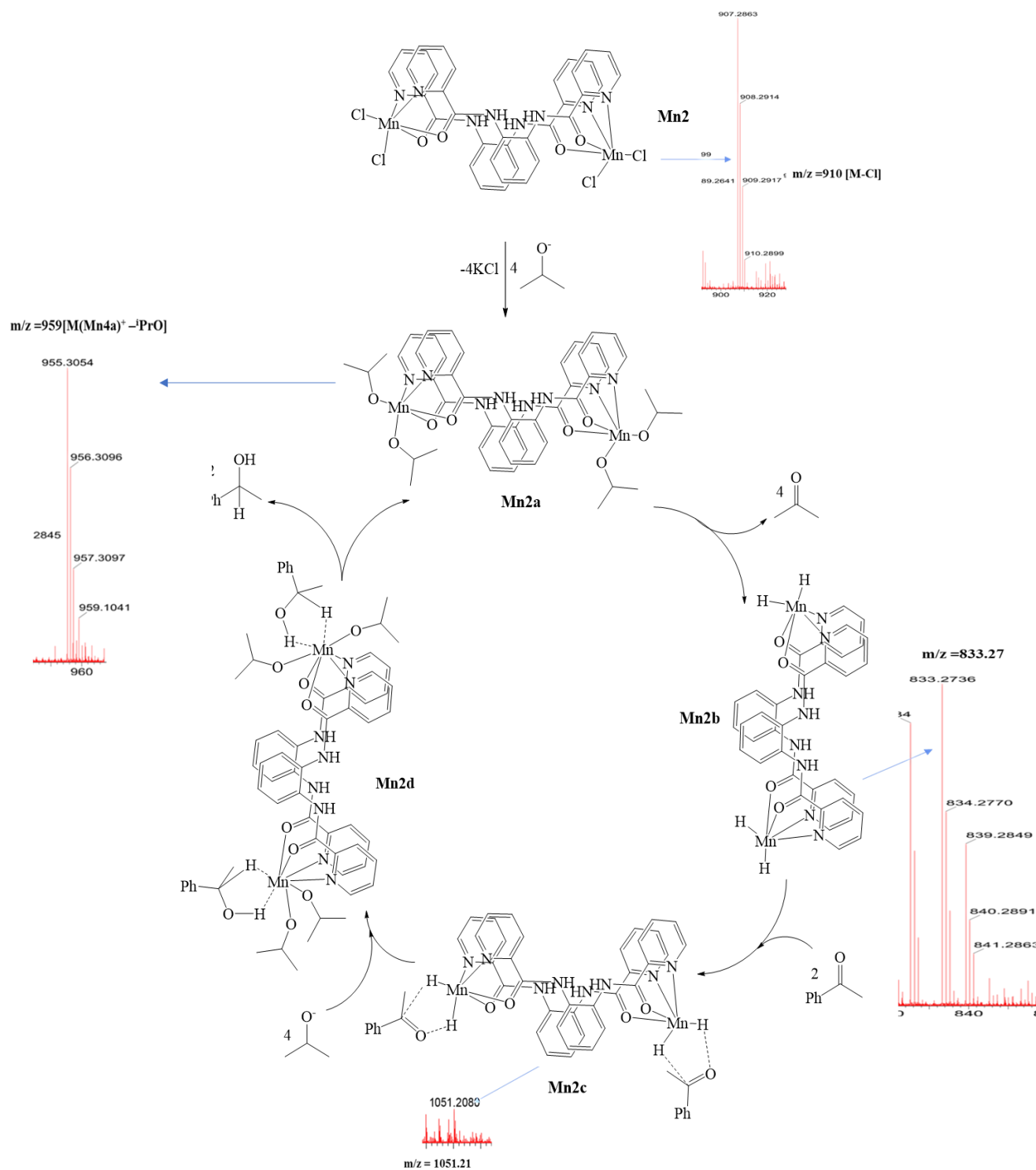
Entry	Substrate	Conversion[%] <sup>b</sup>
1		79
2		90
3		88
4		86
5		80
6		70
7		76
8		81
9		84
10		58
11		63

<sup>a</sup>Condition: Substrate (1.00 mmol, 0.100 mL), K<sup>t</sup>BuO (8.0 mol%) in 2.5 mL of isopropyl alcohol, methoxybenzene (1.00 mmol, 0.11 mL), Mn4(0.015 mol%), time, 8 h, temperature, 82 °C, <sup>b</sup>Determined by using <sup>1</sup>H NMR spectroscopy technique using anisole as internal standard. All experiments were carried out in triplicate to ensure reproducibility.

#### 6.2.6. Plausible catalytic cycle for transfer of ketones using Mn2 as catalysts

On the basis of the mass spectrometry analysis of the aliquots of transfer hydrogenation of acetophenone reaction mixtures, a plausible catalytic cycle dihydride intermediate was proposed using **Mn2** although it was the most active catalysts. From the low-resolution ESI-mass spectrometry data, the mechanism of TH of acetophenone commenced with the displacement of the two chlorides from the Mn(II) centres by isopropoxide to generate the immediate  $[\text{Mn}_2(\text{H}_2\text{L4})_2(\text{iPrO})_4]$  **Mn2a**.<sup>48-49</sup> This could be hypothesised from the signal at  $m/z = 959$  (**Scheme 6.2**). The dihydride active species **Mn2b** was formed as the result of  $\beta$ -elimination of acetone from the **Mn2a** adduct, as evidenced from a signal at  $m/z = 810.63$  (**Scheme 6.2**).<sup>48</sup> The coordination of the substrate acetophenone followed by migration of hydride from the metal centres of the active species **Mn2b** resulted in reactive intermediate **Mn2c**. The formation of the intermediate **Mn2c** could be deduced from the signal at  $m/z = 1050.27$ . Subsequent displacement of the end-product from the metal coordination sphere is proposed to complete the catalytic route and re-generation of the solvated species **Mn2a**.<sup>49-50</sup>





**Scheme 6.2.** The proposed outer-sphere dihydride mechanism of TH of acetophenone using complex **Mn2**.

### 6.3. Conclusions

In summary, dinuclear Mn(II) complexes of carboxamide ligands have been synthesised and characterised using mass spectrometry, FT-IR spectroscopy, magnetic moment measurement, single X-ray crystallography (**Mn2**) and elemental analysis. The first rare less expensive Mn(II) complexes demonstrated good catalytic activities and cooperativity in TH of ketones at lower catalyst loading. The new catalytic system is tolerant to a variety of functional groups such amino, halides, nitro and polyaromatic groups present in the substrates. An outer-sphere dihydride mechanism was proposed for the transfer hydrogenation of ketones catalysed by the new Mn(II) complexes and supported using *in-situ* low resolution mass spectrometry technique.

### 6.4. References

1. Ganesh, K. N.; Zhang, D.; Miller, S. J.; Rossen, K.; Chirik, P. J.; Kozlowski, M. C.; Zimmerman, J. B.; Brooks, B. W.; Savage, P. E.; Allen, D. T., *Green Chemistry: A framework for a sustainable future*. ACS Publications: 2021; Vol. 55, pp 8459-8463.
2. Kurniawan, Y. S.; Priyanga, K. T. A.; Krisbiantoro, P. A.; Imawan, A. C., *Green chemistry influences in organic synthesis: A review. Journal of Multidisciplinary Applied Natural Science* **2021**.
3. Sheldon, R. A.; Arends, I.; Hanefeld, U., *Green chemistry and catalysis*. John Wiley & Sons: 2007.
4. Anastas, P. T.; Bartlett, L. B.; Kirchhoff, M. M.; Williamson, T. C., *Catal. Today* **2000**, 55, 11-22.
5. Li, C.-J.; Trost, B. M., *Proc. Nat. Ac. Sci.* **2008**, 105, 13197-13202.
6. Baidilov, D.; Hayrapetyan, D.; Khalimon, A. Y., *Tetrahedron* **2021**, 98, 132435.
7. Gladiali, S.; Alberico, E., *Chem. Soc. Rev.* **2006**, 35, 226-236.

8. Štefane, B.; Požgan, F., *Catal. Rev.* **2014**, *56*, 82-174.
9. Ahluwalia, V.; Kidwai, M., *New trends in green chemistry*. Springer Science & Business Media: 2004.
10. Albini, A.; Protti, S., *Paradigms in green chemistry and technology*. Springer: 2016.
11. Perez, M.; Elangovan, S.; Spannenberg, A.; Junge, K.; Beller, M., *ChemSusChem* **2017**, *10*, 83-86.
12. van Putten, R.; Benschop, J.; de Munck, V. J.; Weber, M.; Müller, C.; Filonenko, G. A.; Pidko, E. A., *ChemCatChem* **2019**, *11*, 5232-5235.
13. Zhao, Y.; Zhang, L.; Pu, M.; Lei, M., *Dalton Trans.* **2021**, *50*, 14738-14744.
14. Gong, Y.; He, J.; Wen, X.; Xi, H.; Wei, Z.; Liu, W., *Org. Chem. Front.* **2021**, *8*, 6901-6908.
15. Das, K.; Barman, M. K.; Maji, B., *Chem. Commun.* **2021**, *57*, 8534-8549.
16. Ganguli, K.; Shee, S.; Panja, D.; Kundu, S., *Dalton Trans.* **2019**, *48*, 7358-7366.
17. Mata, J. A.; Hahn, F. E.; Peris, E., *Chem. Sci.* **2014**, *5*, 1723-1732.
18. Liu, T.; Wu, K.; Wang, L.; Fan, H.; Zhou, Y.-G.; Yu, Z., *Organometallics* **2019**, *39*, 93-104.
19. Pezük, L. t. G. k.; Sen, B.; Hahn, F. E.; Türkmen, H., *Organometallics* **2019**, *38*, 593-601.
20. Buchwalter, P.; Rosé, J.; Braunstein, P., *Chem. Rev.* **2015**, *115*, 28-126.
21. Liu, T.; Chai, H.; Wang, L.; Yu, Z., *Organometallics* **2017**, *36*, 2914-2921.
22. Pachisia, S.; Kishan, R.; Yadav, S.; Gupta, R., *Inorg. Chem.* **2021**, *60*, 2009-2022.
23. Vijayan, P.; Yadav, S.; Yadav, S.; Gupta, R., *Inorg. Chim. Acta* **2020**, *502*, 119285.
24. Yadav, S.; Vijayan, P.; Gupta, R., *J. Organomet. Chem.* **2021**, *954*, 122081.
25. Panda, C.; Sarkar, A.; Gupta, S. S., *Coord. Chem. Rev.* **2020**, *417*, 213314.
26. Tamer, Ö., *J. Mol. Struc.* **2017**, *1144*, 370-378.

27. Fernandes, T. S.; Vilela, R. S.; Valdo, A. K.; Martins, F. T.; Garcia-Espana, E.; Inclan, M.; Cano, J.; Lloret, F.; Julve, M.; Stumpf, H. O., *Inorg. Chem.* **2016**, *55*, 2390-2401.
28. Sutradhar, M.; Martins, L. M.; da Silva, M. F. C. G.; Alegria, E. C.; Liu, C.-M.; Pombeiro, A. J., *Dalton Trans.* **2014**, *43*, 3966-3977.
29. Wang, S.; Westmoreland, T. D., *Inorg. Chem.* **2009**, *48*, 719-727.
30. Ferenc, W.; Dariusz, O.; Sarzyński, J.; Głuchowska, H., *Eclét. Quím.* **2020**, *45*, 12-27.
31. Raju, K.; Dayakar, G., *Orient. J. Chem.* **2008**, *24*, 237.
32. Allen, F. H., *Acta Crystallogr. Sec. B: Struct. Sci.* **2002**, *58*, 380-388.
33. Allen, F. H.; Davies, J. E.; Galloy, J. J.; Johnson, O.; Kennard, O.; Macrae, C. F.; Mitchell, E. M.; Mitchell, G. F.; Smith, J. M.; Watson, D. G., *J. Chem. Inf. Comput. Sci.* **1991**, *31*, 187-204.
34. Bouteiller, H.; Pasturel, M.; Lemoine, P., *J. Chem. Crystallogr.* **2021**, *51*, 311-316.
35. Martínez-Ferraté, O.; Werlé, C.; Franciò, G.; Leitner, W., *ChemCatChem* **2018**, *10*, 4514-4518.
36. Standfest-Hauser, C.; Slugovc, C.; Mereiter, K.; Schmid, R.; Kirchner, K.; Xiao, L.; Weissensteiner, W., *Dalton Trans.* **2001**, *20*, 2989-2995.
37. Wang, L.; Yang, Q.; Chen, H.; Li, R.-X., *Inorg. Chem. Commun.* **2011**, *14*, 1884-1888.
38. Sato, Y.; Kayaki, Y.; Ikariya, T., *Chem. Asian J.* **2016**, *11*, 2924-2931.
39. Xu, R.; Hua, L.; Li, X.; Yao, Y.; Leng, X.; Chen, Y., *Dalton Trans.* **2019**, *48*, 10565-10573.
40. Dubey, A.; Rahaman, S. W.; Fayzullin, R. R.; Khusnutdinova, J. R., *ChemCatChem* **2019**, *11*, 3844-3852.
41. Azouzi, K.; Valyaev, D. A.; Bastin, S.; Sortais, J.-B., *Curr. Opin. Green Sustain. Chem.* **2021**, *31*, 100511.

42. Zirakzadeh, A.; de Aguiar, S. R.; Stöger, B.; Widhalm, M.; Kirchner, K., *ChemCatChem* **2017**, *9*, 1744-1748.
43. Shvydkiy, N. V.; Vyhivskyi, O.; Nelyubina, Y. V.; Perekalin, D. S., *ChemCatChem* **2019**, *11*, 1602-1605.
44. Zhang, G.-Y.; Ruan, S.-H.; Li, Y.-Y.; Gao, J.-X., *Chin. Chem. Lett.* **2021**, *32*, 1415-1418.
45. Jayaprakash, H., *Dalton Trans.* **2021**, *50*, 14115-14119.
46. Wang, L.; Lin, J.; Sun, Q.; Xia, C.; Sun, W., *ACS Catal.* **2021**, *11*, 8033-8041.
47. Wang, D.; Bruneau-Voisine, A.; Sortais, J.-B., *Catal. Commun.* **2018**, *105*, 31-36.
48. Kumah, R. T.; Tsaulwayo, N.; Xulu, B. A.; Ojwach, S. O., *Dalton Trans.* **2019**, *48*, 13630-13640.
49. Vikse, K. L.; Ahmadi, Z.; McIndoe, J. S., *Coord. Chem. Rev.* **2014**, *279*, 96-114.
50. Ogwen, A. O.; Ojwach, S. O.; Akerman, M. P., *Dalton Trans.* **2014**, *43*, 1228-1237.

## CHAPTER 7

### GENERAL CONCLUSION AND FUTURE PROSPECTS

#### 7.1. Overall concluding remarks

In summary, the thesis examined the synthesis, structural studies, and transfer hydrogenation of ketones and aldehydes of a number of ruthenium(II) and manganese(II) complexes of carboxamide ligands. The work is significant since it unravelled the molecular structures of the ruthenium(II) and manganese(II)-complexes supported on carboxamide ligand motifs and the potential catalytic applications in the transfer hydrogenation of ketones. The project deciphers the role of ligands in the rational design and development of homogeneous catalysts for the efficient transfer hydrogenation of ketones. In this project, the carboxamide ligands and the respective Ru(II) and Mn(II) complexes were synthesised using simple protocols, and their molecular identities were established by  $^1\text{H}$ ,  $^{13}\text{C}$ ,  $^{31}\text{P}$  NMR and  $^{19}\text{F}$  NMR and FT-IR spectroscopies, mass spectrometry, elemental analysis, and single-crystal X-ray crystallography. The solid-state structures of the mononuclear ruthenium(II) complexes **Ru1-Ru5** (**Figure 7.1**) supported on pyrazine-heteroaromatic carboxamide ligands reveal that the ligands coordinated to the Ru(II) ions *via* N<sup>N</sup> bidentate mode. The Ru(II) ion is in a distorted octahedral environment with the C $\equiv$ O, PPh<sub>3</sub>, H and Cl auxiliary ligands occupying the remaining coordinating sites. While dinuclear ruthenium(II) **Ru5** and **Ru6** bearing PPh<sub>3</sub> and C $\equiv$ O auxiliary ligands exhibited distorted octahedral and trigonal bipyramidal geometry with the ligands coordinating *via* the N<sup>O</sup> or N<sup>N</sup> modes, the complexes **Ru8-Ru15** (**Figure 7.1**) adopted a piano-stool geometry around the Ru(II) ions. The dinuclear manganese complex **Mn2** supported on the similar dipicolinamide ligands (**Figure 7.1**) showed that Mn(II) ions reside in a distorted octahedral environment surrounded by two dipicolinamide and *chlorido* ligands.

**Figure 7.1** shows the structures of selected Ru(II) and Mn(II) complexes, demonstrating the highest catalytic activity (TON and TOF) in each Chapter, while **Table 7.1.** presents the summary of catalytic activities of the best performing complexes. All complexes were catalytically active in the transfer hydrogenation of ketones. From **Table 7.1.** it is clear that the nuclearity of the complexes regulated the catalytic activities (TON and TOF) of the complexes. The dinuclear Ru(II) complexes **Ru5** in (**Chapter 3**), and **Ru8-Ru15** (**Chapter 4** and **5**) complexes showed higher catalytic activity compared to the mononuclear Ru(II) complexes **Ru5** and **Ru7** (**Chapter 4**) due to better cooperativity between the metal centres. The *co*-ligands (PPh<sub>3</sub>, CO, Cl<sup>-</sup>, half-sandwich arene) and metal-metal interactions significantly impacted the catalytic activities of the complexes in TH of ketones. Interestingly, the half-sandwich diruthenium complexes **Ru8-Ru11** (**Chapter 4**) displayed relatively higher catalytic activities (TON ranging from 17100 to 48500) compared to the diruthenium complexes **Ru5** bearing the C≡O, PPh<sub>3</sub>, Cl, *co*-ligands (TON range 14300) (**Table 7.1, entries 2 vs 4-7**). This was attributed to the chelating effects and higher cooperativity effects from the Ru(II)-N,N functionality which render the complexes more robust and less prone to deactivation. In addition, the introduction of quinoline moiety into the carboxamide ligand system (**Chapter 5**) leads to a significant increase in the catalytic activity of the complexes **Ru12-Ru15** compared to the analogous complexes **Ru8-Ru11** supported phenylene-dipicolinamide motifs (**Table 7.1**).

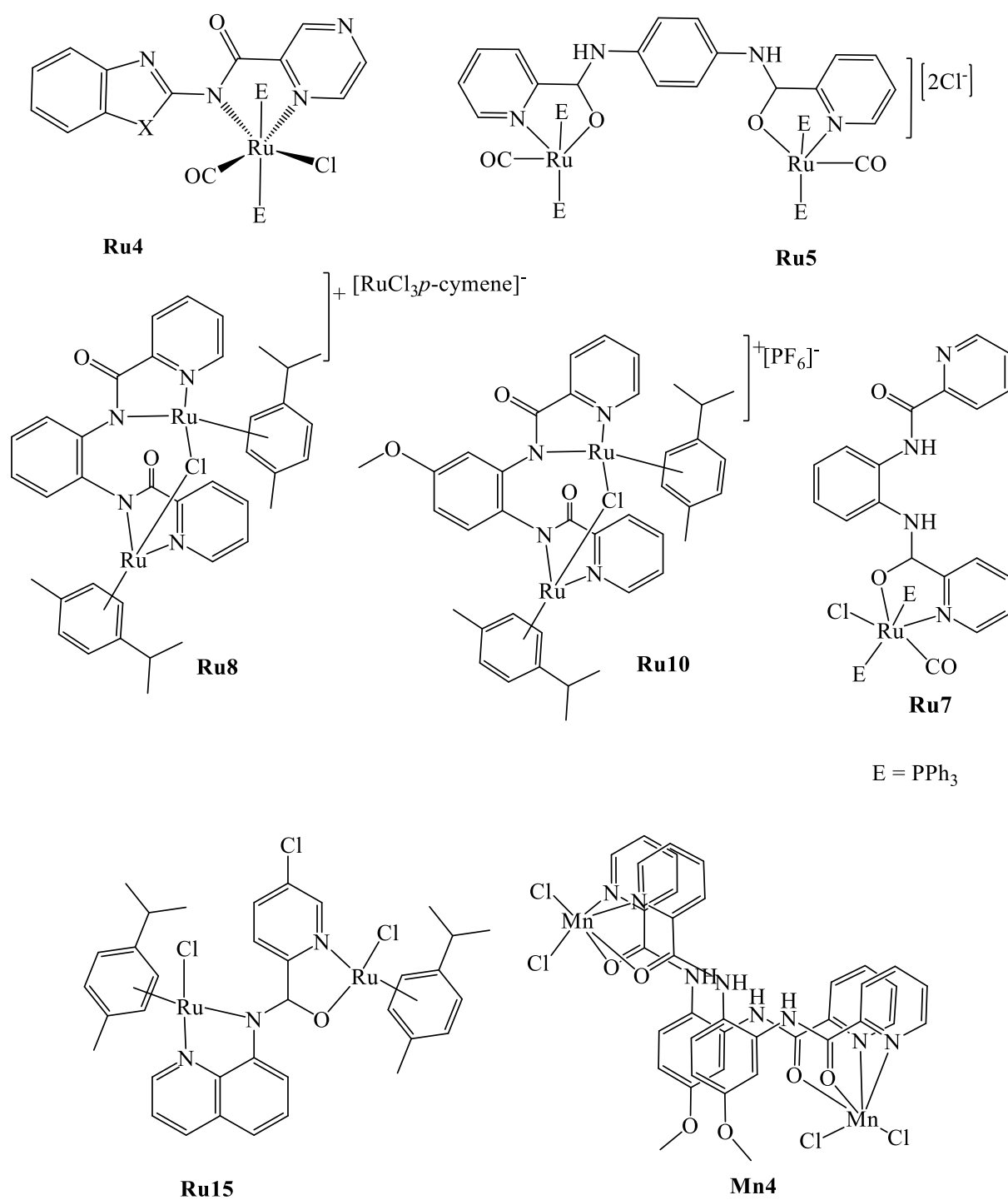


**Figure 7.1.** Selected Ru (II) and Mn(II) complexes displaying the highest and lowest catalytic activities in TH of ketones.



**Table 7.1.** Catalytic activity (TON and  $k_{\text{ob}}/\text{h}^{-1}$ ) of selected Ru(II) and Mn(II) complexes

Entry	Catalyst	TON	TOF/h <sup>-1</sup>	Chapter
1	<b>Ru4</b>	912	152	<b>3</b>
2	<b>Ru5</b>	143 00	2383	<b>4</b>
3	<b>Ru7</b>	94 00	1567	<b>4</b>
4	<b>Ru8</b>	17100	2850	<b>4</b>
5	<b>Ru10</b>	15700	2617	<b>4</b>
6	<b>Ru15</b>	48500	8083	<b>5</b>
7	<b>Mn4</b>	4064	508	<b>6</b>

Turn over number (TON) = moles of product formed/moles of catalyst used. Turn over frequency (TOF) = moles of product /moles of catalyst used/time.

The electropositivity, hardness and the tendency of Ru(II) to form hydride intermediates from isopropyl alcohol compared to Mn(II) (**Mn4**) point to the higher catalytic activities of the Ru(II) complexes (**Ru5-Ru10**). All the new Ru(II) systems followed a similar inner-sphere monohydride reaction pathway in the transfer hydrogenation of acetophenone.

## 7.2. General summary

The study demonstrated the significant roles of carboxamide ligands and ruthenium(II) and manganese(II) catalysts in the transfer hydrogenation of ketones. In summary:

- Ruthenium(II) and manganese(II) carboxamide complexes were synthesised, and their molecular structures were established using spectroscopic techniques and elemental analyses.

- ii. Dinuclear ruthenium(II) complexes exhibited higher catalytic activities than their corresponding mononuclear analogues.
- iii. The dinuclear ruthenium(II) complexes bearing the  $\text{PPh}_3$  and  $\text{C}\equiv\text{O}$  co-ligands showed comparable catalytic activity to half-sandwich ruthenium(II) complexes supported on similar dipicolinamide ligands.
- iv. Metal-metal interactions between the two metal centres in the dinuclear complexes significantly enhanced the catalytic activities.
- v. The manganese(II) complexes supported on the dipicolinamide ligands exhibited relatively lower catalytic activity compared to the analogous ruthenium(II) complexes.
- vi. Despite ruthenium(II) catalysts being more expensive, this thesis affirmed their hitherto superior catalytic activities, though the earth-abundant Mn(II) complexes (**Chapter 6**) showed promising results.

### 7.3. Future prospects

The findings of this study have significantly contributed to the development of organometallic complexes for TH of ketones. For example, the half-sandwich diruthenium(II) complexes supported on picolinamide ligands, as discussed in **Chapter 5**, have demonstrated good catalytic efficiency in the TH of ketones. However, the catalytic activities of these dinuclear Ru(II) complexes were relatively low compared to some previously reported multinuclear ruthenium(II) complexes. Thus, modifying the carboxamide motif will help to minimise the metal-metal interaction and promote better cooperativity and catalytic activity (**Figure 7.2**). It will be more interesting to extend the new system to TH of ketones under base-free reaction conditions.

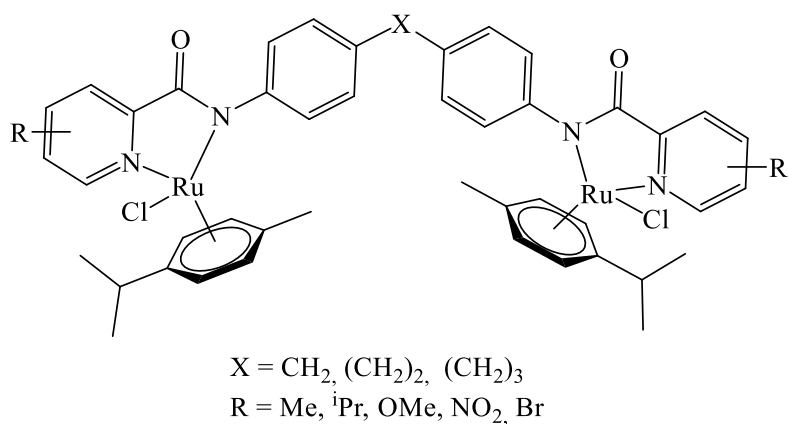


**Figure 7.2.** The general structure of the proposed diruthenium(II) complexes for TH of ketones.

Regarding the principles of green chemistry, heterogeneous catalysts made from earth-abundant and biocompatible metals are more appealing due to ease of separation and recycling. Thus, immobilising the current system using MCM-41 supports will be attractive. MCM-41 is a mesoporous material belonging to a family of M41s discovered in the 1990s. It has an orderly array of channels, high surface area, and excellent stability. New heterogeneous catalysts made up of pinacolinamide carbonyl Mn(I) complexes (**Figure 7.3**) with silanol functionality (CPTMS and CPTES) for anchoring *via* covalent bonding, with MCM-41 mesoporous support would be interesting to study as a catalyst in TH of ketones.

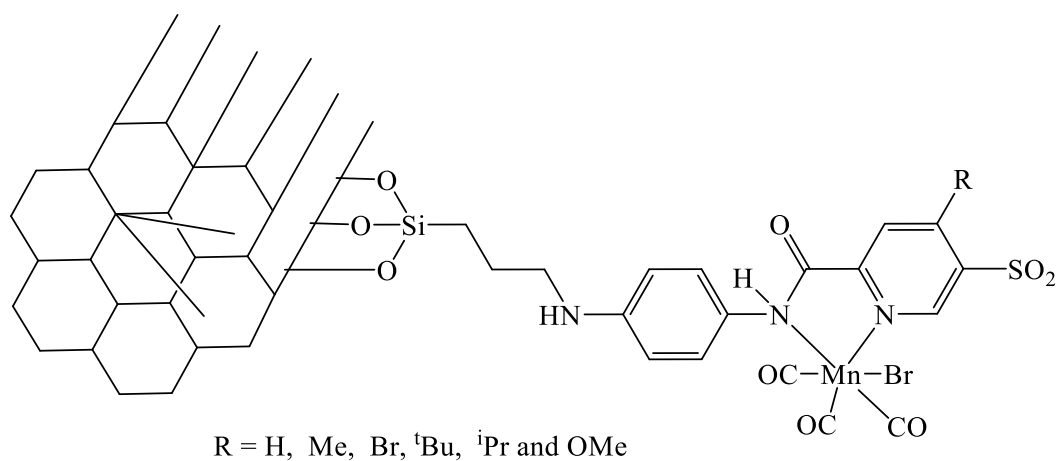


**Figure 7.3.** General structure of Mn(I) carbonyl complexes supported on mesoporous material, MCM-41.